DEPARTAMENTO DE BIOLOGÍA CELULAR, FISIOLOGÍA E INMUNOLOGÍA

Programa de Doctorado en Biomedicina

Mediators of the cellular response to the development of obesity and metabolic disease

Mediadores de la respuesta celular al desarrollo de obesidad y enfermedad metabólica

Directores: Prof. Dra. María del Mar Malagón Poyato y Dra. Rocío Guzmán Ruiz

Julia Sánchez Ceinos

Córdoba, 2021

TITULO: *Mediators of the cellular response to the development of obesity and metabolic disease*

AUTOR: *Julia Sánchez Ceinos*

Campus de Rabanales
Ctra. Nacional IV, Km. 396 A
14071 Córdoba

https://www.uco.es/ucopress/index.php/es/
ucopress@uco.es

DEPARTAMENTO DE BIOLOGÍA CELULAR, FISIOLOGÍA E INMUNOLOGÍA

Programa de Doctorado en Biomedicina

UNIVERSIDAD D CÓRDOBA

Mediators of the cellular response to the development of obesity and metabolic disease

Memoria de Tesis Doctoral presentada por Julia Sánchez Ceinos, Graduada en Biología y Máster en Investigación Biomédica Traslacional, para optar al grado de Doctora en Biomedicina

Los Directores,

Prof. Dra. María del Mar Malagón Poyato
Catedrática de Biología Celular
de la Universidad de Córdoba

Dra. Rocío Guzmán Ruiz
Investigadora Postdoctoral
de la Universidad de Córdoba

En Córdoba, a 11 de Febrero de 2021

DEPARTAMENTO DE BIOLOGÍA CELULAR, FISIOLOGÍA E INMUNOLOGÍA

Dª María del Mar Malagón Poyato (Catedrática de Biología Celular) y Dª Rocío Guzmán Ruiz (Investigadora Postdoctoral), ambas pertenecientes al Departamento de Biología Celular, Fisiología e Inmunología de la Universidad de Córdoba,

INFORMAN

Que Dª Julia Sánchez Ceinos, Graduada en Biología y Máster en Investigación Biomédica Traslacional, ha realizado bajo nuestra dirección el trabajo titulado **"Mediators of the cellular response to the development of obesity and metabolic disease"** y que, bajo nuestro juicio, reúne los méritos suficientes para optar al Grado de Doctora en Biomedicina.

Y para que conste, firmamos el presente documento en Córdoba, 11 de Febrero de 2021.

Fdo.: **Prof. Dra. María del Mar Malagón Poyato**

Fdo.: **Dra. Rocío Guzmán Ruiz**

TÍTULO DE LA TESIS: Mediators of the cellular response to the development of obesity and metabolic disease

DOCTORANDO/A: Julia Sánchez Ceinos

INFORME RAZONADO DE LOS DIRECTORES DE LA TESIS

Durante el desarrollo de la presente Tesis Doctoral, en el periodo comprendido entre junio de 2015 y enero de 2021, la doctoranda Julia Sánchez Ceinos no solo ha superado con creces los objetivos planteados al comienzo de la misma, sino que ha desarrollado y validado técnicas experimentales de una gran utilidad para el grupo de investigación, que le han permitido obtener resultados muy relevantes en el campo de la obesidad contribuyendo a elucidar el papel del tejido adiposo en el desarrollo de resistencia a insulina y diabetes tipo 2 en obesidad. Fruto de este trabajo, la doctoranda ha publicado con primera autoría un trabajo directamente relacionado con su Tesis Doctoral en la revista "*Molecular Therapy – Nucleic Acids*", y cuenta con varios artículos más que serán publicados en un futuro próximo. Además, su colaboración con otros grupos de investigación le ha permitido ser autora de varios trabajos relacionados con su Tesis Doctoral en revistas de elevado prestigio en su área de investigación ("*Nature Communications*"), así como en otras áreas de conocimiento como la química analítica ("*Talanta*") que avalan su amplio conocimiento adquirido durante su periodo predoctoral. Por último, la doctoranda ha presentado sus resultados en diferentes congresos de ámbito nacional (31 comunicaciones, 16 orales y 15 tipo póster) e internacional (6 comunicaciones, 2 orales y 4 tipo póster), sumando 5 premios a las mejores comunicaciones (3 orales y 2 tipo póster), asistido a 36 cursos de formación (25 nacionales y 11 internacionales), y realizado 11 actividades docentes.

Por todo ello, se autoriza la presentación de la Tesis Doctoral.

Córdoba, 11 de Febrero de 2021

Fdo.: **Prof. Dra. María del Mar Malagón Poyato**

Fdo.: **Dra. Rocío Guzmán Ruiz**

Esta Tesis Doctoral ha sido realizada en el Departamento de Biología Celular, Fisiología e Inmunología de la Universidad de Córdoba y en el Instituto Maimónides de Investigación Biomédica de Córdoba (IMIBIC), bajo la dirección de la Prof. Dra. María del Mar Malagón Poyato y la Dra. Rocío Guzmán Ruiz. Dicho trabajo ha sido subvencionado mediante los proyectos del Ministerio de Ciencia, Innovación y Universidades/FEDER (BFU2013-44229-R; BFU2016-76711-R; BFU2017-90578-REDT), del Instituto de Salud Carlos III (ISCIII)/FEDER (PIE14/00005), Conserjería de Salud y Bienestar Social/Junta de Andalucía/FEDER (PI-0159-2016), y fondos propios del grupo de investigación. Durante el transcurso de la presente Tesis Doctoral se ha realizado una estancia de cuatro meses en el Departamento de Medicina, Unidad de Endocrinología y Diabetes del Instituto Karolinska en Estocolmo (Suecia) bajo la supervisión del Dr. Mikael Rydén, financiada por una ayuda de la Universidad de Córdoba (Convocatoria “Becas Movilidad Internacional” 2017/2018) para la realización de estancias destinadas a la obtención de la Mención Internacional en el Título de Doctor.

A Rafa y a mis abuelos

LIST OF ABBREVIATIONS

3D	Three-dimensional
ACAT	CoA:cholesterol O-acyltransferase
ACC	Acetyl-CoA carboxylases
ACLY	ATP-citrate lyase
ADA	American Diabetes Association
ADIPOQ	Adiponectin
ADP	Adenosine-5’-diphosphate
ADSC	Adipose tissue-derived stem cell
AGO	Argonaute
AGPAT	Sn-1-acylglycerol-3-phosphate acyltransferase
ARF	ADP ribosylation factor
AS	Alternative splicing
ATCC	American Type Culture Collection
ATIRI	Adipose tissue insulin-resistance index
ATF	Activating transcription factor
ATGL	Adipose triglyceride lipase
ATM	Adipose tissue macrophage
ATP	Adenosine triphosphate
BAT	Brown adipose tissue
BiP/BIP	Binding immunoglobulin protein
BMI	Body mass index
BMP	Bone morphogenetic protein
BS	Bariatric surgery
BSA	Bovine serum albumin
BSCL	Berardinelli-Seip Congenital Lipodystrophy
C/EBP	CCAAT enhancer binding protein
cAMP	Cyclic adenosine monophosphate
CAV	Caveolin
CCL	Chemokine C-C motif ligand
CHOP	C/EBP homologous protein
ChT-L	Chymotrypsin-like
CIDE	DFFA-like effector
COL	Collagen
CREB	cAMP-response element binding protein
CRP	C-reactive protein
DAG	Diacylglycerol
DAPI	4 ',6-diamidino-2-fenilindol
DGAT	Diacylglycerol acyltransferase
DMEM	Dulbecco's Modified Eagle Medium
DMSO	Dimethyl sulfoxide
DNA	Deoxyribonucleic acid
DNL	De novo lipogenesis
D-PBS	Dulbecco's PBS
DTT	1,4-dithiothreitol
ECM	Extracellular matrix
EDTA	Ethylenediaminetetraacetic acid
EGR	Early growth response protein
eIF	Eukaryotic initiation factor

ER	Endoplasmic reticulum
ERAD	ER-associated degradation
ERK	Extracellular signal–regulated kinase
EV	Extracellular vesicles
FA	Fatty acid
FABP	Fatty-acid-binding protein
FASN/FAS	Fatty acid synthase
FATP	Fatty acid transport protein
FBS	Fetal bovine serum
FFA	Free fatty acid
FGF	Fibroblast growth factor
FIT	Fat storage-inducing transmembrane
FSP	Fat-specific protein
FTO	FTO alpha-ketoglutarate dependent dioxygenase
(E)GFP	Green fluorescent protein
GLUT	Glucose transporter
GO	Gene Ontology
GSV	GLUT4 storage vesicle
HbA1c	Glycosolated haemoglobin
HCA	Hierarchical Clustering Analysis
HDL	High-density lipoprotein
HGHI	High concentrations of glucose and insulin
hnRNP	Heterogeneous nuclear ribonucleoprotein
HOMA-IR	Homeostatic Model Assessment of Insulin Resistance
HRP	Horseradish peroxidase
HSL/LIPE	Hormone sensitive lipase
HURS	"Reina Sofía" University Hospital
HUVR	"Virgen del Rocío" University Hospital
IAA	Iodoacetamide
IBMX	3-isobutyl-1-methylxanthine
IFG	Impaired fasting glucose
IL	Interleukin
IMIBIC	Maimónides Biomedical Research Institute of Córdoba
IPA	Ingenuity Pathway Analysis
IR	Insulin resistance, insulin resistant
IR/INSR	Insulin receptor
IRE	Inositol-requiring transmembrane kinase/endoribonuclease
IRS	Insulin receptor substrate
iTRAQ	Isobaric tags for relative and absolute quantitation
KI	Karolinska Institutet
KO	Knockout
LC-MS/MS	Liquid chromatography-tandem mass spectrometry
LD	Lipid droplet
LDL	Low-density lipoprotein
LPIN	Lipin
LPL	Lipoprotein lipase
LPS	Lipopolysaccharide
LSO	Long-standing obese

MA	Mature adipocyte
MAG	Monoacylglycerols
MCP	Monocyte chemoattractant protein
MGL	MG lipase
miRISC	miRNA-induced silencing complex
miRNA	MicroRNA
mRNA/ARNm	Messenguer RNA
mTOR	Mammalian target of rapamycin
MTT	3-(4,5-dimethylthiazol-2-yl)-2,5-diphenyltetrazolium bromide
MV	Microvesicle
MVB	Multivesicular body
NBCS/NCS	Newborn calf serum
NEFA	Non-esterified fatty acid
NF	Normalization factor
NF-κB	Nuclear transcription factor kappa-B
NG	Normoglycemic
OM	Omental
PAI-1	Plasminogen activator inhibitor-1
PAB	Andalusian Bioinformatics Platform
PANTHER	Protein ANalysis THrough Evolutionary Relationships
PBS	Phosphate buffered saline
PDI	Protein disulphide isomerase
PDK	3-phosphoinositide-dependent protein kinase
PERK	PKR–activated protein kinase-like eukaryotic initiation factor kinase
PGC	Peroxisome proliferator-activated receptor gamma coactivator
PI3K	Phosphatidylinositol 3-kinase
PIP3	Phosphatidyl-inositol-3,4,5-trisphosphate
PK	cAMP-dependent protein kinase
PLIN	Perilipin
PMA	Phorbol-12-myristate-13-acetate
PPAR	Peroxisome proliferator activated receptor
Pref	Preadipocyte factor
PRP/PRPF	Pre-mRNA processing factor
qRT-PCR	Quantitative RT-PCR
RALA	Ras-related protein Ral-A
RNA	Ribonucleic acid
RNF	Ring finger protein
ROS	Reactive oxygen species
RT	Room temperature, retrotranscription
RT-PCR	Real time PCR
RYGB	Roux-en-Y gastric bypass
S1P	Site-1 protease
S2P	Site-2 protease
SAT	Subcutaneous adipose tissue
SC	Subcutaneous
SDS	Sodium dodecyl sulfate
SE	Sterol ester
SEC61	Sec61 translocon

SEL1L	Suppressor/enhancer of Lin1-like
SEPBIO	Proteomics and Bioinformatic Service
SF	Splicing factor
SG	Sleeve gastrectomy
SGBS	Simpson-Golabi-Behmel Syndrome
siRNA	Silencing RNA
SSO	Short-standing obese
SNARE	Soluble NSF attachment receptor
snRNP	Small nuclear ribonucleoprotein
SREBP	Sterol regulatory element-binding transcription factor
SRSF	Serine and arginine rich splicing factor
SVF	Stromal vascular fraction
T2D	Type 2 diabetes
T3	3,3',5-triiodo-l-thyronine
TAG/TG	Triglyceride
TBS	Tris-buffer saline
TEAB	Tetraethylammonium bromide
TEM	Transmission electron microscopy
TGF	Transforming growth factor
TNF	Tumor-necrosis factor
UAB	Autonomous University of Barcelona
UCAIB	Central Unit for Biomedical Research Support
UCP	Uncoupling protein
UGC	Unidad de Gestión Clínica
UPR	Unfolded protein response
UPS	Ubiquitin proteasome system
VAT	Visceral adipose tissue
WAT	White adipose tissue
WHO	World Health Organization
XBP	X-box binding protein
WC	Waist circumference
YBX	Y-box binding protein
ZFP	Zinc finger protein

TABLE OF CONTENTS

GRAPHICAL ABSTRACT

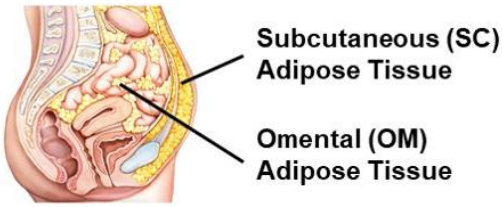

Impaired Adipogenesis in Obese individuals with Insulin Resistance (IR) or Type 2 Diabetes (T2D)

SC Preadipocytes: Down-regulated Splicing machinery

SC/OM Preadipocytes: Umbalanced Endoplasmic Reticulum (ER)-Proteostasis

Dysfuntional Adipose Tissue

Pro-inflammatory conditions (e.g., exposure to TNFα)

miR-223-3p

↓Circulating *miR-223-3p*: Biomarker of Adipose Tissue Dysfunction and T2D onset

Pathogenic accumulation of *miR-223-3p* impairs glucose and lipid metabolism in adipocytes

Graphical elements adapted from Servier Medical Art (SMART) repository.

SUMMARY

Obesity is the pandemic of the 21st century. Overall, about 15% of the world's adult population is obese, and if the rising trend continues, it is estimated that global prevalence reaches 20% by 2025. Obesity poses a major public health issue due to its elevated risks for adverse health consequences, including several serious chronic diseases, such as insulin resistance (IR), type 2 diabetes (T2D), non-alcoholic fatty liver disease (NAFLD), cardiovascular disease, dyslipidemia, hypertension, stroke, hypercholesterolemia, hypertriglyceridemia, arthritis, asthma, neurodegenerative diseases, and even certain forms of cancer. Many factors and mechanisms have been implicated in obesity pathogenesis, but their trigger is uncertain, and the causal relationship between them and the complications of obesity remains in question. However, there is little doubt that obesity is closely associated with adipose tissue dysfunction, and that this condition leads to the development of metabolic diseases.

Adipose tissue is a complex organ with primary roles in energy homeostasis control. Thus, adipose tissue not only acts as a reservoir for energy storage and utilization, but also it senses energy demands and secretes signalling factors to regulate other metabolic tissues. However, in obesity, adipose tissue may become severely dysfunctional and not expand properly to store the energy excess. This induces ectopic fat deposition in other tissues involved in the maintenance of glucose homeostasis, an event commonly defined as "lipotoxicity". It has been extensively demonstrated that excessive lipid accumulation in ectopic tissues leads to local inflammation and IR. Numerous pathogenic processes have been associated with the unhealthy expansion of the adipose tissue, including inflammation, fibrosis, hypoxia, altered adipokines secretion, mitochondrial dysfunction, hyperinsulinemia, endoplasmic reticulum (ER), and oxidative stress. Dietary and lifestyle, as well as therapeutic interventions, can be adequate to treat obesity and prevent metabolic alterations. Nevertheless, the exact molecular and cellular mechanisms underlying adipose tissue dysfunction and its implications in the development of metabolic disturbances are broadly unknown. Improving our understanding in this field might lead to the development of new approaches and the identification of therapeutic targets for treating obesity.

In this Doctoral Thesis, we aimed at identifying potential factors and pathway markers relevant to the loss of adipose tissue function in obesity and their relationship to obesity-related IR/T2D. To this end, we analysed human adipose tissue samples in combination with both human and murine cell lines, using state-of-the-art methodologies to investigate adipose tissue functionality in obesity and in response to weight loss upon bariatric surgery (BS), and their corresponding mechanisms associated with metabolic

alterations or recovery, respectively. Specifically, to reach this general goal, we have carried out two separate studies, which are depicted in detail below.

1. Study 1: Identification of pathogenic markers of metabolic disease in preadipocytes of obese individuals

Adipose precursor cells, the preadipocytes, are essential for the maintenance of adipose tissue homeostasis, regeneration, and expansion. Preadipocytes differentiation into adipocytes (i.e., adipogenesis) enables adipocyte turnover and adipose tissue growth, and ensures adipose tissue plasticity to accommodate surplus energy. It has been proposed that the inability for recruiting new adipose cells, together with the functional impairment of hypertrophied adipocytes that occur in obesity, contributes to lipid spillover from the adipose tissue. Thus, increasing adipogenesis appears as a valuable strategy to facilitate healthy adipose tissue expansion and ensure metabolic health.

Adipocyte differentiation relies on major changes in gene expression programs regulating mRNA and protein production. An increasing body of evidence shows that mRNA processing and, in particular, alternative splicing, is crucial for genome reprogramming during cell differentiation. However, the splicing components relevant to adipogenesis and the cellular events regulated by alternative splicing during adipocyte differentiation have been scarcely explored, and it is yet to be established whether alternative splicing is modified in human obesity. Another crucial mechanism preserving precursor cell function relates to protein homeostasis (i.e., proteostasis), which maintains the capacity of cells to expand in order to sustain tissue growth and regeneration. Several lines of evidence support an important role for the endoplasmic reticulum (ER) protein quality control system in the regulation of adipogenesis. In fact, the unfolded protein response (UPR) is perturbed in the obese adipose tissue, and it has been proposed to contribute to the pathology of obesity. By contrast, it is still unknown whether the other component of the protein control system, the ER-associated protein degradation (ERAD), which is crucial for protecting cells against the accumulation of misfolded/unfolded proteins and proteotoxicity, is altered in the obese adipose tissue.

Here, in order to identify altered molecular pathways that may contribute to metabolic disease in obesity, we set out an iTRAQ-LC-MS/MS proteomic approach for the analysis of subcutaneous (SC) and omental (OM) preadipocytes from obese individuals with normoglycaemia (NG) and T2D. Down-regulation of multiple components of the splicing machinery was observed in SC preadipocytes from obese individuals with insulin

resistance (IR) or T2D, as compared to NG obesity. This, together with the observation that adipogenesis can be modulated by regulating the expression levels of a key spliceosome component, *PRFP8*/PRP8, supports a role for alternative splicing in the development of obesity-associated metabolic complications. In addition, our studies show that not only the UPR is altered in human SC and OM preadipocytes from IR/T2D obese subjects, but also that the ERAD system is hyperactivated. This condition, when mimicked *in vitro*, prevented adipogenesis. Our results provide novel mechanistic explanations for the impaired adipogenic capacity observed in IR/T2D obesity that relates to both mRNA and ER-proteostasis disturbances.

2. Study 2: Characterization of miRNAs as markers of dysfunctional adipose tissue in type 2 diabetes (T2D)

It is increasingly accepted that, besides adipokines, the adipose tissue is a major physiological source of circulating microRNAs (miRNAs). miRNAs, a class of small non-coding RNAs that post-transcriptionally regulate gene expression, have emerged as key molecules for cell function. Anomalous miRNA levels and alterations in their biogenesis machinery have been related to several metabolic diseases, including obesity as well as T2D, and dyslipidemia. miRNAs are also actively secreted into the circulation and have been proposed to act as messengers for intercellular communication. This characteristic has pointed out circulating miRNAs as potential biomarkers for disease and altered circulating levels of numerous miRNAs have been associated with metabolic disorders. In this scenario, in order to design targeted preventive therapeutic strategies, it is critical to identify the early mechanisms that precede disease onset.

Recently, the predictive value of a number of miRNAs for the diagnosis of T2D incidence was assessed in the CORonary Diet Intervention with Olive oil and cardiovascular PREVention (CORDIOPREV) study (ClinicalTrial.gov ID: NTC00924937), a prospective study carried out in 1,002 patients with coronary heart disease and high cardiovascular risk. These studies demonstrated that, when combined with HbA1c, a group of nine miRNAs (*miR-9*, *miR-28-3p*, *miR-29a*, *miR-30a-5p*, *miR-103*, *miR-126*, *miR-150*, *miR-223-3p*, and *miR-375*), provided a higher predictive value in T2D diagnosis than clinical parameters. The relationship between baseline levels of these miRNAs with markers of beta-cell function and systemic and peripheral IR was also investigated. However, their potential association with adipose tissue deregulation was not analyzed. This is of interest as adipose tissue dysfunction has been proposed as a major contributing factor for the development of T2D, and adipose tissue miRNA

expression profile is altered in obesity and T2D. In this line, several cross-sectional human studies have shown that the obesity-related expression pattern of specific circulating miRNAs reflects their miRNA adipose tissue expression profiles, supporting a role for circulating miRNAs as adipose tissue biomarkers. However, the relationship between circulating miRNAs and adipose tissue functional state is not fully understood, yet it might be useful to identify adipose tissue-related metabolic complications.

In this scenario, we aimed at analyzing the relationship between previously established predictive miRNAs for T2D onset in the CORDIOPREV cohort (Jiménez-Lucena et al., 2018) and the loss of adipose tissue insulin sensitivity. Once established that circulating *miR-223-3p* was dysregulated in relation to adipose tissue function, we performed functional analysis to elucidate both the potential of preadipocytes and adipocytes as *miR-223-3p* secreting cells, and the consequences of *miR-223-3p* dysregulation on adipocyte biology. Our results indicate that *miR-223-3p* secretion by preadipocytes and adipocytes is prevented under inflammatory conditions, and that its pathogenic accumulation leads to alterations in both glucose and lipid metabolism in these cells. These observations could answer to the lower circulating levels on this miRNA found in those patients who are going to develop T2D, as well as explain its underlying role as a potential predictor of adipose dysfunction related to T2D development.

We have also demonstrated that the changes that occur in the circulating milieu after BS-induced weight-loss modulate *miR-223-3p* expression by adipocytes. The relevance of these observations was further supported by our functional studies in adipocytes exposed to pre- and post-BS serum, where the post-BS serum improved the insulin-induced glucose uptake in adipocytes, in comparison with those cells exposed to pre-BS. These findings further support the notion that inflammatory mediators present in either the serum, or locally in the adipose tissue, may be responsible for the alterations in *miR-223-3p* regulation.

In sum, when viewed together, our studies indicate that impaired splicing and disturbed ER-proteostasis are components of the pathogenic molecular fingerprint of preadipocytes that could be targeted to prevent and/or improve adipose tissue dysfunction in obesity and its related metabolic disorders. Likewise, our data support the notion that *miR-223-3p* may have a role as a potential predictor of adipose dysfunction related to T2D development, thus unveiling a novel molecular target that may be helpful to design novel therapeutic strategies to prevent T2D.

RESUMEN

La obesidad es la pandemia del siglo XXI. En conjunto, alrededor del 15% de la población adulta mundial es obesa. Si la tendencia al alza continúa, se estima que la prevalencia mundial alcanzará el 20% para el 2025. Así, la obesidad plantea un problema importante de salud pública debido a sus elevados riesgos para la salud, entre ellas varias enfermedades crónicas graves, como resistencia a insulina (IR), diabetes tipo 2 (T2D), enfermedad de hígado graso no alcohólico (NAFLD), enfermedad cardiovascular, dislipidemia, hipertensión, accidente cerebrovascular, hipercolesterolemia, hipertrigliceridemia, artritis, asma, enfermedades neurodegenerativas e incluso ciertas formas de cáncer. Diversos factores y mecanismos han sido implicados en la patogénesis de la obesidad, pero su desencadenante es incierto. Además, la relación causal entre ellos y las complicaciones de la obesidad permanece sin resolver. Sin embargo, hay pocas dudas de que la obesidad está estrechamente asociada con la disfunción del tejido adiposo, y que esta condición conduce al desarrollo de enfermedades metabólicas.

El tejido adiposo es un órgano complejo con funciones principales en el control de la homeostasis energética. Por lo tanto, el tejido adiposo no solo actúa como un depósito para el almacenamiento y la utilización de energía, sino que también detecta las demandas de energía, y secreta factores de señalización para regular otros tejidos metabólicos. Sin embargo, en obesidad, el tejido adiposo puede volverse gravemente disfuncional, y no expandirse adecuadamente para almacenar el exceso de energía. Esto induce el depósito ectópico de grasa en otros tejidos involucrados en el mantenimiento de la homeostasis de la glucosa, un evento comúnmente definido como "lipotoxicidad". Se ha demostrado ampliamente que la acumulación excesiva de lípidos en tejidos ectópicos provoca inflamación local e IR. Numerosos procesos patogénicos se han asociado con la expansión no saludable del tejido adiposo, que incluyen: inflamación, fibrosis, hipoxia, secreción alterada de adipoquinas, disfunción mitocondrial, hiperinsulinemia, y estrés de retículo endoplásmico (ER) y oxidativo. Las intervenciones dietéticas y de estilo de vida, así como las terapéuticas, pueden ser adecuadas para tratar la obesidad y prevenir alteraciones metabólicas. Sin embargo, los mecanismos moleculares y celulares exactos que subyacen a la disfunción del tejido adiposo, y sus implicaciones en el desarrollo de alteraciones metabólicas son ampliamente desconocidos. Mejorar nuestra comprensión en este campo podría conducir al desarrollo de nuevos enfoques y a la identificación de dianas terapéuticas para tratar la obesidad.

En esta Tesis Doctoral, nuestro objetivo fue identificar los posibles factores y marcadores de las vías relevantes para la pérdida de la función del tejido adiposo en

obesidad, y su relación con IR/T2D asociadas. Para ello, analizamos muestras de tejido adiposo humano en combinación con líneas celulares, tanto humanas como murinas, utilizando metodologías de vanguardia para investigar la funcionalidad del tejido adiposo en obesidad, y su respuesta a la pérdida de peso tras cirugía bariátrica (BS). Así como, sus correspondientes mecanismos asociados con alteraciones metabólicas o de recuperación, respectivamente. Específicamente, para alcanzar este objetivo general, hemos llevado a cabo dos estudios separados, que se describen en detalle a continuación.

1. Estudio 1: Identificación de marcadores patogénicos de enfermedad metabólica en preadipocitos de individuos obesos

Las células adiposas precursoras, los preadipocitos, son esenciales para el mantenimiento de la homeostasis, regeneración y expansión del tejido adiposo. La diferenciación de los preadipocitos en adipocitos (adipogénesis) permite el recambio de adipocitos y el crecimiento del tejido adiposo, y asegura la plasticidad de este tejido para acomodar el exceso de energía. Se ha propuesto que la incapacidad para reclutar nuevas células adiposas, junto con el deterioro funcional de los adipocitos hipertróficos que ocurre en obesidad, contribuye al derrame de lípidos del tejido adiposo. Por lo tanto, el aumento de la adipogénesis aparece como una estrategia valiosa para facilitar la expansión saludable del tejido adiposo y salvaguardar la salud metabólica.

La diferenciación de adipocitos se basa en cambios importantes en los programas de expresión génica que regulan la producción de ARNm y proteínas. Un creciente número de evidencias muestra que el procesamiento del ARNm y, en particular, el empalme alternativo, es crucial para la reprogramación del genoma durante la diferenciación celular. Sin embargo, los componentes de empalme relevantes para la adipogénesis y los eventos celulares regulados por este empalme alternativo durante la diferenciación de adipocitos apenas se han explorado. Así mismo, aún no se ha establecido si el empalme alternativo se modifica en la obesidad humana. Otro mecanismo crucial que preserva la función de las células precursoras se relaciona con la homeostasis de las proteínas (proteostasis), que mantiene la capacidad de las células de expandirse para mantener el crecimiento y la regeneración de los tejidos. Varias líneas de evidencia apoyan un papel importante para el sistema de control de calidad proteico del retículo endoplásmico (ER) en la regulación de la adipogénesis. De hecho, la respuesta a proteínas mal plegadas (UPR) se perturba en el tejido adiposo obeso, y se ha propuesto que contribuye a la patología de la obesidad. Por el contrario, todavía se desconoce si

el otro componente del sistema de control de proteínas, la degradación de proteínas asociada a ER (ERAD), que es crucial para proteger las células contra la acumulación de proteínas mal plegadas/desplegadas y la proteotoxicidad, está alterado en el tejido adiposo obeso.

Aquí, con el fin de identificar vías moleculares alteradas que pueden contribuir a la enfermedad metabólica en obesidad, realizamos un estudio proteómico de iTRAQ-LC-MS/MS para el análisis de preadipocitos subcutáneos (SC) y omentales (OM) de individuos obesos con normoglucemia (NG) y T2D. Se observó una disminución de múltiples componentes de la maquinaria de empalme en preadipocitos SC de individuos obesos con IR o T2D, en comparación con los obesos NG. Esto, junto con la observación de que la adipogénesis puede modularse regulando los niveles de expresión de un componente clave del espliceosoma, *PRPF8*/PRP8, respalda el papel de este proceso en el desarrollo de complicaciones metabólicas asociadas a la obesidad. Además, nuestros estudios muestran que no solo el sistema UPR está alterado en preadipocitos humanos SC y OM de sujetos obesos con IR/T2D, sino que también existe una hiperactivación del sistema ERAD. Esta condición, cuando se imita *in vitro*, previene la adipogénesis. Nuestros resultados proporcionan novedosas explicaciones mecanicistas para la capacidad adipogénica deteriorada observada en los obesos IR/T2D que se relaciona tanto con la alteración del procesamiento de ARNm como con la de la proteostasis del ER.

2. Estudio 2: Caracterización de miRNAs como marcadores de tejido adiposo disfuncional en la diabetes tipo 2 (T2D)

Cada vez se acepta más que, además de las adipoquinas, el tejido adiposo es una importante fuente fisiológica de microRNAs (miRNAs) circulantes. Los miRNAs, una clase de pequeños ARN no codificantes que regulan la expresión génica post-transcripcionalmente, han surgido como moléculas clave para la función celular. Los niveles de miRNAs anómalos y las alteraciones en su maquinaria de biogénesis se han relacionado con varias enfermedades metabólicas, incluida la obesidad, así como la T2D y la dislipidemia. Los miRNAs también se secretan activamente a la circulación y se ha propuesto que actúen como mensajeros de la comunicación intercelular. Esta característica ha señalado a los miRNAs circulantes como posibles biomarcadores de enfermedades, y los niveles circulantes alterados de numerosos miRNAs se han asociado con trastornos metabólicos. En este escenario, para diseñar estrategias

terapéuticas preventivas específicas, es fundamental identificar los mecanismos tempranos que preceden al inicio de la enfermedad.

Recientemente, en el estudio CORonary Diet Intervention with Olive oil and cardiovascular PREVention (CORDIOPREV, ClinicalTrial.gov ID: NTC00924937), se evaluó el valor predictivo de varios miRNAs para el diagnóstico de incidencia de T2D, un estudio prospectivo realizado en 1,002 pacientes con enfermedad coronaria y alto riesgo cardiovascular. Estos estudios demostraron que, cuando se combina con HbA1c, un grupo de nueve miRNAs (*miR-9*, *miR-28-3p*, *miR-29a*, *miR-30a-5p*, *miR-103*, *miR-126*, *miR-150*, *miR-223-3p*, y *miR-375*), proporcionaron un valor predictivo más alto en el diagnóstico de T2D que los parámetros clínicos. También se investigó la relación entre los niveles basales de estos miRNAs con marcadores de la función de las células beta y la IR sistémica y periférica. Sin embargo, su posible asociación con la desregulación del tejido adiposo no se analizó. Esto es de interés ya que se ha propuesto que la disfunción del tejido adiposo es un factor importante que contribuye al desarrollo de T2D, y el perfil de expresión de miRNAs del tejido adiposo está alterado en obesidad y T2D. En esta línea, varios estudios transversales en humanos han demostrado que el patrón de expresión de específicos miRNAs circulantes, relacionados con obesidad, refleja los perfiles de expresión de estos miRNAs en el tejido adiposo, lo que respalda el papel de los miRNAs circulantes como biomarcadores del tejido adiposo. Sin embargo, la relación entre los miRNAs circulantes y el estado funcional del tejido adiposo no se comprende completamente, lo cual podría ser útil para identificar las complicaciones metabólicas relacionadas con el tejido adiposo.

En este escenario, nuestro objetivo fue analizar la relación entre los miRNAs predictivos para el inicio de T2D, previamente establecidos en la cohorte CORDIOPREV (Jiménez-Lucena et al., 2018), y la pérdida de sensibilidad a insulina del tejido adiposo. Una vez establecido que el *miR-223-3p* circulante estaba desregulado con relación a la función del tejido adiposo, realizamos un análisis funcional para dilucidar tanto el potencial de los preadipocitos y los adipocitos como células secretoras de *miR-223-3p*, como las consecuencias de la desregulación de este miRNA sobre la biología de los adipocitos. Así, nuestros resultados indican que la secreción de *miR-223-3p* por preadipocitos y adipocitos es inhibida en condiciones inflamatorias, y que su acumulación patológica provoca alteraciones tanto en el metabolismo glucídico como lipídico de estas células. Estas observaciones podrían dar respuesta a los bajos niveles de este miRNA encontrados en aquellos pacientes que van a desarrollar T2D, así como explicar su potencial predictor de la disfunción adiposa relacionada con el desarrollo de esta enfermedad.

También hemos demostrado que los cambios que ocurren en el medio circulante después de la pérdida de peso inducida por BS modulan la expresión de *miR-223-3p* en adipocitos. La relevancia de estas observaciones fue apoyada además por nuestros estudios funcionales en adipocitos expuestos a suero pre- y post-BS, donde el suero post-BS mejoró la captación de glucosa estimulada por insulina en adipocitos, en comparación con aquellos expuestos a sueros pre-BS. Estos hallazgos refuerzan aún más la idea de que los mediadores inflamatorios presentes en el suero, o localmente en el tejido adiposo, pueden ser responsables de las alteraciones en la regulación de *miR-223-3p*.

En resumen, cuando se ven en conjunto, nuestros estudios indican que el empalme deficiente y la alteración de la proteostasis del ER son componentes de la huella molecular patogénica de los preadipocitos que podrían ayudar a prevenir y/o mejorar la disfunción del tejido adiposo en obesidad y sus trastornos metabólicos relacionados. Del mismo modo, nuestros datos respaldan la noción de que *miR-223-3p* puede tener un papel como potencial predictor de la disfunción adiposa relacionada con el desarrollo de T2D, revelando así una nueva diana molecular que puede ser útil para diseñar nuevas estrategias terapéuticas para prevenir la T2D.

INTRODUCTION

1. The adipose tissue

The adipose tissue is increasingly recognized as a critical regulator of systemic metabolism. As a caloric reservoir, this organ is no longer regarded as a passive lipid storage site, but as one of the largest and most dynamic organs in our body, which play pivotal roles in the regulation of energy balance (Luo and Liu, 2016). The adipose tissue stores excess energy in the form of triglycerides (TAGs) during periods of positive energy balance (i.e., lipogenesis), and releases fatty acids (FAs) in periods of nutrient deficiency (i.e., lipolysis), in a tightly regulated manner for usage as fuel by other organs (Kajimura, 2017). Likewise, it is now accepted that the adipose tissue constitutes a primary site for glucose uptake, which is required as a substrate for glycerol synthesis, and formation and accumulation of TAGs in the adipose tissue (Eckel, 2018).

Moreover, great importance has been attributed to the endocrine action of adipose tissue, which may represent the largest endocrine tissue of humans (Coelho et al., 2013). Adipose tissue secretes more than 600 peptide signalling factors termed adipokines (M.-W. Lee et al., 2019), which act in a paracrine, autocrine, and endocrine fashion, communicating this tissue with other organs such as the brain, pancreatic β-cells, the liver, skeletal muscle and the cardiovascular system (Zhu and Scherer, 2018). Adipokines are involved in numerous biological functions, including from food intake, energy homeostasis, and immunity, to cardiovascular function (Parrettini et al., 2020). Besides releasing peptide/proteins such as leptin, adiponectin, resistin, tumor-necrosis factor α (TNFα), interleukin 6 (IL-6), chemokine C-C motif ligand 2 (CCL2), IL-10, and transforming growth factor-β (TGFβ) (Hui and Feng, 2018), the adipose tissue secretome also includes several bioactive lipids (lipokines), and RNA molecules (Scheja and Heeren, 2019).

1.1. Distribution of the adipose tissue

Two main adipose tissue types have been commonly described: white adipose tissue (WAT), which is the main site for energy storage, and brown adipose tissue (BAT), which is dedicated to thermogenesis and energy expenditure (Rosell et al., 2014). BAT dissipates energy through the production of heat by virtue of the expression of the mitochondrial protein, uncoupling protein 1 (UCP1), which disrupts ATP synthesis (Lynes and Tseng, 2018). BAT is significantly smaller than WAT and, in humans, it is located particularly in the cervical-supraclavicular region, yet in adults, it is only recognizable under certain stimuli such as cold exposure (Saito et al., 2016).

Adipose cells (i.e., adipocytes) in WAT are characterized by a single large lipid droplet (LD), whereas the BAT adipocytes contain numerous small LDs and a large number of

mitochondria (Smorlesi et al., 2012). In addition to classical BAT adipocytes, a second type of adipose cells with thermogenic capacity, that are found inter-scattered within WAT, has been identified and termed beige adipocytes (also known as brite or inducible brown adipocytes) (Mueller, 2014). Beige adipocytes are morphologically and functionally very similar to BAT adipocytes, and they transdifferentiate from WAT adipocytes (a process termed “beiging” or “browning”), in response to various stimuli including sustained cold exposure and catecholamines (Gaggini et al., 2017).

WAT is compartmentalized into discrete anatomical depots (Hepler and Gupta, 2017) (**Figure 1**). The most commonly defined and studied are the subcutaneous and the visceral adipose tissues (SAT and VAT, respectively) (Lee et al., 2013). SAT is located under the skin in upper (deep and superficial abdomen), and lower (gluteofemoral) body regions. VAT is associated with digestive organs and includes the omental (OM, hangs off the stomach), the mesenteric (associated with the intestine), and epiploic (along with the colon) depots (Kwok et al., 2016).

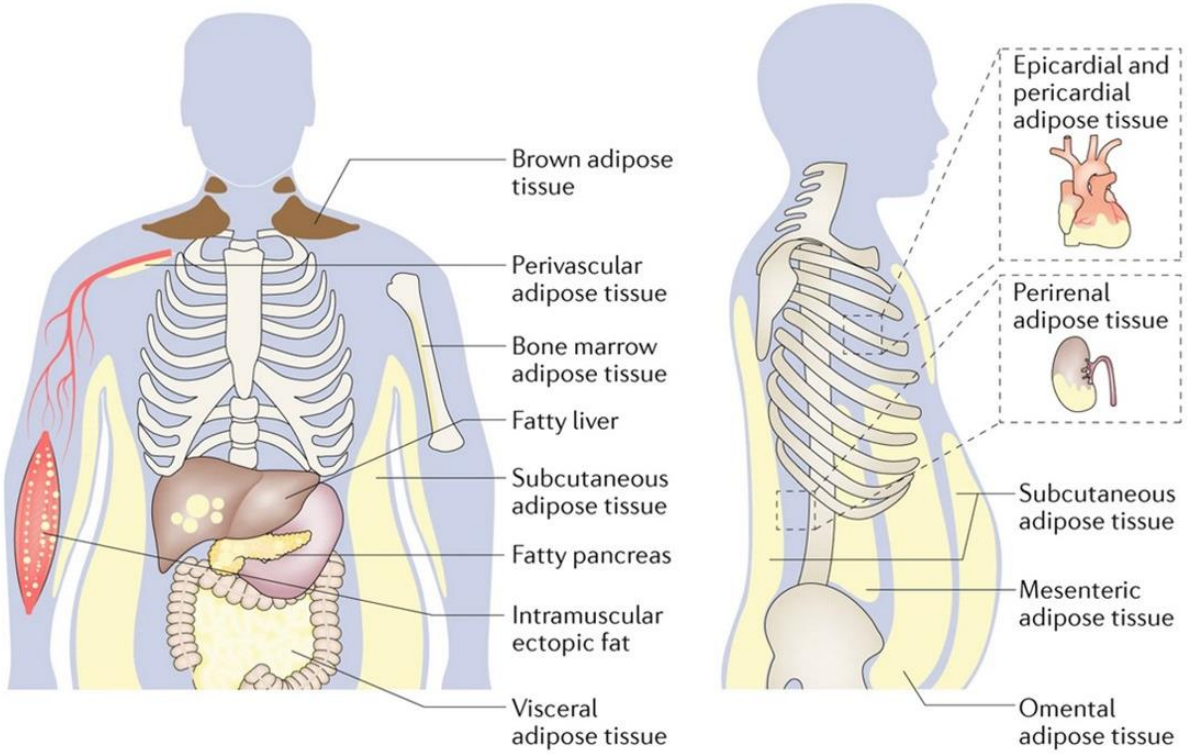

Figure 1. Distribution of BAT and WAT depots in adults (Quail and Dannenberg, 2019).

Regional adipose tissue depots have been considered as distinct mini-organs (Tchkonia et al., 2001). As a matter of fact, SAT and VAT arises from distinct adipocyte precursor cells (Sebo and Rodeheffer, 2019), and they have intrinsic differences in gene/protein expression repertoire (Schleinitz et al., 2020), lipid composition (Hou et al.,

2020), and metabolomic profile (Ose et al., 2020). Therefore, these cellular features provide differential physiological properties (Kwok et al., 2016).

In terms of metabolic characteristics, SAT is the most prominent depot in making up >80% of all adipose tissue (Reddy et al., 2019). Thus, SAT represents a physiological buffer for excess energy intake during times of limited energy expenditure, acting as a metabolic “sink” for excess lipid storage (Karastergiou and Fried, 2013). By contrast, VAT is highly metabolically active, and it is constantly releasing free FAs (FFA) into the circulation (Tchkonia et al., 2013). SAT and vat differ in the proliferation and differentiation capacities of their fat cell precursors, which is higher in SAT (Lafontan, 2014), as well as in their apoptosis rate, which is higher in VAT (Pellegrinelli et al., 2016). Consequently, VAT contains a greater number of large adipocytes in contrast to SAT, which contains smaller (Belligoli et al., 2019).

Adipocytes from VAT, in comparison with those from SAT, are more sensitive to catecholamine-induced lipolysis and less to insulin and a2-adrenergic receptor-dependent inhibition of lipolysis (Bódis and Roden, 2018). Moreover, uptake of non-esterified fatty acids (NEFAs) and lipid synthesis are shown to be higher in VAT compared to SAT (Bjørndal et al., 2011). In the case of glucose uptake, the basal uptake level and insulin-stimulated glucose transport are higher in VAT than in SAT adipocytes (Małodobra-Mazur et al., 2020). The expression levels of mRNA of the glucose transporter GLUT4 is higher in mature adipocytes of VAT than in SAT (Kojta et al., 2020). Similar differences were described for the expression of proteins involved in insulin signalling, such as insulin receptor (IR) and Akt (Cignarelli et al., 2019).

With regards to the angiogenic capacity of the different adipose tissue depots, studies have found SAT to be more vascular, rich in blood supply, more heavily innervated, and seems to express a greater number of angiogenic molecules than VAT (Chait and den Hartigh, 2020).

Finally, there are also differences between VAT and SAT regarding the capacity to synthesize and release adipokines (Dodson et al., 2014). VAT is more infiltrated with inflammatory cells (such as macrophages) (Liu and Nikolajczyk, 2019), and therefore it is more capable of generating pro-inflammatory cytokines such as TNFα, C-reactive protein (CRP), IL-6, monocyte chemoattractant rpotein-1 (MCP-1), and plasminogen activator inhibitor-1 (PAI-1) (Mittal et al., 2018). However, SAT is the major source of leptin and adiponectin (Konigorski et al., 2019).

1.2. Cellular constituents of the adipose tissue

The adipose tissue is a complex tissue containing a host of up to 21 different interacting cell types embedded in an extracellular matrix (ECM) (Lenz et al., 2020) (**Figure 2**). While mature adipocytes are the most characteristic cells and account for the majority of fat pad volume, other cell types, collectively referred to as the stromal vascular fraction (SVF), predominate by overall number (Lago et al., 2018). The SVF cells include mesenchymal stem cells, fibroblasts, preadipocytes, endothelial cells, blood cells (macrophages, neutrophils, lymphocytes, and mast cells), and neural cells (Ramakrishnan and Boyd, 2018). Among them, the preadipocytes are responsible for ~ 10% of the adipocyte pool which allows the adipose tissue to maintain its functional plasticity (Ghaben and Scherer, 2019).

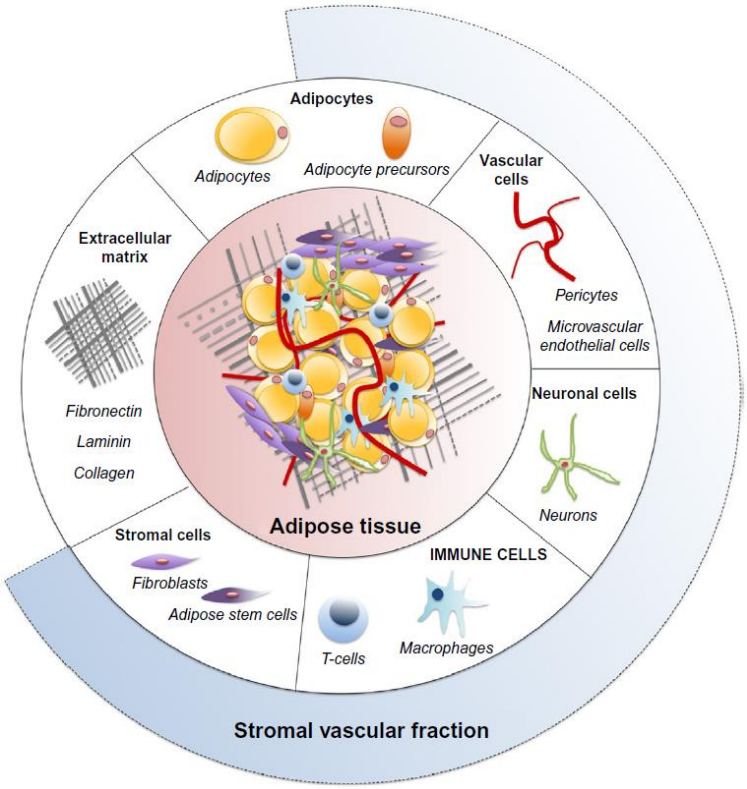

Figure 2. Cellular components of adipose tissue (Lago et al., 2018).

2. Preadipocytes

Multipotent stem cells derived from adipose tissue, or adipose tissue-derived stem cells (ADSCs), have osteogenic, adipogenic, and chondrogenic potential (Moreno-Navarrete and Fernández-Real, 2017). Currently, researchers have adapted the term “preadipocyte” to define the progenitor cell, isolated from the SVF, with the ability to

constantly proliferate and differentiate only into mature adipocytes through the process of adipogenesis (Zuk, 2013).

Although preadipocytes have been characterized by morphology, differentiation capacity, growth kinetics, (epi)genetic analyses, protein secretion, DNA methylation signature, and/or electrophysiological properties (Ejarque et al., 2019), they are most often characterized through their surface markers (Tchkonia et al., 2013). Preadipocyte factor 1 (Pref-1) is a distinguishing early preadipocyte surface marker and maybe the most preferable preadipocyte marker (Hudak and Sul, 2013). Early studies have reported the existence of different preadipocyte subtypes in adipose tissue, whose distribution differs between depots (Ferrero et al., 2020). In particular, single-cell RNA sequencing has recently been used to characterize adipose stem cell populations and has provided new insights into subpopulations of these cells (Vijay et al., 2020).

2.1. Adipogenesis

Adipogenesis is the process whereby fibroblast-like progenitor cells restrict their fate to the adipogenic lineage, accumulate nutrients and become TAG filled mature adipocytes (Ghaben and Scherer, 2019). Adipogenesis is a two-step developmental process (**Figure 3**). In the first step (early adipocyte commitment or adipocyte determination step), a fibroblast-like cell, such as a mesenchymal precursor, restricts itself to the adipocyte lineage without any morphological changes, forming a preadipocyte. This commitment is then followed by a differentiation step (adipocyte differentiation), during which specified preadipocytes undergo growth arrest, accumulate lipids, and form functional mature adipocytes (Ghaben and Scherer, 2019).

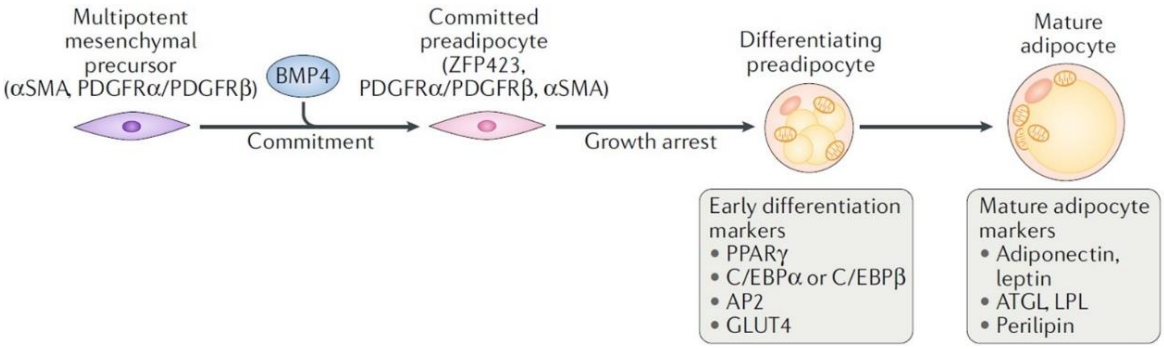

Figure 3. Overview of molecular mechanisms of adipogenesis (Ghaben and Scherer, 2019).

Early studies have identified that the bone morphogenetic proteins (BMPs), BMP2 and BMP4, are sufficient to drive adipocyte commitment. BMPs promote terminal

differentiation by stimulating transcription of peroxisome proliferator-activated receptor γ (PPARγ), the master regulator of adipogenesis (Denton et al., 2019). By contrast, GATA binding proteins, GATA2 and GATA3, inhibit adipogenesis through the prevention of PPARγ transcription (Feng et al., 2016). Other studies have revealed that some zinc-finger proteins (ZFP), such as ZFP423 and ZFP467, promote adipogenesis of the fibroblast-like progenitors by enhancing the expression of another master regulator of adipogenic gene transcription, co-activator CCAAT enhancer-binding protein α (C/EBPα) (Hammarstedt et al., 2018). Finally, early growth response proteins, EGR1 and EGR2, inhibit and stimulate adipogenesis, respectively, by modulating the activation of cAMP-response element-binding protein (CREB), which regulates transcription of C/EBPβ (Bléher et al., 2020).

Thus, adipocyte differentiation is controlled by a network of interacting transcription factors operating to coordinate the expression of many hundreds of proteins responsible for establishing the mature fat cell phenotype (Yi et al., 2020a) (**Figure 4**). The current model suggests that the adipogenic induction rapidly induces expression of C/EBPβ and C/EBPδ (Lowe et al., 2011). Among their targets are the promoters of the genes encoding the key adipogenic transcription factors, C/EBPα and PPARγ, and the regulator of lipogenic genes, sterol regulatory element-binding transcription factor 1 (SREBP1) (Ayala-Sumuano et al., 2011). In addition, PPARγ and C/EBPα induce the expression of genes related to insulin sensitivity, lipogenesis, and lipolysis, including GLUT4, fatty acid-binding protein 4 (FABP4), lipoprotein lipase (LPL), sn-1-acylglycerol-3-phosphate acyltransferase 2 (AGPAT2), perilipin 1 (PLIN1), and the adipokines, adiponectin, and leptin (Moseti et al., 2016).

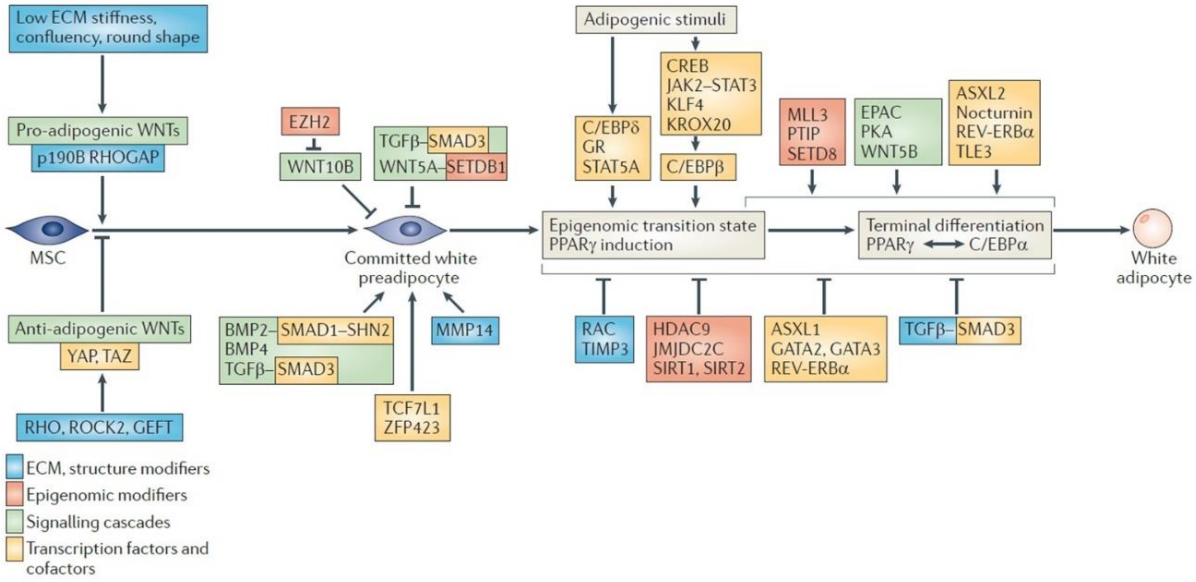

Figure 4. Integration of pro- and anti-adipogenic factors in the regulation of white adipogenesis (Cristancho and Lazar, 2011).

SC preadipocytes are capable of more extensive replication (Baglioni et al., 2012), and appear to be more responsive to adipogenic stimulation than OM preadipocytes (Lessard and Tchernof, 2012). In this line, adipose tissue expression levels of transcription factors and many mature adipocyte-related transcripts such as C/EBPα, PPARγ2, SREBP1, LPL, FABP4, diacylglycerol (DAG) acyltransferase 1 and 2 (DGAT1 and DGAT2) and PLIN1 are higher in SC than OM adipose tissue (Sarjeant and Stephens, 2012).

2.2. Lipid droplets (LDs)

Lipid droplets (LDs) are evolutionarily conserved cellular organelles consisting of a core of neutral lipids encircled by a phospholipid monolayer that is studded with integral and peripheral proteins (Olzmann and Carvalho, 2019). Apart from store neutral lipids, most commonly TAGs and sterol esters (SEs) (such as cholesterol), which prevent lipotoxicity, LDs also regulate a number of cellular processes (Brasaemle and Wolins, 2012).

LDs originate from specialized endoplasmic reticulum (ER) subdomains, that harbours the majority of enzymes required for neutral lipid synthesis (Nettebrock and Bohnert, 2020). DGAT1 and DGAT2 catalyse the synthesis of TAG from DAG (Løvsletten et al., 2020), and acyl CoA:cholesterol O-acyltransferase 1 and 2 (ACAT1 and ACAT2) catalyse the synthesis of SE (Rogers et al., 2015). Conceptually, there are a few key steps from the synthesis of TAG/SE to the appearance of mature LDs (Henne et al., 2020), discussed below (**Figure 5**).

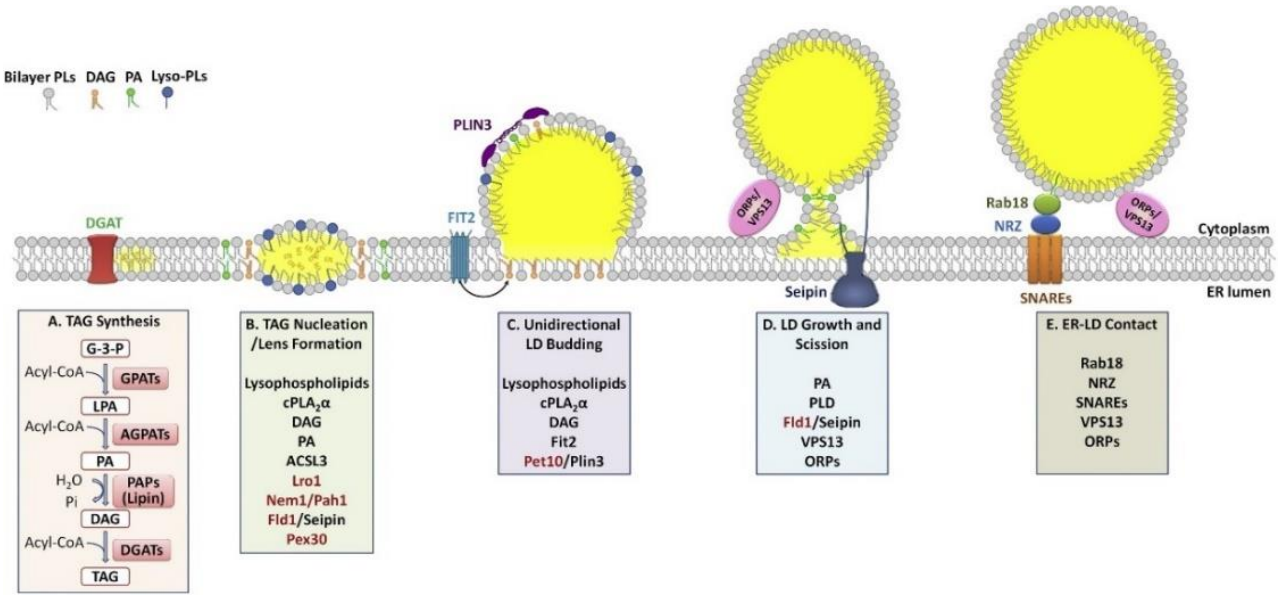

Figure 5. Proposed steps in the biogenesis of LDs and the involvement of candidate proteins and lipids at each step (Gao et al., 2019).

At low concentrations, TAG/SE molecules are dispersed between the two leaflets of the ER bilayer. As their concentration increases, neutral lipids eventually coalesce and undergo phase separation, leading to lens formation (pre-LDs). Several candidate proteins acting at the initial steps of LD formation have been identified (Dhiman et al., 2020). The most studied of these proteins is seipin/BSCL2. Seipin was initially isolated as a human disease gene since loss-of-function mutations in *seipin* cause the most severe form of human congenital generalized lipodystrophy (Magré et al., 2001). A structural role of seipin at the LD-ER interface for the biogenesis and/or maintenance of LDs has been proposed (Salo et al., 2016). In the absence of seipin, LD formation is delayed (Wang et al., 2016), resulting in LDs with aberrant morphologies and properties (Salo et al., 2016). Thus, seipin is essential for adipogenesis (W. Chen et al., 2012), and the maintenance of healthy adipose tissue (Zhou et al., 2016). After TAG nucleation and initial lens formation, LDs bud into the cytoplasmic side of the ER (Nguyen and Olzmann, 2019) with the assistance of fat storage-inducing transmembrane (FIT) proteins (Choudhary et al., 2015), and PLIN1 (Q. Gao et al., 2017). Once separated from the ER, LDs will continue to grow into the cytoplasm, which occurs through LD–LD fusion, through the transfer of TAGs to LDs via ER membrane bridges, or through TAG synthesis directly on the LD surface (Thiam and Beller, 2017).

LDs fusion is mediated by the cell death-inducing DFFA-like effector (CIDE) family of proteins: CIDEA, CIDEB, and CIDEC/FSP27 (Chen et al., 2020) (**Figure 6**). CIDE proteins are enriched at LD-LD contact sites, physically tethering the adjacent organelles (Gong et al., 2011). The CIDE oligomers are thought to assemble into a pore or channel that mediates the transfer of TAG between LDs (Lo et al., 2013).

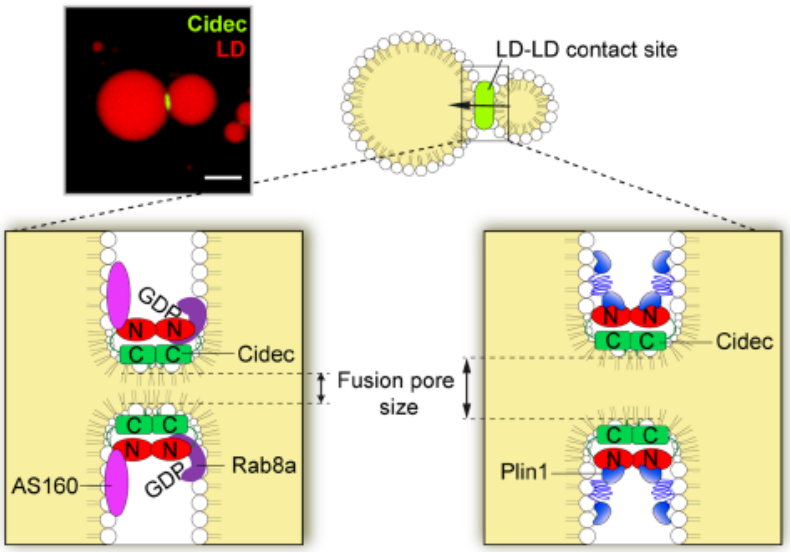

Figure 6. Schematic diagram showing the mechanism of CIDE-mediated LD fusion and growth (Chen et al., 2020).

3. Adipocytes

Adipocytes vary dramatically in size, ranging from <20 to 300 μm in diameter, with this variation mainly depending on cellular TAG content (Stenkula and Erlanson-Albertsson, 2018). Adipocytes provide a safe and specific compartment for lipid accumulation (Gupta, 2014), and their classical function is to serve as a strictly regulated energy bank. Hence, LDs are specialized structures expressing the necessary lipid machinery components for the production and release of their lipid cargo (Church et al., 2012). During times of energy excess, FFAs enter adipocytes following the hydrolysis of TAGs, which are esterified for storage in adipocyte LDs via lipogenesis (Karpe et al., 2011). Adipocytes can also synthesize lipid from carbohydrates through *de novo* lipogenesis (DNL) (Song et al., 2018). When energy is required, TAGs undergo lipolysis and they are hydrolysed from glycerol to release NEFA into the circulation (Saponaro et al., 2015).

3.1 Regulation of lipid metabolism

Feeding stimulates the lipogenic pathway, while fasting induces the activation of the lipolytic pathway in adipocytes (Festuccia et al., 2011) (**Figure 7**). The balance between lipogenesis and lipolysis is under a complex regulatory system, where insulin and catecholamines are the main endocrine regulators (Luo and Liu, 2016).

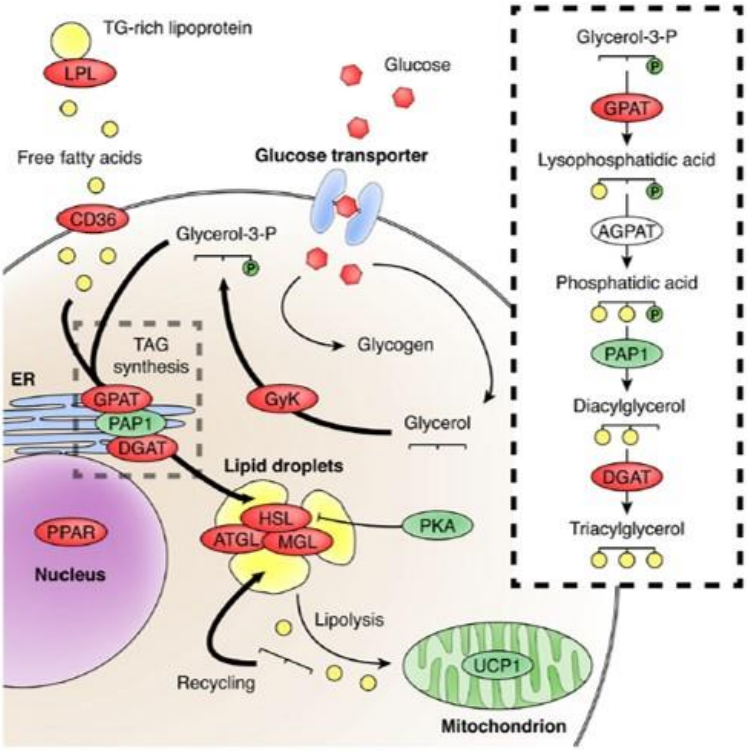

Figure 7. Modulation of lipid metabolism in adipocytes (Festuccia et al., 2011).

3.1.1. Lipogenesis

Post-prandial increase in insulin exerts a critical control on anabolic responses in adipose tissue by stimulating glucose and FFA uptake and stimulating *de novo* FA synthesis in adipocytes (Cisa-Wieczorek and Hernández-Alvarez, 2020). On the other hand, insulin is the most potent antilipolytic hormone (Cignarelli et al., 2019). NEFAs released by LPL from circulating TAGs enter adipocytes through passive diffusion or protein-facilitated transfer, i.e., FA transporters such as CD36 and fatty acid transport protein-1 (FATP1). Within the adipocytes, FAs are activated into acyl-CoA and three acyl-CoA are esterified with glycerol to form TAGs stored into the LD (Cisa-Wieczorek and Hernández-Alvarez, 2020).

In *de novo* lipogenesis (DNL), glucose undergoes glycolysis and tricarboxylic acid (TCA) cycle to produce citrate in the mitochondria, which is transported to the cytosol and then releases acetyl-CoA by ATP-citrate lyase (ACLY). The resulting acetyl-CoA is converted by acetyl-CoA carboxylase (ACC) to malonyl-CoA, which is, in turn, converted into palmitate by fatty acid synthase (FASN) (Song et al., 2018). Finally, palmitate undergoes elongation and desaturation reactions to generate the complex FAs (Solinas et al., 2015).

3.1.2. Lipolysis

Lipolysis is under the primary control of catecholamines (Mullins et al., 2014). It consists of lipase-based breakdown of tri-, di-, and monoacylglycerides (MAGs) into individual FFAs. This process requires three consecutive steps that involve three different enzymes: adipose triglyceride lipase (ATGL) that catalyses the initial step of lipolysis, converting TAGs to DAGs; hormone sensitive lipase (HSL) is mainly responsible for the hydrolysis of DAGs to MAGs; and MG lipase (MGL) that hydrolyses MAGs (Lass et al., 2011).

3.2. Regulation of glucose metabolism by insulin

Despite daily feeding, plasma glucose levels are normally maintained within a narrow range owing, in part, to insulin (Czech, 2017). This hormone promotes glucose uptake into adipose tissue (Bogan, 2012). Glucose uptake is the rate-limiting step in glucose utilization and/or storage and as such has a key role in the maintenance of glucose homeostasis (Krycer et al., 2017). This process is important for controlling whole-body

energy homeostasis, as adipocytes serve as a cellular 'rheostat' that senses the energy status (Skorobogatko et al., 2018).

As depicted in **Figure 8**, upon insulin binding and autophosphorylation of its receptor, there is rapid phosphorylation of insulin receptor substrate (IRS) 1 and IRS2, which lead to phosphatidylinositol 3-kinase (PI3K) activation (Klip et al., 2014). PI3K phosphorylates phosphatidylinositol lipids in the plasma membrane and yields phosphatidyl-inositol-3,4,5-trisphosphate (PIP3), which recruits the 3-phosphoinositide-dependent protein kinase 1 (PDK1) and AKT to the plasma membrane (Świderska, 2020). AKT controls several biological functions such as cell survival, glycogen metabolism, and glucose uptake (Petersen and Shulman, 2018). On the other hand, activation of the extracellular signal-regulated kinase (ERK) pathway is implicated in the control of cell growth of preadipocytes and differentiation (Ozaki et al., 2016).

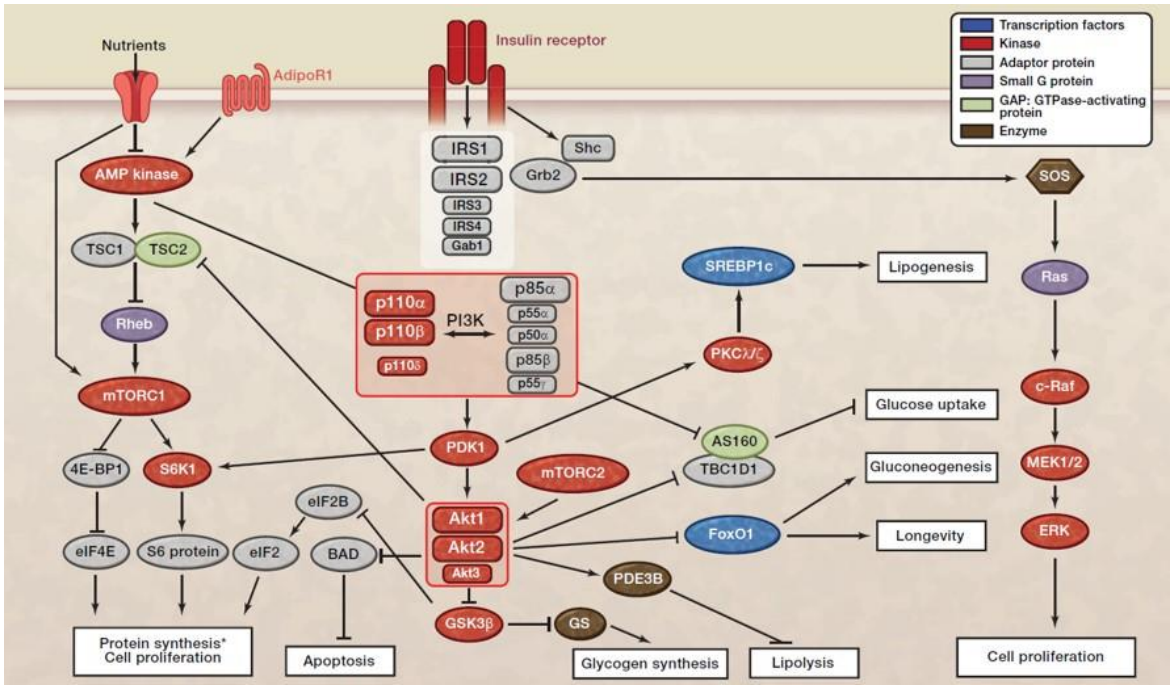

Figure 8. Schematic illustration of insulin signalling pathways (Kadowaki et al., 2012).

3.2.1. GLUT4 traffic

GLUT4 is a high-affinity glucose transporter and the most abundant glucose transporter in adipocytes (Klip et al., 2019). In the basal state (in the absence of any stimuli), GLUT4 locates to cytosol-dispersed vesicles [specialized GLUT4 storage vesicles (GSVs)] in the cell perinuclear area, with only a small proportion at the plasma membrane (Brewer et al., 2016). The exclusion of GLUT4 from the cell surface depends on efficient sorting and sequestration into GSVs that do not readily cycle to the plasma

membrane (Olson, 2012). In addition, in the absence of insulin, hypoglycaemia is avoided by rapid endocytosis and slow exocytosis of GLUT4.

In response to insulin, the majority of the intracellular GLUT4 reaches within minutes the plasma membrane, while endocytosis decreases (Stöckli et al., 2011), which results in a 10- to 40-fold increase in glucose uptake, a process generically called ‘GLUT4 translocation’ (Habtemichael et al., 2011) (**Figure 9**).

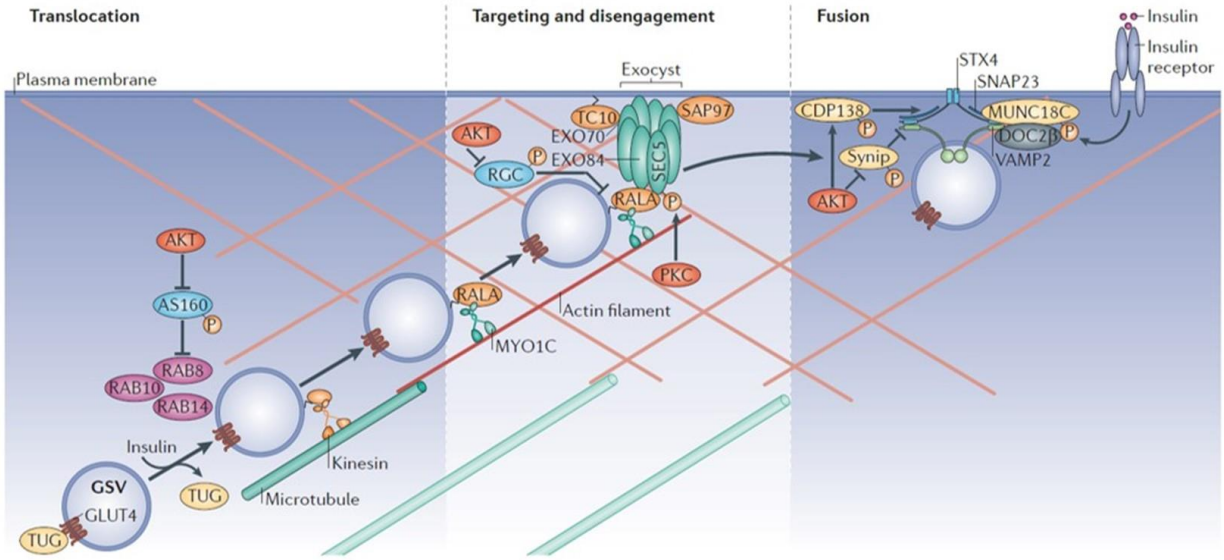

Figure 9. GLUT4 exocytosis (Leto and Saltiel, 2012)

A crucial component of the GLUT4 targeting machinery is the exocyst, an octameric complex that assembles at sites of exocytosis and tethers exocytic vesicles to the plasma membrane (Fujimoto et al., 2019). The exocyst is thought to mediate the initial flexible contact between exocytic vesicles and the plasma membrane (Chen et al., 2011). The exocyst is recognized by GSVs via the small GTPase Ras-related protein Ral-A (RALA), which is present on GLUT4-containing vesicles (Wu and Guo, 2015). Finally, following GSV tethering, SNARE proteins on both the GSV and the plasma membrane form tight complexes that provide the driving to membrane fusion (Bryant and Gould, 2011).

Once at the plasma membrane, GLUT4 may be endocytosed through at least two separate pathways: clathrin-mediated endocytosis and cholesterol-dependent endocytosis (Lizunov et al., 2013) (**Figure 10**). GLUT4 trafficking through the endosomal system and the formation of GSVs require the actions of multiple small GTPases, ADP ribosylation factor 6 (ARF6), and RALA (Tunduguru and Thurmond, 2017).

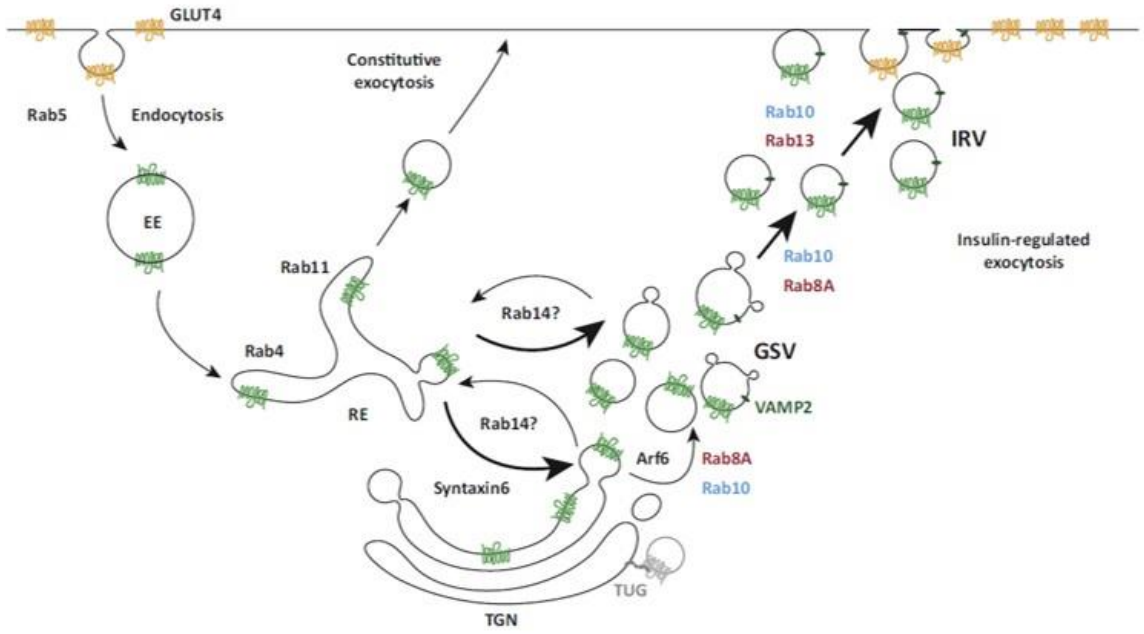

Figure 10. GLUT4 cycling to and from the plasma membrane. (Jaldin-Fincati et al., 2017)

4. Adipose tissue and obesity

According to the World Health Organization (WHO), obesity is a heterogeneous disease defined as an excessive fat accumulation that presents a risk to health. Over the past ~50 years, the prevalence of obesity has increased worldwide to pandemic proportions (Yanovski, 2018), and, along with overweight, affects over a third of the world's population (Ng et al., 2014) (**Figure 11**). If secular trends continue, by 2030 an estimated 38% of the world's adult population will be overweight and another 20% will be obese (Hruby and Hu, 2015).

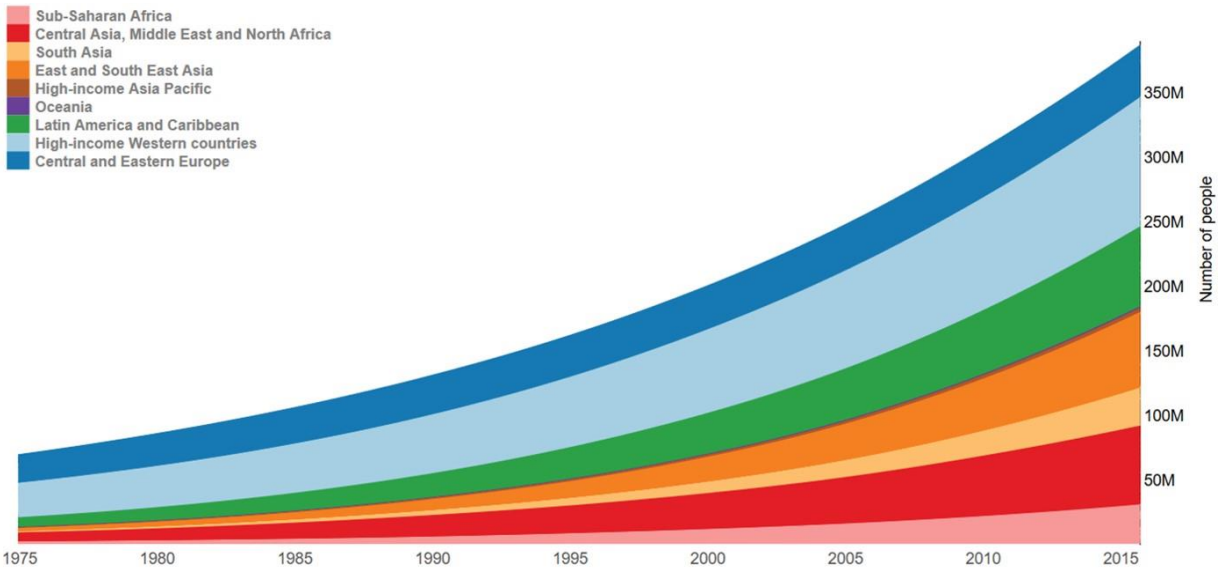

Figure 11. Stacked plot representing the worldwide evolution of obesity (www.ncdrisc.org).

This situation has become a worldwide health concern because obesity affects nearly all physiological functions of the body (Chooi et al., 2019), affecting several hallmarks of health (López-Otín and Kroemer, 2020). Obesity substantially increases the risk for metabolic diseases [insulin resistance (IR), type 2 diabetes mellitus (T2D) and fatty liver disease (NAFLD)] (Singh et al., 2013), cardiovascular diseases (hypertension, myocardial infarction, and stroke) (Singh et al., 2013), musculoskeletal disease (osteoarthritis) (Palazzo et al., 2016), some types of cancer (breast, ovarian, prostate, liver, kidney, and colon) (Stone et al., 2018), and infertility (Mintziori et al., 2020). Overall, obesity is associated with a decreased life expectancy of an estimated 5–20 years lost and it is responsible for 10-13% of premature deaths (Leung et al., 2017).

Intriguingly, expansion of adipose tissue (total fat mass) does not necessarily translate into increased metabolic risk (Collins et al., 2018). In contrast, body fat distribution is a strong metabolic risk factor (Nimptsch et al., 2019). Thus, the accumulation of adipose tissue in the upper body (VAT) is associated with the development of obesity-related comorbidities and even all-cause mortality (Koster et al., 2015), whereas the accumulation of fat in the lower body (SAT) is associated with a protective lipid and glucose profile as well as a decrease in cardiovascular and metabolic disease prevalence (McLaughlin et al., 2016).

Moreover, adipose tissue remodelling and dysfunction may be also a key factor in the pathophysiology of obesity-related metabolic disease (Longo et al., 2019). In obesity, “healthy” WAT expansion is achieved by recruiting and differentiating preadipocytes (hyperplasia) rather than by hypertrophy of mature adipocytes (Pellegrinelli et al., 2016). Specifically, alterations in SAT adipogenesis have been associated with the metabolic complications of obesity (Lessard et al., 2014). When the storage capacity of SAT, the largest adipose tissue depot, is exceeded, further caloric overload leads to lipid spillover into the circulation (Goossens and Blaak, 2015). This induces ectopic fat deposition and dysfunction in other tissues (liver, skeletal muscle, and heart, among others), through an event commonly defined as “lipotoxicity”, as well as in VAT (Montgomery et al., 2019). It has been largely demonstrated that excessive lipid accumulation in ectopic tissues leads to IR (Reilly and Saltiel, 2017), probably being the major contributor to subsequent associated complications in a high percentage of obese patients (Czech, 2020).

WAT undergoes various cellular and structural remodelling processes to accommodate the excess energy during the course of obesity: i) adipose tissue expansion (Wang et al., 2013), ii) recruitment of inflammatory cells (Corrêa et al., 2019), and iii) remodelling of the vasculature and the ECM to allow adequate tissue expansion, oxygenation, and mobilisation of nutrients (Åkra et al., 2020). However, when obesity is

sustained, these adaptive homeostatic mechanisms fail, leading to WAT dysfunction characterised by impaired secretion of adipokines, abnormal lipid storage and adipogenesis, exacerbated fibrosis deposition, and IR (Quail and Dannenberg, 2019) (**Figure 12**).

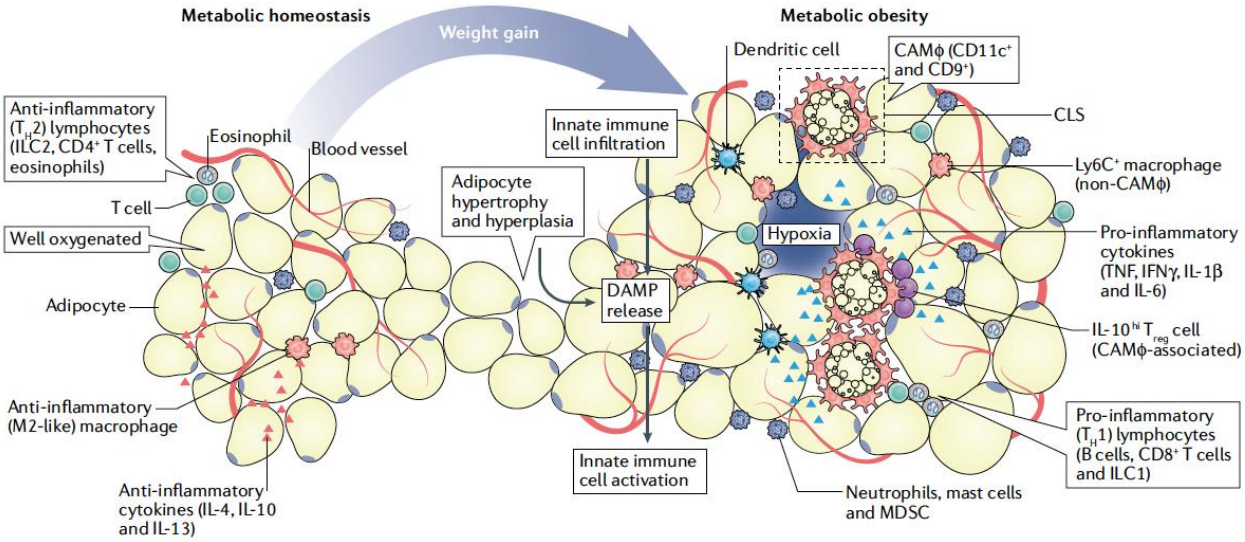

Figure 12. Remodelling of the WAT in obesity (Quail and Dannenberg, 2019).

4.1. Pathological adipose tissue expansion in obesity

4.1.1. Impaired adipogenesis

A likely mechanism for the limited expandability of adipose tissue is reduced recruitment and differentiation of precursor cells (Vishvanath and Gupta, 2019). Consistent with this idea, a number of studies have shown that individuals with an inappropriate expansion of their adipocytes (hypertrophic adipocytes) are characterized by reduced recruitment and adipogenic differentiation of their SVF precursor cells (Hammarstedt et al., 2018), whereas high generation rates of adipogenesis are associate with adipose tissue hyperplasia (White and Ravussin, 2019). Most studies propose that preadipocytes become dysfunctional in response to obesity in terms of altered patterns of cell surface marker expression, decreased differentiation, proliferation, migration, and viability, and a pro-inflammatory transcriptome (Pachón-Peña et al., 2016). In particular, expression of adipogenic genes (i.e. *PPARG2*, *FABP4*, *ADIPOQ*, and *FASN*) and, therefore, adipogenic potential, are decreased in obesity and this is further exacerbated in IR and T2D (Belligoli et al., 2019). However, the specific molecular mechanisms and signalling factors involved in the loss of function of these cells in relation of obesity and

associated metabolic disturbances remains to be fully elucidated, which could be key to develop novel strategies to promote adipogenesis and, in turn, the metabolic health.

4.1.2. Adipocyte hypertrophy

Adipocyte hypertrophy (*vs.* hyperplasia) contributes to obesity-associated metabolic abnormalities (Longo et al., 2019). In obesity, the adipocyte size reaches a critical threshold before recruiting precursor cells to increase the adipocyte number (Cotillard et al., 2014). The adipocytes that reach the critical cell size become lipid-overloaded and IR, and adipose tissue hyperplasia, which is considered as a “recovery mechanism” to overnutrition, attempts to repair metabolic alterations (Blüher, 2016). Adipocyte hypertrophy induces several stress responses (i.e., oxidative stress, ER stress, autophagy, etc) (Blüher, 2013), which, together with mechanical stress arising from accumulation of ECM, i.e. fibrosis (Spencer et al., 2011), have been proposed to trigger an inflammatory response (Reilly and Saltiel, 2017). These processes are depicted in detail below.

4.2. Inflammatory response

Inflammation occurs as a consequence of obesity and numerous studies support that it may play a causal role in inducing IR (Alcalá et al., 2017). The adipose tissue of obese humans exhibits altered adipokine secretion toward a pro-inflammatory pattern (M.-W. Lee et al., 2019). Importantly, the levels of the pro-inflammatory cytokine, TNFα, are increased, which has been shown to induce IR, while the production of anti-inflammatory mediators, such as adiponectin, apelin, and IL-10 are reduced in obese states (Makki et al., 2013).

The inflammatory response, greater in VAT, is accompanied by a dramatic shift in the immune landscape due to the recruitment of immune cells (Catrysse and van Loo, 2018). This shift is most apparent in adipose tissue macrophages (ATMs) (Jia et al., 2020). These cells greatly expand in number (Orliaguet et al., 2020), but also, ATMs adopt a metabolic activation state or M1 phenotype, with the main purpose to clear dead adipocytes (Coats et al., 2017), at the expense of M2, anti-inflammatory macrophages (Li et al., 2020). According to the current hypothesis, this phenotypic switch of ATMs is believed to be crucial to promote the pro-inflammatory environment in obese adipose tissue, affecting insulin sensitivity in peripheral organs (Zatterale et al., 2020).

4.3. Oxidative stress

The association of adipose oxidative stress with the pathogenesis of metabolic disorders in obesity has been firmly established (Masschelin et al., 2020). Adipocytes help maintain the appropriate balance between energy storage and expenditure, which requires normal mitochondrial function, for the central roles of these organelles in ATP production, energy expenditure, and disposal of reactive oxygen species (ROS) (Heinonen et al., 2020). Excessive energy substrates during obesity leads to mitochondrial dysfunction with consequential effects on intracellular signalling pathways that contribute to the formation of IR adipocytes (Sergi et al., 2019). Preadipocytes from VAT exhibit excessive oxidative stress and higher ROS, compared to SC preadipocytes (Sriram et al., 2019). Since adipocyte differentiation involves changes in the abundance, morphology, and organization of mitochondria, increased oxidative stress disrupts adipogenesis and inhibits healthy adipose expansion (Fernando et al., 2020). In fact, several studies have demonstrated the requirement of limited ROS levels for adipogenesis, and only when their levels peak or if they become persistent in cells, ROS may also impede adipogenesis (Castro et al., 2016).

4.4. Endoplasmic Reticulum (ER) stress

ER is responsible for several homeostatic responses including protein, lipid and glucose metabolism, lipoprotein secretion, and calcium homeostasis (Liu et al., 2015). It is mainly recognized as a primary site for protein biosynthesis, post-translational modifications, folding, and maturation, and together with the Golgi apparatus, also for protein transportation and release (Malhotra and Kaufman, 2011). These complex cellular processes are governed by a highly regulated quality control system within the ER known as the “Unfolded Protein Response” (UPR) (Gardner et al., 2013), which is initiated in response to homeostatic de-arrangements, which trigger ER stress (Amen et al., 2019). Thus, ER stress is referred to as a condition where an accumulation of unfolded or misfolded proteins occurs in the ER lumen while the degradation machinery does not work properly (Mohan et al., 2019).

The role of severe ER stress in adipose tissue and metabolic disease outcomes such as T2D in obesity has already been established (Piperi et al., 2012). It has been demonstrated that adipocytes from obese individuals and from animal models of obesity exhibit increased mRNA and/or protein levels of several markers of ER stress, such as CHOP, irrespective of the fat depot origin (Díaz-Ruiz et al., 2015). The components of the ER stress response and UPR are described in detail below.

As for oxidative stress (Sriram et al., 2019), current studies support the notion that during adipogenesis, differentiating adipocytes exhibit signs of moderate ER stress (Lowe et al., 2011). These stress processes can be considered as adaptive responses to achieve the increasing demands of growing cells (Cao and Kaufman, 2014). Nevertheless, few studies have addressed whether obese preadipocytes display enhanced ER stress or whether this may have an influence on the development of IR/T2D in obese individuals.

Briefly, the abundant literature indicates that obesity significantly decreases mechanisms associated with proteome maintenance in the adipose tissue. In this direction, we have previously reported that proteasome dysfunction and proteotoxicity in adipocytes constitute major pathogenic mechanisms in the development of IR in obesity (Díaz-Ruiz et al., 2015). However, whether these processes are also altered in other cellular components of the adipose tissue, such as preadipocytes, or if they also include alterations in specific mechanisms involved in the ER proteostasis (i.e., UPR and ERAD) have not been assessed yet.

4.4.1. Unfolded Protein Response (UPR)

During UPR, perturbations in ER homeostasis are sensed and transduced to the cytoplasm and nucleus causing a compensatory response. Three branches of UPR have been described and defined by a class of transmembrane ER-resident signalling components or ER stress sensors: (1) the inositol-requiring transmembrane kinase/endoribonuclease 1 (IRE1); (2) the double-stranded RNA (PKR)–activated protein kinase-like eukaryotic initiation factor 2α kinase (PERK); and (3) the activating transcription factor 6 (ATF6) (Bravo et al., 2013). Each UPR sensor binds to the ER luminal chaperone binding immunoglobulin protein (BiP). When misfolded proteins accumulate in the ER, they bind to and sequester BiP, thereby activating the sensors (Vincenz et al., 2013) (**Figure 13**).

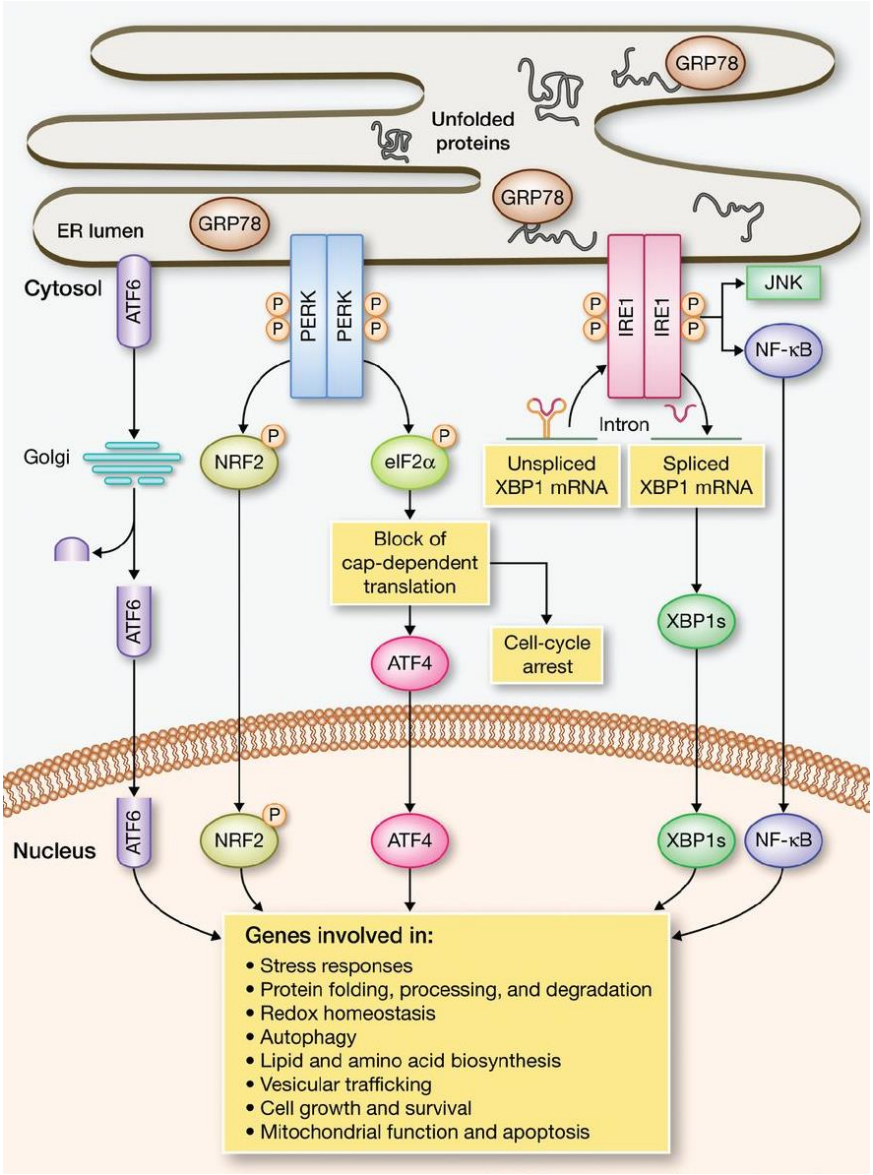

Figure 13. Signalling pathways of the unfolded protein response (UPR) (Vincenz et al., 2013).

IRE1 pathway: IRE1 is the most highly conserved branch of the UPR (Zhang et al., 2016). It is a bifunctional transmembrane kinase/endoribonuclease that uses a unique mechanism of non-conventional mRNA splicing to transmit the UPR signal (Walter and Ron, 2011). When activated, IRE1 cleaves a 26-base fragment from the mRNA encoding the X-box binding protein 1 (XBP1) (Peschek et al., 2015). Spliced *XBP1* mRNA is translated into a potent transcription factor, XBP1s, which targets a wide variety of genes involved in ER membrane biogenesis, ER protein synthesis, folding, glycosylation, ERAD, redox metabolism, autophagy, lipid biogenesis, and vesicular trafficking and protein secretion from the cell (Acosta-Alvear et al., 2018).

PERK pathway: PERK is structurally related to IRE1α, with an ER luminal dimerization domain and a cytoplasmic portion that displays protein serine/threonine kinase activity (Mendez et al., 2015). When activated, upon ER stress, PERK oligomerizes and phosphorylates itself and the ubiquitous translation initiation factor, eIF2α, inhibiting mRNA translation, decreasing global protein synthesis, and reducing the ER load (Guan et al., 2014).

ATF6 pathway: ATF6 is an ER-associated type 2 transmembrane basic leucine zipper transcription factor (Hillary and FitzGerald, 2018). During ER stress conditions, ATF6 is transported on vesicles toward the Golgi apparatus, where it is sequentially cleaved by Site-1 and Site-2 Proteases (S1P and S2P, respectively) (Gallagher and Walter, 2016). Then, the liberated N-terminal cytosolic active fragment of ATF6, $ATF6^{p50}$, is translocate to the nucleus where it promotes the transcription of UPR genes (Dufey et al., 2014).

The integral response of the UPR: ER stress sensors use different mechanisms and effectors to activate the UPR, but at some points, the three pathways communicate. One example is the close relationship between the IRE1α and ATF6 pathways. XBP1s does not only function as a negative regulator of XBP1 but also targets the active form of ATF6 to the proteasome, while ATF6, on the other hand, also controls the transcription of XBP1 (Hetz and Papa, 2018). Additionally, ATF6 heterodimerizes with XBP1 to promote degradation of ERAD components, and the PERK pathway is also linked to IRE1α and ATF6 (Bravo et al., 2013). All these studies underscore the notion that the individual branches of the UPR are connected in ways that permit generating integrated responses. In adipose tissue, ER stress is initiated by nutrient overload along with high demand for protein translation, decreased vascularization, and local glucose deprivation due to IR (Cnop et al., 2012). During this condition, ER homeostasis will collapse, and UPR will be initiated (Pagliassotti et al., 2016).

The UPR activates the ER-associated degradation (ERAD) system so that miss-folded/unfolded proteins get transported from the ER lumen to the cytosol for subsequent degradation by the proteasome (Tepedelen and Kirmizibatrak, 2019).

4.4.2. Endoplasmic reticulum-associated protein degradation (ERAD)

An imbalanced UPR lead to a significant increase in the ratio of incorrectly folded proteins (Morito and Nagata, 2015). ER-associated protein degradation (ERAD) detects misfolded proteins in the ER lumen and then extracts them through membrane channels

to the cytosolic proteasome (Olzmann et al., 2013). ERAD is a highly complicated and regulated mechanism that occurs in a multistep process, including protein recognition and targeting, retrotranslocation, ubiquitination, and proteasomal targeting and degradation (Christianson et al., 2011) (**Figure 14**).

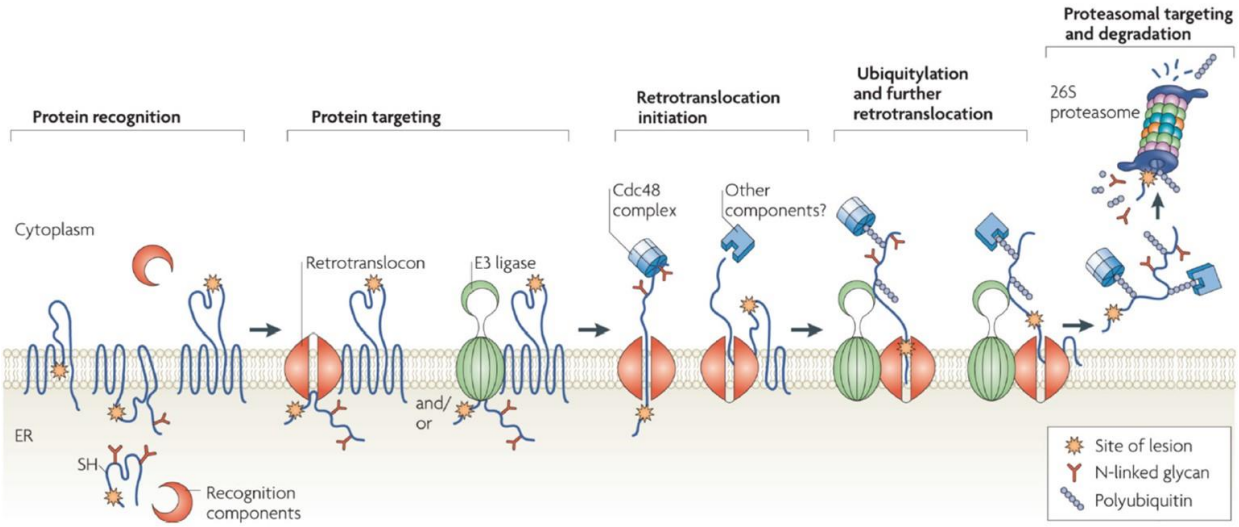

Figure 14. Step-by-step illustration of endoplasmic reticulum-associated protein degradation (ERAD) (Vembar and Brodsky, 2008).

Recognition: The substrate recognition step of ERAD is a complicated mechanism, in which several different enzymes and chaperones are involved. In a simplified model of ERAD, chaperones and lectins (e.g., BiP, EDEM, ERdj, OS9, XTP3B, etc.) within the ER lumen recognize and bind to the misfolded protein, and hold it in a retrotranslocation component form until transfer to the retrotranslocation complex (Ushioda et al., 2013). Suppressor/enhancer of Lin12-like (SEL1L) appears to link luminal factors that recognize misfolding to components of the retrotranslocon (Williams et al., 2013).

Retrotranslocation: The ERAD substrates must be retrotranslocated to the cytosol for proteasomal degradation (Tepedelen and Kirmizibatrak, 2019). Several putative retrotranslocation channels have been proposed such as the Sec61 complex, members of Derlin family, VCP, and polytopic E3s such as Hrd1 and gp78 (Vasic et al., 2020).

Ubiquitination: Once retrotranslocated from the ER to the cytosol, ERAD substrates should be rapidly targeted to the proteasome for degradation in order to avoid the accumulation of aggregates in the cytosol (Lopata et al., 2020). Ubiquitin is a 76 amino acid polypeptide that can be covalently conjugated to other proteins through a complex, highly regulated process called ubiquitination (Preston and Brodsky, 2017). Among its regulators, there are multiple E3 ligases in ERAD, including the transmembrane proteins

gp78/AMFR (Lemus and Goder, 2014), TRC8 (Tsai and Weissman, 2011), RNF185 (van de Weijer et al., 2020), MARCH6/TEB4 (Kreft and Hochstrasser, 2011), and CHIP (Matsumura et al., 2013).

Proteasome: The ubiquitin-proteasome system (UPS) is responsible for most of the protein degradation (Collins and Goldberg, 2017). Since polypeptides are digested irreversibly to short peptides, this system involves intricate mechanisms to avoid failures and to ensure efficient and selective degradation (Bard et al., 2018). Therefore, the proteasome is not only essential for general protein and amino acid homeostasis but also controls a myriad of essential cellular processes, including the cell cycle, DNA replication, transcription, signal transduction, and stress responses (Bhattacharyya et al., 2014).

The 26S proteasome is a large multi-catalytic ATP-dependent protease complex that can be divided into two functionally distinct sub-complexes, the core particle (20S) and the regulatory particle (19S) (Livneh et al., 2016). The 19S receives assists in deubiquitylation and unfolds ubiquitinated protein substrates, that are subsequently translocated into an enclosed cavity formed by the 20S (Kors et al., 2019). Here, a variety of catalytic sites degrade the substrate into short peptides that are subsequently broken down to amino acids by peptidases and recycled by the cell (Marshall and Vierstra, 2019).

ERAD regulation: Deficiencies in proteostasis can lead to metabolic, oncogenic, neurodegenerative, and cardiovascular disorders (Hipp et al., 2014). It is thought that ERAD functions at relatively low levels under basal conditions, but under proteotoxic stress its activity is enhanced (Qi et al., 2017). Since ERAD is crucial for the maintenance of the integrity of the ER proteome (Guerriero and Brodsky, 2012), and for protecting cells from proteotoxicity caused by the formation of protein aggregates, it has been shown that aberrations in ERAD function play a role in the pathology of nearly 70 diseases such as cystic fibrosis, diabetes, neurodegenerative diseases, and infectious diseases (Baldridge and Rapoport, 2016). Regulation of ERAD in normal and pathological conditions is also of great importance since hyper-ERAD may cause loss-of-function phenotypes upon unnecessary degradation of folding intermediates (El Khouri et al., 2013), and hypo-ERAD may result in gain-of-function phenotypes upon accumulation and/or aggregation of misfolded and unassembled proteins (Byun et al., 2014). However, it is still unknown whether ERAD is dysregulated in the adipose tissue in obesity and its potential role on obesity-related metabolic disease remains unexplored.

Likewise, aberrations in the proteasome have been linked to several diseases. Some diseases are due to the increased lifetime of disease-related proteins, whereas others are caused by accelerated protein degradation (Hanna et al., 2019). The occurrence of alterations in ERAD have never been explored in human preadipocytes as yet.

5. Therapeutic management of obesity-related metabolic disease

Despite significant investigation in the development of drugs for obesity and IR/T2D, to date, the success of weight-loss strategies has been mainly limited to surgical interventions as compared to diet or pharmacotherapy (Hendricks, 2017). While lifestyle adjustments such as physical activity and diet, together with pharmacotherapy, can have moderate effects at the individual level, they are clearly insufficient at population levels (Botchlett et al., 2017). Therefore, bariatric surgery (BS) is the most effective available therapy for obesity and its comorbidities (Gloy et al., 2013).

5.1. Bariatric surgery (BS)

Over the past decade, the number of bariatric and metabolic interventions performed worldwide has more than doubled (Pareek et al., 2018), with BS reportedly being the most cost-effective therapy for sustained weight loss in patients with morbid obesity (Buchwald and Oien, 2013). All contemporary procedures include different techniques, among which Roux-en-Y gastric bypass (RYGB) and sleeve gastrectomy (SG) (**Figure 15**) are the most commonly performed (Khorgami et al., 2017).

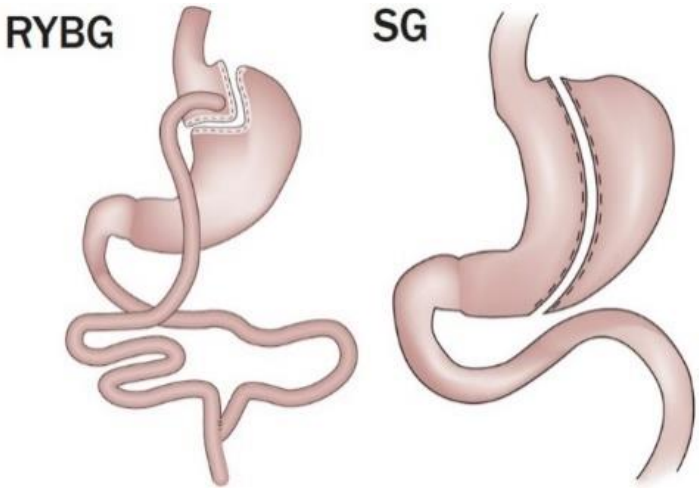

Figure 15. Anatomical alterations of Roux-en-Y gastric bypass (RYGB) and sleeve gastrectomy (SG) procedures (Frühbeck, 2015).

The mechanisms of action of BS are complex and involve multiple neuroendocrine signals that exert effects on the central nervous system as well as in peripheral organs (Pappachan and Viswanath, 2015). BS also improves the metabolic status of patients, ameliorating hypertension and improving the blood lipid profile, thus decreasing cardiovascular risk (Sjöström et al., 2012). On average, BS can achieve a sustained weight loss of up to 40%, which leads to important benefits, even remission, for hypertension, dyslipidaemia, and T2D in a huge proportion of patients (Rubino et al., 2016). One of the most illuminating aspects of bariatric operations is that the favourable modulation of comorbidities does not take place uniformly or gradually for all comorbidities, thereby highlighting the involvement of both weight-dependent and weight-independent effects (Adams et al., 2017). Most cardiovascular risk factors and mechanically related comorbidities ameliorate slowly and mainly in parallel with weight loss (Schauer et al., 2014). By contrast, T2D tends to improve rapidly and soon after surgery, even before major reductions in body weight occur (Madsbad et al., 2014).

5.1.1. Adipose tissue remodelling after BS

The most obvious effect of BS is the loss of up to half of the total adipose tissue mass within the first year after surgery along with improvements in systemic metabolism (Frikke-Schmidt et al., 2016). These metabolic improvements associated with BS do not correlate directly with reduction of adipose mass *per se*, but also relate to the extent to which different adipose tissue anatomic depots are affected (Mardinoglu et al., 2015). Most studies of depot-specific fat mass find pronounced reductions in both VAT and SAT within the first few months after surgery (Faria et al., 2015). These data suggest that the beneficial effects of BS result not only from the overall loss of fat mass but also a metabolically beneficial redistribution among different anatomic depots.

Reduction in adipocyte hypertrophy is a dominant feature of fat mass loss (Carvalho and Sparks, 2019). Studies investigating adipocyte size after BS find that, at least, SC adipocytes become smaller (Aghamohammadzadeh et al., 2013), ultimately approaching diameters similar to lean controls, yet, total adipocyte number, and therefore adipogenesis, remains unchanged (Andersson et al., 2014). Moreover, previous studies have reported that, at least in SAT, the obesity-induced IR is reduced after surgery (Hansen et al., 2015). As would be predicted based on fat mass changes, leptin decreases, whereas adiponectin increases after BS (Sams et al., 2016). These findings point strongly towards adipose tissue regaining its endocrine capacity after surgery (Frikke-Schmidt et al., 2016).

6. In the search of biomarkers of metabolic disease in the adipose tissue

In recent decades, overwhelming evidence has indicated that the pathogenesis of adipose tissue dysfunction in metabolic disorders, including obesity, IR, and T2D, involves multiple biological pathways yet our knowledge of the underlying mechanisms is still incomplete (Zhang et al., 2019). In this scenario, biological markers may provide the needed breakthrough to propel our understanding, and may as well represent useful indicators of physio-pathogenic processes or pharmacological responses to therapeutic interventions (O'Neill et al., 2016).

In this scenario, lessons may be learned from the knowledge gained from other complex diseases and processes such as cancer or aging. There is a number of essential alterations in cell physiology that have been proposed to collectively trigger cell dysfunction leading to disease. In 2013, Lopez-Otín and collaborators defined the hallmarks of aging as those perturbations that are common denominators of this process in different organisms (López-Otín et al., 2013). These hallmarks included: genomic instability, telomere attrition, epigenetic alterations, loss of proteostasis, deregulated nutrient sensing, mitochondrial dysfunction, cellular senescence, stem cell exhaustion, and altered intercellular communication. Interestingly, many of these pathogenic processes are shared by other diseases, such as neurodegenerative diseases (Mattson and Arumugam, 2018). Based on the current knowledge, they may also embrace the various mechanisms that are dominant contributors to the pathogenesis of dysfunctional adipose tissue (Díaz-Ruiz et al., 2015) (**Figure 16**). However, additional candidate hallmarks (or groups of) should be considered in the context of adipose tissue in obesity, including inflammation/fibrosis/hypoxia (Crewe et al., 2017; Guzmán-Ruiz et al., 2020), alterations in lipids/metabolites (Fernández-Vega et al., 2020; López-Bascón et al., 2018), and impaired organelle interaction (Pulido et al., 2011).

Figure 16. Proposed scheme of the hallmarks of adipose tissue dysfunction in obesity. Modified from (López-Otín et al., 2013).

It is likely that other mechanisms operating in adipocytes and, for that matter in preadipocytes, that are important for maintaining cell homeostasis may be altered in obesity. Precisely, adipocyte differentiation is a complex process involving striking changes in size, morphology, metabolism, and responsiveness to signals. This, in turn, relies on major changes in gene expression programs regulating RNA and protein production (de Sá et al., 2017). An increasing body of evidence shows that mRNA processing and, in particular, alternative splicing, is crucial for genome reprogramming during cell differentiation (Fiszbein and Kornblihtt, 2017). In this line, the recent identification of PPARγ protein variants with opposing effects on preadipocyte differentiation, supports a role for alternative splicing in adipogenesis (Aprile et al., 2018, 2014). Nevertheless, neither the splicing components relevant to adipogenesis nor the cellular events regulated by alternative splicing during this process have been elucidated (Lin, 2015), and it is yet to be established whether this process is modified in human obesity.

On the other hand, it is widely accepted that the changes occurring in the secretory profile of the adipose tissue of obese individuals alters the intercellular communication of this organ with other tissues, thus representing a hallmark of obesity (Rodríguez et al., 2015). This essentially relates to adipokines yet this classic view has been challenged by recent data demonstrating that the adipose tissue is also a major source of circulating miRNAs (Thomou et al., 2017). Specifically, several cross-sectional human studies have shown that the obesity-related expression pattern of specific circulating miRNAs reflects their miRNA adipose tissue expression profiles (Mori et al., 2019), supporting a role for circulating miRNAs as adipose tissue biomarkers. However, the relationship between circulating miRNAs and adipose tissue functional state is not fully understood, yet it might be useful to identify adipose tissue-related metabolic complications.

An overview of alternative mRNA splicing as well as of miRNAs, both as intracellular effectors and as extracellular messengers, is provided in the following sections, including available information related to adipose tissue.

6.1. Alternative mRNA splicing (AS)

Alternative splicing (AS) is a key process for the generation of multiple mRNAs during pre-mRNA maturation, resulting in the generation of multiple proteins from a single gene (Lee and Rio, 2015). During this process, the exons of a gene will be included within or excluded from the final mature mRNA, and the resulting transcripts generate diverse protein isoforms (Harvey and Cheng, 2016). Recent evidence demonstrates that approximately 95% of human genes with multiple exons undergo AS during pre-mRNA maturation, highlighting the important role of AS in determining gene function as one of the major mechanisms contributing to protein diversity (Kelemen et al., 2013). In the same line, AS is regulated by physiological signals, allowing an organism to adapt to the alterations in the environment (Tapial et al., 2017). Thus, dysregulation of AS is associated with diseases, such as cancer, diabetes, and neurodegenerative diseases (Zhao et al., 2014), suggesting that this mechanism could serve as a disease-specific biomarker (Tang et al., 2013). Likewise, modulating this process might prevent the development and/or alter the course of diseases, implying the potential targeting for new drug development (Bates et al., 2017).

Pre-mRNA splicing is catalysed by the spliceosome, a complex molecular machinery that recognizes and excises introns (Will and Lührmann, 2011). The human spliceosome is composed of ~170 different proteins, including five small nuclear ribonucleoproteins (snRNPs) and additional non-snRNP associated protein factors (Will and Lührmann,

2011). Each of the five snRNPs contains one small nuclear RNA (snRNA) and a number of protein components (Lee and Rio, 2015). The genomes harbour two different types of introns that are removed by two, similar but distinct, spliceosomes (Toroney et al., 2019). Major spliceosome splices the 95% of the introns, which are referred to as major or U2-type introns, whereas minor or U12-type introns, that only account for 0.5% of all introns, are spliced by the minor spliceosome (Turunen et al., 2013). As shown in **Figure 17**, introns are removed through two transesterification reactions (Lin et al., 2016).

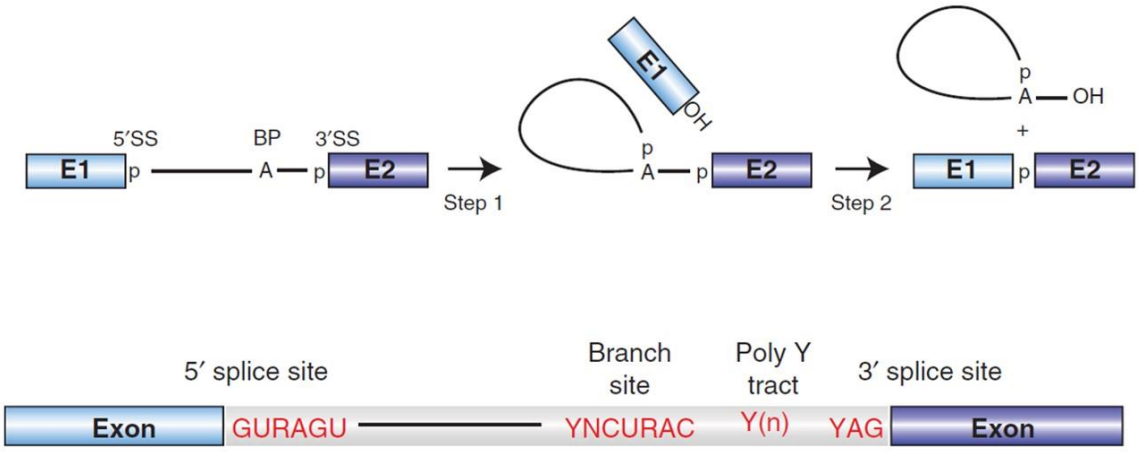

Figure 17. Schematic representation of the two-step mechanism of pre-mRNA splicing (top panel), and conserved sequences found at U2-type pre-mRNA introns (bottom panel) (Will and Lührmann, 2011).

The major spliceosome contains five snRNPs, U1, U2, U4, U5, and U6, the latter three of which form a U4/U6.U5 tri-snRNP (Nguyen et al., 2016). These components assemble on pre-mRNA in a stepwise manner (Will and Lührmann, 2011) (**Figure 18**). The first spliceosome assembly step involves the initial recognition of an intron by the spliceosome and the formation of the E complex (Shi, 2017). Subsequently, the U2 snRNP joins the spliceosome, replaces SF1 at branch point sequence, and forms the pre-splicesome (A complex) and, at later stages, the U4/U6.U5 tri-snRNP stably associates with the spliceosome (B complex) (Yan et al., 2019). Extensive structural rearrangements lead to the formation of the catalytically active spliceosome (B* complex) that catalyses the first transesterification reaction (X. Li et al., 2013). After the first transesterification reaction, the spliceosome repositions the substrate to form the C complex, which is ready for the second catalytic reaction (Matera and Wang, 2014). The second reaction is followed by post-catalytic rearrangements to liberate the mature mRNA for export and release the lariat intron to be degraded and snRNPs to be recycled (L. Zhang et al., 2013).

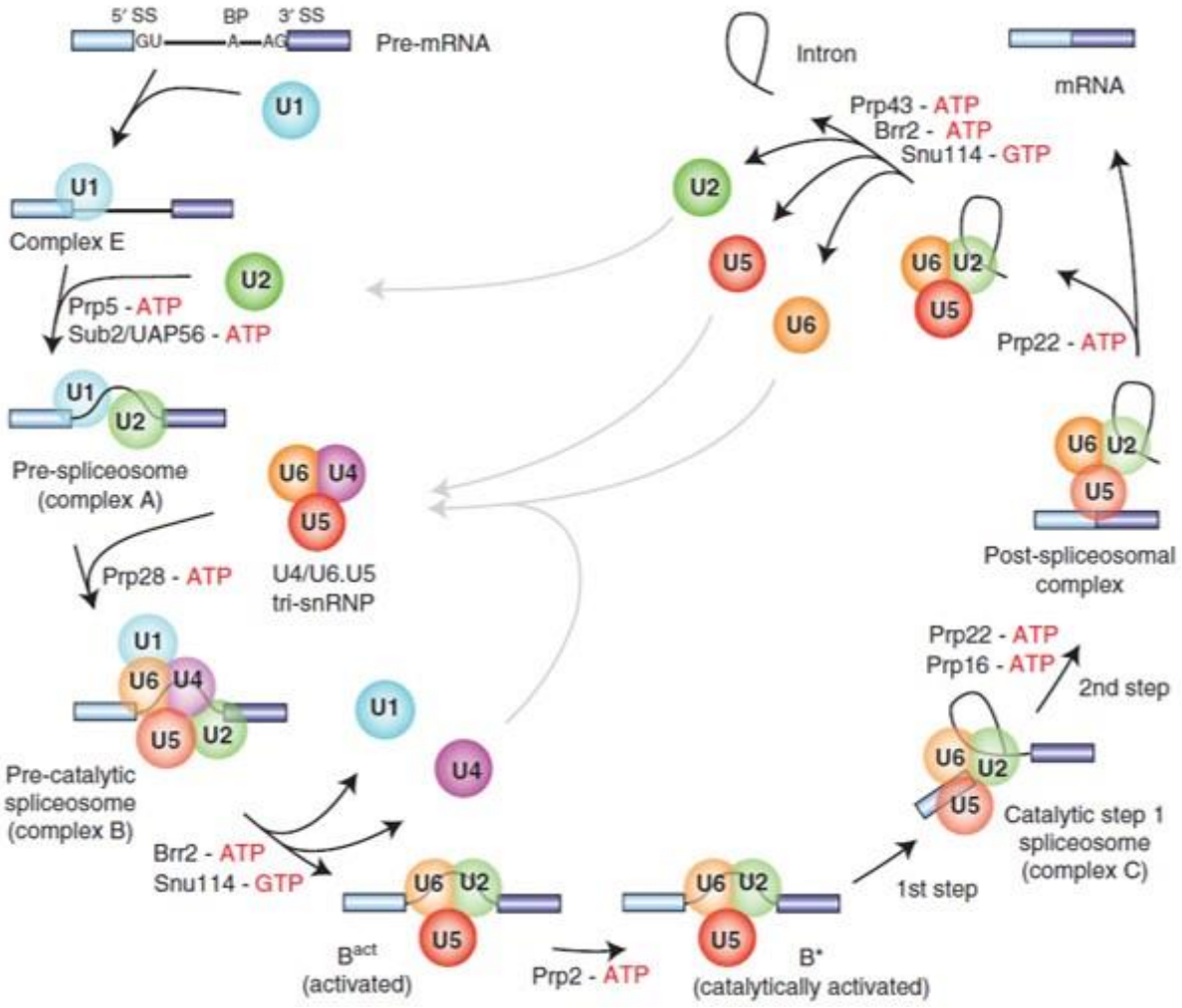

Figure 18. Canonical cross-intron assembly and disassembly pathway of the major spliceosome (Will and Lührmann, 2011).

The minor spliceosome contains four specific snRNPs: U11, U12, U4atac, and U6atac, each of which contains a specific snRNA component with a secondary structure that is equivalent to but distinct from its major counterpart, i.e., U1, U2, U4, and U6, respectively (Turunen et al., 2013). U5 snRNP is shared between the two spliceosomes, whereas U4atac, U6atac, and U5 associate into a tri-snRNP, similar to the major U4/U6.U5, and the protein composition of the major and minor tri-snRNPs appears to be very similar, if not identical (Verma et al., 2018).

6.1.1. AS in the adipose tissue

Although the role of alternative splicing (AS) in adipose tissue metabolism is unclear, a number of adipose tissue-related genes are regulated by AS (Kaminska and

Pihlajamäki, 2013). For instance, the phosphatase, lipin1 (gene *LPIN1)*, has two splicing isoforms (α and β). The β isoform associates with increased expression of lipogenic genes while the α isoform promotes proliferation (Zhang and Reue, 2017). Insulin receptor (*INSR*) exists in two splicing isoforms: INSR-A promotes growth while INSR-B regulates glucose homeostasis (Payankaulam et al., 2019).

In addition, AS of several genes has been reported to be important in adipogenesis (Yi et al., 2020c). *Pref-1* has four major AS products (*Pref-1 A–D*). Only Pref-1A and Pref-1B severely inhibit adipogenesis whereas Pref-1C and Pref-1D do not affect adipocyte differentiation (Hudak and Sul, 2013). The human PPARγ gene consists of nine exons and transcribes four major transcripts (PPARγ1, PPARγ2, PPARγ3, and PPARγ4), though the PPARγ transcripts only encode two variants. PPARγ1, PPARγ3, and PPARγ4 encode the PPARγ1 isoform that is ubiquitously expressed, whereas the PPARγ2 transcript encodes the PPARγ2 isoform which is enriched in WAT (J. C. Lin, 2015). In recent years, three distinct splice PPARγ isoforms with dominant-negative activity have been identified: γORF4, PPARγ1(tr), and PPARγΔ5 (Aprile et al., 2018). These isoforms are expressed in the adipose tissue and regulated during adipocyte differentiation (Aprile et al., 2014). In particular, PPARγΔ5 impairs adipocyte differentiation and its expression is higher in human SAT of overweight or obese and diabetic patients compared to control individuals (Aprile et al., 2018). Moreover, *in vitro* hypertrophic-like adipocytes displaying PPARG isoforms unbalance recapitulate adipocyte dysfunction i*n vivo* (Aprile et al., 2020).

Other examples demonstrating the importance of AS in obesity have been reported. The RNA-binding protein, Sam68, regulates mTOR AS during adipogenesis (Huot et al., 2012). SRSF10 is required for adipocyte differentiation due to its role on AS of *ACLY, Axin1*, *UPF1*, and *Lipin1* (Li et al., 2014). *In vivo* studies indicated that FTO specifically mediated the demethylation of RNA N6-methyladenosine (m6A), which is essential for RNA splicing (Yue et al., 2015). The adipogenic transcriptional cofactor, ZNF638, interacts with splicing regulators and influences AS (Meruvu et al., 2011). Protein kinase Cδ (PKCδ) splice variants modulate the apoptosis pathway during adipogenesis (Patel et al., 2013).

Moreover, it is important to note that insulin signalling pathways lead to phosphorylation of spliceosome components and splicing factors (Jiang et al., 2017). Therefore, it is plausible to postulate that IR in obese individuals and improved insulin signalling after weight loss could modify AS.

6.2. microRNAs (miRNAs)

miRNAs are endogenous small non-coding single-stranded RNAs (O'Brien et al., 2018). miRNAs negatively modulate gene expression by interacting with mRNA 3′- UTR of target genes, leading to mRNA degradation and/or translational repression (Ha and Kim, 2014). As biological regulators, miRNAs play important roles in physiological processes such as development, cell growth, proliferation, differentiation, survival, apoptosis, metabolism, and homeostasis (Sun and Lai, 2013).

miRNAs are found in all tissues, but recent studies have suggested that they can also be secreted from cells and enter the bloodstream, serving as signalling molecules to mediate cell-cell communication (Bayraktar et al., 2017). Previous studies have indicated that the dysregulated expression levels of circulating miRNAs are associated with a variety of human diseases (Paul et al., 2018). Thus, miRNAs show great promise in becoming novel diagnostic and prognostic non-invasive biomarkers for multiple human diseases, and manipulating relevant miRNA expression or function may serve as potential therapeutic strategies (Huang, 2017) (**Figure 19**).

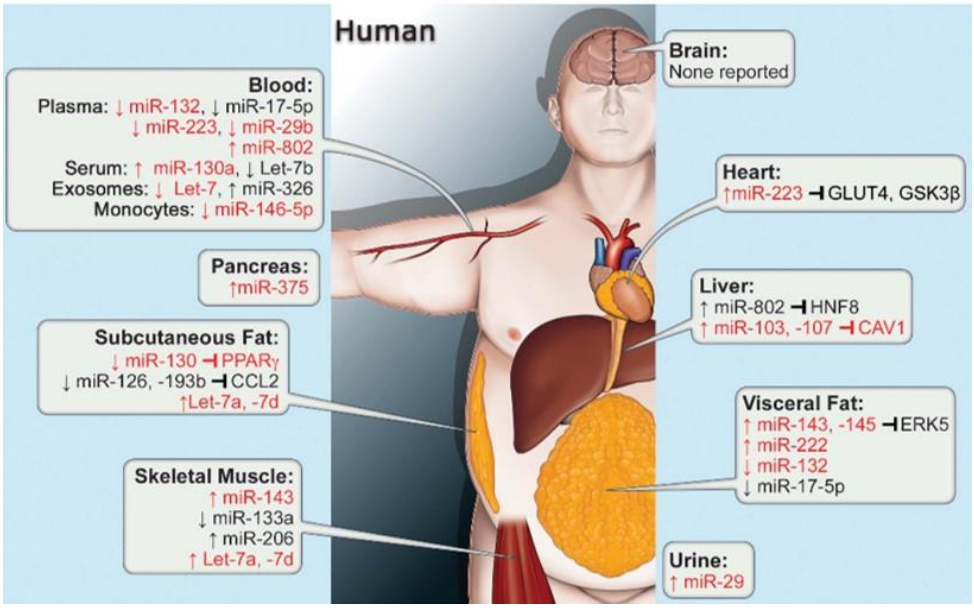

Figure 19. Obesity/IR-related miRNA expression changes in humans (Deiuliis, 2016)

6.2.1. Biogenesis of miRNAs

miRNA biogenesis starts in the nucleus by RNA polymerase II/III to generate the long primary miRNA transcripts (pri-miRNA). The biogenesis of miRNA is classified into canonical and non-canonical pathways (Zhao et al., 2019) (**Figure 20**).

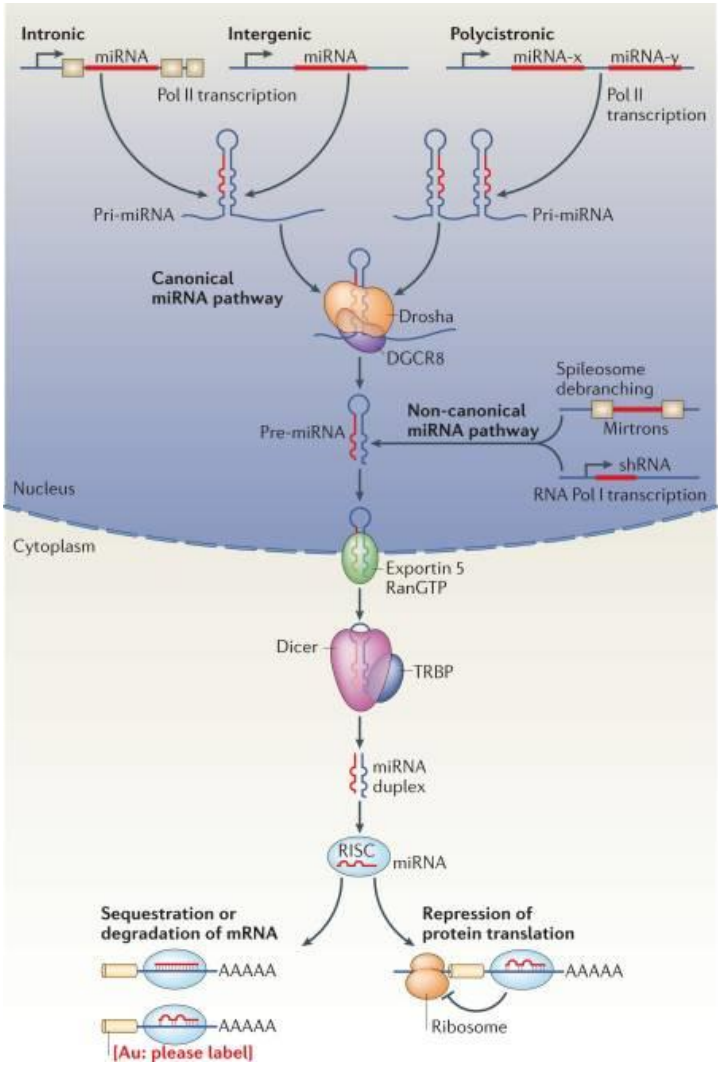

Figure 20. The miRNA biogenesis pathway and function (Rottiers and Näär, 2012).

The canonical biogenesis pathway is the dominant pathway by which miRNAs are processed (Jiang and Yan, 2016). In this pathway, pri-miRNAs are cleaved into pre-miRNAs by the microprocessor complex, consisting of an RNA binding protein, DGCR8, and a ribonuclease III enzyme, Drosha (Alarcón et al., 2015). Once pre-miRNAs are generated, they are exported to the cytoplasm by an exportin 5 (XPO5)/RanGTP complex through the nuclear pores and then the terminal-loop is cleaved by the RNase III endonuclease, Dicer (Koscianska et al., 2011). This processing involves the removal of the terminal loop, resulting in a mature miRNA duplex (Creugny et al., 2018). The directionality of the miRNA strand determines the name of the mature miRNA form. The 5p strand arises from the 5′ end of the pre-miRNA hairpin while the 3p strand originates from the 3′ end (Meijer et al., 2014). Generally, the strand with lower 5′ stability or 5′ uracil is preferentially loaded into argonaute (AGO), which are the direct binding partners of

small RNAs (Meister, 2013), and it is deemed the guide strand (Yoda et al., 2013). The unloaded strand is called the passenger strand, which will be unwound from the guide strand through various mechanisms based on the degree of complementarity.

To date, multiple non-canonical miRNA biogenesis pathways have been elucidated (Stavast and Erkeland, 2019). These pathways make use of different combinations of the proteins involved in the canonical pathway. In general, the non-canonical miRNA biogenesis can be grouped into Drosha/DGCR8-independent and Dicer-independent pathways (Treiber et al., 2019). Pre-miRNAs produced by the Drosha/DGCR8-independent pathway resemble Dicer substrates (Pong and Gullerova, 2018). An example of such pre-miRNAs is mirtrons, which are produced from the introns of mRNA during splicing (Schamberger et al., 2012), and the 7-methylguanosine (m^7G)-capped pre-miRNA (Xie et al., 2013). On the other hand, Dicer-independent miRNAs are processed by Drosha from endogenous short hairpin RNA (shRNA) transcripts (Sheng et al., 2020).

6.2.2. Function of miRNAs

Most studies to date have shown that miRNAs bind to a specific sequence at the 3′ UTR of their target mRNAs to induce translational repression (Ameres and Zamore, 2013). Such peculiar properties of miRNAs regulation of gene expression generate a complex network of interactions in which a single miRNA can target multiple genes and, concomitantly, a single target gene can be regulated by multiple miRNAs, thus conferring them a powerful post-transcriptional expression control activity (Ferro et al., 2019). The miRNA-induced silencing complex (miRISC) consists of the guide strand and AGO (O'Brien et al., 2018). The target specificity of miRISC is due to its interaction with complementary sequences on target mRNA (Nishimura and Fabian, 2016).

6.2.3. Secretion and uptake of miRNAs

Many studies have demonstrated that extracellular miRNAs can exert biological functions in recipient cells to regulate their activity, thereby acting as intercellular signalling molecules (Vickers et al., 2011). miRNAs are released to the extracellular space via three different pathways (Sebastiani et al., 2017) (**Figure 21**): (1) passive leakage from broken cells caused by tissue injury, inflammation, cell necrosis or apoptosis (apoptotic bodies) (Turchinovich et al., 2015); (2) Active secretion via extracellular microvesicles (MVs) (Sohel, 2016); (3) Active secretion via association with

lipoproteins (e.g., HDL) (Vickers et al., 2011), or RNA-binding proteins (e.g., Ago2) (Arroyo et al., 2011).

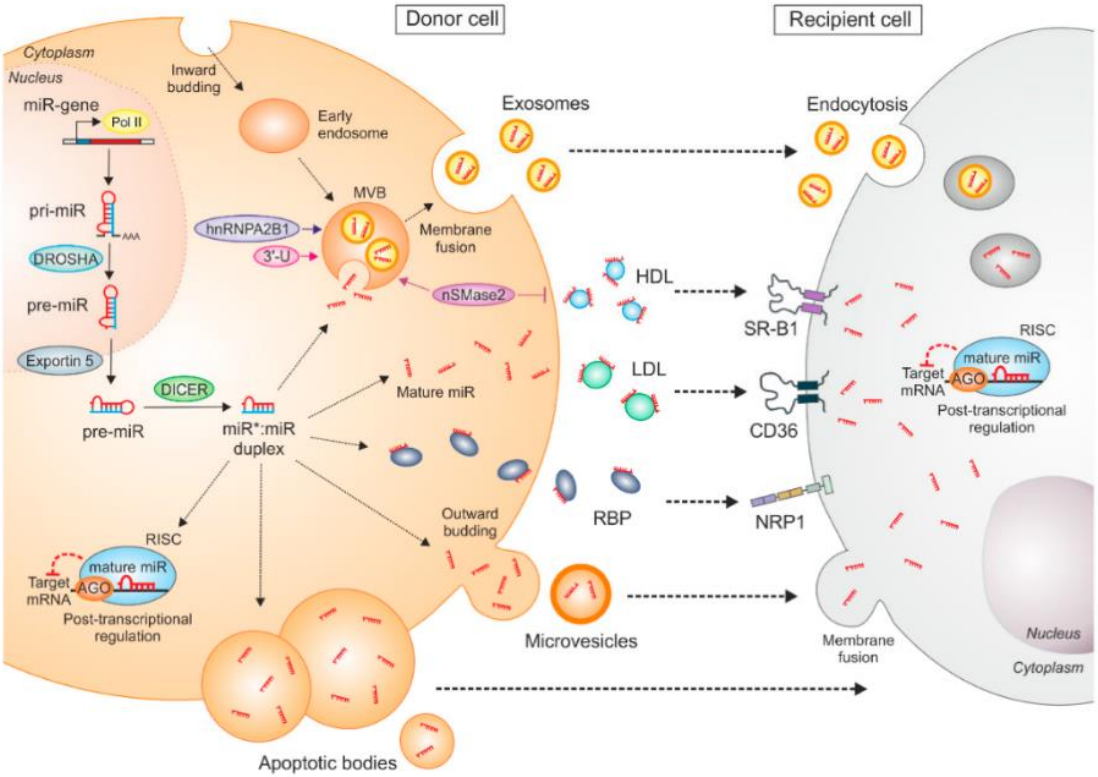

Figure 21. Mechanisms of miRNAs intercellular communication (Syed et al., 2019).

It is clear from the definition that apoptotic bodies are formed during apoptosis from dying cells. Therefore, it is uncertain whether extracellular miRNAs incorporated with these structures might solely be the waste product from dying cells or they could mediate a warning signal to the organism about cellular dysfunction (Rayner and Hennessy, 2013). On the other hand, MVs and miRNA-protein complex are found to be released from viable cells in a tightly regulated manner, according to cell type and status, leaving without doubt about their physiological and pathological implications (Mori et al., 2019). Despite being functionally important, MV-associated and lipoprotein-bound miRNAs are just a minor fraction of all the miRNAs found in circulation. In fact, although it was assumed that circulating miRNAs must be encapsulated in vesicles to be protected from RNases (Zhao et al., 2019), it has been demonstrated that the majority (90-99%) of extracellular miRNA are MVs-free and associated with proteins of the AGO family. These findings revealed that there are at least two populations of circulating miRNAs, and suggest that circulating Ago2 complexes are a mechanism responsible for the stability of plasma miRNAs (Arroyo et al., 2011; Turchinovich et al., 2011).

Two major MVs can package and deliver miRNAs: shedding vesicles and exosomes. As a heterogeneous population, shedding vesicles are larger, 100 to 1000 nm in diameter vesicles that are released from the plasma membrane through outward budding and fission, while exosomes are 30–100 nm in diameter and they are released by exocytosis from multivesicular bodies (MVBs) (Stahl and Raposo, 2019). Evidence has indicated that cells may preferentially select the particular miRNA populations and sort them into MVs. Thus far, research has identified several miRNA sorting mechanisms, but the specific details remain incompletely understood (Janas et al., 2015). These mechanisms broadly include RNA-binding proteins (such as hnRNPA2B1, Ago-2, Ybx1, Mex3c, MVP, and La protein), but also membranous proteins involved in MVs biogenesis (such as Caveolin-1, nSMase2, and Vps4A) (Groot and Lee, 2020). Some studies have confirmed that the protein heterogeneous nuclear ribonucleoprotein A2B1 (hnRNPA2B1) recognizes a special EXOmotif GGAG present in miRNAs and controls their loading into exosomes (Villarroya-Beltri et al., 2013). Ago2 has also been implicated in binding and sorting miRNA into EVs through the KRAS-MEK-ERK signalling pathway (McKenzie et al., 2016). Y-Box Binding Protein 1 (YBX-1) is another protein with RNA-binding, and it was found to be required to selectively package into exosomes (Shurtleff et al., 2016). Caveolin-1 is integral in the trafficking process of hnRNPA2B1 and hnRNPA2B1-associated miRNAs into MVs (H. Lee et al., 2019). Finally, as ceramide has been implicated in exosome biogenesis, neural Sphingomyelinase 2 (nSMase2) has been also reported to be a regulator of exosome synthesis (Kosaka et al., 2013).

In recent years, extraordinary progress has been made in terms of finding the origin and function of miRNA and their potential use in research and clinical practice, for both healthy and diseased patients (Condrat et al., 2020). However, probably the most promising role of miRNAs is that of a potential biomarker. Numerous authors have investigated this opportunity in various medical fields and evidence suggests that the circulating miRNA signature (i.e. miRNome), comprising more than 1,000 miRNAs (Castro-Magdonel et al., 2020), change in pathological conditions (such as cancer, and neuronal, cardiovascular, infectious, and metabolic diseases), and that it could play an essential role as a biomarker (Párrizas and Novials, 2016).

With respect to target cells, it has been proposed that vesicle-associated extracellular miRNAs may enter cells by endocytosis, phagocytosis, or direct fusion with the plasma membranes, while vesicle-free secreted miRNAs may be taken up by specific receptors on the cell surface (X. Chen et al., 2012). miRNAs have also been shown to transfer between co-cultured cells via direct cell-cell contact and gap junctions (Zong et al., 2016).

6.2.4. miRNAs in the adipose tissue

Distinct circulating miRNA profiles have been reported in overweight/obese patients as compared to lean individuals (Ortega et al., 2020), as well as in relation to the degree of IR and T2D prevalence, incidence, progression, and its complications (Jiménez-Lucena et al., 2018), obesity-related T2D (Landrier et al., 2019), and in response to obesity treatment strategies (Catanzaro et al., 2020).

On the one hand, many miRNAs are differentially regulated in WAT of obese subjects compared to non-obese individuals and in relation to T2D manifestation (Brovkina et al., 2019). Notably, profiling analysis has also shown that numerous miRNAs are expressed differently in SAT and VAT (Yang et al., 2018). Several studies have illustrated a correlation between the expression of miRNAs in adipose tissue and different metabolic parameters (Heyn et al., 2020). Collectively, these different facts highlighted the interest in the role of miRNAs in the field of obesity and related diseases. Particularly, alterations in miRNA expression could induce changes in the pattern of genes controlling a range of biological processes including from adipogenesis to inflammation in the adipose tissue, as well as lipid metabolism and IR (Yi et al., 2020b).

In line with adipose tissue producing a variety of miRNAs and bearing in mind the size of the fat depots, also in lean individuals, it is increasingly accepted that adipose tissue-derived circulating miRNAs are an important source of all circulating miRNAs and are considered a new form of adipokine (Thomou et al., 2017). In this study Thomou et al., isolated miRNAs from the serum of a generated mice specifically lacking Dicer in adipose tissue (ADicerKO), and wild-type control mice. They observed that there was a broad reduction in total miRNAs in the serum of ADicerKO mice when compared to the wild type. Similar results were found when miRNA profiling on the serum was compared between patients with congenital generalized lipodystrophy or patients with HIV-associated lipodystrophy and control individuals. Moreover, restoration of circulating miRNAs was observed in ADicerKO mice upon fat transplant from normal mice.

Therefore, miRNAs in adipose tissue have a critical function in paracrine actions (Engin, 2017), as well as endocrine actions that facilitate crosstalk between metabolic organs (Kita et al., 2019) (**Figure 22**). This has led to the suggestion that adipose tissue-derived circulating miRNAs are essential for the physiological regulation of energy metabolism (Ji and Guo, 2019). According to the present evidence, adipose tissue-derived miRNAs are mainly released from adipocytes (Thomou et al., 2017), and macrophages (Ying et al., 2017), and their levels are governed by the degree of obesity and its metabolic complications (Ortega et al., 2014).

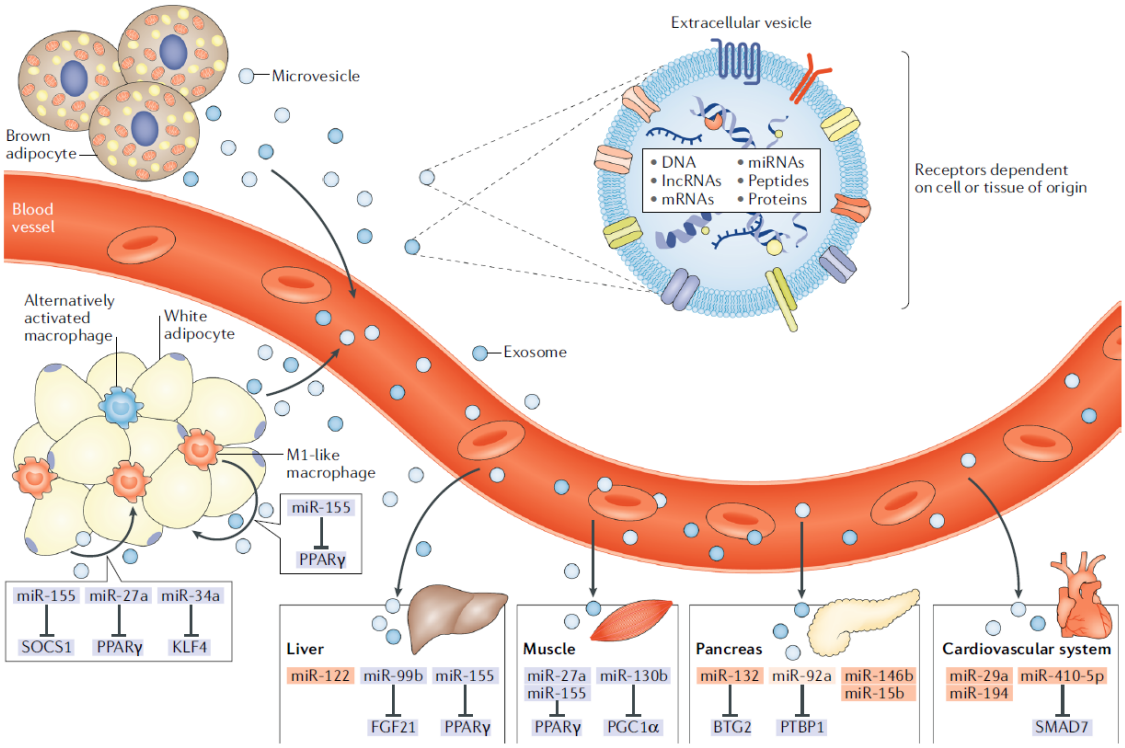

Figure 22. Adipose derived-circulating miRNAs as endocrine factors (Ji and Guo, 2019).

OBJECTIVES

Based on the existing evidence mentioned until this point, the present Doctoral Thesis was based on the notion that the alteration of the normal, physiologic function of the adipose tissue is a hallmark of the disturbed metabolic state of the individuals.

For this reason, the general aim of this investigation was to explore and characterize novel mediators of the cellular response of different components of the adipose tissue that could be closely implicated in the development and progression of metabolic diseases [i.e., insulin resistance (IR), and type 2 diabetes (T2D)] in obesity.

These findings could represent a potential source for the identification of signalling pathways and/or molecular factors that could serve as prognostic and therapeutic targets in highly prevalent and health-threatening diseases such as IR and T2D. To achieve this main aim, we proposed the following specific objectives:

Objective 1: Identification and characterization of signalling pathways and/or molecular factors altered in subcutaneous (SC) and omental (OM) preadipocytes that may contribute to metabolic disease in obesity. This was pursued through the analysis of the proteome of SC and OM preadipocytes from obese individuals with normoglycemia (NG) and T2D, complemented with protein and/or gene expression analysis also including SC and OM preadipocytes from obese individuals with IR. The modulation of the signalling pathways and/or molecular factors of interest (i.e., alternative mRNA splicing and ER-proteostasis) and its implication in the process of adipogenesis was further studied in human adipocytes using different *in vitro* approaches.

Objective 2: Determination of the relationship between predictive miRNAs for T2D onset and the loss of adipose tissue function. To do that, the relationship between circulating levels of previously established miRNAs for T2D onset in the CORDIOPREV cohort (Jiménez-Lucena et al., 2018), and the adipose tissue insulin-resistance index (ATIRI) of these individuals was evaluated. The regulation (i.e., expression and secretion) of the miRNA of interest, *miR-223-3p*, by adipocytes and its role in adipocyte biology was next explored using different *in vitro* approximations.

MATERIAL AND METHODS

1. Study cohorts

This Doctoral Thesis includes studies derived from four different cohorts, which are described below. For all these cohorts, written consent was obtained from the participants prior to recruitment. The study protocols were approved by the Ethics and Research Committees of the corresponding hospitals, all of which follow the Helsinki Declaration and good clinical practices.

1.1. Study cohort 1

In this study, a total of 69 morbidly obese subjects (BMI >40 kg/m^2) undergoing bariatric surgery (BS) were recruited at the General and Digestive Surgery Unit and the Lipids and Atherosclerosis Unit of the "Reina Sofía" University Hospital (HURS; Córdoba, Spain). Anthropometrical and biochemical parameters were obtained as described (Díaz-Ruiz et al., 2015). Type 2 diabetes (T2D) in treatment with insulin, serious systemic disease not related to obesity (infectious disease, cancer, kidney disease or severe liver disease), or major cardiovascular disease in the 6 months prior to the inclusion of the study, as well as pregnancy, breastfeeding, and acute or chronic inflammatory diseases were considered as exclusion criteria.

Subjects were matched by age and BMI, and classified into three groups according to the criteria of the American Diabetes Association (ADA, 2020): normoglycemic (NG Obese, n = 27): Glucose <100 mg/dL and HbA1c <5.7%; impaired fasting glucose (IFG Obese, n = 25): Glucose 100–126 mg/dL and HbA1c 5.7-6.4%; and with type 2 diabetes (T2D Obese, n = 17): Glucose >126 mg/dL and HbA1c >6.4%. The clinical characteristics of the subjects are shown in **Table 1**. IFG individuals exhibited significantly higher HOMA-IR values than NG individuals, as well as other clinical and plasma parameters that are within the cut-off points for identifying insulin resistance (IR) in hyperinsulinemia-euglycemic clamp studies (Tam et al., 2012). Thus, they will be referred hereinafter to as IR subjects (Díaz-Ruiz et al., 2015).

Table 1. Anthropometric and biochemical characteristics of study subjects from cohort 1.

	NG Obese	IR Obese	T2D Obese
N	27	25	17
Gender (female/male)	13 / 14	13 / 12	11 / 6
Post-menopause (n, %)	2 (15)	2 (15)	3 (27)
Lipid-lowering therapy (n, %)	0 (0)	5 (20)	4 (24)
Antidiabetic therapy (n, %)	0 (0)	3 (12)	8 (47)
Antihypertensive therapy (n, %)	1 (4)	6 (24)	5 (29)
Age (years)	43 ± 3	43 ± 2	46 ± 2
Weight (kg)	140.4 ± 7.0	153.4 ± 10.0	145.4 ± 7.5
Height (m)	1.67 ± 0.03	1.69 ± 0.02	1.65 ± 0.03
Body mass index (kg/m^2)	50.2 ± 2.1	52.8 ± 2.9	52.9 ± 1.9
Fat mass (%)	43.1 ± 1.9	41.2 ± 2.0	42.1 ± 1.7
Lean mass (%)	39.1 ± 3.2	36.1 ± 1.1	35.0 ± 1.0
Water mass (%)	23.0 ± 3.5	22.7 ± 1.6	22.9 ± 1.3
Waist circumference (cm)	144.2 ± 5.9	156.1 ± 8.1	149.9 ± 4.6
Systolic pressure (mm/Hg)	128.1 ± 2.3	127.0 ± 3.5	122.1 ± 2.6
Diastolic pressure (mm/Hg)	78.5 ± 4.4	75.5 ± 3.1	71.5 ± 2.6
Fasting glucose (mg/dL)	88.9 ± 1.8	105.2 ± 2.4 ^{aaa}	159.2 ± 10.0 $^{aaa, bbb}$
Fasting glucose (mmol/L)	4.93 ± 0.10	5.84 ± 0.13 ^{aaa}	8.83 ± 0.56 $^{aaa, bbb}$
Fasting insulin (mU/L)	15.4 ± 1.8	25.9 ± 2.9 ^{aa}	17.9 ± 2.7 ^{b}
HbA1c (%)	5.45 ± 0.06	6.25 ± 0.11 ^{a}	8.51 ± 0.56 $^{aaa, bbb}$
HbA1c (mmol/mol)	32.2 ± 0.6	41.0 ± 1.2 ^{a}	65.7 ± 6.1 $^{aaa, bbb}$
HOMA-IR (units)	3.42 ± 0.44	6.77 ± 0.74 ^{aa}	6.74 ± 1.05 ^{aa}
Total cholesterol (mg/dL)	167.4 ± 10.0	181.6 ± 8.3	198.1 ± 8.6
LDL cholesterol (mg/dL)	122.9 ± 11.1	112.9 ± 6.6	124.2 ± 8.5
HDL cholesterol (mg/dL)	39.5 ± 3.3	36.3 ± 2.1	36.7 ± 1.6
Triglycerides (mg/dL)	108.2 ± 7.0	132.7 ± 12.2	152.0 ± 12.9 ^{a}
Free fatty acids (mmol/L)	66.7 ± 6.3	74.4 ± 7.2	83.5 ± 6.2
C-reactive protein (mg/L)	9.61 ± 1.68	11.4 ± 2.3	17.4 ± 5.3
Uric acid (mg/dL)	6.30 ± 0.32	7.03 ± 0.36	6.85 ± 0.68

NG, normoglycemic; **IR**, insulin-resistant; **T2D**, type 2 diabetes; **LDL**, low-density lipoprotein; **HDL**, high-density lipoprotein; **HbA1c**, glycated hemoglobin; **HOMA-IR**, homeostasis model assessment of insulin resistance. ^{a}P<0.05, ^{aa}P<0.01, ^{aaa}P<0.001 *vs.* NG Obese; ^{b}P<0.05, ^{bbb}P<0.001 *vs*. IR Obese.

1.2. Study cohort 2

In this study, a total of 43 subjects undergoing scheduled non-acute surgical procedures, including laparoscopic surgery for hiatus hernia repair or cholecystectomies, were recruited by the Endocrinology and Surgery Departments at the University Hospital Joan XXIII (Tarragona, Spain) as reported previously (Ejarque et al., 2017). Anthropometrical and biochemical parameters were obtained as described (Serena et al., 2016). All subjects were of caucasian origin and reported that their body weight had been stable for at least 3 months before the study. They had no systemic disease other than obesity, and all had been free of infection in the previous month before the study.

Primary liver disease, cardiovascular disease, arthritis, acute inflammatory disease, infectious disease, neoplastic, and renal diseases were specifically excluded by a biochemical workup.

Subjects were classified by BMI into two groups, according to World Health Organization criteria, as lean (n = 18, BMI <25 kg/m^2), and obese (n = 25, BMI >30 kg/m^2). Obese subjects were subclassified into NG (n = 15), and T2D (n = 10) groups, as previously described (Serena et al., 2016). Anthropometric and biochemical variables from this cohort are presented in **Table 2**.

Table 2. Anthropometric and biochemical characteristics of study subjects from cohort 2.

	Lean	**NG Obese**	**T2D Obese**
N	18	15	10
Gender (female/male)	10 / 8	9 / 6	6 / 4
Antidiabetic therapy (n, %)	0 (0)	0 (0)	7 (70)
Age (years)	51 ± 13	54 ± 14	60 ± 8
Weight (kg)	65.6 ± 8.7	92.2 ± 10.7 ^{aaa}	90.0 ± 11.7 ^{aaa}
Height (m)	1.68 ± 0.07	1.66 ± 0.10	1.68 ± 0.12
Body mass index (kg/m^2)	23.3 ± 2.1	33.6 ± 2.7 ^{aaa}	32.1 ± 2.9 ^{aaa}
Systolic pressure (mm/Hg)	125.1 ± 17.3	138.7 ± 17.5	142.2 ± 15.0
Diastolic pressure (mm/Hg)	74.2 ± 8.3	76.2 ± 9.8	81.6 ± 12.3
Fasting glucose (mg/dL)	88.0 ± 13.2	97.3 ± 15.3	121.6 ± 41.4 $^{aa, b}$
Fasting glucose (mmol/L)	5.51 ± 0.96	5.84 ± 0.80	8.24 ± 5.61 $^{aa, b}$
Fasting insulin (mU/L)	11.4 ± 2.2	12.7 ± 6.7	18.4 ± 1.3
HOMA-IR (units)	2.82 ± 0.94	3.28 ± 1.81	6.91 ± 5.08
Total cholesterol (mg/dL)	184.7 ± 33.6	192.8 ± 51.8	172.2 ± 24.6
LDL cholesterol (mg/dL)	104.1 ± 37.1	124.8 ± 43.9	98.7 ± 10.5
HDL cholesterol (mg/dL)	54.0 ± 11.0	49.7 ± 16.1	43.0 ± 14.0
Triglycerides (mg/dL)	106.7 ± 62.1	142.3 ± 60.1	226.6 ± 162.5 ^{aa}
Urid acid (mg/dL)	4.65 ± 0.68	5.13± 0.97	6.48 ± 0.96 $^{aa, b}$

NG, normoglycemic; **T2D**, type 2 diabetes; **LDL**, low-density lipoprotein; **HDL**, high-density lipoprotein; **HOMA-IR**, homeostasis model assessment of insulin resistance. ^{aa}P<0.01, ^{aaa}P<0.001 *vs.* Lean; ^{b}P<0.05 *vs*. NG Obese.

1.3. Study cohort 3

Participants of this study belonged to the CORonary Diet Intervention with Olive oil and cardiovascular PREVention (CORDIOPREV) study registered in ClinicalTrials.gov (NTC00924937). Detailed study design and biochemical and anthropometrical characteristics of participants have been published elsewhere (Delgado-Lista et al., 2016). Briefly, the CORDIOPREV study is a prospective study carried out in 1,002 patients with coronary heart disease and high cardiovascular risk. Patients who had their last coronary event more than 6 months previously to the inclusion, aged between 20-75 years old, and without other serious diseases or a life expectancy of fewer than 5 years were included. Subjects were randomized into two different dietary models (Mediterranean and low-fat diets). For the present study, those patients without diagnosed T2D at baseline (n = 462) were included (CORDIOPREV-DIAB) (Blanco-Rojo et al., 2016). Anthropometrical and biochemical parameters were obtained as described (Jiménez-Lucena et al., 2018). Patients were classified into two groups according to T2D incidence (ADA diagnosis criteria) (ADA, 2020), during a median follow-up of 60 months: non-T2D group (participants who did not develop T2D during the follow-up, n = 355), and incident-T2D (participants who developed T2D during the follow-up; n = 107). No statistical differences were found in the demographic and metabolic characteristics between dietary interventions in the CORDIOPREV-DIAB cohort (Chi^2 = 1.948; p = 0.163).

A sub-cohort (n = 64; 32 non-T2D and 32 Incident-T2D) of the CORDIOPREV-DIAB study was employed for *in vitro* experiments as detailed below. The biochemical and anthropometric characteristics of the subjects included in this sub-cohort are shown in **Table 3**. Subjects were matched by BMI, waist circumference, and biochemical variables as determined at the beginning of the study.

Table 3. Biochemical and anthropometric characteristics of the study groups from cohort 3.

	Non-T2D	Incident-T2D	*P Value*
N	32	32	-
Age (years)	60.88 ± 1.30	62.09 ± 1.29	0.508
WC (cm)	104.06 ± 1.84	103.44 ± 1.57	0.799
BMI (Kg/m^2)	29.94 ± 0.55	29.88 ± 0.63	0.941
TG (mg/dL)	102.38 ± 8.87	117.71 ± 10.14	0.259
Chol (mg/dL)	159.81 ± 5.72	156.52 ± 5.16	0.671
c-HDL (mg/dL)	44.42 ± 1.22	42.48 ± 1.23	0.269
hs-CRP (mg/L)	2.35 ± 0.53	2.66 ± 0.59	0.695
Glucose (mg/dL)	91.97 ± 1.87	95.19 ± 2.08	0.253
HbA1c (%)	5.78 ± 0.07	5.97 ± 0.08	0.069
Insulin (mU/L)	7.07 ± 0.78	8.80 ± 0.85	0.140
HOMA-IR (units)	2.36 ± 0.21	2.23 ± 0.19	0.640

Non-T2D, Subjects who did not develop T2D; **Incident-T2D**, subjects who developed T2D; **WC,** Waist circumference; **BMI**, body mass index; **TG**, triglycerides; **c-HDL**, high-density lipoprotein; **hs-CRP**, high-sensitivity C-reactive protein; **HbA1c**, glycosylated hemoglobin; **HOMA-IR**, homeostasis model assessment-insulin resistance.

Adipose tissue insulin resistance index (ATIRI) was determined for subjects from study cohort 3 according to the formula: ATIRI = fasting plasma NEFA (mM) x fasting plasma insulin (pmol/L), which has been proposed as a suitable and useful method in clinical practice to estimate adipose tissue insulin sensitivity (Ter Horst et al., 2017).

1.4. Study cohort 4

In this study, a total of 14 morbidly obese subjects (BMI >40 kg/m^2) undergoing BS were recruited at the Surgery Unit of the “Virgen del Rocío” University Hospital (HUVR; Sevilla, Spain), and monitored at the moment of the surgery intervention (Pre-BS), and approximately 1.5 years (15 ± 2 months) after (Post-BS), during plastic surgery interventions to reduce excess skin after weight loss. Anthropometrical and biochemical parameters were obtained as described (Martín-Rodríguez et al., 2014; Moreno-Castellanos et al., 2016). Exclusion criteria included acute or chronic inflammatory disease, malignant disease, asthma, or any history of alcohol or drug abuse. The Pre-

and Post-BS biochemical and anthropometric characteristics of the subjects are shown in **Table 4**.

Subjects were subclassified into two groups according to their obesity duration, [short-standing obese (SSO, n = 8), and long-standing obese (LSO, n = 6), with an average of 15 ± 2 and 32 ± 2 years of obesity medical history, respectively. The biochemical and anthropometric characteristics of the subjects at Pre- and Post-BS are shown in **Table 5**.

Table 4. Anthropometric and biochemical characteristics of studied subjects before (Pre-) and after (Post-) bariatric surgery (BS) from cohort 4.

	Pre-BS	**Post-BS**	***P value***
N	14	-	-
BS type (SG/RYGB)	9 / 5	-	-
Gender (female/male)	11 / 3	-	-
T2D diagnosis (n, %)	3 (21.4)	1 (7.1)	-
Lipid-lowering therapy (n, %)	3 (21.4)	2 (14.3)	-
Antidiabetic therapy (n, %)	4 (28.6)	1 (7.1)	-
Antihypertensive therapy (n, %)	5 (35.7)	3 (21.4)	-
Age (years)	42 ± 3	+16 ± 1 m	-
Body mass index (kg/m^2)	50.5 ± 1.7	32.9 ± 1.9	***
Fat mass (%)	51.4 ± 4.5	36.4 ± 3.6	*
Lean mass (%)	12.4 ± 0.5	18.4 ± 1.3	**
Water mass (%)	35.8 ± 1.2	45.2 ± 2.3	*
Waist circumference (cm)	133.5 ± 4.2	97.3 ± 4.5	***
Hip circumference (cm)	149.1 ± 3.7	116.0 ± 5.1	***
Waist to hip ratio (units)	0.90 ± 0.03	0.84 ± 0.02	*
Fasting glucose (mg/dL)	101.0 ± 9.5	79.3 ± 2.4	**
Fasting glucose (mmol/L)	5.61 ± 0.53	4.40 ± 0.13	**
Fasting insulin (mU/L)	24.5 ± 2.5	7.41 ± 1.32	***
HbA1c (%)	6.16 ± 0.28	5.29 ± 0.08	***
HbA1c (mmol/mol)	43.7 ± 3.0	34.2 ± 0.9	***
HOMA-IR index (units)	6.53 ± 1.29	1.46 ± 0.27	***
Total cholesterol (mg/dL)	195.1 ± 8.3	184.9 ± 7.8	ns
LDL cholesterol (mg/dL)	126.8 ± 9.3	110.4 ± 7.1	ns
HDL cholesterol (mg/dL)	45.8 ± 2.1	59.8 ± 3.6	**
Triglycerides (mg/dL)	116.0 ± 7.8	76.7 ± 6.4	**
Adiponectin (µg/mL)	46.7 ± 6.0	99.0 ± 11.1	***
FABP4 (ng/mL)	13.5 ± 1.2	11.5 ± 1.1	ns
C-reactive protein (ng/L)	14.4 ± 3.8	2.2 ± 0.7	***
PAI-1 (ng/mL)	54.3 ± 12.6	23.7 ± 9.1	ns
sTNFR-2 (ng/mL)	5.33 ± 0.37	4.98 ± 0.25	ns
Circulating DNA (ng/mL)	327.9 ± 116.2	582.5 ± 123.6	ns
Oxidized LDL (ng/mL)	258.5 ± 62.4	109.0 ± 17.0	*
TAS (mmol/L)	3.45 ± 1.16	19.97 ± 12.38	ns
GSH (µmol/g Hb)	5.84 ± 0.70	7.64 ± 0.60	ns
GSSG (µmol/g Hb)	0.41 ± 0.05	0.47 ± 0.10	ns
GPX (U/g Hb)	824.1 ± 523.4	1292 ± 672	ns
SOD (U/g Hb)	947.4 ± 28.3	992.4 ± 40.1	ns

Pre-BS, before bariatric surgery; **Post-BS,** after bariatric surgery; **HbA1c,** glycated haemoglobin; **HOMA-IR,** homeostasis model assessment of insulin resistance; **LDL,** low-density lipoprotein; **HDL,** high-density lipoprotein; **FABP4**, Fatty Acid-Binding Protein 4; **PAI-1**, plasminogen activator inhibitor type1; **sTNFR-2**, serum tumour necrosis factor receptor 2; **TAS**, total antioxidant status; **GSH**, glutathione; **GSSG**, glutathione disulphide; **GPX**, glutathione peroxidase. **ns,** no significant; *****P<0.05, ******P<0.01, *******P<0.001 Post-BS *vs.* Pre-BS.

Table 5. Anthropometric and biochemical characteristics of studied subjects before (Pre-) and after (Post-) bariatric surgery (BS) from cohort 4 subclassified according to obesity time evolution.

	Short-Standing Obese (SSO)			Long-Standing Obese (LSO)		
	Pre-BS	**Post-BS**	***P***	**Pre-BS**	**Post-BS**	***P***
N	8	-	-	6	-	-
BS type (SG/RYGB)	5 / 3	-	-	4 / 2	-	-
Obesity duration (years)	15 ± 2	-	-	32 ± 2 ^{aaa}	-	-
Gender (female/male)	5 / 3	-	-	6 / 0	-	-
T2D diagnosis (n, %)	0 (0)	0 (0)	-	3 (50)	1 (17)	-
Lipid-lowering therapy (n, %)	2 (25)	1 (13)	-	1 (17)	1 (17)	-
Antidiabetic therapy (n, %)	1 (13)	0 (0)	-	3 (50)	1 (17)	-
Antihypertensive therapy (n, %)	2 (25)	1 (13)	-	3 (50)	2 (33)	-
Age (years)	37 ± 3	+15 ± 2 m	-	48 ± 5	+16 ± 1 m	-
Body mass index (kg/m^2)	49.5 ± 2.9	30.0 ± 2.7	***	51.8 ± 1.1	36.2 ± 2.3	**
Fat mass (%)	50.1 ± 2.2	25.3 ± 5.0	***	53.0 ± 1.3	41.9 ± 2.7 ^{a}	ns
Lean mass (%)	12.4 ± 0.9	22.4 ± 2.2	**	12.3 ± 0.6	16.4 ± 1.0 ^{a}	ns
Water mass (%)	37.1 ± 2.6	52.3 ± 2.8	*	34.7 ± 0.8	41.7 ± 1.8 ^{a}	ns
Waist circumference (cm)	137.7 ± 6.7	92.8 ± 6.4	***	127.8 ± 4.5	105.2 ± 4.6	**
Hip circumference (cm)	147.2 ± 4.3	109.1 ± 5.7	***	151.6 ± 7.2	128.0 ± 7.8	*
Waist to hip ratio (units)	0.94 ± 0.04	0.85 ± 0.03	*	0.85 ± 0.04	0.82 ± 0.05	ns
Fasting glucose (mg/dL)	88.1 ± 4.9	75.2 ± 2.1	ns	118.1 ± 21.2	84.1 ± 4.3	*
Fasting glucose (mmol/L)	4.89 ± 0.27	4.17 ± 0.12	ns	6.56 ± 1.18	4.67 ± 0.24	*
Fasting insulin (mU/L)	23.9 ± 3.2	6.27 ± 1.99	*	25.1 ± 4.6	8.73 ± 1.70	**
HbA1c (%)	5.9 ± 0.2	5.1 ± 0.1	*	6.4 ± 0.6	5.4 ± 0.1	*
HbA1c (mmol/mol)	41.8 ± 2.1	32.7 ± 1.1	*	46.4 ± 7.0	36.0 ± 1.3	*
HOMA-IR index (units)	5.24 ± 0.72	1.14 ± 0.34	*	8.03 ± 2.66	1.83 ± 0.41	*
Total cholesterol (mg/dL)	198.5 ± 9.2	178.7 ± 10.9	*	190.6 ± 17.1	192.1 ± 12.4	ns
LDL colesterol (mg/dL)	128.7 ± 8.9	104.1 ± 8.6	*	124.2 ± 21.0	119.2 ± 3.3	ns
HDL cholesterol (mg/dL)	47.4 ± 2.8	61.2 ± 4.0	*	43.6 ± 3.0	57.8 ± 7.7	ns
Triglycerides (mg/dL)	117.0 ± 10.5	65.1 ± 7.0	**	116.1 ± 14.1	90.3 ± 9.3 ^{a}	ns
Adiponectin (ng/mL)	40.2 ± 6.7	110.3 ± 15.0	**	55.3 ± 11.1	85.7 ± 17.6	*
FABP4 (ng/mL)	10.9 ± 1.2	10.5 ± 1.0	ns	16.1 ± 1.5 ^{a}	12.6 ± 2.0	ns
C-reactive protein (ng/L)	16.6 ± 6.8	2.65 ± 1.30	*	11.4 ± 1.9	1.68 ± 0.33	**
PAI-1 (ng/mL)	67.3 ± 20.0	12.7 ± 6.3	ns	36.2 ± 8.0	36.4 ± 17.8	ns
sTNFR-2 (ng/mL)	5.14 ± 0.50	5.06 ± 0.44	ns	5.55 ± 0.56	4.89 ± 0.23	ns
Circulating DNA (ng/mL)	802.9 ± 173.1	431.6 ± 132.5	ns	394.5 ± 83.3	758.5 ± 208.3	ns
Oxidized LDL (ng/mL)	259.3 ± 95.3	104.5 ± 22.9	ns	257.5 ± 81.5	114.4 ± 27.5	ns
TAS (mmol/L)	3.92 ± 1.70	1.22 ± 0.04	ns	2.83 ± 1.62	40.8 ± 25.1	ns
GSH (µmol/g Hb)	6.04 ± 1.18	7.16 ± 0.87	ns	5.57 ± 0.60	8.20 ± 0.83	ns
GSSG (µmol/g Hb)	0.30 ± 0.06	0.40 ± 0.12	ns	0.57 ± 0.03 ^{aa}	0.56 ± 0.17	ns
GPX (U/g Hb)	1376 ± 888	59.1 ± 10.4	ns	88.1 ± 10.2	2730 ± 1259 ^{a}	ns
SOD (U/g Hb)	980.4 ± 43.0	918.1 ± 37.3	ns	903.4 ± 26.9	1079.0 ± 60.1	**

Pre-BS, before bariatric surgery; **Post-BS,** after bariatric surgery; **HbA1c,** glycated haemoglobin; **HOMA-IR,** homeostasis model assessment of insulin resistance; **LDL,** low-density lipoprotein; **HDL,** high-density lipoprotein; **FABP4**, Fatty Acid-Binding Protein 4; **PAI-1**, plasminogen activator inhibitor type1; **sTNFR-2**, serum tumour necrosis factor receptor 2; **TAS**, total antioxidant status; **GSH**, glutathione; **GSSG**, glutathione disulphide; **GPX**, glutathione peroxidase. ***P***, *P value*. **ns,** no significant; *****P<0.05, ******P<0.01, *******P<0.001 Post-BS *vs.* Pre-BS; ^{a}P<0.05, ^{aa}P<0.01, ^{aaa}P<0.001 *vs.* SSO group.

2. Biological material

2.1. Collection of serum samples

Serum samples were collected from participants of cohorts 3 and 4 as described (Jiménez-Lucena et al., 2018). Briefly, venous blood from the participants was collected in tubes containing EDTA or gelose. Then, the tubes were centrifuged at 2,000 x g for 10 min for plasma separation from blood cells, and plasma samples were frozen in liquid nitrogen and stored at -80 ºC for further analysis.

2.2. Collection and processing of human adipose tissue samples

Paired abdominal subcutaneous (SC) adipose tissue samples were collected from participants of cohort 4 during and 1.5 years after BS. Samples were frozen in liquid nitrogen and stored at -80 ºC for further analysis. Likewise, SC and omental (OM) adipose tissue samples were obtained from participants of cohorts 1 and 2, and they were processed to obtain the different cellular components.

Freshly isolated adipose tissue samples (from cohorts 1 and 2) were processed to isolate the mature adipocytes and the stromal-vascular fraction (SVF) as previously described (Díaz-Ruiz et al., 2015). Briefly, samples were washed with Dulbecco`s phosphate-buffered saline (D-PBS; Sigma-Aldrich; Madrid, Spain) to remove blood contaminants and mechanically dispersed in DMEM/F-12 (1:1) (Lonza; Basilea, Switzerland). Next, samples were enzymatically dispersed by incubation in DMEM/F-12 (1:1), containing 400 units/mL of collagenase type V (Sigma), at 37 ºC for 30 min in a shaking bath. Undigested tissue was removed by filtering through a sterile 100 μm pore Cell Strainer (BDFalcon; Glendale, AZ), and the remaining was centrifuged at 600 x g for 10 min to separate the floating mature adipocyte layer and the pelleted SVF. SVF was resuspended in DMEM/F-12 (1:1), filtered through a 40 μm pore Cell Strainer (BDFalcon), and centrifuged at 400 x g for 5 min. Then, pelleted SVF was resuspended in 500 µL of erythrocyte lysis buffer (Norgen Biotek Corp.; Thorold, Canada) and incubated for 3 min at room temperature (RT). After centrifugation at 400 x g for 10 min, SVF was frozen in liquid nitrogen and stored at -80 ºC for further analysis, and/or seeded onto culture flasks.

2.3. Culture and *in vitro* differentiation of human primary preadipocytes

Human preadipocytes were cultured and *in vitro* differentiated into adipocytes as previously described (Serena et al., 2016). Specifically, SVF cells, obtained from fresh SC and OM adipose tissue, were seeded in preadipocyte-proliferation medium [DMEM/F-12 (1:1) supplemented with 8 mM biotin, 18 mM d-pantothenate acid, 100 mM ascorbate, and 1% penicillin-streptomycin (Sigma)] with 10% new-born calf serum (NCS; ThermoFisher Scientific; Madrid, Spain), at 37 ºC in a humidified atmosphere with 95% air: 5% CO_2. The medium was replaced every 48 h until confluence. Once at confluence (i.e., ~80%), cells were detached with a trypsin-EDTA solution (Sigma) and sub-cultured at 4,000 cells/cm^2 2-3 times to purify and amplify the cell culture following established methods (Palumbo et al., 2018). Thereafter, 1 x 10^6 preadipocytes were collected, frozen in liquid nitrogen, and stored at -80 ºC for immunophenotyping analysis and proliferation studies, or directly induced for adipogenic differentiation, as indicated in detail in the following sections.

Preadipocytes were seeded at 4,000 cells/cm^2 in a preadipocyte proliferation medium until they reached 70-80% of confluence. Then (day 0 of differentiation), primary preadipocytes were differentiated using differentiation medium [preadipocyte-proliferation medium with 3% NCS, and 17.5 mM glucose] supplemented with 10 µg/mL insulin, 0.1 µM dexamethasone, 1 µM rosiglitazone, and 0.5 mM IBMX (Sigma) for the first 3 days. Then, the medium was removed and replaced by a differentiation medium supplemented with 10 µg/mL insulin and 0.1 µM dexamethasone for 3 more days (day 6), when the medium was refreshed and maintained until day 10. Adipogenesis was monitored by the appearance of doubly refractile lipid inclusions under light microscopy and images of the cultures were taken using a camera (Moticam 1080; Motic, Barcelona, Spain) coupled to the microscope. Experiments were carried out using cells from passages 3 to 4.

2.4. Culture and differentiation of adipocyte and macrophage cell lines

This Doctoral Thesis includes studies using three adipocyte cell lines and one macrophage cell line. Protocols of culture and differentiation are described below. All of them were tested for mycoplasma contamination and incubated at 37 ºC in a humidified atmosphere with 95% air: 5% CO_2. Adipogenesis and macrophage polarization were monitored by the appearance of doubly refractile lipid inclusions and cellular appearance, respectively, under light microscopy and images of the cultures were taken. *In vitro* experiments were undertaken using cells from passages 3 to 20.

2.4.1. Simpson-Golabi-Behmel Syndrome (SGBS) cell line

SGBS cell line, a human-derived preadipocyte cell line isolated from the SVF of SC adipose tissue from a 3-months male infant with Simpson-Gobali-Behmel syndrome, was kindly donated by Prof. Dr. José Manuel Fernández-Real (Institut d'Investigació Biomèdica; Girona, Spain). This cell model has been largely used in studies pertaining to preadipocytes and differentiated adipocytes (Kalkhof et al., 2020). SGBS cells growth and differentiation into adipocytes were performed as previously described (Moure et al., 2016). Cells were seeded at a density of 4,000 cells/cm^2 and proliferated to 80% confluence in basal medium: DMEM/F12 (1:1) (Thermo), supplemented with 32.7 µM biotin, 16.78 µM d-pantothenic acid, and 1% penicillin-streptomycin.

Confluent cells (day 0 of differentiation) were differentiated in differentiation medium [serum-free basal medium supplemented with 0.01 mg/mL human transferrin, 20 nM human insulin, 100 nM hydrocortisone, 0.2 nM 3,3',5-triiodo-l-thyronine (T3) (Sigma), 25 nM dexamethasone, 0.5 mM IBMX, and 2 µM rosiglitazone] for the first 4 days. Next, the medium was removed and replaced by a differentiation medium supplemented with 0.01 mg/mL human transferrin, 20 nM human insulin, 100 nM hydrocortisone, and 0.2 nM T3 for 6 days (day 10). Then, the medium was refreshed, and cells were maintained in culture until day 14. The differentiation process was also monitored by Oil Red-O staining and expression analysis of known markers of adipogenesis (*PPARG*, *SREBF1*) and LD biogenesis and growth (*CIDEC*) (**Figure 23**).

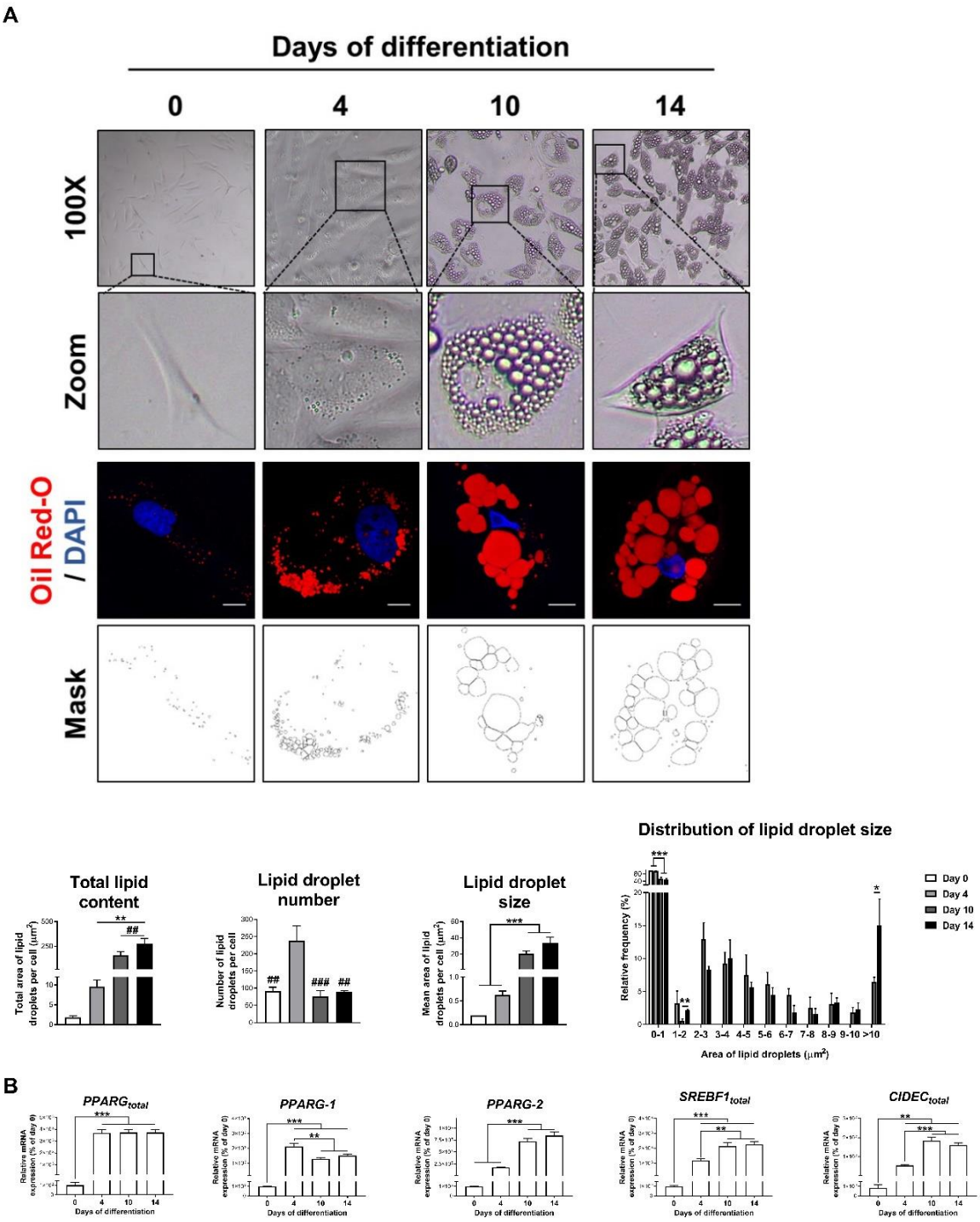

Figure 23. Representative light and confocal micrographs, and LD morphometrical analysis **(A)**, and mRNA levels of the genes indicated **(B)** in SGBS cells during differentiation (days 0-14). *****P<0.05, ******P<0.01, *******P<0.001 *vs.* previous days; ##P< 0.01, ###P<0.001 *vs.* day 4. Cells were stained with Oil-Red O (LDs, red) and DAPI (nuclei, blue). Scale bar = 10 µm.

2.4.2. Human adipose-derived stem cells (hADSCs)

Studies with hADSCs were carried out in the Lipid Laboratory lead by Prof. Dr. Mikael Rydén at the Karolinska Institutet (KI; Stockholm, Sweden). hADSCs were isolated from

SC adipose tissue of a male lean donor (aged 16 years, BMI 24 kg/m^2). This cell model was developed and validated in previous works (Rodriguez et al., 2005). Cells were isolated, propagated, and differentiated into adipocytes (H. Gao et al., 2017). Cells were cultured at 20,000 cells/cm^2 in proliferation medium [DMEM with 1 g/L glucose (Panreac AppliChem; Barcelona, Spain), supplemented with 1% hepes buffer 1 M (Thermo), 0.5% penicillin (10,000 U/mL) / streptomycin (10,000 µg/mL) (Thermo), and 10% fetal bovine serum (FBS; Thermo)] with 2.5 ng/mL FGF2 (Sigma). Cells were maintained until reaching 80% of confluence and the medium was replaced for proliferation medium without FGF2 for one more day.

Cells at day 0 of differentiation were differentiated in differentiation medium [serum-free proliferation medium:Ham's F12 (1:1) (Thermo)] supplemented with 5 µg/mL human insulin, 10 µg/mL transferrin, 0.2 nM T3, 1 µM rosiglitazone (CaymanChemical; Ann Arbor, MI), 100 µM IBMX, and 1 µM dexamethasone (Sigma) for 3 days. Next, the medium was removed and replaced by a differentiation medium supplemented with 5 µg/mL human insulin, 10 µg/mL transferrin, 0.2 nM T3, and 1 µM rosiglitazone. The medium was refreshed each 2-3 days until the day of the experiments.

2.4.3. 3T3-L1 cell line

3T3-L1 cells were purchased from ATCC (Manassas, VA). Cells were cultured and differentiated into adipocytes according to our previously established protocols (Moreno-Castellanos et al., 2017). Briefly, cells were seeded at a density of 3,000 cells/cm^2 and proliferated until 80% of confluence in maintenance medium [DMEM 4.5 g/L glucose (Thermo) with 4 mM L-glutamine (Sigma), 1.5 g/L sodium bicarbonate, and 1% antibiotic-antimycotic (Sigma)], supplemented with 10% NCS.

Then, cells (at day 0 of differentiation) were cultured in differentiation medium [maintenance medium with 10% FBS supplemented with 0.5 mM IBMX, 0.25 µM dexamethasone, and 10 µg/mL bovine insulin (Sigma)] for 72 h (day 3). Next, the medium was replaced by a differentiation medium supplemented with 10 µg/mL bovine insulin for 72 h (day 6), and by a differentiation medium without hormones for 4 more days (day 10).

2.4.4. THP-1 cell line

THP-1 cells were purchased from ATCC and grown in RPMI-1640 culture medium (Biowest; Nuaillé, France) supplemented with 10% FBS, 2 mM L-glutamine, 4,500 mg/L glucose, and 1% penicillin/streptomycin, following the supplier's recommendations. To

induce macrophage differentiation, THP-1 cells were transferred to RPMI-1640 medium supplemented with 3% FBS, 2 mM L-glutamine, 4,500 mg/L glucose, and 1% penicillin/streptomycin, seeded in 12-well plates at $2x10^5$ cells/mL, and treated with 10 ng/mL Phorbol 12-Myristate 13-Acetate (PMA; Sigma) for 48 h.

2.5. Isolation of extracellular vesicles

We analysed the release of extracellular vesicles (EVs), including exosomes, to the culture media by 3T3-L1 cells at day 0 and 10 of differentiation, and at day 6 of differentiation upon exposure to TNFα (5 nM) or control medium (24 h). EVs were isolated following established methods (Théry et al., 2006). Serum-free culture media was employed to avoid contamination from FBS and the culture media corresponding to a 24 h-period was collected and centrifuged at 300 x g for 10 minutes to remove cells in suspension. Thereafter, supernatants were centrifuged at 2,000 x g for 20 minutes and at 10,000 x g for 30 minutes to remove cell debris. Finally, supernatants were ultracentrifuged at 100,000 x g for 1 h to pellet EVs. All centrifugations were performed at 4 ºC. EVs pellets were resuspended in 1 mL sterile PBS, stored at 4 ºC, and utilized within 1 week of isolation for subsequent analysis.

3. Silencing and overexpression studies

3.1. *PRPF8*/PRP8 silencing

In this study, one component of the major spliceosome, Pre-MRNA Processing Factor 8 (*PRPF8*), was selected for its further characterization in adipocytes. To this end, we performed silencing studies in SGBS cells and hADSCs. SGBS preadipocytes, cultured on 6-wells or 12-wells plates, were stably transfected at day 4 of differentiation with targeted double-stranded siRNA oligonucleotides against *PRPF8* or a specific negative control siRNA (Thermo) using Lipofectamine RNAiMAX Transfection Reagent (Invitrogen; Carlsbad, CA), following manufacturer's instructions. Transfection efficiency was checked by RT-PCR, western blotting, or by cotransfecting cells with the N-terminal end of phrGFP-N1 (Agilent Technologies; Santa Clara, CA), as a reporter (Moreno-Castellanos et al., 2017) using Lipofectamine 2000 Transfection Reagent (Invitrogen). Briefly, the cells were washed twice with D-PBS and submerged into 1 mL of OPTI-MEM™ medium (Thermo), containing 100 nM of the corresponding siRNA and, when required, 3 µg of phrGFP-N1 during 24 h. Thereafter, the transfection medium was

removed, and a fresh culture medium was added. Finally, after 3-5 days of transfection, silenced cells were stained with Oil Red-O. The effects of *PRPF8* silencing were also explored by RT-PCR and quantitative immunoblotting. In another series of experiments, siRNA-treated cells were exposed to 100 mM insulin for 15 min.

hADSCs were transfected one day before differentiation induction through electroporation by Kit Neon™ Transfection System (Invitrogen) (Kim et al., 2008). The cells were trypsinised and washed with D-PBS (without Ca^{2+} and Mg^{2+}; Thermo) and resuspended in resuspension buffer R at a final density of 1 x 10^6 cells/mL. The NEON system (Invitrogen) 10-µL electroporation tips were used with 1 x 10^6 cells per reaction. One pulse (1,200 V, 40 ms) was used to transfect a final concentration of 40 nM siRNA to cells, which were seeded in a medium without antibiotic/antimycotic. Twenty-four h after electroporation, the medium was replaced, and differentiation started following the standard protocol. Finally, the effects of *PRPF8* silencing were evaluated at different days of differentiation (7 or 10), after 3 or 5 days of transfection, respectively.

3.2. *PRPF8*/PRP8 and BIP overexpression

Rescue experiments were carried out by overexpressing *PRPF8* in SGBS cells silenced for this splicing-related gene. To be more specific, SGBS preadipocytes, cultured on 6-wells or 12-wells plates, were stably transfected at day 4 of differentiation with a plasmid vector coding for *PRPF8* (PRPF8-pcDNA3.1; Thermo), its corresponding empty plasmid vector alone (pcDNA3.1; Invitrogen) as a negative control, or co-transfected with PRPF8-pcDNA3.1 and PRPF8-siRNA (PRPF8-pcDNA3.1+PRPF8-siRNA) using Lipofectamine 2000 Transfection Reagent following manufacturer's instructions. The effects of *PRPF8* recovery were evaluated after 3-5 days of transfection.

In another set of experiments, SGBS preadipocytes were stably transfected with a plasmid vector coding for BIP (pCMV BiP-Myc-KDEL-wt; AddGene; Watertown, MA) or its corresponding empty vector (pCMV-Myc; Clontech Laboratories; Mountain View, CA). Briefly, the cells were washed twice with D-PBS and submerged into 1 mL of OPTI-MEM™ medium containing 3 µg of corresponding plasmid vector during 24 h. Thereafter, the transfection medium was removed, and a fresh culture medium was added. The effects of *BiP* overexpression were evaluated after 3 days of transfection (day 7 of differentiation).

Expression efficiency upon transfection was explored by RT-PCR, and/or quantitative immunoblotting. All constructs were verified by DNA sequencing.

3.3. *miR-223-3p* overexpression

Overexpression studies were also carried out to evaluate the effects of *miR-223-3p* in adipocytes. Briefly, the mirVana miRNA mimic *hsa-miR-223-3p*, or miRNA control mirVana miRNA Negative Control #1 (Thermo) were transfected into 3T3-L1 cells using different methodologies according to the differentiation state. To be more specific, transfection was carried out in cells at day 3 of differentiation, whereas electroporation was performed at day 6 of differentiation in order to increase the efficiency of gene transfer. In both cases, the transfection efficiency was checked by the co-transfection of the Cye3™-labeled Pre-miR™ Negative Control #1 (Thermo) designed for monitoring uptake of Pre-miR™ miRNA Precursors by fluorescence microscopy, or with a phrGFP-N1 empty vector (Invitrogen), as a reporter in confocal, and RT-PCR studies (Moreno-Castellanos et al., 2017).

***Transfection of 3T3-L1 cells*:** 3T3-L1 preadipocytes were transfected at day 3 of differentiation using 1 mL of OPTIMEM medium containing Lipofectamine 2000 or RNAiMAX Reagent and 30 nM of the corresponding miRNA during 24 h. Next, the transfection medium was removed, and a fresh culture medium was added. Finally, the effects of *miR-223-3p* overexpression were evaluated 72 h after transfection (day 5 of differentiation).

***Electroporation of 3T3-L1 cells*:** 3T3-L1 adipocytes were transfected at day 6 of differentiation through electroporation using our established protocol (Pulido et al., 2011). Cells cultured on 150-mm dishes were mechanically resuspended, washed with D-PBS, and submerged into 100 µL D-PBS containing 100 nM of the corresponding miRNA. Electroporation was performed in 2-mm thick electroporation cuvettes using a Gene Pulser Xcell (Bio-Rad Laboratories; Hercules, CA), which delivered a 500 µF pulse at 110 V. After electroporation, cells were seeded in the medium. Twenty-four h after electroporation, the medium was replaced and finally, the effects of *miR-223-3p* overexpression were evaluated 72 h after electroporation (day 8 of differentiation).

4. *In vitro* models and experimental treatments

4.1. Obesogenic insults

We have previously developed several *in vitro* models mimicking obesogenic conditions (Díaz-Ruiz et al., 2015). Herein, SGBS and 3T3-L1 cells were exposed to a combination of high glucose (4.5 g/L) and insulin (100 nM) (HGHI), to mimic the

hyperglycaemia and hyperinsulinemia characteristic of the patients with IR (Stumvoll et al., 2010); 5 nM of the inflammatory cytokine, tumor necrosis factor α (TNFα; Sigma), whose expression in adipose tissue has been associated with obesity-linked IR (Hotamisligil et al., 1993); 500 μM of saturated (palmitate, C16:0) and unsaturated (oleate, C18:1) fatty acids (Sigma), to mimic the lipid-overloaded, enlarged adipocytes that appear in obesity-related IR (Kim et al., 2015). The TNFα model was also employed for studies in THP-1 cells.

To guarantee cell viability, the different treatments were adapted to the nature of the culture. SGBS cells were exposed for 30 h to the four models at day 4 of differentiation. On the other hand, 3T3-L1 cells at day 3 and 6 of differentiation were exposed to pre-treatment medium (without FBS) for 2 h, and then to TNFα for 24 h. Palmitate and oleate were dissolved in methanol and ethanol, respectively, and diluted in a pre-treatment medium containing 2% fatty acid-free bovine serum albumin (BSA; Sigma). Parallel sets of cells were used to obtain control responses in the presence of the solvent.

4.2. Adipocyte culture in a 3D model of fibrosis

We have recently developed a 3D model of fibrosis consisting of collagen I-enriched hydrogels supplemented with the proteoglycan, lumican, which mimics the composition of the extracellular matrix of SC adipose tissue of IR, as compared to NG obese individuals (Guzmán-Ruiz et al., 2020). Culture in the fibrotic 3D matrix containing lumican impairs adipogenesis and decreases lipid accumulation in 3T3-L1 adipocytes (Guzmán-Ruiz et al., 2020). In the present study, we prepared 3D cultures of 3T3-L1 cells by mixing with 3.6 mg/mL collagen type I (COL-I; Thermo) solution. Cells were seeded onto 24-well plates and differentiated following our standard protocol in the absence or presence of lumican (10 or 30 ng/mL; R&D Systems; Minneapolis, MI). The medium was renewed every 3 days until day 10 when cells were processed for RT-PCR studies. We could not replicate these experiments in SGBS cells because cell viability was severely compromised when these cells were grown in 3D collagen I-enriched matrices (**Figure 24**).

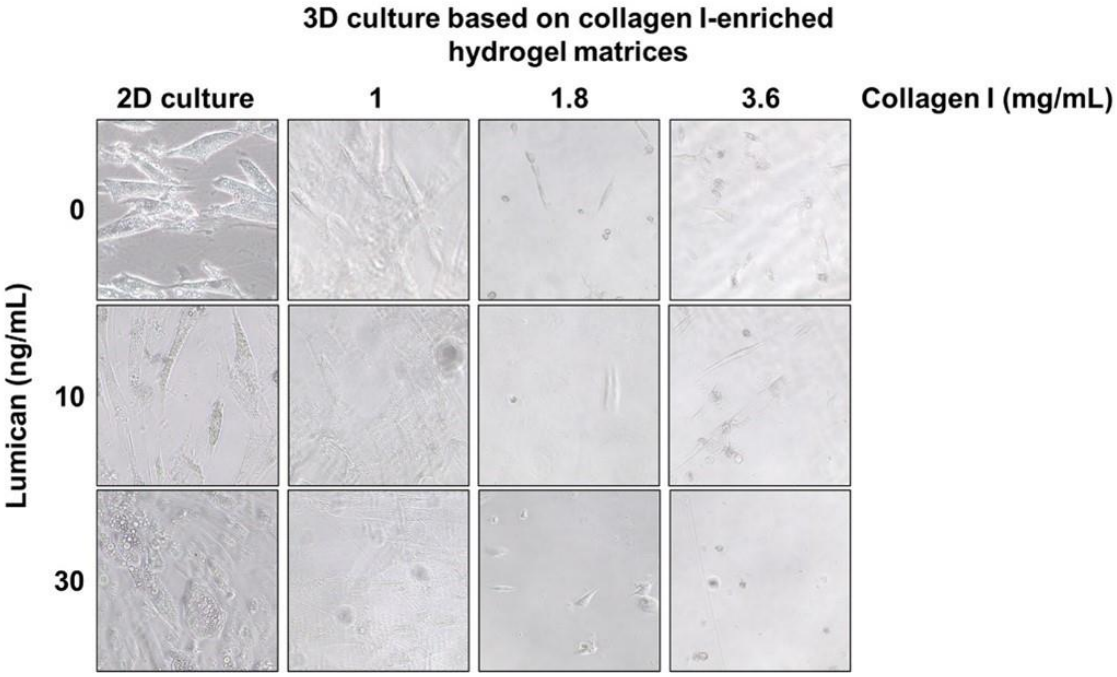

Figure 24. Representative light microscopy images of SGBS adipocytes differentiated in conventional 2D or 3D culture based on hydrogel matrices enriched in collagen I (1-3.6 mg/mL) containing increasing concentrations of lumican (0-30 ng/mL).

4.3. Exposure of cells to conditioned media.

To elucidate the response of adipocytes to circulating factors, SGBS and 3T3-L1 adipocytes (at day 14 and 10 of differentiation, respectively) were exposed for 24 h to medium containing 10% heat-inactivated serum from study subjects (cohorts 3 and 4) following our previously established protocols (Arias de la Rosa et al., 2018). 3T3-L1 cells were exposed for 2 h to a pre-treatment medium before serum treatment.

4.4. Effects of splicing inhibition on adipogenesis

To evaluate the effects of splicing inhibition in adipocyte function, we employed Pladienolide B. Pladienolide B is a natural product produced by *Streptomyces platensis* (Mizui et al., 2004) (**Figure 25A**), which directly binds to the splicing factor 3b (SF3b) in the spliceosome (Kotake et al., 2007), and inhibits the splicing process through interfering with the proper recognition of the branch site (BS) region of the intron (Cretu et al., 2018) (**Figure 25B**). SGBS cells at day 4 of differentiation were treated with Pladienolide B (Santa Cruz Biotechnology; Dallas TX) or vehicle and incubated for 24 hours (Jiménez-Vacas et al., 2019). Pladienolide B was initially used in the 10^{-11} M to 10^{-7} M range, being 10^{-8} M the higher dose that did not compromise cell viability.

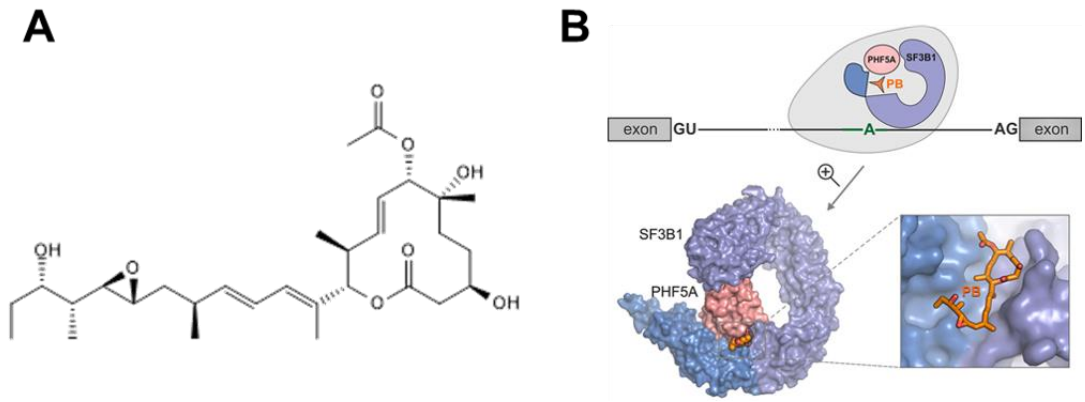

Figure 25. (A) Chemical structure of Pladienolide B (data sheet). **(B)** Surface representation of Pladienolide B (orange) in the Sf3B1 (blue), and PHF5A (pink) pocket bonded to SF3B, preventing the formation of the BS-binding pocket (Cretu et al., 2018).

4.5. Insulin signalling studies

To investigate the response to insulin in SGBS and 3T3-L1 cells under the different experimental conditions tested in this Doctoral Thesis, the levels of phosphorylation of specific enzymes involved in insulin signalling were evaluated. For this, cells were exposed for 2 h to pre-treatment medium [DMEM 1g/L glucose with 4 mM L-glutamine, 1.5 g/L sodium bicarbonate, 1% antibiotic-antimycotic but without serum] and then, with 100 nM insulin for different short-time periods (0, 5, 15, and 30 min). At the end of the experiments, cells were recovered from the culture plates, and protein extracts were prepared and analysed by immunoblotting.

5. Gene expression analysis

5.1. RNA extraction

RNA was extracted through different methodologies according to the nature of the sample. In all cases, the samples were treated with DNase (Qiagen; Hilden, Germany), and both RNA integrity and concentration were assessed using a NanoDrop2000 or DS-11 spectrophotometer (Thermo) at the Genomics Unit of the UCAIB of the IMIBIC and frozen at -80 ºC. The quality of the samples was considered optimal when the 260/280 nm absorbance ratio was between 1.60 and 2.20 units.

For human preadipocytes and hADSC, total RNA isolation and purification was performed using the RNeasy kit (Qiagen). Total RNA isolation and purification was performed for adipose tissue, SVF and cell lines following our established protocols

(Pulido et al., 2011). 20 mg of tissue samples were disrupted in TRIzol Reagent Reagent (Invitrogen). Then, 200 µL chloroform (Sigma) per mL of TRIzol were added and mixed. After centrifugation at 12,000 x g for 15 min at 4 ºC, the aqueous phase containing the RNA was separated from the organic phase containing DNA and proteins and collected. The RNA was then precipitated with isopropanol (Sigma) incubation for 15 min, maintaining a 1:1 ratio with the amount of sample collected and 1 µL of glycogen (Qiagen). The RNA was pelleted after a 12,000 x g centrifugation for 10 min at 4 ºC, washed with 1 mL 75% ethanol (Panreac), and reconstituted in 11 µL of RNAse-free water (Qiagen).

5.2. Retrotrancription

One µg of RNA was retrotranscribed to cDNA (Peinado et al., 2010) using the Revertaid First Strand Synthesis kit (Thermo) or iScript cDNA Synthesis Kit (Bio-Rad). A sample without RNA was always prepared as a control.

5.3. Primer design and validation

Primers were selected using Primer3 software and StepOneTM Real-Time PCR System software v2.3, with selection parameters set to identify primer pairs that: 1) span an intron (when possible), 2) differ by no more than 1 ºC in annealing temperature, 3) are at least 20 bp in length, 4) have a GC content between 45 and 55%, and 5) do not form primer-dimers. Sequences of selected primers were used in BLAST (NCBI) searches to check for potential homology to sequences other than the designated target. Primers were purchased from Metabion (Munich, Germany) or STAB Vida (Caparica, Portugal).

Initial screening of primer efficiency using real-time detection was performed by amplifying 2-fold dilutions of RT products, where optimal efficiency was demonstrated by a difference of one cycle threshold between dilutions and a clear melting peak followed by a graded temperature-dependent dissociation to verify that only one product was amplified. The thermocycling profile consisted of 1) 95 ºC for 1 min; 2) 35 cycles of denaturing (95 ºC for 5 s) and annealing/extension (60 ºC for 20 s); and 3) a last cycle where final PCR products were subjected to graded temperature-dependent dissociation (60 ºC to 95 ºC for 20 s, increasing 1 ºC / 3 s). PCR products were then column purified (Thermo). The primers for splicing-machinery components used for the qPCR dynamic array are listed elsewhere (Gahete et al., 2018), and those used for quantitative RT-PCR are listed in **Table 6**.

Table 6. Sequences and transcript sizes of primers used in quantitative RT-PCR. **bp,** base pairs.

	Primer sequences (5' → 3')		
Gene (NCBI reference)	**Forward**	**Reverse**	**Size (bp)**
Hsa 18S (Bialesova et al., 2017)	TGACTCAACACGGGAAACC	TCGCTCCACCAACTAAGAAC	-
Hsa ACTB (NM_001101.3)	ACTCTTCCAGCCTTCCTTCTT	CAGTGATCTCCTTCTGCATCC	176
Hsa ADIPOQ (NM_009605.4)	TGGAGAAGCCGCTTATGTGT	GTCCCGGAATGTTGCAGTAG	159
Hsa GRP78/BiP (X87949.1)	CTATGAAGCCCGTCCAGAAA	GTCGAGCCACCAACAAGAAC	85
Hsa BSCL2-1 (NM_001122955.3)	TCAGATCCTGGAGCATACCAA	CAGGCAGTGAACTAGCGACA	94
Hsa BSCL2-2/3 (KU178595.1)	GCCTCCTGCTATTTGGCTTT	TCTTCAGGGCTCTCACCATC	309
Hsa CCL2 (NM_002982.4)	CTGGACAAGCAAACCCAAAC	GGGGAAAGCTAGGGGAAAA	90
Hsa CD206 (NM_002438.4)	ATGGATGGAAGCAAAGTGGA	TATGTCGCTGGCAAATGAA	154
Hsa CD80 (NM_005191.4)	CACCATCCAAGTGTCCATACC	GTCAGCACCATTTTCTTCTCCT	196
Hsa CIDEB-1 (NM_001318807.2)	GCCTACAGCCTGCCTCTTTT	TTGTGTTTGAGGTGGGGTCT	72
Hsa CIDEB-2 (NM_014430.3)	GGGCCTACAGGACACAGAAA	TGGACGTGACAGAGATGTGAA	237
Hsa CIDEC-5 (NM_001321142.2)	GAGGCTGTGAGGGGGAGAA	CTTGTCAGCTGGACTGCGTT	154
Hsa CIDE$_t$ (NM_001321142.2)	ATGGGAGAGAGGAGGCTTTG	CACTGACACATGCCTGGAGA	147
Hsa DERL1 (NM_001134671.2)	AAGACAAGCAGCGGATGAAG	AGGAAACAAACACCCAGCAA	175
Hsa FABP4 (NM_001442.3)	TGCAGCTTCCTTCTCACCTT	GGCAAAGCCCACTCCTACTT	134
Hsa FABP5 (DN991192)	GAAGGAGCTAGGAGTGGGAATAG	TCTCTCCCAGGGTACAAGAAAA	146
Hsa GAPDH (NM_002046.5)	AATCCCATCACCATCTTCCA	AAATGAGCCCCAGCCTTC	122
Hsa HPRT (S79316.1)	TAATCCAGCAGGTCAGCAAAG	CTGAGGATTTGGAAAGGGTGT	157
Hsa HRD1 (AB085847.1)	TGATGGGCAAGGTGTTCTTT	GCCAGTGGAAACATTTGAGG	177
Hsa IL-1β (NM_000576.2)	GGACAGGATATGGAGCAACAA	TCATCTTTCAACACGCAGGA	131
Hsa IL-10 (NM_000572.3)	AGAACCAAGACCCAGACATCAA	AAGGCATTCTTCACCTGCTC	142
Hsa KI67 (NM_002417)	GACATCCGTATCCAGCTTCCT	GCCGTACAGGCTCATCAATAAC	233
Hsa NOVA1 (NM_002515.2)	TACCCAGGTACTACTGAGCGAG	CTGGTTCTGTCTTGGCCACAT	124
***Hsa γORF4* (Aprile et al., 2014)**	AAACCCAAAACAACTTCCCG	CTTGCAGTGGGGATGTCTCA	279
Hsa PDGFRA (NM_006206.6)	CCTTTTTGTGACGGTCTTGG	AAAGGCTACATCTGGGTCTGG	148
Hsa PPARG-2 (NM_015869.4)	AGGAGTGGGAGTGGTCTTCC	TTTTAACGGATTGATCTTTTGC	255
Hsa PPARG-3 (NM_138711.3)	TGGGTGTGTAGTCGTGGTACTTT	CTCGGTTACTCCCCGTTTCT	82
Hsa PPARG-4 (NM_005037.6)	GCCGTGGCCGCAGAAA	CCACGGAGCTGATCCCAAAG	76
***Hsa PPARG$_t$* (Aprile et al., 2014)**	ATGGCCACCTCTTTGCTCT	GAGAAGGAGAAGCTGTTGGC	272
Hsa RAD23A (D21235.1)	TGGCCCAAATCTTTCCATC	TGAGCTGATGTTAGCCCTTCTC	100
Hsa RNF185 (NM_152267.3)	CAACAGGACCCCAGAGAGAA	CCACCATCTCCAAATCCAAA	101
Hsa SEC61A1 (NM_013336.3)	GAGTGGACCTGCCAATCAAG	AGCTGAGAGCATTTGGGAGA	146
Hsa SEL1L (AF052059.1)	CCTGCCACTTCCCTTTTCTT	CCATTTCTGCTTCCTGCATC	180
Hsa SREBF1-1 (NM_001005291.3)	GACCGACATCGAAGGTGAAG	GGTCAAATAGGCCAGGGAAG	158
Hsa SREBP1$_t$ (NM_001005291.3)	AGCTCAAGGATCTGGTGGTG	TGTGTTGCAGAAAGCGAATG	93
Hsa STT3A (NM_001278503.1)	AGCTATGGCAAACCGAACAA	CCTCCAAAAATGACCAGCAC	153
Hsa STT3B (NM_178862.2)	CCCTCCTCCTTTTTCTTCCTC	ACGACTTGTGCTTGCTCTCC	153

Hsa TGFB1 (NM_000660.6)	GCAACAATTCCTGGCGATAC	CTAAGGCGAAAGCCCTCAA	136
Hsa TNFα (NM_000594.4)	CGTGGAGCTGAGAGATAACCA	GCTCTTGATGGCAGAGAGGA	178
Hsa UBQLN1 (NM_013438.4)	CAACACACCAGGAATGCAGA	CTTCTCATGTAGGGGGCAGA	90
Hsa UPK3B (NM_030570.3)	TGCACTCAGGAGGGTTTAGG	ATGGTGGAGCAGGAGAGACA	135
Hsa XBP1s (NM_001079539.1)	TGGATGCCCTGGTTGCT	CACCTGCTGCGGACTCA	87
Hsa XBP1u (NM_005080.3)	CGCAGCACTCAGACTACGTG	CTGGGTCCAAGTTGTCCAGA	147
Mmu Acly (NM_001199296.1)	CACCTCCAAGAAGCCAAATC	CCAATGAAGCCCATACTCCTT	87
Mmu Actb (NM_007393.5)	GCCTTCCTTCTTGGGTATGG	AGCACTGTGTTGGCATAGAGG	108
Mmu Ago2 (NM_153178.4)	ATGCCTTCAAACCTCCACCT	TGCTCCACAATTTCCCTGTT	169
Mmu Agpat3 (NM_053014.3)	CCTCATCCTGACGTTCTTGG	CGCATCAGGTTATGGGTGTT	69
Mmu Atgl (NM_001163689.1)	ATGGTCCTCCGAGAGATGTG	AGGGTTGGGTTGGTTCAGTAG	68
Mmu Bscl2 (NM_001136064.3)	CGTGATCGGGTACTGATGTATG	CACTGAGCGTGAAGAAGTGG	57
Mmu Cd36 (NM_001159558.1)	GGCAAAGAACAGCAGCAAA	CAACAGACAGTGAAGGCTCAAA	73
Mmu Cd63 (NM_001042580.1)	CAAGGAATCCACTATCCATACCC	TTCCCAAGACCTCCACAAAA	119
Mmu Cebpa (NM_001287523.1)	GTGGACAAGAACAGCAACGA	TCACTGGTCAACTCCAGCAC	128
Mmu Cidea (NM_007702.2)	ATGGGATTGCAGACTAAGAAGG	TAACCAGGCCAGTTGTGATG	47
Mmu Cidec (NM_178373.4)	TCCCAGAAGCCAACTAAGAAGA	CAGGTCATAGGAAAGCGAGTATG	54
Mmu Dgat2 (NM_026384.3)	CTACTCCAAGCCCATCACCA	CAGTTCACCTCCAGCACCTC	50
Mmu Fabp1 (NM_017399.5)	ATCCGTCTGGTCAAGGTCAA	GGGCAATCTTCTTGTTGGTG	69
Mmu Fabp4 (NM_024406.3)	AAGAAGTGGGAGTGGGCTTT	CTGTCGTCTGCGGTGATTT	84
Mmu Fabp5 (NM_010634.3)	AGGATCTCGAAGGGAAGTGG	CTCGGTTTTGACCGTGATGT	44
Mmu Fasn (NM_007988.3)	ATACAATGGCACCCTGAACC	TTACAGAGGAGAAGGCCACAA	159
Mmu Gapdh (NM_001289726.1)	GTGGCAAAGTGGAGATTGTTG	CTCCTGGAAGATGGTGATGG	164
Mmu Glut4 (AB008453.1)	AAGAGTCTAAAGCGCCTGACC	TTGGACGCTCTCTCTCCAAC	94
Mmu hnrnpa2b1 (NM_016806.3)	GCGATGGAGAGAGAAAAGGAA	GATCCCGCATAACCACACA	133
Mmu Hprt (NM_013556.2)	TGGATACAGGCCAGACTTTGTT	TTGCGCTCATCTTAGGCTTT	153
Mmu Hsl (NM_010719.5)	TCTAAATCCCACGAGCCCTAC	AAGGCATATCCGCTCTCCA	69
Mmu Insr (NM_010568.3)	GTTCAAGACCAGACCCGAAG	TCCAGACCATAGACACGGAAG	155
Mmu Lpl (NM_008509.2)	AGCCAAGAGAAGCAGCAAGA	CCATCCTCAGTCCCAGAAAA	72
Mmu Mgl (NM_001166251.1)	TCCACAGAATGTTCCCTACCA	GCTCATCATAACGGCCACA	80
Mmu Pck1 (NM_011044.3)	CTTTGGAAGCGGATATGGTG	TGCCTTCGGGGTTAGTTATG	59
Mmu Plin1 (NM_175640.2)	TGACGACCAGACAGACACAGA	TCACTGCGGAGATGGTGTT	51
Mmu Pparg (NM_001127330.2)	GCCTCCCTGATGAATAAAGATG	AGGCTCCATAAAGTCACCAAAG	108
Mmu Prpf8 (NM_138659.2)	TACATGACGGCCAAGAACAA	TGCAATCCCAGTACAAGCAA	146
Mmu Scd1 (NM_009127.4)	CAAAGAGAAGGGCGGAAAA	AGCACCAGAGTGTATCGCAAG	89
Mmu Srebf1 (NM_011480.4)	AGGTCACCGTTTCTTTGTGG	AATACAGTTCAACGCTCGCTCT	151
Mmu Ybx1 (NM_011732.2)	GTCATCGCAACGAAGGTTTT	TCAAACTCCACAGTCTCTCCATC	176

5.4. Real time PCR (RT- PCR)

5.4.1. Digital RT-PCR

For the analysis of splicing machinery components in SC and OM preadipocytes from NG, IR, and T2D obese subjects, a 48.84 Dynamic Array based on microfluidic technology (Fluidigm; South San Francisco, CA) was implemented (Gahete et al., 2018). Specifically, the expression of 48 transcripts was determined, including components of the major (n = 13) and minor spliceosome (n = 4), associated splicing factors (SFs; n = 28), and 3 housekeeping genes (*ACTB*, *GAPDH*, and *HPRT*) in 36 samples (n = 6 per group), simultaneously. The panel of splicing machinery components was selected on the basis of two main criteria: 1) the relevance of the given spliceosome components in the splicing process (such as the components of the spliceosome core), and 2) the demonstrated implication in the regulation of splicing variants implicated in the pathophysiology of T2D (as it is the case for the 28 splicing factors selected in this study).

Generation of standard curves: Standard curves were generated (del Río-Moreno et al., 2019). The concentration of purified products was determined, and PCR products were serially diluted to obtain standards containing 1, 10^1, 10^2, 10^3, 10^4, 10^5, and 10^6 copies of the synthetic template. Standards were then amplified by qPCR, and standard curves were generated using Stratagene Mx3000p software (Thermo). The slope of a standard curve for each template examined was approximately -3.33 ($R2 \approx 1$), indicating that the efficiency of amplification of our primers was 100%, meaning that all templates in each cycle were copied.

qPCR dynamic array based on microfluidic technology: 12.5 ng of cDNA of each sample were pre-amplified using 1 µL of all primers mix (500n M) in a T100 Thermal cycler (Bio-Rad), using the following program: 1) 2 min at 95 ºC; 2) 15 s at 94 ºC and 4 min at 60 ºC (14 cycles). Then, samples were treated with 2 µL of 4 U/µL Exonuclease I solution (New England BioLabs; Ipswich, MA) and diluted with 18 µL of TE Buffer (Invitrogen), and 2.7 µL were mixed with 3 µL of EvaGreen Supermix (Bio-Rad) and 0.3 µL of cDNA Binding Dye Sample Loading Reagent (Fluidigm). Primers were diluted to 5 µM with 2X Assay Loading Reagent (Fluidigm). Control line fluid was charged in the chip and Prime script program was run into the IFC controller MX (Fluidigm). Finally, 5 µL of each primer and 5 µL of each sample were pipetted into their respective inlets on the chip and the Load Mix script in the IFC controller software was run. After this program, the qPCR was run in the Biomark System (Fluidigm) following the thermal cycling program: 1) 9 ºC for 1 min; 2) 35 cycles of denaturing (95 ºC for 5 s) and annealing/extension (60 ºC for 20 s); and 3) a last cycle where final PCR products were

subjected to graded temperature-dependent dissociation (60 ºC to 95 ºC, increasing 1 ºC/3 s). Data were processed with Real-Time PCR Analysis Software 3.0 (Fluidigm).

5.4.2. Quantitative RT-PCR

Transcript levels in cell samples were quantified by RT-PCR with GoTaq qPCR Master Mix (Promega; Madison, WI) (Peinado et al., 2010). The cDNA was amplified at the following conditions: hot-start activation at 95 ºC for 2 min, followed by 40 cycles of denaturation (95 ºC for 15 s), then annealing/extension (60 ºC for 60 s), and finally, a dissociation cycle (melting curve; 60 ºC to 95 ºC, increasing 0.5 ºC / 30 s) to verify that only one product was amplified, using the Light-Cycler 480 II instrument (Roche; Basilea, Switzerland). Relative quantification was calculated using the ΔΔCT formula (Catalán et al., 2007).

The expression level of each transcript was adjusted by a normalization factor (NF) obtained from the expression levels of different housekeeping genes (*ACTB*, *GAPDH*, and *HPRT*) for 3T3-L1 and SGBS cells; *18S* for hADSCs; *RPS9* and *HPRT* for THP-1 cells (Catalán et al., 2007), using Gernorm 3.3 or by geometric averaging method (Vandesompele et al., 2002). This selection was based on the stability of these housekeeping genes among the experimental groups to be compared, wherein the expression of these housekeeping genes was not significantly different among groups.

6. miRNA expression analysis

6.1. miRNA extraction

miRNAs were extracted using miRNeasy Serum/Plasma Kit (Qiagen) following previously established procedures (Jiménez-Lucena et al., 2018). miRNAs purity and concentration were evaluated by spectrophotometry using NanoDrop ND-2000 or DS-11 (Thermo).

6.2. miRNA retrotranscription and preamplification

The retrotranscription of miRNA was carried out using the TaqMan MicroRNA Reverse Transcription Kit (Life Technologies; Carlsbad, CA). RT mix contained 2 µL miRNA and 3 µL RT custom primer pool in a final volume of 7.5 µL. RT primer pool was customized selecting specific primers of our set of target miRNAs in the database of Thermo. Plates were incubated in the iQ5 thermocycler (Bio-Rad) at 16 ºC for 30 min,

followed by 42 ºC for 30 min, and finally at 85 ºC for 5 min. In this step, the cDNA was stored at -20 ºC for a maximum of 1 week. Then, the mixture was prepared containing 10 µL customized PreAmp primer pool specific for our set of target miRNAs and 7.5 µL RT mix and 20 µL TaqMan PreAmp Master Mix (Life Technologies) to a final volume of 40 µL. Next, the mixture was incubated in the iQ5 Thermocycler using the following steps: denaturation at 95 ºC for 10 min, 55 ºC for 2 min, and 72 ºC for 2 min; 20 cycles of preamplification for 15 s at 95 ºC, and 4 min at 60 ºC per cycle; and final incubation at 99.9 ºC for 10 min. The pre-amplified products were then diluted with RNase-free water at a ratio 1:40.

6.3. RT-PCR for miRNA quantification

The levels of miRNAs were measured with the OpenArray platform (Life Technologies) (Jiménez-Lucena et al., 2018). The levels of intracellular and/or extracellular miRNAs in 3T3-L1, SGBS, and THP-1 cells in culture were measured using TaqMan Universal PCR Master Mix II (Bio-Rad). The mixture containing 10 µL TaqMan Universal PCR Master Mix II, 1 µL customized primers (Applied Biosystems; Foster City, CA), and 1.5 diluted cDNA to a final volume of 20 µL, was incubated in the iQ5 Multicolor Real Time PCR Detection System (Bio-Rad) using the following steps: 95 ºC for 10 min, 40 cycles of preamplification for 15 s at 95 ºC 15 s, and 1 min at 60 ºC per cycle.

As a normalization method, the circulating miRNAs that showed the least variability in their Ct values in all samples were selected. To this end, the NormFinder Bioinformatic tool was used (MOMA-Department of Molecular Medicine, Aarhus University Hospital, Denmark) (Andersen et al., 2004), a software extensively used in expression studies (Danese et al., 2017; De Spiegelaere et al., 2015). This showed that the most stable miRNAs were *miR-143-3p* and *miR-144-3p*. Second, the BestKeeper method was used to calculate the geometric mean of the pair-wise Ct values (Pfaffl et al., 2004). The relative expression data was analysed using OpenArray Real-Time qPCR Analysis Software (Life Technologies). The intracellular level of each miRNA was normalized by the intracellular level of *miR-17-3p* in 3T3-L1 and SGBS cells, as validated previously (Andersen et al., 2010), whereas in THP-1 cells they were normalized by a NF obtained from the expression levels of 2 housekeeping genes (*RPS9* and *HPRT*). In turn, intracellular miRNA levels were used for the normalization of their corresponding extracellular miRNA levels.

7. Protein expression analysis

7.1. Protein extraction

Proteins were extracted using different procedures according to the nature of the sample and its final purpose, as described in detail in the following sections. For proteomic studies, protein content was quantified by Qubit Protein Assay kit or RcDc assay kit (Bio-Rad), whereas Bradford assay (Bradford, 1976) was used in routine studies. In all the cases, protein samples were maintained at -20 ºC.

1 x 10^6 human preadipocytes obtained from subjects of cohort 1 were used for extracting proteins for proteomic and immunoblotting studies (Díaz-Ruiz et al., 2015). For proteomic analyses, preadipocyte samples were homogenized in lysis buffer containing 8 M urea, 4% CHAPS, 30 mM Tris base (Sigma), and sonicated. For immunoblotting studies, preadipocyte samples were disrupted in lysis buffer containing 20mM Tris-HCl pH7.4 (Sigma), 150mM NaCl (Merck; Darmstadt, Germany), 1mM EDTA, 1% Tritón X-100, and 1 µg/mL anti-protease cocktail (Sigma).

SVF and cell lines were used for extracting proteins for immunoblotting and functional assays (Moreno-Castellanos et al., 2017). Thus, cells were lysed in SDS-DTT [62.5 mM Tris-HCl, 100 mM DTT (Thermo), 2% SDS (Sigma), 20% glycerol (VWR; West Chester, PE); pH 7.6] and lysis buffers, respectively.

7.2. Proteomic study: *iTRAQ labelling and high-resolution LC-MS/MS*

Isobaric tags for relative and absolute quantitation (iTRAQ) coupled to liquid chromatography-tandem mass spectrometry (LC-MS/MS) (Wiese et al., 2007) was performed for the quantitative proteomic study of paired preadipocytes samples from SC and OM adipose tissue of NG obese and T2D obese subjects. iTRAQ proteomics was carried out at the Proteomics and Bioinformatic Service (SEPBIO) of the Autonomous University of Barcelona (UAB; Spain) (**Figure 26**).

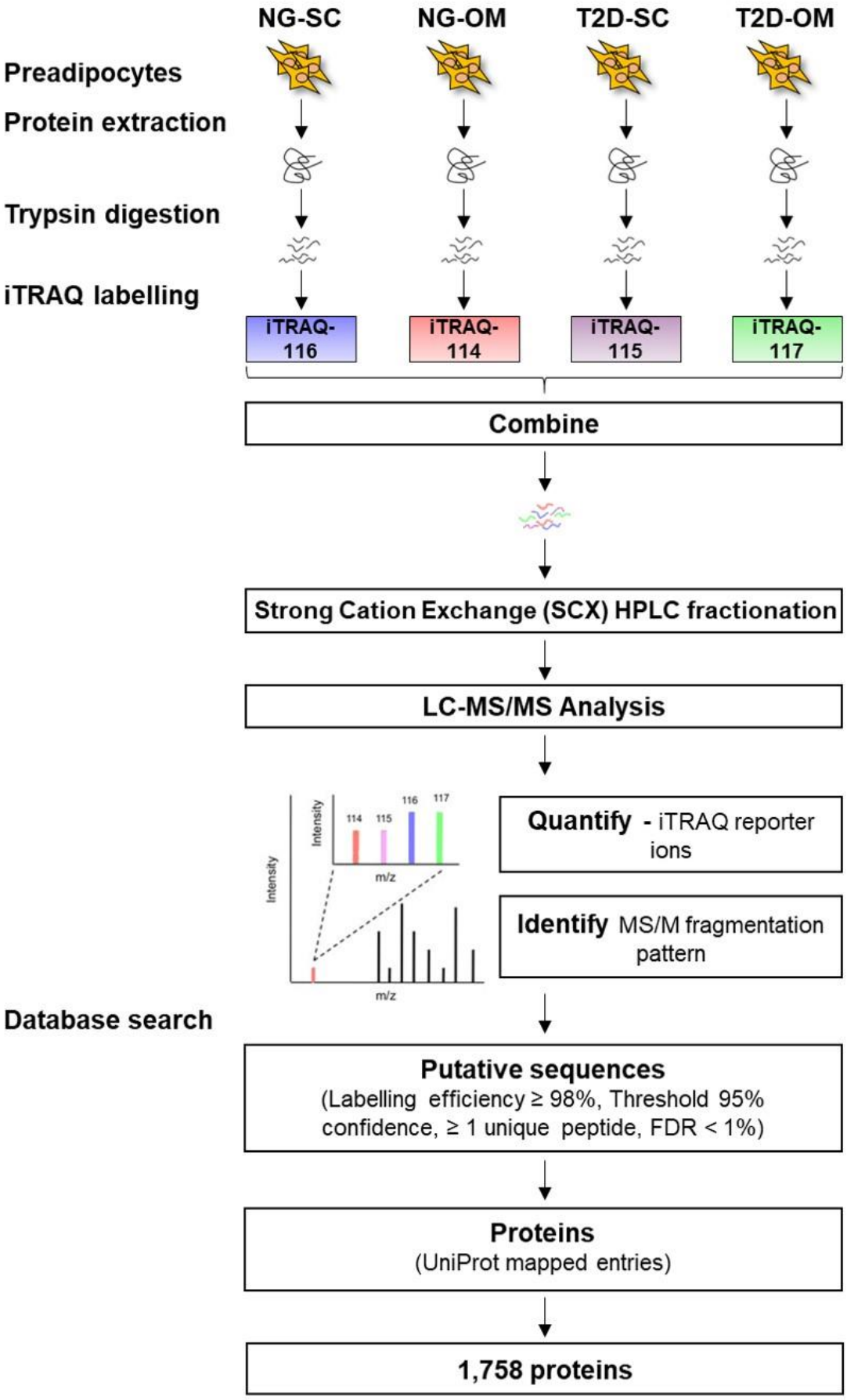

Figure 26. Graphical workflow of the iTRAQ labelling and high-resolution LC-MS/MS performed.

Sample preparation: Human preadipocytes were reduced and alkylated by addition of 2 mM 1,4-dithiothreitol (DTT), and 7 mM iodoacetamide (IAA; Sigma), respectively, for 15 min at RT. Then, samples from 2-3 individuals per group and fat depot were pooled and used for two separate iTRAQ experiments (n = 5-6 subjects per group and fat depot). Protein samples were precipitated using 10% trichloroacetic acid (TCA; Sigma), diluted in tetraethylammonium bromide (TEAB; Sigma) with 0.1% sodium dodecyl sulfate (SDS) (Sigma), and quantified. Samples were diluted 1:2 with TEAB and digested with 2% trypsin (Promega).

iTRAQ labelling and relative quantification: Tryptic peptides (240 µg per group and fat depot) were employed for proteomic analysis using 4-plex isobaric tags for iTRAQ, according to the manufacturer's instructions (Applied Biosystems). Samples were tagged with the corresponding iTRAQ reagent (Applied Biosystems), mixed, desalted, and fractionated by strong cation exchange (SCX). Six fractions were collected, and each fraction was desalted, evaporated to dryness, and diluted in 20 µL of injection phase. Then, 8 µL of extract were diluted with 5% methanol (MeOH; VWR)/1% formic acid (Scharlau; Barcelona, Spain) and analysed by liquid chromatography-tandem mass spectrometry (LC-MS/MS). The MS system used was an Orbitrap XL (Thermo), equipped with a microESI ion source (Proxeon; Madrid, Spain), and coupled to an Agilent 1200 series LC-system (Agilent). The SCX fractions were loaded onto a chromatographic system consisting of a C18 preconcentrating cartridge (Agilent Technologies), connected to a 15 cm long, 100 µm i.d. C18 column (Nikkyo Technos Co., Ltd.; Tokyo, Japan). The separation was performed at 0.4 µL/min in a 90-min acetonitrile gradient from 3 to 40% [solvent A: 0.1% formic acid, solvent B: acetonitrile (Sigma) 0.1% formic acid]. The Orbitrap XL was operated in the positive ion mode with a spray voltage of 2 kV. The scan range for full scans was m/z 400-1800. The spectrometric analysis was performed in a data dependent mode, acquiring a full scan followed by 8 MS/MS scans of the 4 most intense signals detected in the MS scan. For each MS signal, two MS/MS spectra were acquired using higher energy collisional dissociation (HCD) and ion-trap-based collision-induced dissociation (CID) as fragmentation devices. The HCD spectra were used to measure the intensity of iTRAQ fragments and the CID spectra were used for database search and peptide identification. An exclusion time of 30 sec and a spectral count of 2 were included to avoid repetitive MS/MS analysis of the dominant MS signals.

Data search and protein identification: Peak lists were searched against the complete human proteome (UniProt release 2014_08, with 68.049 proteins) using SEQUEST (Proteome Discoverer 1.3, Thermo) as a search engine. The search tolerances were set as follows: peptide mass tolerance 10 ppm, fragment tolerance 0.8 Da, with trypsin as

an enzyme (allowing up to two missed cleavages), methionine oxidation (+15.995 Da), and 4-plex iTRAQ (K, Y, N-terminal, +144.102) as variable modifications, and cysteine carbamidomethylation (+57.021 Da) as a fixed modification. Peptide identifications were filtered for 0.5% FDR and only proteins identified with two or more peptides were considered.

Data normalization and statistical analysis: Protein intensities, for each of the two iTRAQ experiments, were normalized using protein median intensities in each comparison (iTRAQ reagents 115/116: 0.987, 115/117: 0.958, 116/114: 1.142, 117/114: 1.191 for replicate 1; and 115/116: 1.026, 115/117: 0.933. 116/114: 1.090, 117/114: 1.180 for replicate 2). Proteins identified in the two replicates were matched. To discard duplicate proteins between replicates, the following parameters were considered: absence of missing values, # unique peptides, # peptide and coverage (the higher, the better). Proteins showing quantification values within a fixed average ratio (±1.5) and a coefficient of variation (CV) under 20% were considered for further statistical analysis. Specifically, the Perl module "Statistic R" was used to calculate the average, the standard deviation (SD), the coefficient of variation (CV), and the fold change ratios for each protein between groups. Data normality was tested by Shapiro-Wilk test, and a Student's t test was performed to obtain the statistical significance (*p-value*).

7.3. Quantitative immunoblotting and dot-blot assays

Tissue and cell samples were processed for immunoblotting studies (Moreno-Castellanos et al., 2017; Díaz-Ruiz et al., 2015) . First, protein extracts were prepared for their electrophoretic separation mixing them with loading buffer [500 nM Tris-HCl, 7.5% SDS, 10 mM EDTA, 50% sucrose, 5% β-mercaptoethanol, 250 mM DTT, 5 mg/mL bromophenol blue (Sigma); pH 6.8]. Then, the proteins were denatured by 5 min boiling at 95 ºC.

Thirty to 50 µg of protein per sample were separated by 4-20% SDS-PAGE gels under denaturing conditions in the electrophoresis system Mini-Protean tetra (Bio-Rad) at 80-120 V in running buffer (25 mM Tris, 190 mM glycine, 1% SDS). Once finished, the proteins were transferred to a nitrocellulose membrane (Bio-Rad) using a humid system at a constant amperage of 330 mV for 60-90 min in a continuous recirculation of transference buffer [25 mM Tris, 190 mM glycine, 0.2% SDS, 20% methanol (VWR)] or Trans-Blot Turbo Transfer system (Bio-Rad). For dot-blot assays, 7 µL of samples mixed with 3 µL of Glycerol:PBS (3:1) were laid in dots onto nitrocellulose membranes (Díaz-Ruiz et al., 2015). To ensure equal sample loading, the membrane was stained with

Ponceau [0.1% Ponceau S (Sigma), 1% acetic acid (VWR)] and blocked in Tris-buffer saline [(TBS); 25 mM Tris, 150 mM NaCl] including 0.05% Tween 20 (TTBS), and 5% non-fat dry milk (Panreac) for 1 h at RT. Blots were then incubated overnight at 4 ºC with the corresponding primary antibody (**Table 7**). The antigen-antibody complexes were visualized using horseradish peroxidase (HRP)-conjugated secondary antibodies, which were incubated at RT for 1 h, and the enhanced chemiluminescence ECL Plus detection system (Bio-Rad).

Table 7. Antibodies used for immunoblotting studies.

Antibody	Commersial Source	Reference	Host Specie	Dilution
Anti-ADRP	Santa Cruz	sc-377429	Mouse	1/1,000
Anti-AKT	Cell Signaling Technology (Danvers, MA)	#9272	Rabbit	1/1,000
Anti-ARF6	Santa Cruz	sc-7971	Mouse	1/1,000
Anti-AS160	Merck	#07-741	Rabbit	1/1,000
Anti-ATF6α	Santa Cruz	sc-22799	Rabbit	1/1,000
Anti-CASPASE3	Cell Signaling	#9665	Rabbit	1/1,000
Anti-CD14	Santa Cruz	sc-9150	Rabbit	1/1,000
Anti-CD45	Santa Cruz	sc-25590	Rabbit	1/1,000
Anti-CD63	Sigma	SAB4301607	Rabbit	1/1,000
Anti-CHOP	Cell Signaling	#2895	Mouse	1/1,000
Anti-DGAT2	Novus Biologicals (Littleton, CO)	NB100-57851	Goat	1/1,000
Anti-DLK/PREF1	Santa Cruz	sc-25347	Rabbit	1/1,000
Anti-eIF2α	Santa Cruz	sc-517214	Mouse	1/1,000
Anti-FAS	Santa Cruz	sc-16147	Goat	1/1,000
Anti-GLUT4	Abcam (Cambrigde, UK)	ab35826	Mouse	1/1,000
Anti-BiP/GRP78	Santa Cruz	sc-376768	Mouse	1/1,000
Anti-GRP94	Cell Signaling	#2104	Rabbit	1/1,000
Anti-GSS	Abcam	ab133592	Rabbit	1/1,000
Anti-HSL/LIPE	Abcam	ab45422	Rabbit	1/1,000
Anti-IRE1α	Santa Cruz	sc-390960	Mouse	1/1,000
Anti-IRS1	Santa Cruz	sc-7200	Rabbit	1/1,000
Anti-JNK	R&D Systems	AF387	Rabbit	1/1,000
Anti-pAKT$^{(S473)}$	Cell Signaling	#4060	Rabbit	1/750
Anti-pAS160$^{(S666)}$	Merck	#09-489	Rabbit	1/750
Anti-PDI	Cell Signaling	#3501	Rabbit	1/1,000
Anti-peIF2α$^{(S51)}$	Santa Cruz	sc-101670	Rabbit	1/750
Anti-PERK	Santa Cruz	sc-377400	Mouse	1/1000
Anti-PGC1α	Abcam	ab54481	Rabbit	1/1,000
Anti-pHSL$^{(S563)}$	Cell Signaling	#4139	Rabbit	1/750

Anti-pIRE1α $^{(S724)}$	Abcam	ab48187	Rabbit	1/750
Anti-pIRS1$^{(S307)}$	Santa Cruz	sc-33956	Rabbit	1/750
Anti-pIRS1$^{(T612)}$	Merck	09-432	Rabbit	1/750
Anti-pJNK$^{(T183/Y185)}$	R&D Systems	AF1205	Rabbit	1/750
Anti-PLIN1	Progen (Heidelberg, Germany)	GP29	Guineapig	1/5,000
Anti-PPARγ	Cell Signaling	#2430	Rabbit	1/1,000
Anti-pPERK$^{(T980)}$	Santa Cruz	sc-32577	Rabbit	1/750
Anti-PRP8	Santa Cruz	Sc-55533	Mouse	1/1,000
Anti-PSMB8	R&D Systems	AF7710	Sheep	1/1,000
Anti-SOD1	Sigma	HPA001401	Rabbit	1/1,000
Anti-UBIQUITIN	Cell Signaling	#3933	Rabbit	1/1,000
Anti-UCP1	Abcam	ab23841	Rabbit	1/750
Anti-Goat/Sheep IgG	Sigma	A-9452	Mouse	1/2,500
Anti-Guinea pig IgG	Sigma	A-7289	Goat	1/2,500
Anti-Mouse IgG	Sigma	A-9044	Rabbit	1/2,500
Anti-Rabbit IgG	Sigma	A-8275	Goat	1/10,000

8. Microscopy studies

8.1. Determination of fat cell volume

To measure the size of human fat cells, freshly isolated mature adipocytes were washed with DMEM/F-12 (1:1) and suspended in Krebs Ringer Phosphate (KRP) buffer [0.9% NaCl, 15 mM NaH_2PO_4 (Thermo), 6 mM KCl (Merck), 1.5 mM $MgSO_4$ (Panreac), 1.6 mM $CaCl_2$ (Sigma), supplemented with 2% BSA, 1 mg/mL glucose, and 0.1 mg/mL ascorbic acid (Sigma); pH 7.4]. Fat cell volume was determined as described (Tchoukalova et al., 2003). In brief, light microscopy images of 100 cells were captured with a coupled camera, and their diameters (*d*) were measured in μm using ImageJ 1.50b. Mature adipocytes are assumed to be spheres so that fat cell volume (expressed in pL) was calculated as $[(\pi \times d^3)/6]$.

8.2. Confocal microscopy studies

Coverslips bearing the cells were mounted on slides with fluorescent mounting medium (Agilent), containing 1 μg/mL DAPI (Sigma), to visualize the nuclei, and examined by a confocal microscopy LSM 710 (Zeiss; Germany), fitted with a Plan-Fluor

63X oil immersion objective (n.a.=1.4) in the facilities of the "Flow Cytometry and Advanced Optical Microscopy Unit" of the IMIBIC (Córdoba, Spain), as described previously (Pulido et al., 2011).

To capture the DAPI signal, the excitation of the sample was at 405 nm and the emission was collected between 420 and 480 nm, whereas in the case of the Cye™3-labeled Pre-miR™ Negative Control #1 signal, the excitation of the sample was at 547 nm and the emission was at 540 and 580 nm. Depending on the location of the fluorescence signal and the cell depth, 10-20 stacks per channel were collected. The set of all the stacks for each image and channel underwent a deconvolution process with the Huygens Essential 2.4.4 software (Scientific Volume Imaging) (Lam et al., 2017), and images were processed and analysed using the ImageJ software (Hartig, 2013).

8.2.1. Quantitative analysis of lipid droplets (LDs)

Oil Red-O staining of cellular lipids was performed in SGBS and 3T3-L1 cells grown on glass coverslips under different conditions as previously described (Pulido et al., 2011). Cells were washed with D-PBS and fixed with 4% paraformaldehyde for 8 min at RT. Coverslips were washed with 60% isopropanol and then left to dry. Subsequently, an Oil Red-O stock solution was prepared [0.35 g Oil Red-O (Sigma) dissolved in 100 mL 100% isopropanol]. Before use, the solution was diluted 6:4 with distilled water, allowed to stand for 10 min, and then filtered through Whatman No. 1 paper. Cells were exposed to this solution for 30 min at RT in darkness and the unbound dye was rinsed with distilled water. Images were captured with an inverted light microscope coupled to a camera.

For morphometric studies of the lipid droplets (LDs), Oil Red-O staining was observed through excitation at 543 nm and collection of the emission between 610 and 700 nm. When used, GFP signal was observed through excitation at 488 nm and collection of the emission between 500 and 550 nm. At least 30 cells were randomly selected for each experimental condition and the LD number and size were then estimated by using ImageJ 1.50b (Mohan et al., 2019). The analysis was performed by converting the 8-bit image into a binary image, that consists of the pixels comprising the LDs. Following binarization, the image was subjected to watershed object separation for image processing, which is used to identify borders of adjacent LDs (Abdolhoseini et al., 2019). After separation, the binary image was manually compared with the original image for consistency and correct binary conversion. After setting the scale of the image, the amount and individual size of the LDs in the image, displayed by ImageJ as surface area

in μm^2, were measured. Incomplete LDs located at the edge of the image were excluded. The sum of the areas of all the LDs present in a cell was used as the total lipid content.

Staining of neutral lipids and DNA was also performed in *PRPF8* silencing experiments of hADSCs cultured on 96-wells plates. To be more specific, hADSCs were washed with PBS and fixed with 4% paraformaldehyde solution (PFA; Bosterbio; Pleasanton, CA) containing 0.123 M $NaH_2PO_4x2H_2O$ (Sigma), 0.1 M NaOH (Sigma), and 0.03 M glucose for 10 min at RT. Fixed cells were washed with PBS and stained with Bodipy 500/510 (0.2 µg/ml PBS; Invitrogen) and Hoechst (2 µg/ml PBS; Invitrogen) for 20 min at RT. After washing with PBS, accumulation of intracellular lipids (Bodipy staining) and cell number (Hoechst staining for nuclei) were quantified with Cell Insight CX5 High-Content Screening (HCS) Platform and High-Content Screening (HCS) Studio Cell Analysis Software 2.0 (Thermo). Total lipid content, and LD number and size were normalised by cell size.

8.2.2. Intracellular localization of GLUT4

The intracellular localization of the glucose transporter 4 (GLUT4), and specifically its redistribution to the plasma membrane in response to insulin, was studied in 3T3-L1 cells by confocal microscopy (Patki et al., 2001). 3T3-L1 cells were transfected at day 3 of differentiation whereas at day 6, they were electroporated with 10 and 50 µg, respectively, of the cMyc-GLUT4-EGFP expression vector and seeded on glass coverslips. This vector was kindly donated by Professor Dr. Jeffrey E. Pessin (Albert Einstein College of Medicine, NY), and codes for a GLUT4 recombinant protein containing cMyc epitope tag in the first exofacial N-loop as well as EGFP fused in frame at the carboxy terminus (Watson and Pessin, 2006) (**Figure 27A**). As shown in **Figure 27B**, this reporter enables the measurement of GLUT4 localization. In non-permeabilized conditions, in the basal stage, GLUT4 is present in the perinuclear region and small vesicular structures dispersed in the cytoplasm, as revealed by the intrinsic EGFP fluorescence, whereas no cMyc labelling is detectable since the anti-cMyc primary antibody and red fluorescent-conjugated secondary antibody does not reach the vesicular interior, where the Myc-epitope is exposed. In response to insulin, GLUT4-containing vesicles translocate and fuse with the cell surface, thereby exposing the cMyc-epitope to the surface of the cell where it can be recognized by the antibody. Thus, EGFP fluorescence and cMyc labelling are readily visible and colocalize at the plasma membrane giving yellow fluorescence.

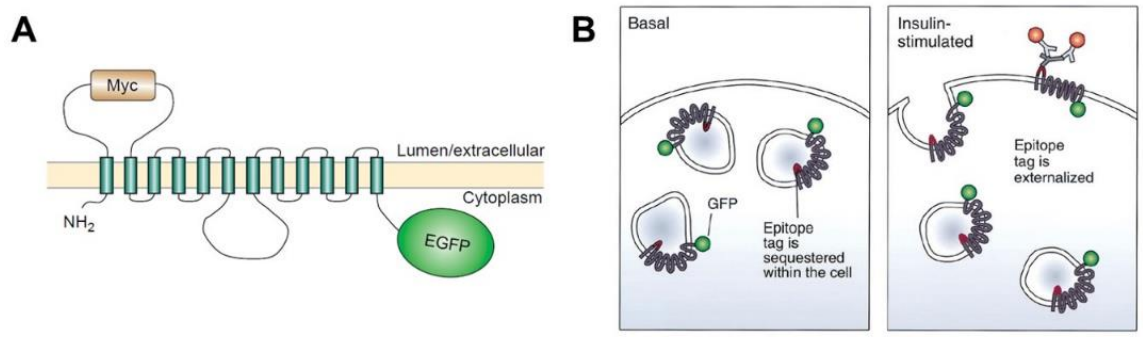

Figure 27. Graphical representation of the cMyc-GLUT4-EGFP recombinant protein inserted in the membrane **(A)**, and of cells expressing cMyc-GLUT4-EGFP in basal and insulin-stimulated conditions **(B)** (Bogan et al., 2001; Watson and Pessin, 2006).

Transfected cells were washed with PBS and fixed in 4% paraformaldehyde for 8 min at RT. Paraformaldehyde was then removed and cells were washed with PBS and incubated for 1 h at RT with Block Buffer without saponin (Sigma). Subsequently, the cells were incubated overnight at 4 ºC with anti-cMyc primary antibody (1:500, developed in mouse; Bio-Rad) diluted in Antibody Buffer without saponin. The unbonded primary antibody was removed through washings with PBS and the cells were incubated with Alexa Fluor® 594-conjugated secondary antibody (1:500; Thermo) at RT for 2 h. Finally, cells were washed with PBS and then immunostained coverslips were mounted.

For the acquisition of the EGFP signal in cells overexpressing the cMyc-GLUT4-EGFP construct, the samples were excited at 488 nm and the emitted fluorescence was acquired between 500 and 550 nm. In the case of the fluorochrome Alexa 594, the excitation was performed at 543 nm and the emission between 610 and 700 nm was collected.

8.3. Transmission electron microscopy (TEM)

Transmission electron microscopy (TEM) studies were carried for studies of adipocyte extracellular vesicles (EVs). Isolated EVs were fixed in glutaraldehyde (Electron Microscopy Sciences; Industry Road Hatfield, PA) (1%, v/v) for 30 minutes at room temperature. Then, 10 µl-droplets of fixed isolated EVs were placed onto 200 mesh copper grids with carbon film (Agar Scientific; Essex, UK), and allowed to air dry for 30 minutes. Grids were washed (2x2 minutes in Milli-Q water) before negative staining with 2% (v/v) uranyl acetate (Electron Microscopy Sciences) for 4 minutes. The surplus stain was washed (2x2 minutes in Milli-Q water) and grids were allowed to air dry before being examined in a Jeol JEM-1400 Transmission Electron Microscope (TEM) (Jeol Ltd.; Tokyo, Japan) with Gatan Microscopy Suite software (Gatan; Pleasanton, CA, USA) in

the facilities of the "Central Research Support Service" (SCAI) of the University of Córdoba (UCO; Córdoba, Spain).

9. Functional analysis

9.1. Determination of preadipocyte proliferation rate

Cell counting in culture flasks was carried out to monitor the growth rates of the preadipocytes *in vitro*. At passage 3, cells were detached from the culture flasks, an aliquot was stained with trypan blue (Sigma) to discard dead cells, and live cells were counted in a Neubauer chamber. Cell proliferation was calculated as the total number of live cells per initial seeding number (Morten et al., 2016).

9.2. Determination of cell viability and cytotoxicity

To determine cell viability and cytotoxicity in the *in vitro* experiments, two assays were performed.

MTT cell viability assay: Cell viability of SGBS and 3T3-L1 cell lines under the different experimental conditions were evaluated by MTT assay (van Meerloo et al., 2011). Cells were incubated for 2 h with 0.1 mg/mL of MTT (Sigma), dissolved in PBS. Washing with PBS was followed by the addition of DMSO (Sigma), and gentle shaking for 10 min so that complete dissolution was achieved. Aliquots of the resulting solutions were transferred into 96-well plates and absorbance was recorded at 570 nm using a microplate spectrophotometer system (Flex Station 3; BioNova Scientific; Fremont, CA). Results were analysed with the SoftMax Pro software 2.2.1 (Molecular Devices; San José, CA).

LDH cytotoxicity assay: The cytotoxicity of gene expression manipulation in hADSCs was evaluated by Cytotoxicity Detection Kit^{PLUS} (LDH; Roche). The culture medium was aspirated and centrifuged at 3,000 rpm for 10 min in order to obtain a cell-free supernatant. Aliquots of media and warm reagent were mixed in a 96-well plate and absorbance was recorded using a microplate reader (Tecan Infinite 2000). Results were analysed with Magellan software 7.2 SP1 (Tecan; Männedorf, Switzerland).

9.3. Determination of glucose uptake

To measure the capacity of the cells to uptake glucose, glucose uptake analysis in SGBS and 3T3-L1 cell cultures were performed using the luminescence method Glucose Uptake-Glo™ Assay (Promega). This assay is based on the detection of 2-deoxyglucse-6-phosphate (2DG6P) (Valley et al., 2016). After 2 h of pre-treatment, cells were incubated with 1 mM 2DG, diluted in PBS, and exposed to 100 nM insulin for 1 h. To determine nonspecific glucose uptake, 25 mM cytochalasin B (Sigma) was used as a control. Luminescence was measured in a Flex Station 3 and results were analysed with the SoftMax Pro software 2.2.1.

9.4. Determination of lipolysis and lipogenesis

Free glycerol released into cell culture medium and intracellular triglycerides (TAGs) were determined in 3T3-L1 cells as an index of lipolysis and lipogenesis, respectively. To this end, two different commercial kits were used and adapted to increase the sensitivity using in combination with the fluorescent reagent, Amplex UltraRed® (Invitrogen). A glycerol standard curve run alongside each assay was used to determine the final glycerol concentration and values were normalized to the protein content measured by Bradford method. Fluorescence was measured in a Flex Station 3 and results were analysed with the SoftMax Pro software 2.2.1.

Free glycerol determination: 3T3-L1 cells were washed with PBS, and then incubated in phenol red-free DMEM (Sigma) for 24 h. The culture medium was aspirated and centrifuged at 6,000 x g for 10 min in order to obtain a cell free supernatant, which was tested using the Free Glycerol Determination Kit (Sigma).

Triglycerides determination: 3T3-L1 cells were washed with PBS, lysed in lysis buffer, sonicated, and the extracts were tested using the Serum Triglyceride Determination Kit (Sigma).

9.5. Determination of proteasome activity

The 26S proteasome activity (ATP stimulated) and 20S (SDS stimulated) was measured in SGBS cells exposed to HGHI conditions following established conditions (Díaz-Ruiz et al., 2015; Li et al., 2008). Assays for proteasome activity were performed using Suc-LLVY-AFC product, which is proteolyzed by the chymotrypsin-like (ChT-L)

active site of the proteasome forming a fluorogenic substrate (AFC) (Keita et al., 2014; Martín-Clemente et al., 2004) (**Figure 28**).

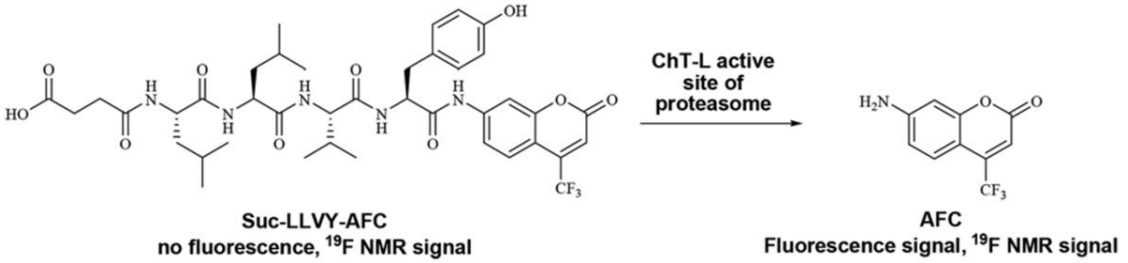

Figure 28. Representation of the enzymatic reaction releasing the bimodal probe AFC from the substrate Suc-LLVY-AFC (Keita et al., 2014).

At the end of the treatments, cells were washed with PBS and scraped from plates in lysis buffer without DTT, Triton X-100 nor protease inhibitors because these compounds interfere with the assay. The reaction was conducted in 250 µL of activity assay buffer in a 96-well plate containing 50 µg/ml protein lysate in Proteasome buffer [20 mM Tris–HCl, pH 7.8, 1 mM EDTA, 0.5 mM DTT, 5 mM $MgCl_2$ (Merck), and 50 µM Suc-LLVY-AFC (Sigma)], plus 2 mM ATP (Sigma), or 0.02% SDS for the determination of 26S and 20S proteasome activities, respectively. In order to confirm the specificity of the findings for proteasome activity, parallel reactions containing the proteasome inhibitor, MG132 (25 µM; Merck), were run as controls. The reaction mixture was incubated for 3 h at 37 ºC and the fluorescence of the released AMC product was kinetically followed each 10 min in a Flex Station 3 microplate reader at an emission wavelength of 355 nm and an excitation wavelength of 460 nm. The background fluorescence values obtained by incubating the lysates with MG132 were subtracted from activity values (Dasuri et al., 2011). Results were analysed with the SoftMax Pro software 2.2.1 and the values reported for proteasome peptidase activity are expressed as relative fluorescence arbitrary units/min/mg of total protein.

9.6. EV size and concentration analysis

To characterize the size and frequency distribution of the EVs isolated from 3T3-L1 cells culture media, we used nanoparticle tracking analysis (NTA) as described before (Mehdiani et al., 2015). Briefly, NTA uses the light scattering properties and Brownian motion of laser-illuminated particles in suspension to determine EV size and concentration. NTA was undertaken using the NanoSight NS300 configured with a 488 nm laser (Malvern Panalytical; Madrid, Spain) using NTA software version 3.3 in the facilities of the University Institute of Nanochemistry (IUNAN/UCO; Córdoba, Spain).

Camera shutter speed was maintained at 30 ms. Samples were diluted in PBS to concentrations between $2x10^8$ and $3x10^9$ particles/mL. Sixty-second videos were recorded in replicates of 5 per sample with camera sensitivity and detection threshold set to 13 and 8, respectively. The temperature was monitored manually and ranged from 24 to 26 ºC. EV concentration and distribution were normalized to the cell protein content as determined by Bradford assay and expressed as [particles]/mg of protein.

9.7. Determination of cytokines

PRPF8- and control-silencing hASCs cell culture supernatants were collected at different points during differentiation (day 3-10) and cytokines (IL-1β, IL-6, IL-8, IL-10, MCP-1, and MIF) secretion were measured using at MesoScale Discovery (MSD; Thermo) by the U-PLEX assay and run according to manufactures protocol. Biotinylated capture antibodies are coupled to U-PLEX linkers, which self-assemble onto unique spots on the U-PLEX plate. Analytes in the sample bind to the capture reagents; detection antibodies conjugated with electro-chemiluminescent labels (MSD GOLD SULFO-TAG) bind to the analytes to complete the sandwich immunoassay. Once the sandwich immunoassay is complete, the U-PLEX plate is loaded into an MSD instrument where a voltage applied to the plate electrodes causes the captured labels to emit light. The instrument measures the intensity of emitted light, which is proportional to the amount of analyte present in the sample and provides a quantitative measure of each analyte in the sample. Data were acquired using a Sector S 6000 (MSD), and analysed using MSD Discovery workbench software.

10. Bioinformatic studies

To predict the biological meaning of the different protein lists generated in this Doctoral Thesis, together with the search of potential target genes of *PRPF8* and *miR-223-3p*, *in silico* analyses were performed as described in the sections below. UniProt IDs of each protein were retrieved from UniProt knowledgebase (UniProtKB) and then submitted to the corresponding software. Moreover, to get further insights on the regulation of interested processes during adipogenesis, we explored the expression of genes related to these processes in previously published transcriptomic datasets on *in vitro* differentiation of SC preadipocytes isolated from a lean healthy donor (Ehrlund et al., 2017a).

10.1. Gene Ontology (GO) analysis

Gene Ontology (GO) enrichment analyses were conducted using PANTHER 14.1 (Protein ANalysis THrough Evolutionary Relationships) classification system (Mi et al., 2019). This software clusters the proteins into different groups related to their biological process, according to GO annotation (GO terms). Significant over- and under-represented GO terms and pathways were identified by Fisher's Exact with FDR multiple test correction < 0.05 taking all the Homo sapiens genes in the data set as a reference list.

10.2. Ingenuity Pathway Analysis (IPA)

To interpret our comparative proteomic data sets in the context of canonical pathways and upstream regulators, the Ingenuity Pathways Analysis (IPA; Qiagen), kindly provided by the Andalusian Bioinformatics Platform (PAB) centre located at the University of Málaga (Málaga, Spain), were used. To determine quantitative changes, the differentially expressed proteins were characterized by the "Core Analysis" function. A value of ± 1.5-fold change, with *P value* < 0.05 (determined by Student's t-test) was set as the threshold for categorizing up-regulated and down-regulated proteins.

IPA Canonical Pathway analysis: Canonical pathway analysis identified the pathways from the IPA library of canonical pathways that were most significant to the data set. The significance of the association between the data set and the canonical pathway was measured in two ways: 1) A ratio of the number of proteins from the data set that mapped to the pathway divided by the total number of proteins that mapped to the canonical pathway displayed, and 2) Fisher's exact test was used to calculate a p-value determining the probability that the association between the proteins in the dataset and the canonical pathway was explained by chance alone. Pathways with FDR < 0.05 by the Benjamini-Hochberg method (Benjamini, Yoav ; Hochberg, 1995) were considered statistically significant.

IPA Upstream Regulator analysis: The goal of the IPA Upstream Regulator analysis is to identify the cascade of upstream transcriptional regulators that can explain the observed gene expression changes in our dataset. The upstream regulator prediction is based on prior knowledge of expected effects between transcriptional regulators and their target genes stored in the Ingenuity® Knowledge Base. For each potential transcriptional regulator (TR) two statistical measures, an overlap *P-value,* and an activation z-score are computed. The overlap *P-value* calls likely upstream regulators based on the significant overlap between dataset genes and known targets regulated by

a TR. The activation z-score is used to infer likely activation states of upstream regulators based on comparison with a model that assigns random regulation directions. The upstream regulators were considered significant if they had a significant prediction Z score greater than 2. The program gives a *P-value* of overlap with the downstream targets. The Z scores can independently predict the activation or inhibition of an upstream regulator independent of the *P-value* of overlap.

10.3. *PRPF8* target genes analysis

The target genes of *PRPF8* were analysed *in silico* through CLIP_Seq data using ENCORI (The Encyclopedia of RNA Interactomes) (J.-H. Li et al., 2013), and in the HumanBase tool database (Greene et al., 2015).

10.4. miRNA target genes analysis

The list of potential target genes of *miR-223-3p* was obtained from *in silico* search of four web-based tools. These included the computationally predicted microRNA target databases: TargetScan (Agarwal et al., 2015), miRDB (Liu and Wang, 2019), and microRNA.org (Betel et al., 2010); and the experimentally verified microRNA target database miRTarBase (Chou et al., 2018). The redundant genes were removed, and consensus targets were defined as genes predicted by at least two algorithms.

11. Statistics analysis

The data showed in the figures are represented as mean ± SEM (Standard Error Mean) of the results obtained from at least three independent experiments. Statistical differences were analysed, and plots generated by GraphPad Prism 7.00. The quantitative data were evaluated for normal distribution by the Shapiro-Wilk test, with the cut off for normal distribution set at *P-value* > 0.05. When comparing two experimental groups, Student's t-test was used for parametric data, whereas the Mann-Whitney U test was used for non-parametric data. When comparing more than two experimental groups, the statistical analysis was performed using analysis of variance: Two- or One-way ANOVA test followed by Tukey's test as a Post Hoc test. The differences between experimental groups were considered statistically significant from a confidence level higher than 95% (*P-value* < 0.05).

11.1. Correlations

The relationship between the plasma levels of nine miRNAs (*miR-9*, *miR-28-3p*, *miR-29a*, *miR-30a-5p*, *miR-103*, *miR-126*, *miR-150*, *miR-223-3p*, *miR-375*), and adipose tissue insulin resistance index (ATIRI) was evaluated through a linear regression analysis adjusted by age, gender, BMI, TGs, and c-HDL, as well as with the R packet MASS by the Akaike Information Criterion (AIC) multivariate regression analysis with the stepAIC method (Akaike, 1974; Heinze et al., 2018).

11.2. Hierarchical Clustering Analysis (HCA)

Hierarchical Clustering Analysis (HCA) was used as a method for cluster analysis in transcriptomics data mining aiming to establish a hierarchy of clusters (Petushkova et al., 2014). It was performed using the MetaboAnalyst 4.0 (Chong et al., 2019), which also generates a heat map wherein the orders of columns and rows are reordered to facilitate the better presentation of dendrograms. Dendrograms are used to describe the similarity between clusters and/or observations.

RESULTS

All the Appendixes within this section have been deposited to the Mendeley Data repository (DOI: 10.17632/572rgjrzrw.1).

1. Study 1: Identification of pathogenic markers of metabolic disease in preadipocytes of obese individuals

This study was aimed at analysing the proteins and pathways that are differentially regulated in preadipocytes in obese individuals with different degrees of insulin sensitivity for their characterization and relevance as potential biomarkers of obesity-associated metabolic disease.

1.1. Preadipocytes display distinct features in obesity-related IR/T2D

Preadipocytes from SC and OM adipose tissue were isolated from 69 morbidly obese subjects (BMI <40 kg/m^2) (hereinafter referred to as obese individuals) (cohort 1) (**Table 1**; *Material and Methods* section), who were subclassified into three groups [normoglycemic (NG Obese): Glucose <100 mg/dL, HbA1c <5.7 %; impaired fasting glucose (IFG Obese): Glucose 100-126 mg/dL, HbA1c 5.7-6.5 %; and with type 2 diabetes (T2D Obese): Glucose >126 mg/dL, HbA1c >6.5 %], according to the criteria of the American Diabetes Association (ADA, 2020). IFG individuals exhibited significantly higher HOMA-IR values than NG individuals and they will be referred to as insulin-resistant (IR) subjects (Díaz-Ruiz et al., 2015; Tam et al., 2012). No significant differences were found among groups in blood pressure, inflammation, or lipid parameters except triglycerides, whose levels were enhanced in T2D *vs.* NG obese groups.

Paired SC and OM adipose tissue samples were processed immediately after tissue removal for the isolation of the stroma-vascular fraction (SVF) and mature adipocytes. Microscopic analysis and morphometric quantification of micrographs from freshly isolated mature adipocytes revealed that these cells were larger in IR/T2D than in NG obese individuals (**Figure 29**).

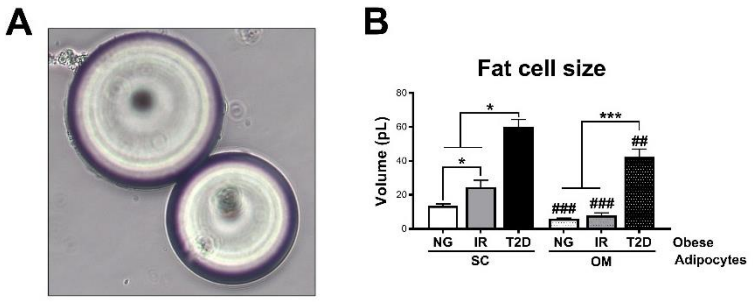

Figure 29. Representative light microscopy images **(A)**, and cell size **(B)** of SC and OM mature adipocytes from NG, IR, and T2D obese subjects (cohort 1, n=6-8). *****P<0.05, *******P<0.001 *vs.* NG and/or IR obese subjects; ##P<0.01, ###P<0.001 *vs.* SC preadipocytes from the same subjects.

SC and OM preadipocytes were obtained after serial passaging (2-3 passages) of the corresponding SVFs following established methods (Palumbo et al., 2018). The purity of the preadipocyte cultures was confirmed by the presence of preadipocyte markers (DLK1/PREF1, *ADIPOQ*, *CCL2*, *FABP4*, *PDGFRA*, *PPARG*, *TGFB2*, and *UPK3B*), and the absence of blood cell markers (CD45 and CD14) in RT-PCR and immunoblotting studies using protein (**Figure 30A**), and RNA (**Figure 30B**), extracts, respectively.

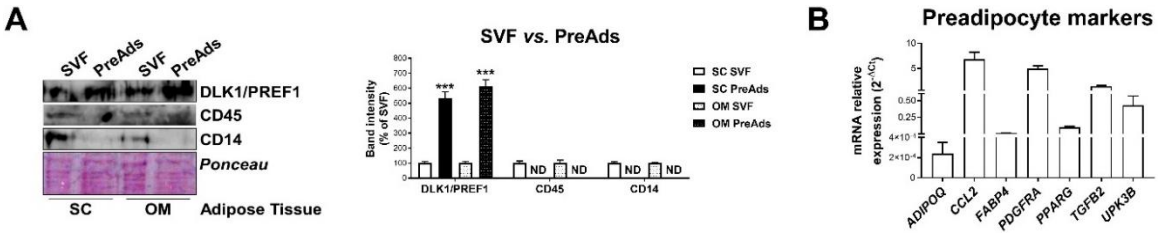

Figure 30. (A) Representative blot and protein level quantification of the proteins indicated in the SVF and preadipocytes (PreAds) isolated from SC and OM adipose tissue (cohort 1, n=3). *******P<0.001 *vs.* SVF; ND, non-detected. **(B)** mRNA levels of the genes indicated in SC and OM preadipocytes (cohort 1, n=12).

In addition, expression levels of the proliferation marker, *KI67*, and the proliferation rate, as assessed by cell count, were higher in SC than in OM preadipocytes, and both parameters decreased in IR/T2D (**Figure 31**).

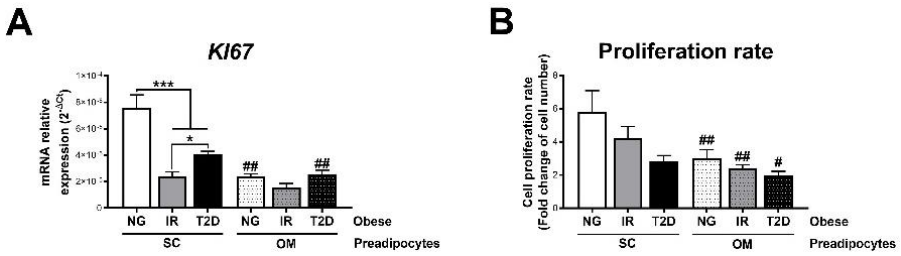

Figure 31. (A) mRNA levels of *KI67* in SC and OM preadipocytes from NG, IR, and T2D obese subjects (cohort 1, n=6). *****P<0.05, *******P<0.001 *vs.* NG and/or IR obese subjects; ##P<0.01 *vs.* SC preadipocytes from the same subjects. **(B)** Proliferation rate of SC and OM preadipocytes from NG, IR, and T2D obese subjects (cohort 1, n=20-22). #P<0.05, ##P<0.01 *vs.* SC preadipocytes from the same subjects.

As shown in **Table 8**, preadipocyte proliferation rate negatively correlated with obesity and IR markers (BMI, glucose, insulin, and HbA1c).

Table 8. Lineal regression analyses of the proliferation rate of SC and OM preadipocytes from obese subjects and their anthropometric and biochemical parameters (cohort 1).

	SC Preadipocytes		**OM Preadipocytes**	
	r	***P value***	**r**	***P value***
Age (years)	-0.024	0.875	0.240	0.113
Weight (kg)	-0.373	0.023 *****	-0.461	0.004 ******
Height (m)	-0.147	0.386	-0.152	0.369
BMI (kg/m^2)	-0.518	0.001 *******	-0.593	<0.0001 *******
Fat mass (%)	-0.585	0.024 *****	-0.714	0.004 ******
Lean mass (%)	-0.093	0.741	0.696	0.005 ******
Water mass (%)	-0.161	0.567	0.436	0.105
Waist circumference (cm)	-0.201	0.341	-0.204	0.352
Systolic pressure (mm/Hg)	-0.617	0.001 ******	-0.127	0.553
Diastolic pressure (mm/Hg)	-0.468	0.021 *****	-0.053	0.805
Fasting glucose (mg/dL)	-0.324	0.028 *****	-0.406	0.005 ******
Fasting insulin (mU/L)	-0.418	0.019 *****	-0.427	0.017 *****
HbA1c (%)	-0.417	0.007 ******	-0.442	0.004 **
HOMA-IR (units)	-0.546	0.002 ******	-0.512	0.003 **
Total cholesterol (mg/dL)	0.112	0.474	0.075	0.632
LDL cholesterol (mg/dL)	0.160	0.365	0.074	0.679
HDL cholesterol (mg/dL)	0.030	0.865	0.116	0.514
Triglycerides (mg/dL)	-0.170	0.281	-0.337	0.029 *****
Free fatty acids (mmol/L)	0.239	0.262	0.431	0.036 *****
C-reactive protein (mg/L)	-0.225	0.259	-0.530	0.004 ******
Uric acid (mg/dL)	0.047	0.782	0.107	0.527

r=Spearman's correlation coefficient, n=44-47. *****P<0.05, ******P<0.01, *******P<0.001.

Microscopic observation of lipid droplets (LDs) in cell preparations showed that both SC and OM preadipocytes from NG obese subjects differentiated well, while those from IR/T2D obese groups differentiated poorly (**Figure 32A**). In this line, the mRNA levels of the adipocyte markers, *PPARG*, *FABP4,* and *ADIPOQ* were lower in IR obese subjects than in their NG counterparts throughout differentiation (**Figure 32B**).

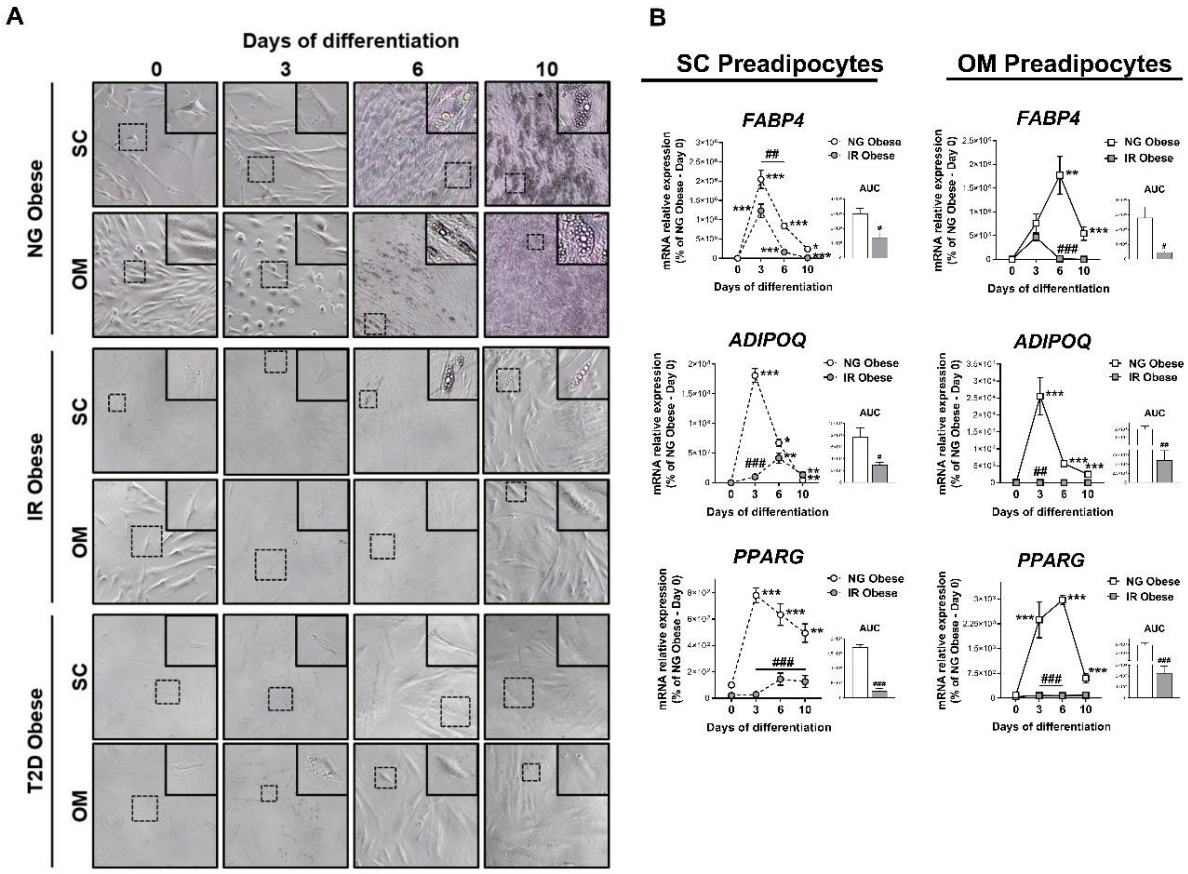

Figure 32. Representative light microscopy images **(A)**, and mRNA levels of the genes indicated **(B)** during *in vitro* differentiation of SC and OM preadipocytes from NG, IR, and T2D obese subjects (cohort 1, n=6). *****P<0.05, ******P<0.01, *******P<0.001 *vs.* previous days; ##P<0.01, ###P<0.001 *vs.* NG Obese.

1.2. Comparative proteomics of human obese preadipocytes

In order to identify marker pathogenic pathways of dysfunctional preadipocytes in obesity-associated metabolic disease, we employed iTRAQ proteomics of SC and OM preadipocytes from obese individuals of cohort 1 with extreme metabolic phenotypes, NG *vs.* T2D. This study enabled the identification of a total of 1,758 proteins that were present in both SC and OM fat from NG and T2D obese individuals, thus defining the human obese preadipocyte proteome (**Figure 26**; *Material and Methods* section). According to GO Biological Process annotation, 55.5% of these proteins were related to cellular and metabolic processes (**Figure 33A**), including metabolism of mRNA, proteins, glucose, and lipids (**Figure 33B**). All the proteomic data related to this study are available

at the ProteomeXchange Consortium via the Proteomics IDEntifications (PRIDE) partner repository (Perez-Riverol et al., 2019) with the dataset identifier PXD015621.

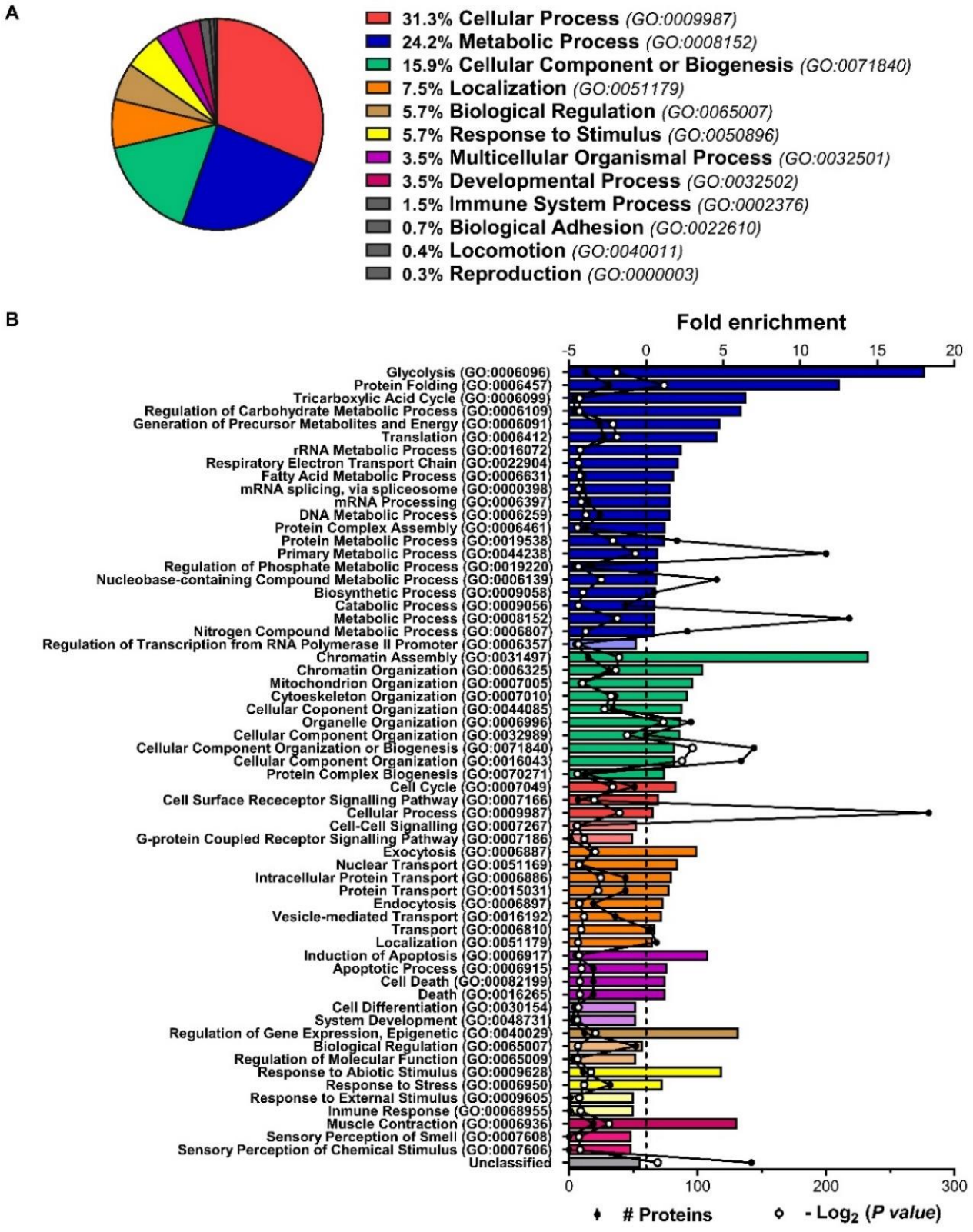

Figure 33. Pathway analysis of the proteome of SC and OM preadipocytes from NG and T2D obese subjects (cohort 1; n=5-6). Proteins were categorized according to GO biological processes **(A)** and depicted in significantly over- and under-represented according to their fold enrichment **(B)**. The black line represents the number of identified proteins per each GO pathway and the white line represents -Log_2(*P value*).

Comparison of proteomic data from SC and OM preadipocytes revealed marked differences between the cells of the two fat depots regarding the number of differentially expressed proteins and protein-related functional pathways (**Figure 34** and **Appendix 1**). To be more specific, 617 proteins and 512 proteins were differentially expressed between SC and OM preadipocytes in NG and T2D obese individuals, respectively (**Figure 34A**). Accordingly, T2D obese individuals exhibited a lower number of pathways with dissimilar regulation in SC preadipocytes *vs*. OM preadipocytes (5 down-regulated and 7 up-regulated pathways) than NG obese individuals (37 down-regulated and 25 up-regulated pathways) (**Figures 34B** and **34C**).

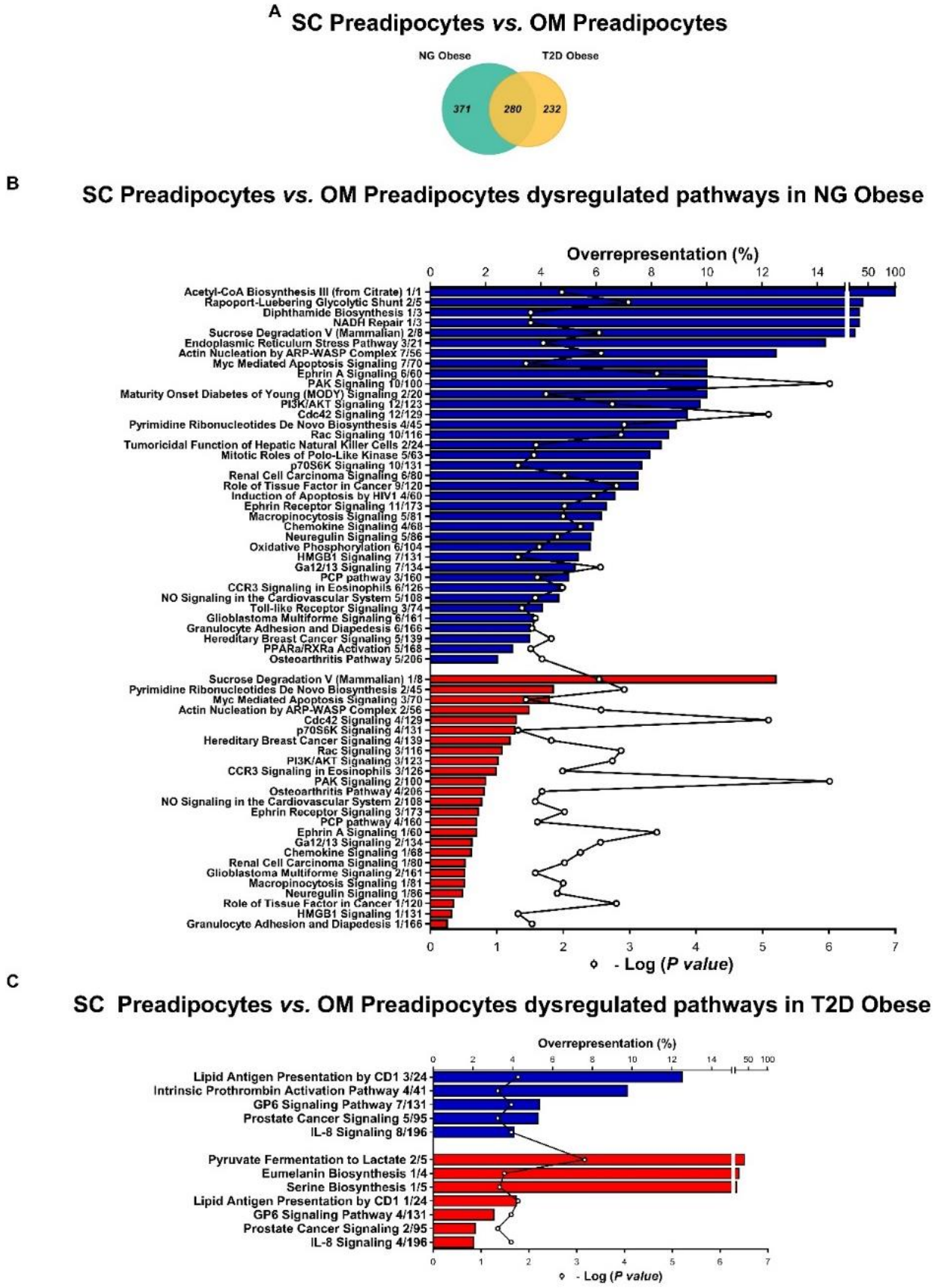

Figure 34. Venn diagram showing overlap of differentially regulated proteins **(A)**, and significant over-represented IPA pathways in SC *vs.* OM preadipocytes from NG **(B)**, and T2D **(C)** obese subjects (cohort 1, n=5-6). Blue and red bars indicate down- and up-regulated pathways, respectively. Numbers indicate the number of identified proteins/total proteins annotated to the pathway. Black line indicates $-Log_2$(*P value*).

In addition, when we compared T2D *vs.* NG obese individuals, 378 proteins and 372 proteins were differentially regulated in SC preadipocytes and OM preadipocytes, respectively (**Figure 35A**). To investigate enrichment for functional pathways in each depot, canonical pathway analysis of the proteomic data was performed using IPA (**Appendix 2**). Among the top ten IPA canonical pathways that were overrepresented in SC preadipocytes in T2D obesity, the highest ranked down-regulated pathway was the spliceosomal cycle (**Figure 35B**). The unfolded protein response (UPR) was also modified in SC preadipocytes from T2D obese group (**Figure 35B**), while pathways related to endoplasmic reticulum (ER) stress were up-regulated in OM preadipocytes (**Figure 35C**) in T2D *vs.* NG obesity.

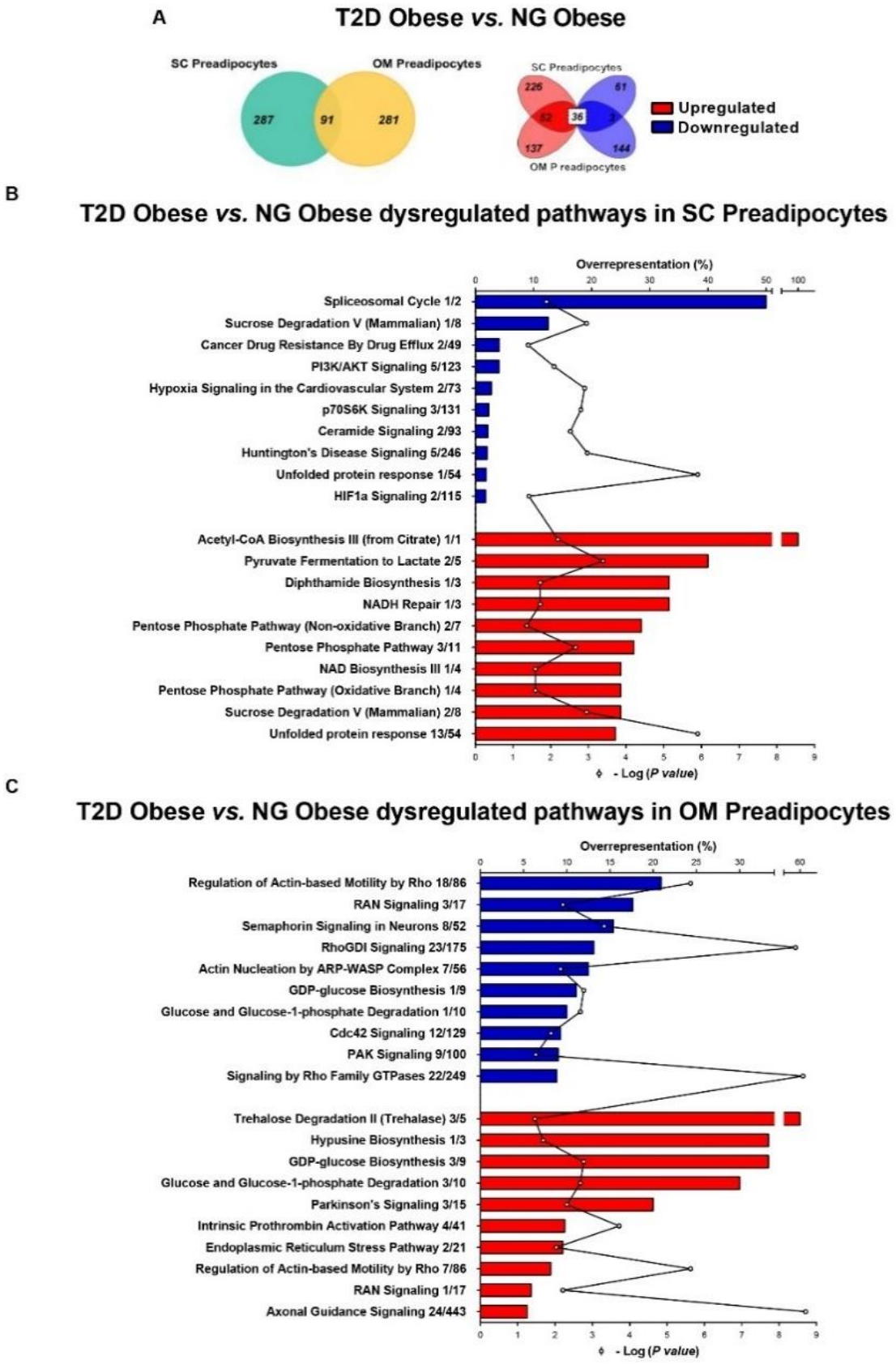

Figure 35. Venn diagrams showing overlap of differentially regulated proteins **(A)**, and Top10 significant over-represented IPA pathways in SC **(B)**, and OM preadipocytes **(C)** in T2D *vs.* NG obese subjects (cohort 1, n=5-6). Blue and red bars indicate down-regulated and up-regulated pathways, respectively. Numbers indicate the number of identified proteins/total proteins annotated to the pathway. Black line indicates - Log_2(*P value*).

Based on these findings, we next characterized the splicing machinery and ER control system in preadipocytes and their contribution to adipocyte differentiation.

1.3. Splicing Down-regulation as a marker of SC preadipocytes in obesity-related metabolic disease

To get further insights on the regulation of alternative splicing in preadipocytes, we explored the expression of genes related to this process in previously published transcriptomic datasets on human SC preadipocytes (Ehrlund et al., 2017). Specifically, IPA analysis of global gene expression profiles during *in vitro* differentiation of SC preadipocytes isolated from a lean healthy donor revealed that splicing of RNA/mRNA and processing of RNA/mRNA were among the top ten disease and functions (**Figure 36A**). Hierarchical clustering of expression values of splicing-related genes *(GO:0008380)* revealed that 60% of these genes were more expressed at early stages of adipocyte differentiation (D1-D4) (**Figure 36B**).

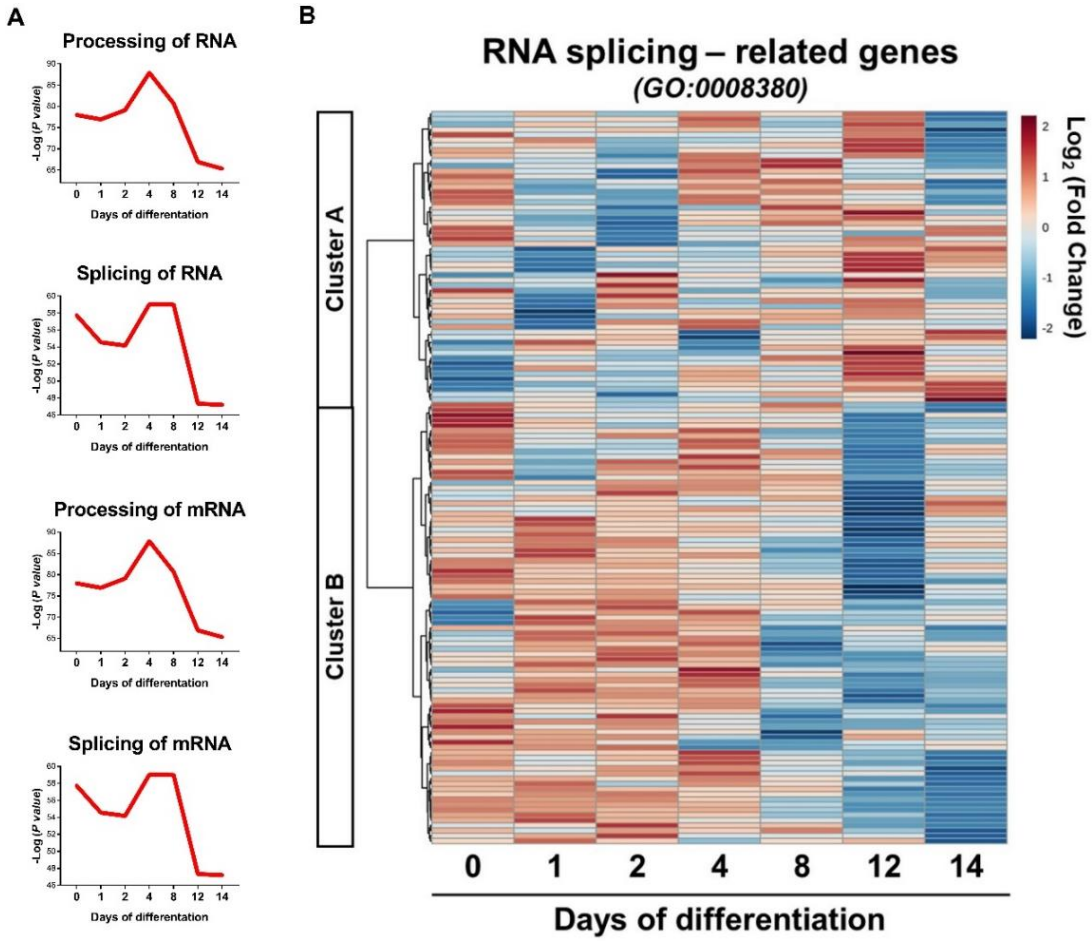

Figure 36. RNA metabolism-related IPA pathways **(A)**, and hierarchical clustering dendrogram heatmap of the mRNA expression of RNA splicing GO pathway-related genes **(B)** during *in vitro* differentiation of hADSCs. Rows stand for genes, while columns stand for differentiation time. The scale in the colour bar is Log_2(Fold Change).

To complement our proteomic observations, we assessed the expression of splicing-related genes in human preadipocytes using a microfluidic-based dynamic qPCR array comprising 45 splicing-related components (Gahete et al., 2018). Preadipocytes isolated from the SC and OM fat pads of NG, IR, and T2D obese individuals (n=6 per group) from cohort 1 were employed for this study. Analysis of gene expression profiles by hierarchical clustering revealed a marked gene expression shift between NG and IR/T2D SC preadipocytes, which was not evident for OM preadipocytes (**Figure 37**).

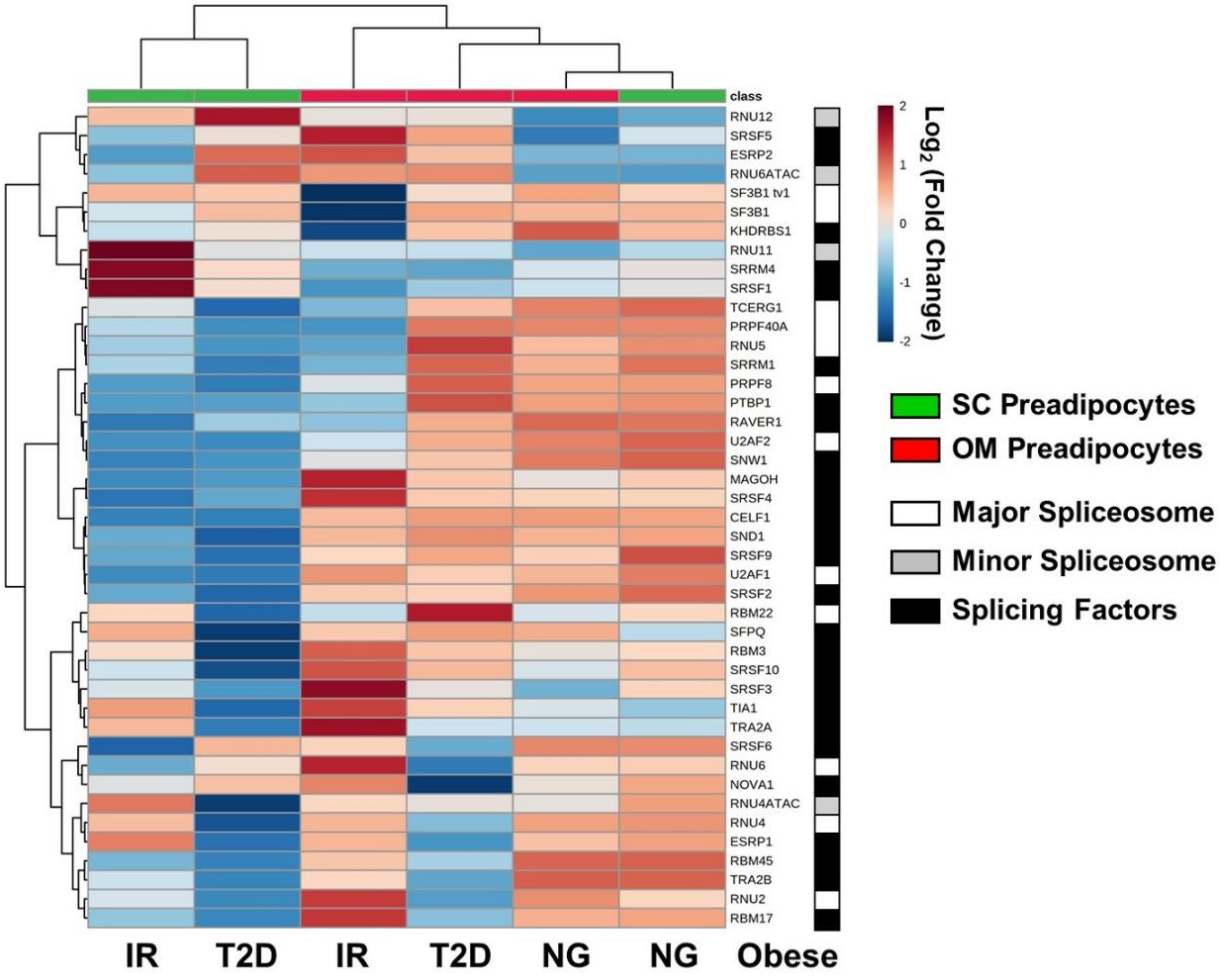

Figure 37. Hierarchical clustering dendrogram heatmap of splicing-related genes in SC (green) and OM (red) preadipocytes from NG, IR, and T2D obese subjects (cohort 1, n=6) measured by qPCR array. Rows stand for genes (white, mayor spliceosome; grey, minor spliceosome; black, splicing factors), while columns stand for subject groups. The scale in the colour bar represents -Log_2(Fold Change).

SC preadipocytes from IR/T2D obese individuals exhibited lower expression levels of splicing-related genes than NG obese subjects, including components of the major spliceosome (*PRPF8*, *RNU5*, *SF3B1 tv1*, *TCERG1*, and *U2AF1*), and splicing factors (*CELF1*, *MAGOH*, *RBM3*, *RBM45*, *SFPQ*, and *SNW1*) (**Figure 38A** and **38C**). Notably, only the minor spliceosome component, *RNU12*, was up-regulated in T2D *vs*. NG SC

preadipocytes (**Figure 38B**). No differences in OM preadipocytes were observed among the three groups of obese individuals (**Figure 38**).

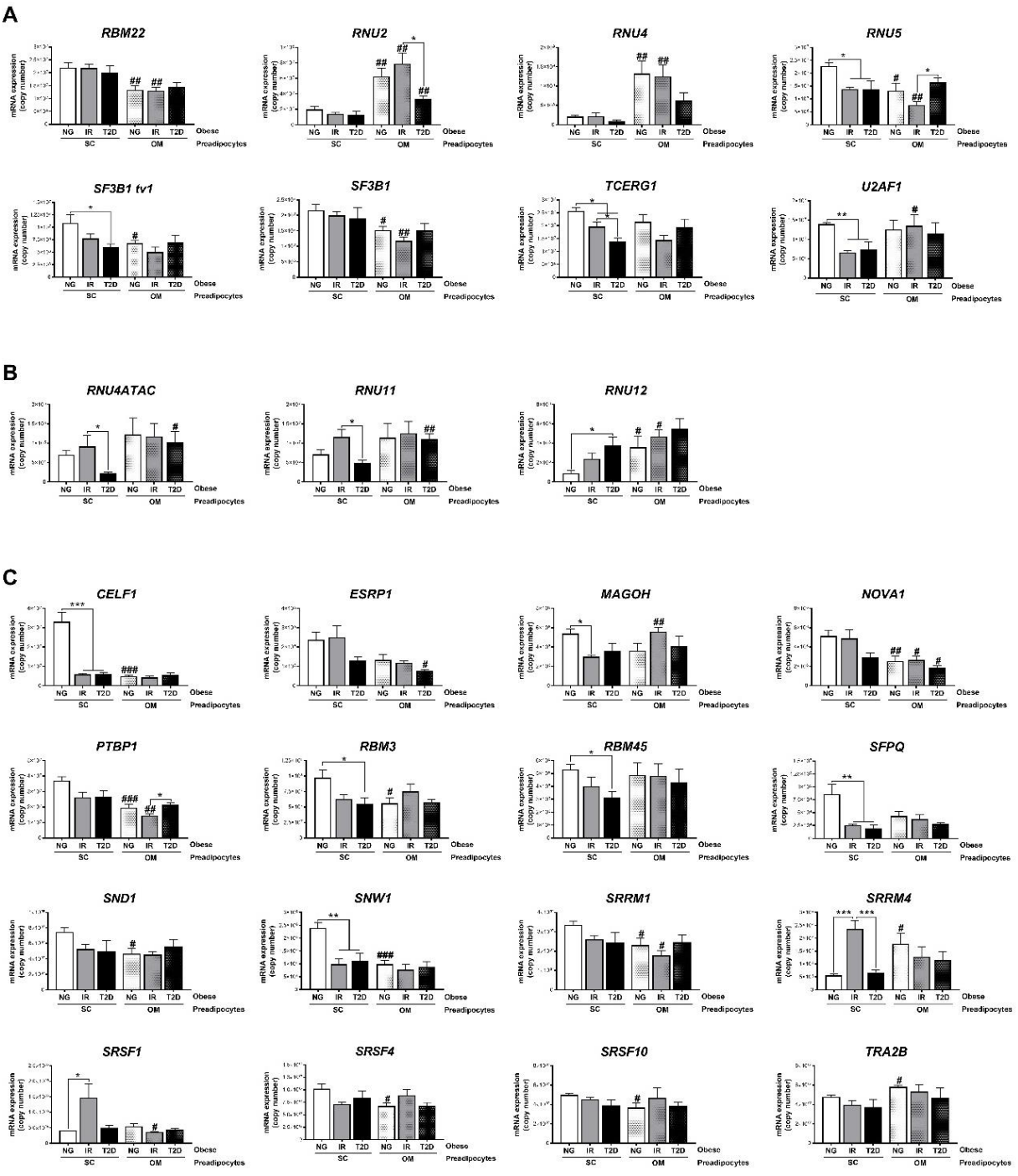

Figure 38. mRNA levels of components of the major spliceosome **(A)**, minor spliceosome **(B)**, and splicing factors **(C)** in SC and OM preadipocytes from NG, IR, and T2D obese subjects (cohort 1, n=6) measured by qPCR array. Only the genes that were significantly regulated are represented (27 out of 43; *PRPF8* is shown in **Figure 42**). *****P<0.05, ******P<0.01, *******P<0.001 *vs.* NG and/or IR subjects; #P<0.05, ##P<0.01, ###P<0.001 *vs.* SC preadipocytes from the same subjects.

Notably, only one major spliceosome component (*RNU1*) and one splicing factor (*CELF4*) could not be detected in the preadipocyte samples, whereas no statistical

differences were found among the six groups of obese preadipocytes in the remaining 15 splicing-related genes analysed (3 major and 1 minor spliceosome components, and 11 splicing factors) (**Figure 39**).

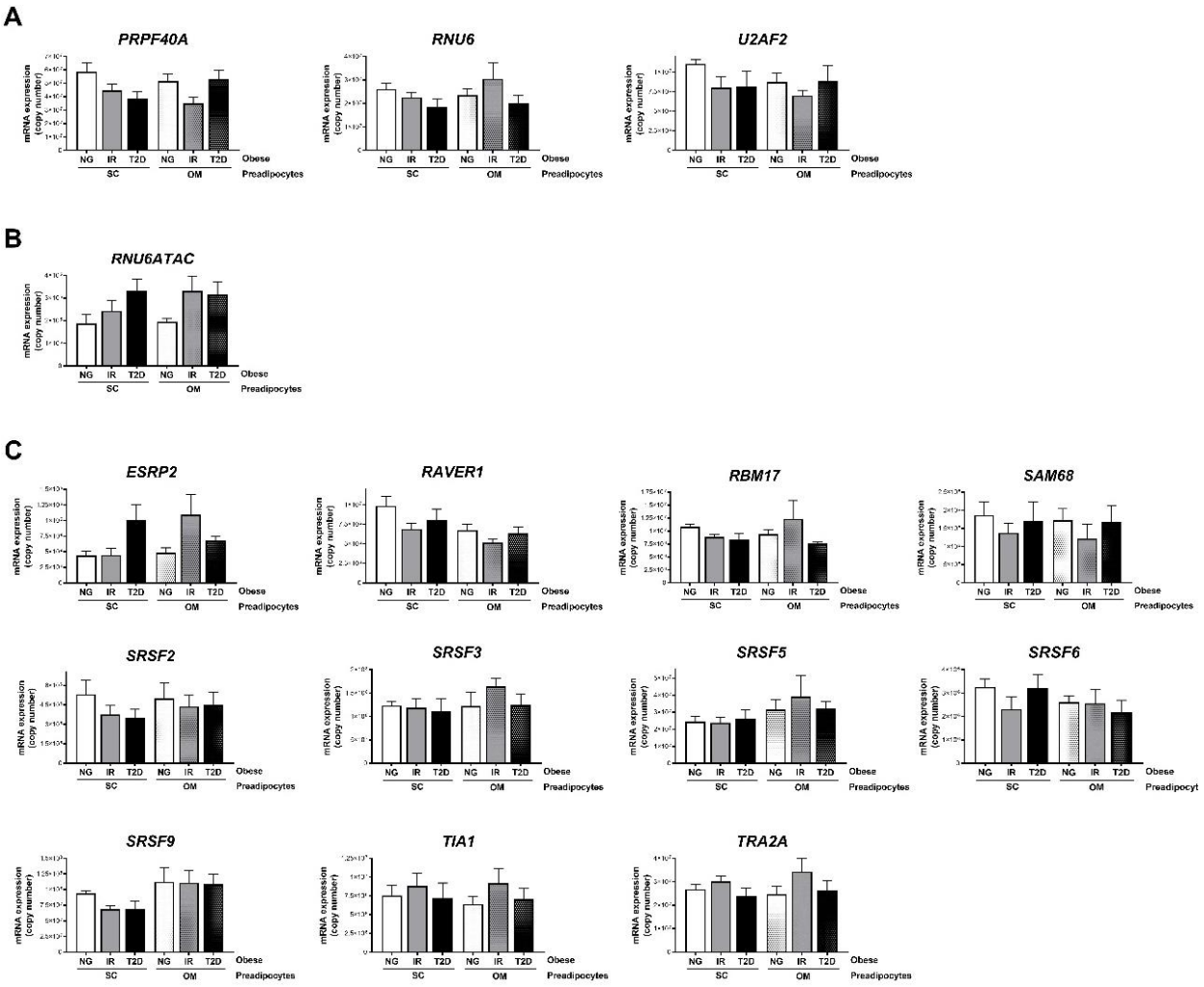

Figure 39. mRNA levels of components of the major spliceosome **(A)**, minor spliceosome **(B)**, and splicing factors **(C)** in SC and OM preadipocytes from NG, IR, and T2D obese subjects (cohort 1, n=6) measured by qPCR array. Only the genes that were not significantly regulated between the different groups are represented (15 out of 43).

These observations were largely confirmed by RT-PCR in RNA samples from SC and OM preadipocytes that were obtained from a second independent subset of samples (n=6) obtained from additional obese individuals (**Figure 40**).

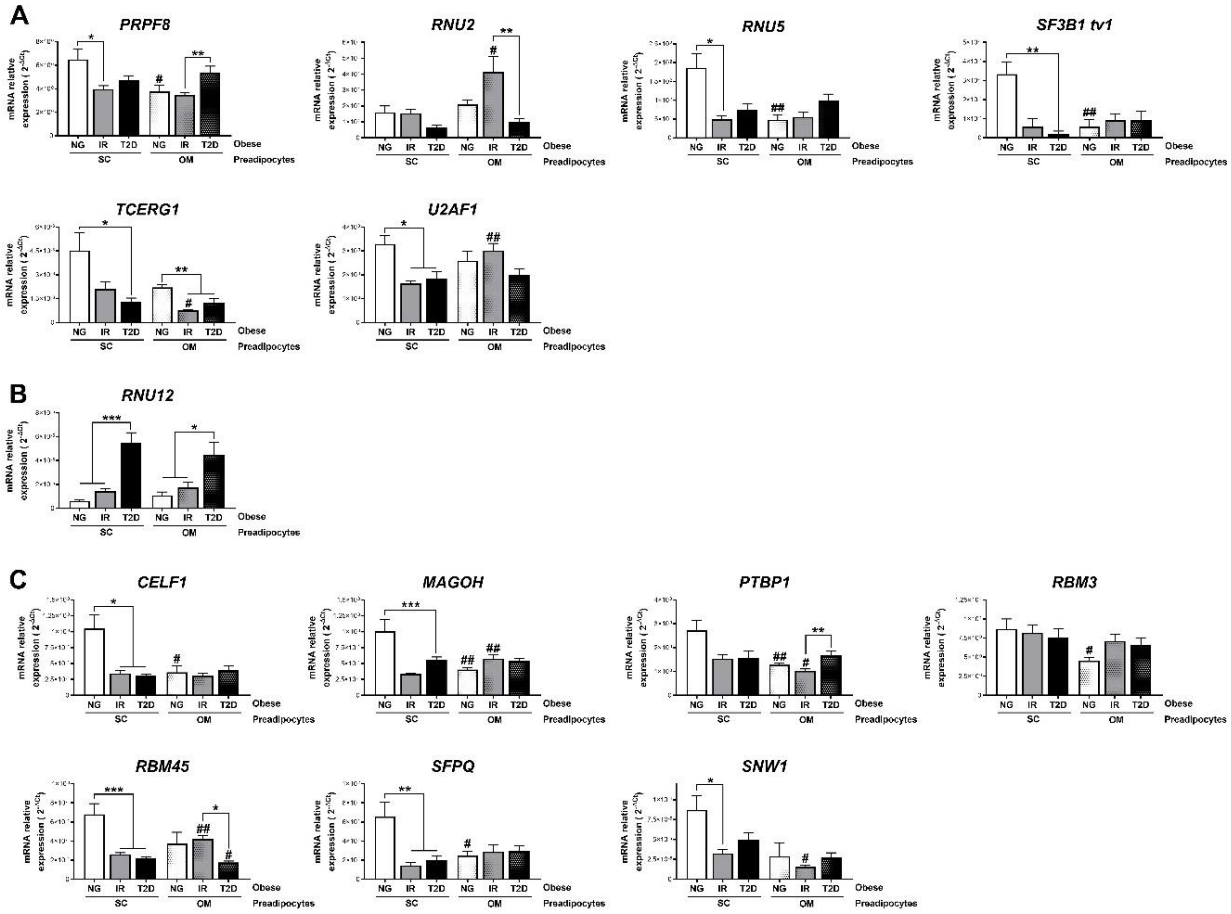

Figure 40. mRNA levels of components of the major spliceosome **(A)**, minor spliceosome **(B)**, and splicing factors **(C)** in SC and OM preadipocytes from NG, IR and T2D obese subjects (cohort 1, n=6) measured by RT-PCR. *****P<0.05, ******P<0.01, *******P<0.001 *vs.* NG and/or IR subjects; #P<0.05, ##P< 0.01 *vs.* SC preadipocytes from the same subjects.

Based on these findings, we next investigated whether inhibition of pre-mRNA splicing by use of pladienolide B, which binds to the SF3B complex (Aouida et al., 2016), had an effect on SGBS cell differentiation. As shown in **Figure 41**, exposure of SGBS cells to pladienolide B impaired lipid accumulation in these cells.

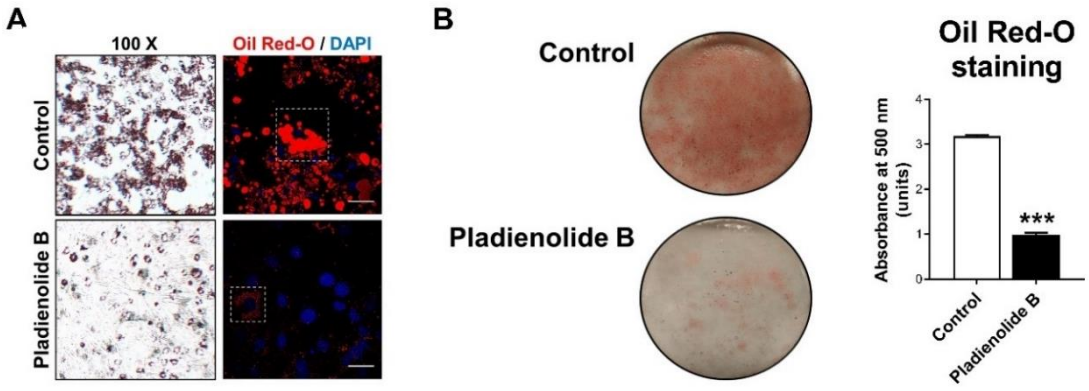

Figure 41. Representative images of light and confocal microscopy **(A)**, and quantification of Oil Red-O staining **(B)** of SGBS cells (day 4) treated with Pladienolide B (10^{-8} M), or vehicle (control) for 24h. *******P<0.001 *vs.* control. Scale bar = 10 µm.

1.4. *PRPF8*/PRP8 expression studies in human preadipocytes

One of the most highly expressed genes in SC preadipocytes from NG obese individuals that was significantly down-regulated in both IR and T2D obese subjects as compared to NG SC preadipocytes, was *PRPF8*/PRP8. Specifically, mRNA and protein levels of this key component of the major spliceosome were reduced by 51% and 56%, respectively, in IR SC preadipocytes, and by 49% and 82%%, respectively, in T2D SC preadipocytes as compared to NG levels (**Figure 42**). No differences in *PRPF8*/PRP8 expression were observed among groups in OM preadipocytes (**Figure 42**).

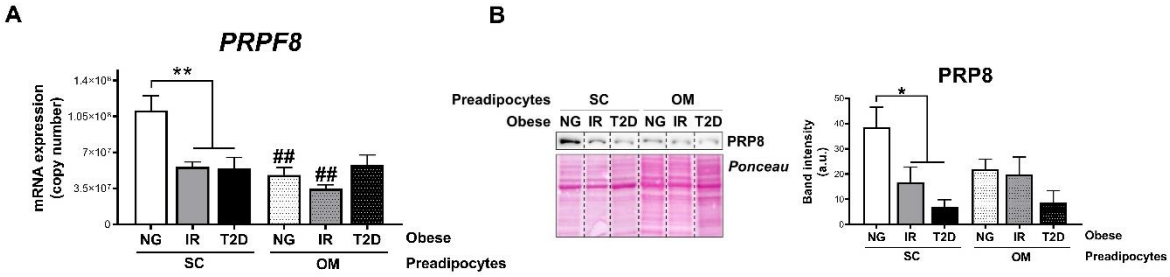

Figure 42. mRNA levels measured by qPCR dynamic array **(A)**, and representative blot and protein level quantification protein levels **(B)** in SC and OM preadipocytes from NG, IR, and T2D obese subjects (cohort 1, n=6). *****P<0.05, ******P<0.01 *vs.* NG and/or IR subjects, ##P<0.01 *vs*. SC preadipocytes from the same subjects.

We also examined *PRPF8* expression levels during in vitro differentiation of preadipocytes isolated from NG and IR individuals (**Figure 43**). These studies revealed that while *PRPF8* transcript content remained low throughout adipogenesis in IR preadipocytes, *PRPF8* levels peaked at day 3 (D3) of differentiation and thereafter remained above D0 levels in NG preadipocytes (**Figure 43**). *PRPF8* mRNA remained constant or decreased at the end of differentiation of NG and IR OM preadipocytes, respectively (**Figure 43**).

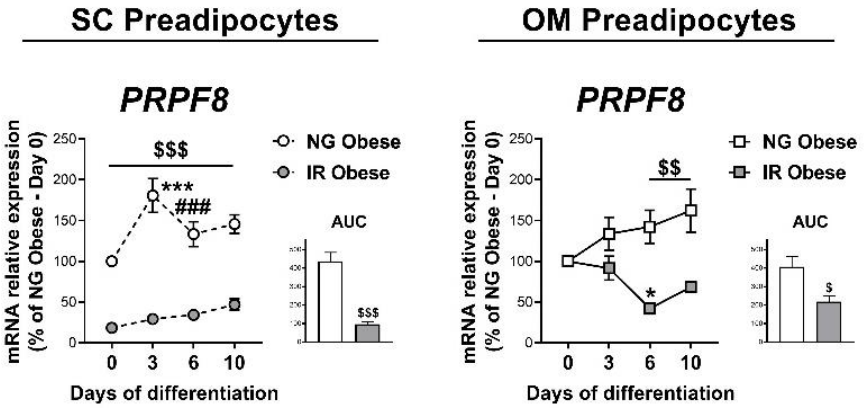

Figure 43. *PRPF8* mRNA levels during *in vitro* differentiation of SC and OM preadipocytes from NG and IR obese subjects (cohort 1, n=6). *****P<0.05, *******P<0.001 *vs.* day 0; ###P<0.001 *vs.* day 3; $$P<0.01, $$$P<0.001 *vs.* NG.

PRPF8 was also investigated in a second cohort comprising lean subjects and NG and T2D individuals with simple obesity (BMI >30 kg/m^2) (cohort 2). These studies showed significantly higher *PRPF8* expression levels in SC preadipocytes from NG obese *vs.* lean individuals (**Figure 44A**). Similar to that observed for morbidly obese individuals from cohort 1 (**Figure 42A**), significantly decreased *PRPF8* transcript levels were detected in T2D *vs.* NG individuals with simple obesity (**Figure 44A**). No differences in *PRPF8* transcript levels were observed in OM preadipocytes among groups (**Figure 44A**). Similar to that found for *PRPF8*, the expression levels of other component of the major spliceosome, *SF3B1 tv1*, and the splicing factors, *CELF1* and *SNW1*, were lower in T2D than in NG preadipocytes from individuals with simple obesity (**Figures 44B** and **44C**). Moreover, as observed in cohort 1 of morbidly obese individuals, the member of the minor spliceosome, *RNU12*, was more highly expressed in T2D than in NG preadipocytes in simple obesity (**Figure 44B**).

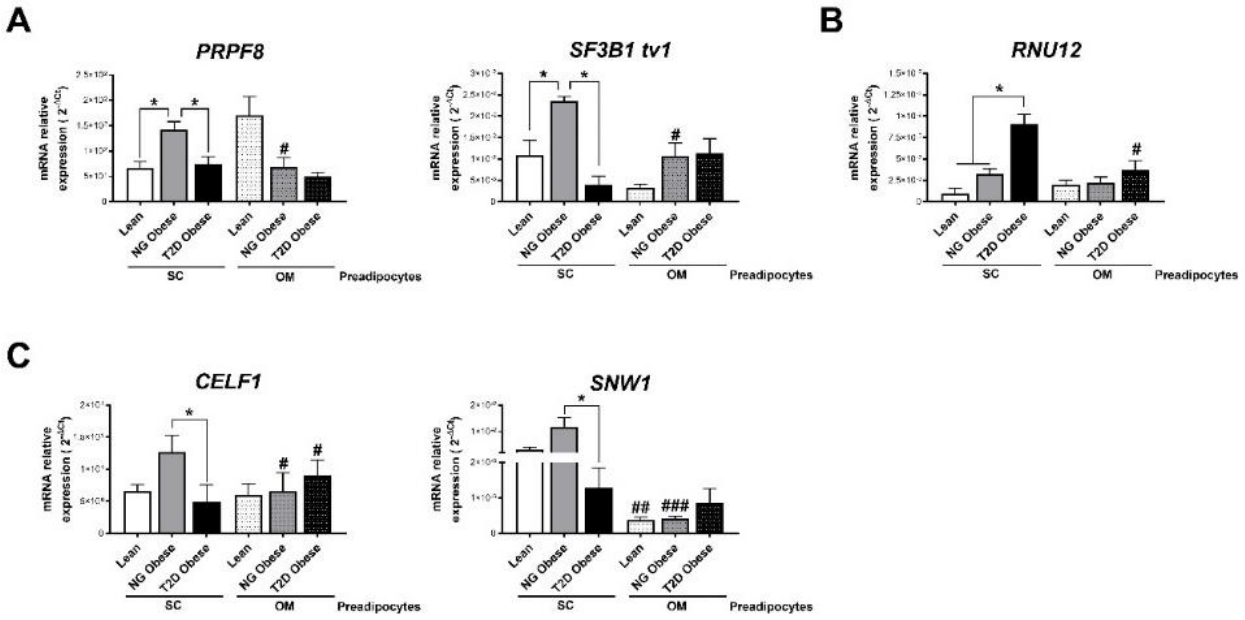

Figure 44. mRNA levels of representative components of the splicing machinery, including the major spliceosome **(A)**, minor spliceosome **(B)**, and splicing factors **(C)** in SC and OM preadipocytes from lean subjects and NG and T2D obese subjects (cohort 2, n=5-11 per group). *****P<0.05 *vs.* lean and/or NG obese subjects; #P<0.05, ##P<0.01, ###P<0.001 *vs.* SC preadipocytes from the same subjects.

1.5. Down-regulation of *PRPF8* expression in response to fibrotic conditions

We have recently shown that 3T3-L1 adipocytes cultured in 3D matrices based on collagen I-enriched hydrogels containing the proteoglycan, lumican, which mimic the fibrotic conditions occurring in the SC adipose tissue of IR morbidly obese individuals, exhibit impaired adipogenesis (Guzmán-Ruiz et al., 2020). To be more specific, 3D fibrotic matrices containing lumican reduced LD accumulation as well as the expression

levels of *PPARG* and in these cells as compared to 3D matrices containing collagen I alone (Guzmán-Ruiz et al., 2020). Herein, we show that 3T3-L1 cells differentiated in 3D collagen I-enriched matrices in the presence of increasing doses of lumican also exhibited lower *PRPF8* mRNA levels than control cells (**Figure 45C**).

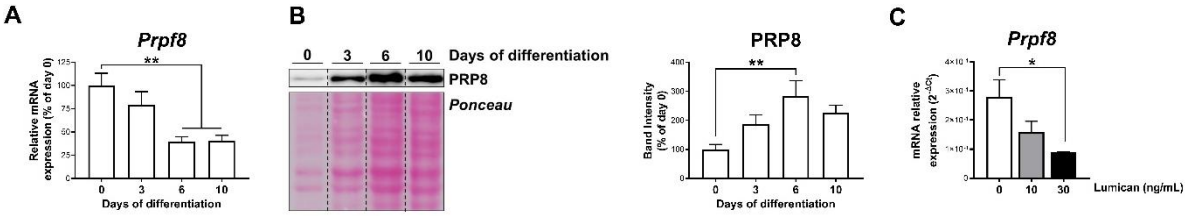

Figure 45. mRNA levels **(A)**, and representative blot, and protein level quantification **(B)** of *Prpf8*/PRP8 in 3T3-L1 cells during differentiation (days 0-10). ******P<0.01 *vs.* day 0. **(C)** mRNA levels of *Prpf8* in 3T3-L1 adipocytes (day 10 of differentiation) cultured in 3D matrices based on collagen I-enriched hydrogels containing or not increasing concentrations of the proteoglycan, lumican (0-30 ng/mL). *****P<0.05 *vs.* 0 ng/mL lumican.

Unfortunately, we could not replicate these experiments in SGBS cells because SGBS cell viability was severely compromised when these cells were grown in 3D collagen I-enriched matrices, even at the lowest collagen I concentration forming 3D gels (i.e., 1 mg/mL) (**Figure 24**; *Material and Methods* section).

Moreover, we cannot exclude the possibility that other pathogenic processes that are activated in obesity may also alter *PRPF8*/PRP8 expression, though no differences were observed in *PRPF8* mRNA levels in SGBS cells grown in other *in vitro* models of obesity-associated IR that have been previously validated in our laboratory (Díaz-Ruiz et al., 2015) (**Figure 84**). Specifically, neither hypertrophy or inflammation, induced by exposure to palmitate and TNFα, respectively, nor hyperglycaemia/hyperinsulinemia, induced upon treatment with high concentrations of glucose and insulin (HGHI), modified *PRPF8* transcript content in SGBS adipocytes (**Figure 46**). Likewise, exposure of SGBS adipocytes to oleate, which induces hypertrophy but does not impair insulin signalling in these cells (Díaz-Ruiz et al., 2015), had no effect on *PRPF8* expression levels (**Figure 46**).

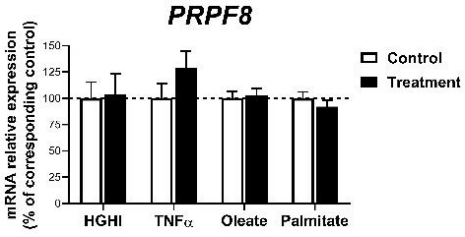

Figure 46. mRNA levels of *PRPF8* in SGBS preadipocytes (at day 4 of differentiation) exposed during 30 h to high glucose (4.5 g/L)/high insulin (100 nM) (HGHI), 5 nM TNFα, 500 μM Oleate, 500 μM Palmitate or corresponding vehicle (control).

1.6. *PRPF8*/PRP8 down-regulation in preadipocytes impairs adipogenesis

In order to unveil the relevance of *PRPF8*/PRP8 in adipocyte differentiation, we employed a siRNA strategy to down-regulate *PRPF8* gene expression levels in preadipocytes that mimicked the conditions found in IR/T2D obese SC preadipocytes as compared to NG obesity (**Figure 47**). These studies were carried out using the human SC adipocyte cell line, SGBS cells, given the limitations imposed by the low number of primary preadipocytes that can be obtained from human adipose tissue samples and the low transfection efficiency of these cells. As observed for NG SC human primary preadipocytes (**Figure 43**), *PRPF8* mRNA levels reached a peak at early stages of SGBS cell differentiation (D4) (**Figure 47**). Accordingly, siRNA treatment of SGBS cells started at D4 and cells were collected 72 h or 144 h post-transfection (D7 or D10 of differentiation, respectively).

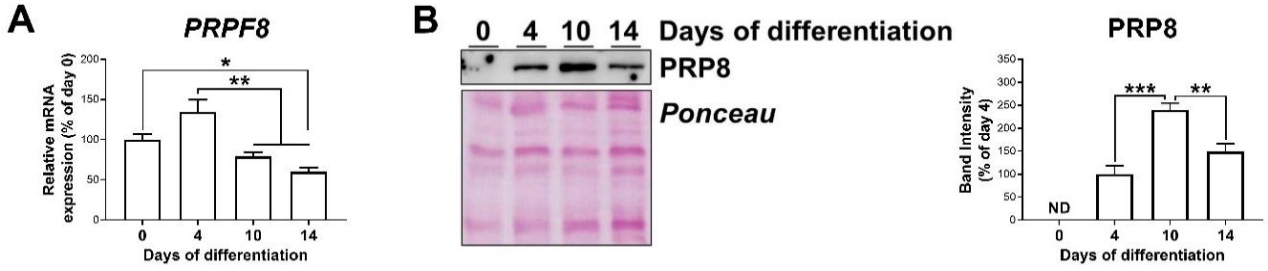

Figure 47. mRNA levels **(A)**, and representative blot, and protein level quantification **(B)** of *PRPF8*/ PRP8 in SGBS cells during differentiation (days 0-14). *****P<0.05, ******P<0.01; *******P<0.001 *vs.* previous days; ND, non-detected.

siRNA treatment of SGBS preadipocytes decreased by 67% and 65% *PRPF8* mRNA and protein levels, respectively, at day 3 post-transfection (D7), without changing cell viability (**Figure 48**).

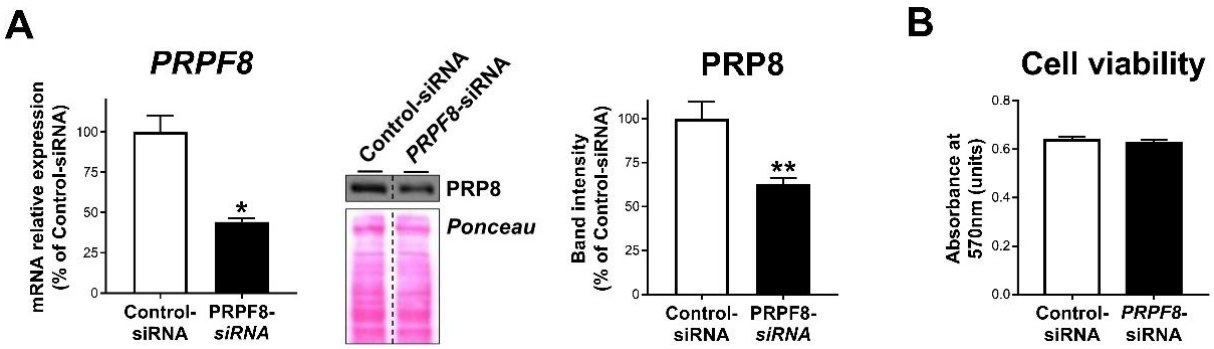

Figure 48. mRNA levels and representative blot and protein level quantification of *PRPF8*/PRP8 **(A)**, and cell viability **(B)** in SGBS adipocytes at day 3 post-transfection with Control-siRNA or *PRPF8*-siRNA. *****P<0.05, ******P<0.01 *vs.* control-siRNA.

Morphometric evaluation of Oil Red-O staining in confocal micrographs revealed that *PRPF8*-silenced preadipocytes accumulated more but smaller LDs than control cells, which resulted in an increase in the total lipid content in cells exposed to *PRPF8* siRNA (**Figure 49**).

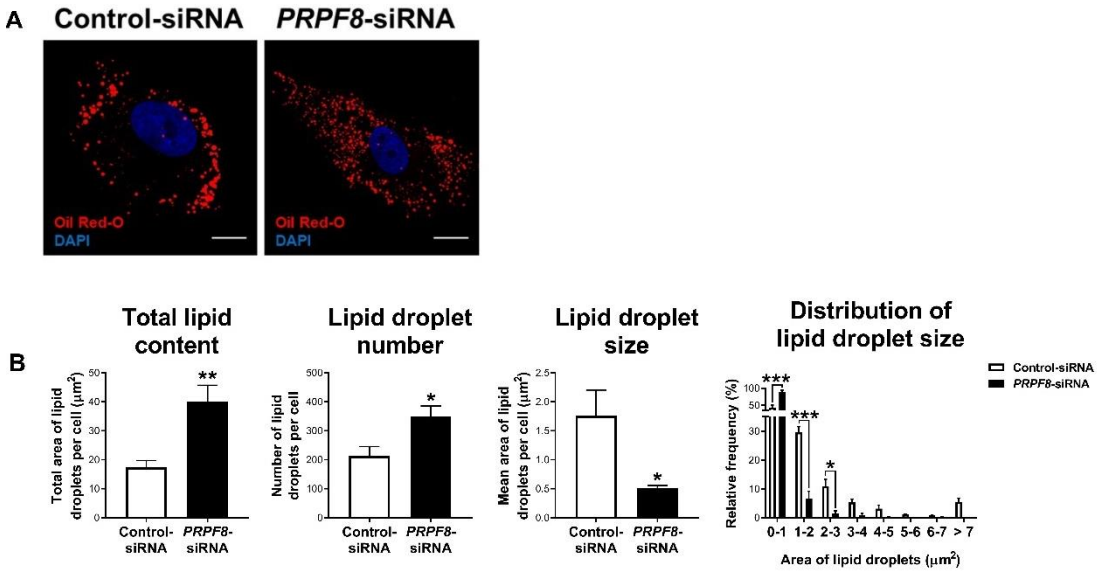

Figure 49. Representative confocal micrographs **(A)**, and LD morphometric analysis **(B)** of SGBS adipocytes at day 3 post-transfection with control-siRNA or *PRPF8*-siRNA stained with Oil Red-O (LDs, red) and DAPI (nuclei, blue). *****P<0.05, ******P<0.01, *******P<0.001 *vs.* control-siRNA. Scale bar = 10 µm.

In silico analysis of CLIP_Seq data using ENCORI (The Encyclopedia of RNA Interactomes) (J.-H. Li et al., 2013) revealed that both adipogenic (*PPARG* and *SREBF1)* and LD biogenesis and growth markers (*BSCL2*, *CIDEB*, and *CIDEC*) are PRP8 target genes (**Appendix 3**). Enrichment analysis of PRP8-RNA interactions revealed pathways such as insulin signalling, adipokine signalling, and fatty acid metabolism to be significantly overrepresented (**Appendix 3**). Similarly, the HumanBase tool (Greene et al., 2015) identified several adipogenesis-related genes, including *ADIPOQ*, *CAV1*, and *CD36*, among the Top10 genes showing functional interactions with *PRPF8* (**Figure 50** and **Appendix 4**).

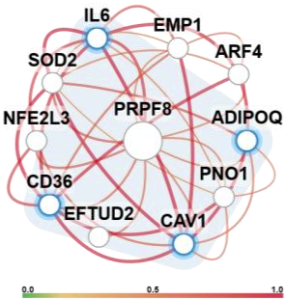

Figure 50. Top10 adipose tissue-specific network of *PRPF8* functional interactions according to HumanBase tool database (Greene et al., 2015).

To further explore this *in-silico* data, we evaluated the mRNA content of the transcription factors, *PPARG* and *SREBF1*, and the LD-related genes, *BSCL2*, *CIDEB*, and *CIDEC*, in SGBS cells considering either the expression of all the mRNA isoforms potentially derived from these genes or that of those isoforms which could be selectively amplified using specific primers (i.e., total and isoform expression levels, respectively) (**Figure 51A-C**). Thus, in accordance with the *in silico* data, expression of total *PPARG* and *SREBF1* transcript contents and the abundances of some of their isoforms were altered in *PRPF8*-silenced cells (**Figure 51A**). In particular, mRNA and protein levels of the fat specific *PPARG* isoform, *PPARG-2*, were up-regulated upon *PRPF8* silencing (**Figures 51A** and **51B**). Decreased levels and/or altered splicing patterns of *BSCL2*, *CIDEB*, and *CIDEC,* were also observed in silenced cells (**Figure 51C**).

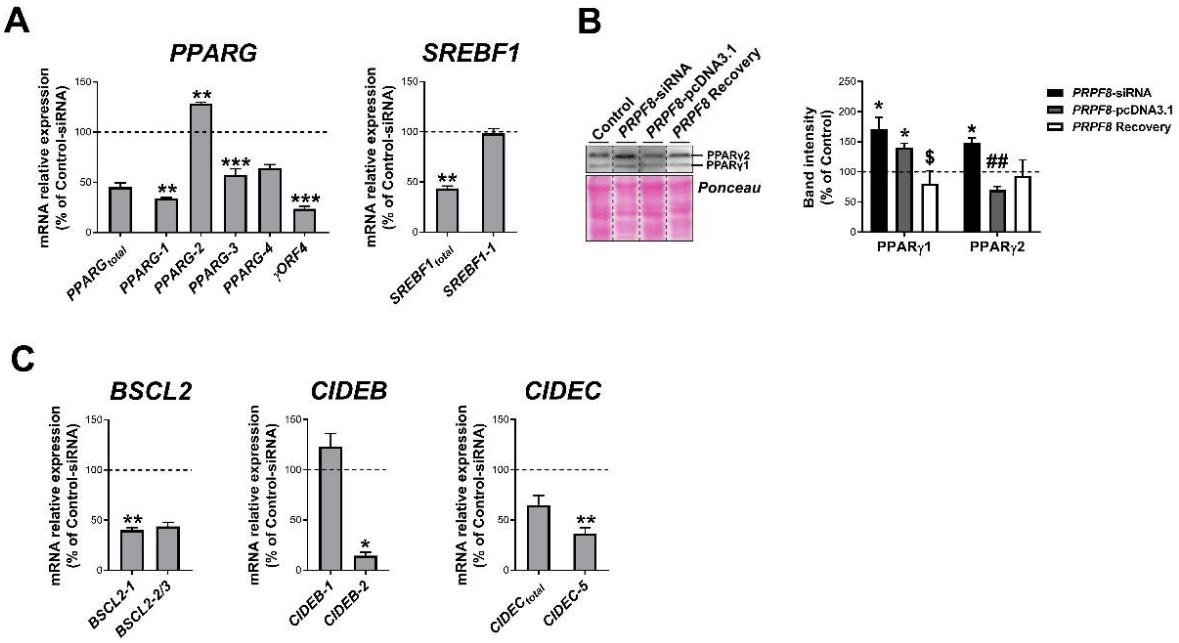

Figure 51. mRNA levels of splicing variants of the genes indicated **(A, C)**, and representative blot and protein level quantification of PPARγ1 and PPARγ2 **(B)** in SGBS adipocytes 3 days post-transfection with control, *PRPF8*-siRNA or *PRPF8*-pcDNA3.1, alone or in combination (*PRPF8* Recovery). *****P<0.05, ******P<0.01, *******P<0.001 *vs.* control; ##P<0.01 *vs. PRPF8*-siRNA; $P<0.05 *vs. PRPF8*-pcDNA3.1.

Other proteins showing significant changes in *PRPF8*-silenced cells included enzymes involved in lipid synthesis (FAS and DGAT2), and the LD-associated protein, ADRP, while neither PLIN1 nor HSL/pHSL, which are related to lipolysis, were modified (**Figure 52A**). *PRPF8* silencing also activated stress responses in SGBS adipocytes, as indicated by the increased protein levels of the ER stress marker, CHOP, the immunoproteasome component, PSMB8, and CASP3/Pro-CASP3 ratio, as a marker of apoptosis (**Figure 52A**). Contrarily to control cells, *PRPF8*-silenced cells did not respond to an insulin challenge (**Figure 52B**).

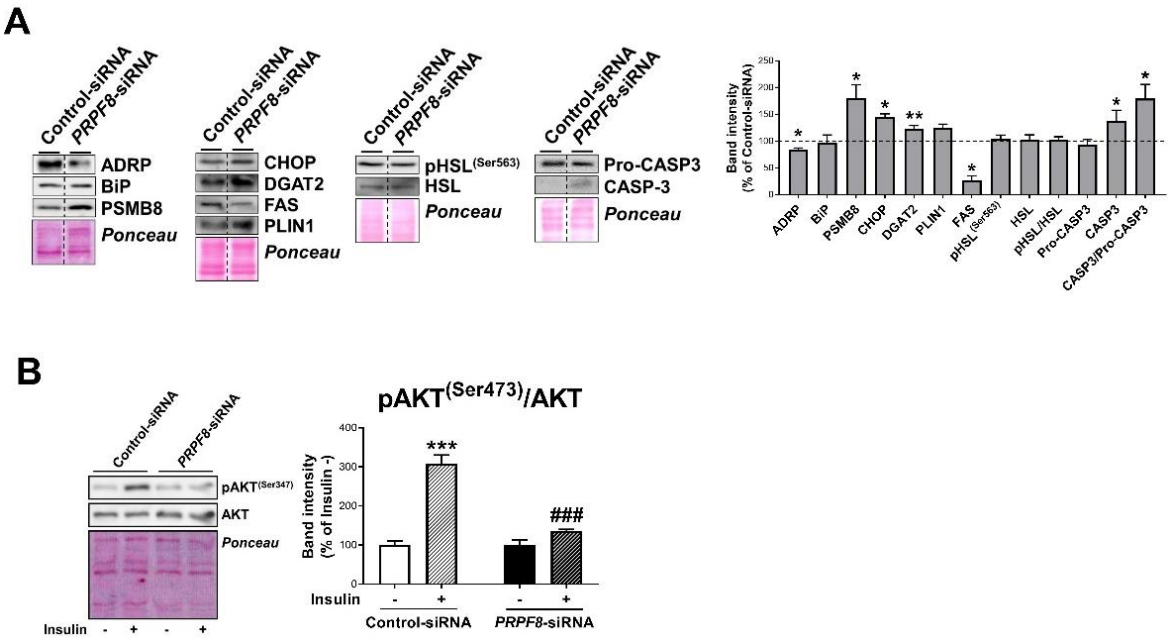

Figure 52. (A) Representative blot and protein level quantification of the proteins indicated in SGBS adipocytes 3 days post-transfection with Control-siRNA or *PRPF8*-siRNA. *****P<0.05, ******P<0.01 *vs.* control-siRNA. **(B)** Representative blots and protein level quantification of pAKT$^{(Ser473)}$ and AKT in SGBS adipocytes 3 days post-transfection treated with/without insulin (100nM, 15min). *******P<0.001 *vs.* control-siRNA -Insulin; $^{###}$P<0.001 *vs.* control-siRNA +Insulin.

Most of the effects depicted for silenced SGBS cells at D7 remained significant at D10 (**Figures 53-56**).

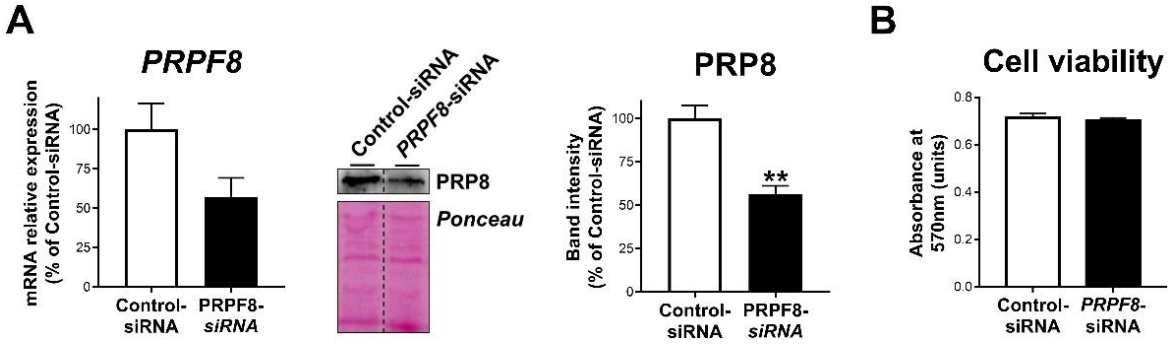

Figure 53. mRNA levels and representative blot and protein level quantification of *PRPF8*/PRP8 **(A)**, and cell viability **(B)** in SGBS adipocytes at day 5 post-transfection with Control-siRNA or *PRPF8*-siRNA. ******P<0.01 *vs.* control-siRNA.

Nevertheless, silenced cells at D10 still exhibited abundant LDs but of small size, thus resulting in a drastic decrease in the total amount of lipids stored in *PRPF8* siRNA-treated cells as compared with controls (**Figure 54**).

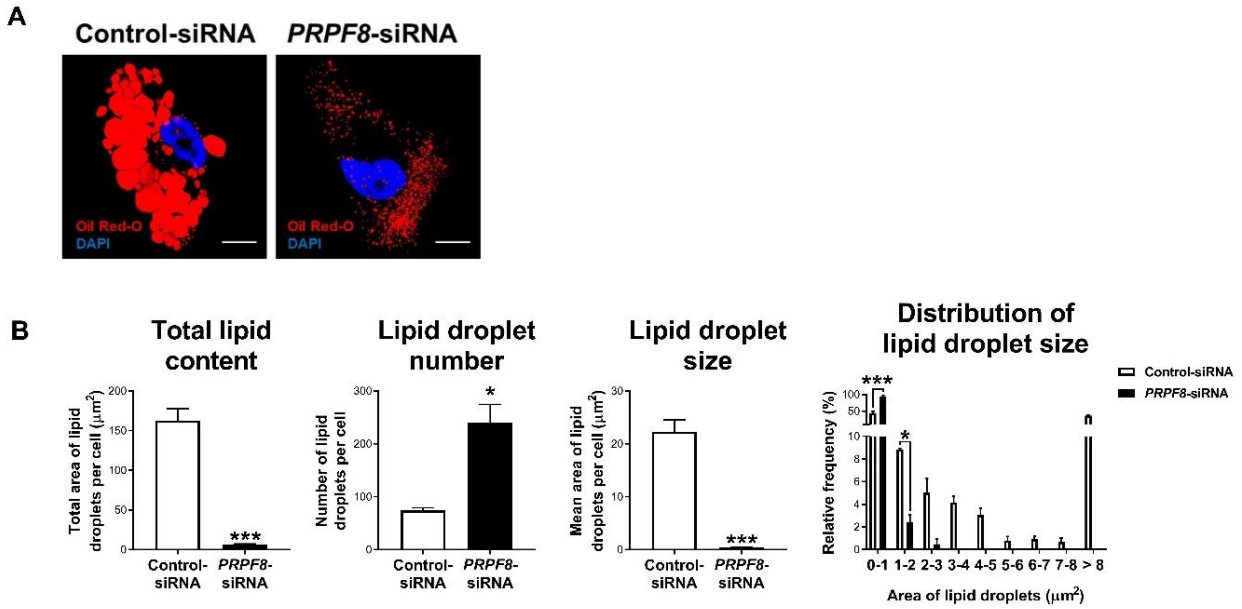

Figure 54. Representative confocal micrographs **(A)**, and LD morphometric analysis **(B)** of SGBS adipocytes at day 5 post-transfection with control-siRNA or *PRPF8*-siRNA stained with Oil Red-O (LDs, red) and DAPI (nucleus, blue). *****P<0.05, *******P<0.001 *vs.* control-siRNA. Scale bar = 10 µm.

PPARG-2 mRNA and protein, and the late adipocyte markers, *ADIPOQ* and *FABP4*, were down-regulated at D10 in *PRPF8*-silenced cells (**Figures 55** and **56**).

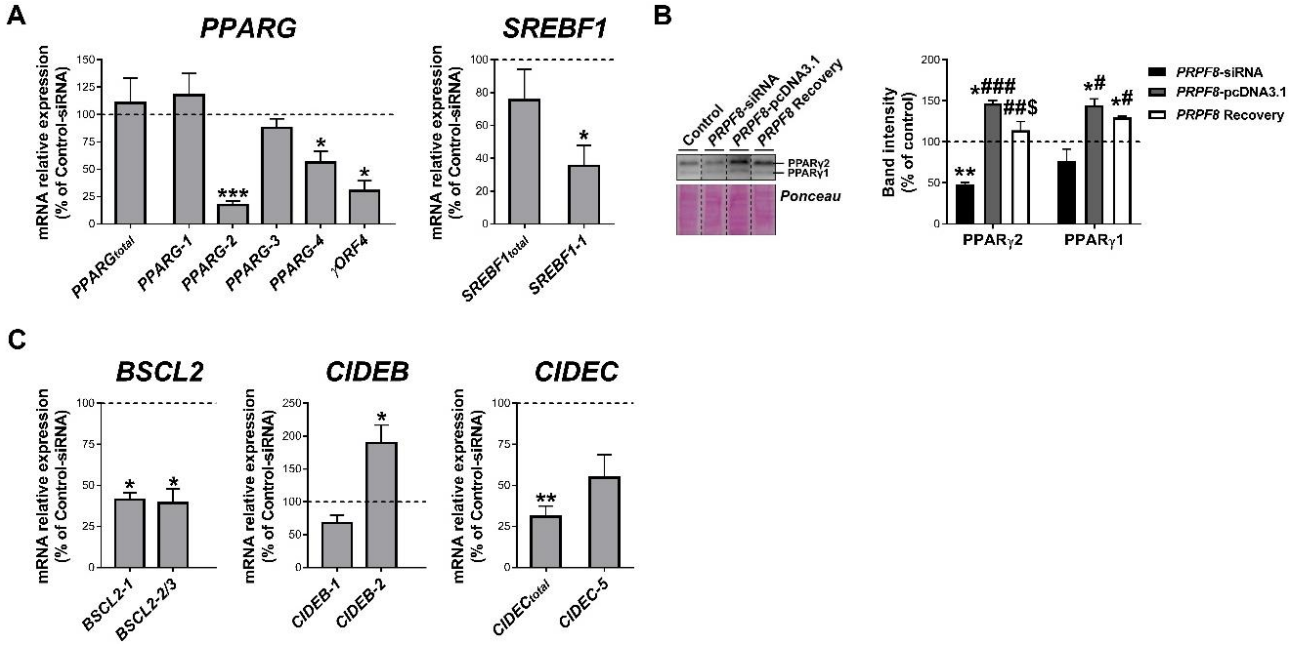

Figure 55. mRNA levels of splicing variants of the genes indicated **(A, C)**, and representative blot and protein level quantification of PPARγ1 and PPARγ2 **(B)** in SGBS adipocytes 5 days post-transfection with Control-siRNA or *PRPF8*-siRNA. *****P<0.05, ******P<0.01, *******P<0.001 *vs.* control-siRNA; #P<0.05, ##P<0.01, ###P<0.001 *vs. PRPF8*-siRNA; $P<0.05 *vs. PRPF8*-pcDNA3.1.

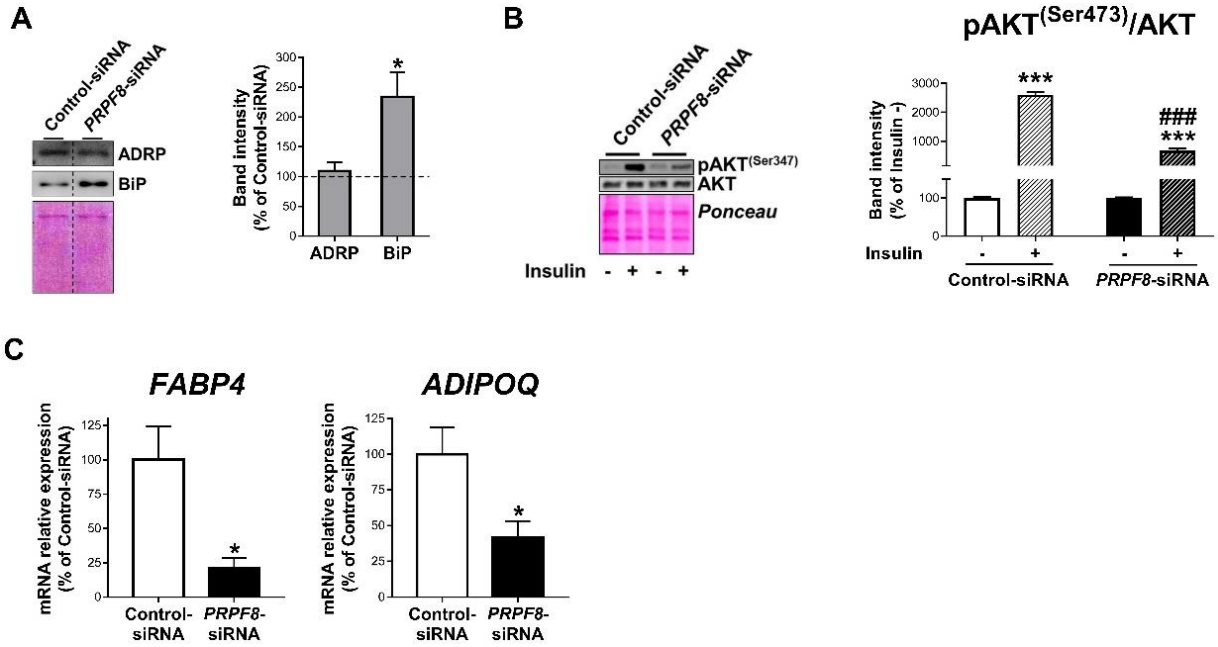

Figure 56. (A) Representative blot and protein level quantification of ADRP and BiP in SGBS adipocytes 5 days post-transfection with Control-siRNA or *PRPF8*-siRNA. *****P<0.05 *vs.* contro-siRNA. **(B)** Representative blots and protein level quantification of pAKT$^{(Ser473)}$ and AKT in SGBS adipocytes 5 days post-transfection treated with/without insulin (100nM, 15min). *******P<0.001 *vs.* control-siRNA -Insulin; $^{###}$P<0.001 *vs.* control-siRNA +Insulin. **(C)** mRNA levels of *FABP4* and *ADIPOQ* in SGBS adipocytes 5 days post-transfection. *****P<0.05 *vs.* control-siRNA.

In order to check the specificity of the effects induced by *PRPF8* silencing, we carried out rescue experiments using an expression vector coding for this protein (*PRPF8*-pcDNA3.1) (**Figure 57-61**).

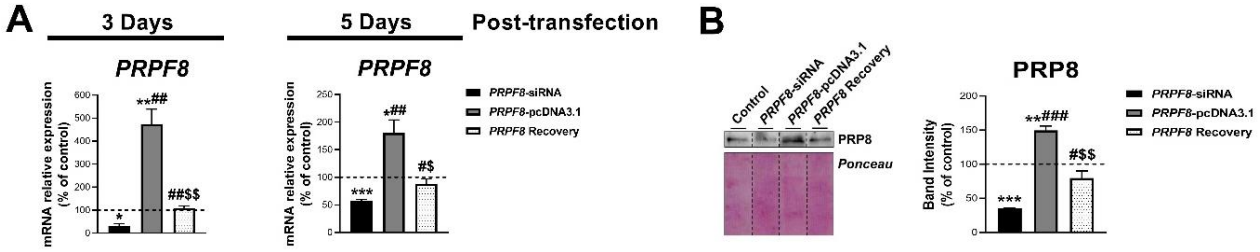

Figure 57. (A) mRNA levels of *PRPF8* in SGBS adipocytes at day 3 or 5 post-transfection with control, *PRPF8*-siRNA or *PRPF8*-pcDNA3.1, alone or in combination (*PRPF8* Recovery). **(B)** Representative blot and protein level quantification of PRP8 in SGBS adipocytes at day 5 post-transfection. *****P<0.05, ******P<0.01, *******P<0.001 *vs.* control; $^{#}$P<0.05, $^{##}$P<0.01, $^{###}$P<0.001 *vs. PRPF8*-siRNA; $^{\$}$P<0.05, $^{\$\$}$P<0.01 *vs. PRPF8*-pcDNA3.1.

Recovery of PRP8 protein levels by co-transfection of *PRPF8*-silenced SGBS cells with *PRPF8*-pcDNA3.1 reverted the effects induced by *PRPF8* silencing on adipocyte and LD markers at D7 (**Figure 58**).

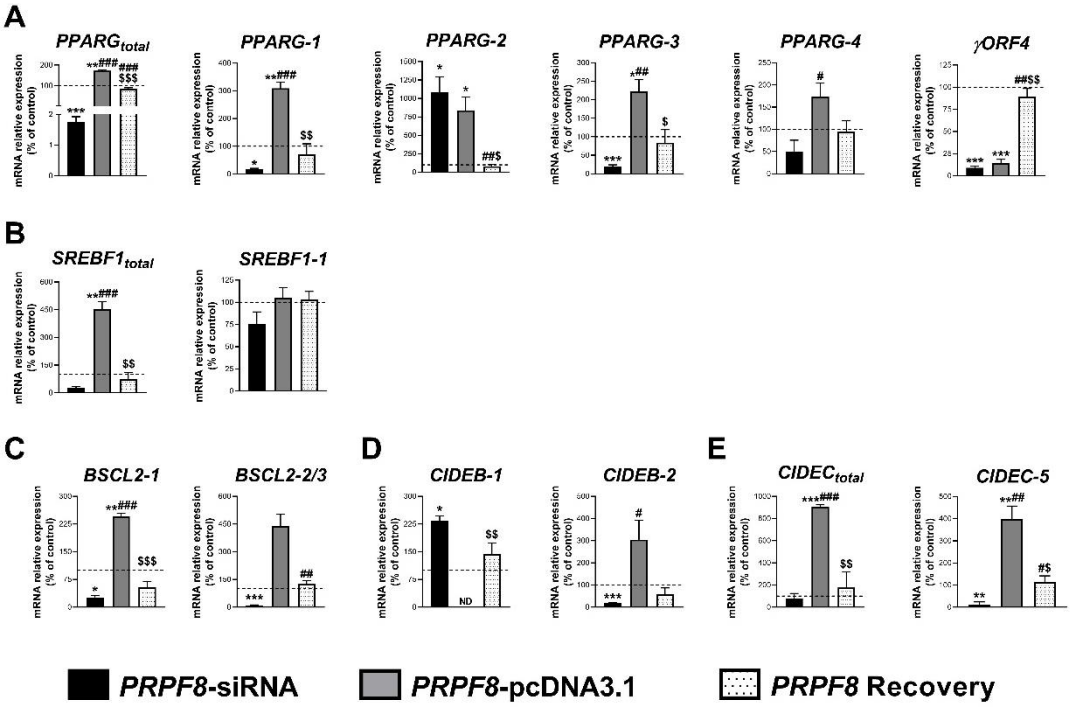

Figure 58. (A-E) mRNA levels of splicing variants of the genes indicated in SGBS adipocytes at day 3 post-transfection with control, *PRPF8*-siRNA or *PRPF8*-pcDNA3.1, alone or in combination (*PRPF8* Recovery). *****P<0.05, ******P<0.01, *******P<0.001 *vs.* control; #P<0.05, ##P<0.01, ###P<0.001 *vs. PRPF8*-siRNA; $P<0.05, $$P<0.01, $$$P<0.001 *vs. PRPF8*-pcDNA3.1.

Similar results were observed when *PRPF8*-silenced SGBS cells were observed at later stages of differentiation (D10) (**Figure 59**).

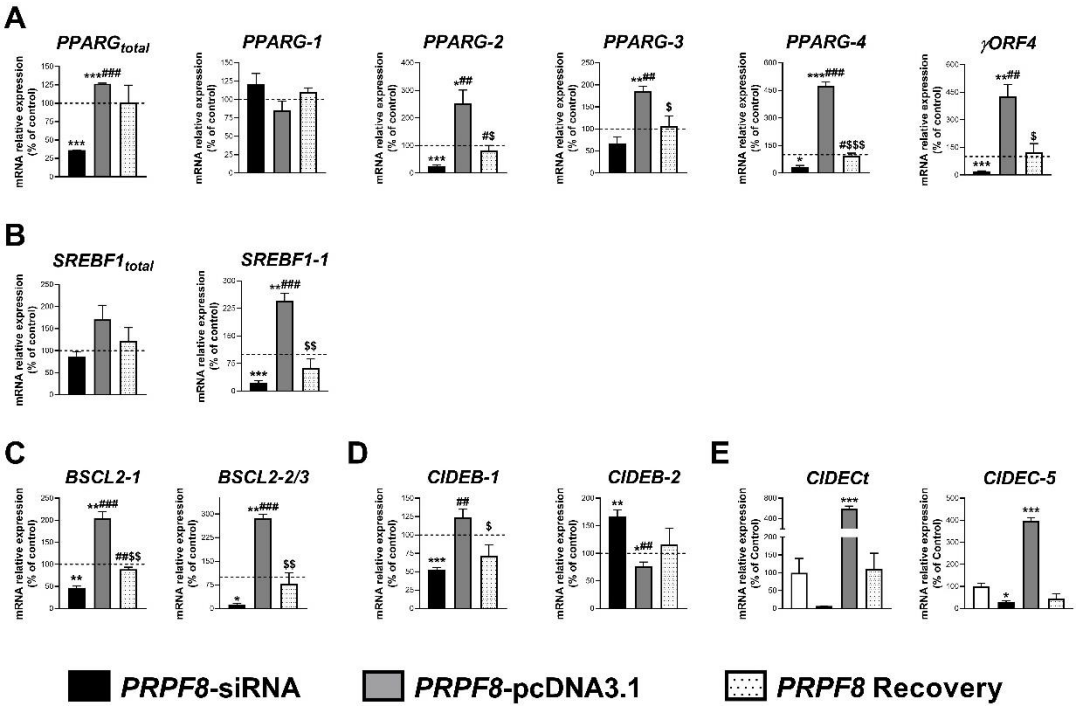

Figure 59. (A-E) mRNA levels of splicing variants of the genes indicated in SGBS adipocytes at day 5 post-transfection with control, *PRPF8*-siRNA or *PRPF8*-pcDNA3.1, alone or in combination (*PRPF8* Recovery). *****P<0.05, ******P<0.01, *******P<0.001 *vs.* control; #P<0.05, ##P<0.01, ###P<0.001 *vs. PRPF8*-siRNA; $P<0.05, $$P<0.01, $$$P<0.001 *vs. PRPF8*-pcDNA3.1.

Silencing-induced changes in both LD number and size were also reverted in rescue experiments by *PRPF8* re-expression as soon as 3 days post-transfection (**Figure 60**).

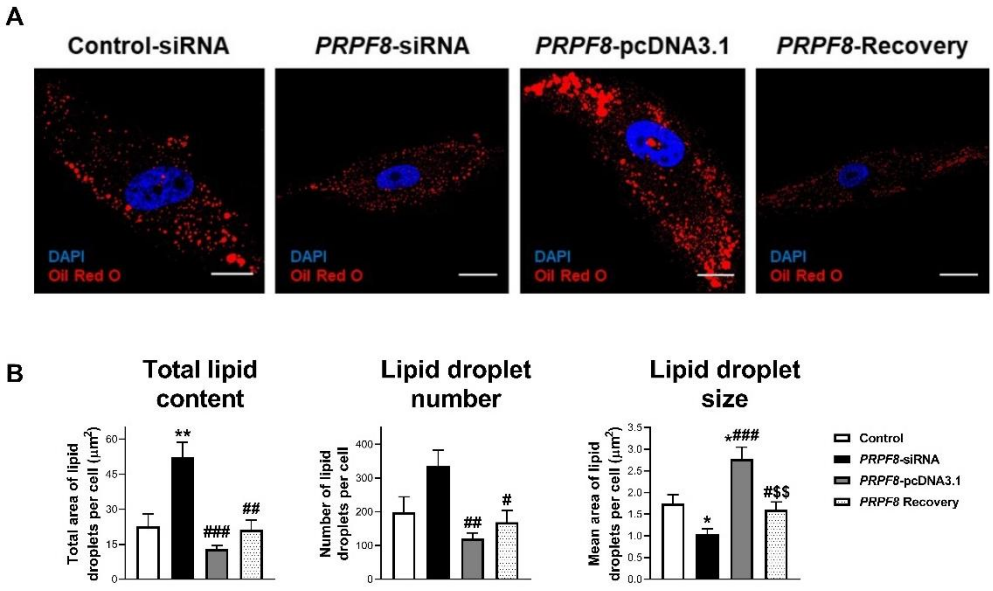

Figure 60. Representative confocal micrographs **(A)**, and LD morphometric analysis **(B)** of SGBS adipocytes at day 3 post-transfection with control, *PRPF8*-siRNA or *PRPF8*-pcDNA3.1, alone or in combination (*PRPF8* Recovery) stained with Oil Red-O (LDs, red) and DAPI (nuclei, blue). *****P<0.05, ******P<0.01 *vs.* control; $^{\#}$P<0.05, $^{\#\#}$P<0.01, $^{\#\#\#}$P<0.001 *vs. PRPF8*-siRNA; $^{\$\$}$P<0.01 *vs. PRPF8*-pcDNA3.1. Scale bar = 10 µm.

Recovery of LD number and size by *PRPF8* expression could be also observed in silenced SGBS adipocytes at late stages of differentiation (D5 post-transfection) (**Figure 61**).

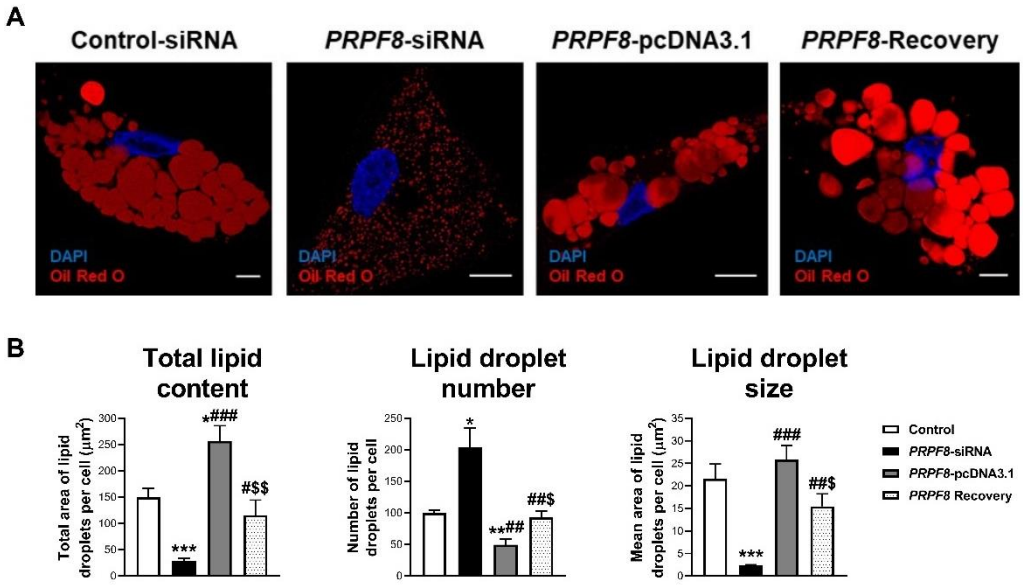

Figure 61. Representative confocal micrographs **(A)**, and LD morphometric analysis **(B)** of SGBS adipocytes at day 5 post-transfection with control, *PRPF8*-siRNA or *PRPF8*-pcDNA3.1, alone or in combination (*PRPF8* Recovery) stained with Oil Red-O (LDs, red) and DAPI (nuclei, blue). *****P<0.05, ******P<0.01, *******P<0.001 *vs.* control; $^{\#}$P<0.05, $^{\#\#}$P<0.01, $^{\#\#\#}$P<0.001 *vs. PRPF8*-siRNA; $^{\$}$P<0.05, $^{\$\$}$P<0.01 *vs. PRPF8*-pcDNA3.1. Scale bar = 10 µm.

Finally, we also investigated the effects of *PRPF8* silencing in human adipose-derived stem cells (hADSCs) (**Figures 62-65**). In these cells, wherein *PRPF8* levels remained constant throughout differentiation (**Figure 62A**), *PRPF8* siRNA was effective in reducing endogenous *PRPF8* mRNA levels (**Figure 62B**). *PRPF8* silencing did not affect cell viability (**Figure 62C**).

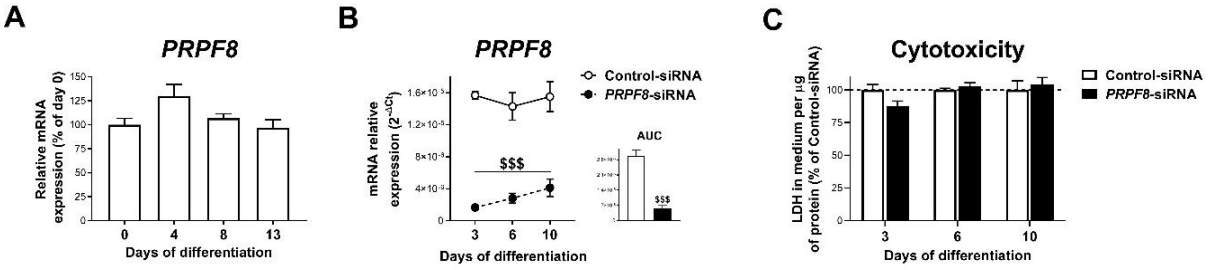

Figure 62. (A) mRNA levels of *PRPF8* in hADSCs cells during *in vitro* differentiation (days 0-13). mRNA levels of *PRPF8* **(B)**, and cytotoxicity **(C)** in hADSCs cells transfected with *PRPF8*-siRNA or Control-siRNA during differentiation (days 3-10). $^{\$\$\$}$P<0.001 *vs.* control-siRNA.

Similar to that observed for SGBS cells, *PRPF8* silencing modified LD content and size in hADSCs (**Figures 63**).

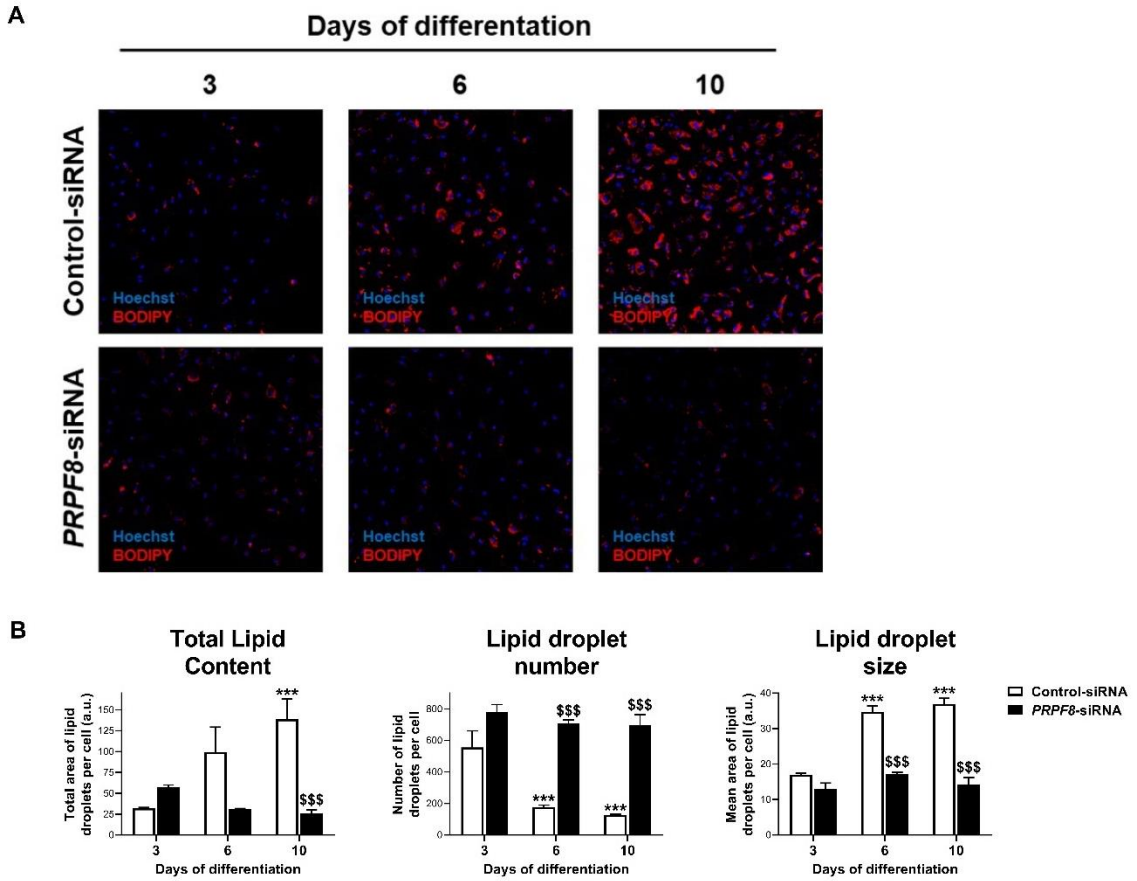

Figure 63. Representative micrographs **(A)**, and and LD morphometric analysis **(B)** of hADSCs cells transfected with *PRPF8*-siRNA or Control-siRNA after staining with BODIPY (LDs, red) and Hoechst (nuclei, blue) during differentiation (days 3-10). *******P<0.001 *vs.* day 3; $^{\$\$\$}$P<0.001 *vs.* control-siRNA.

Likewise, changes in the expression levels of markers of adipogenesis and LD biogenesis and growth, either global or affecting to specific isoforms, were observed in hADSCs-silenced for *PRPF8* as compared to control cells (**Figure 64**).

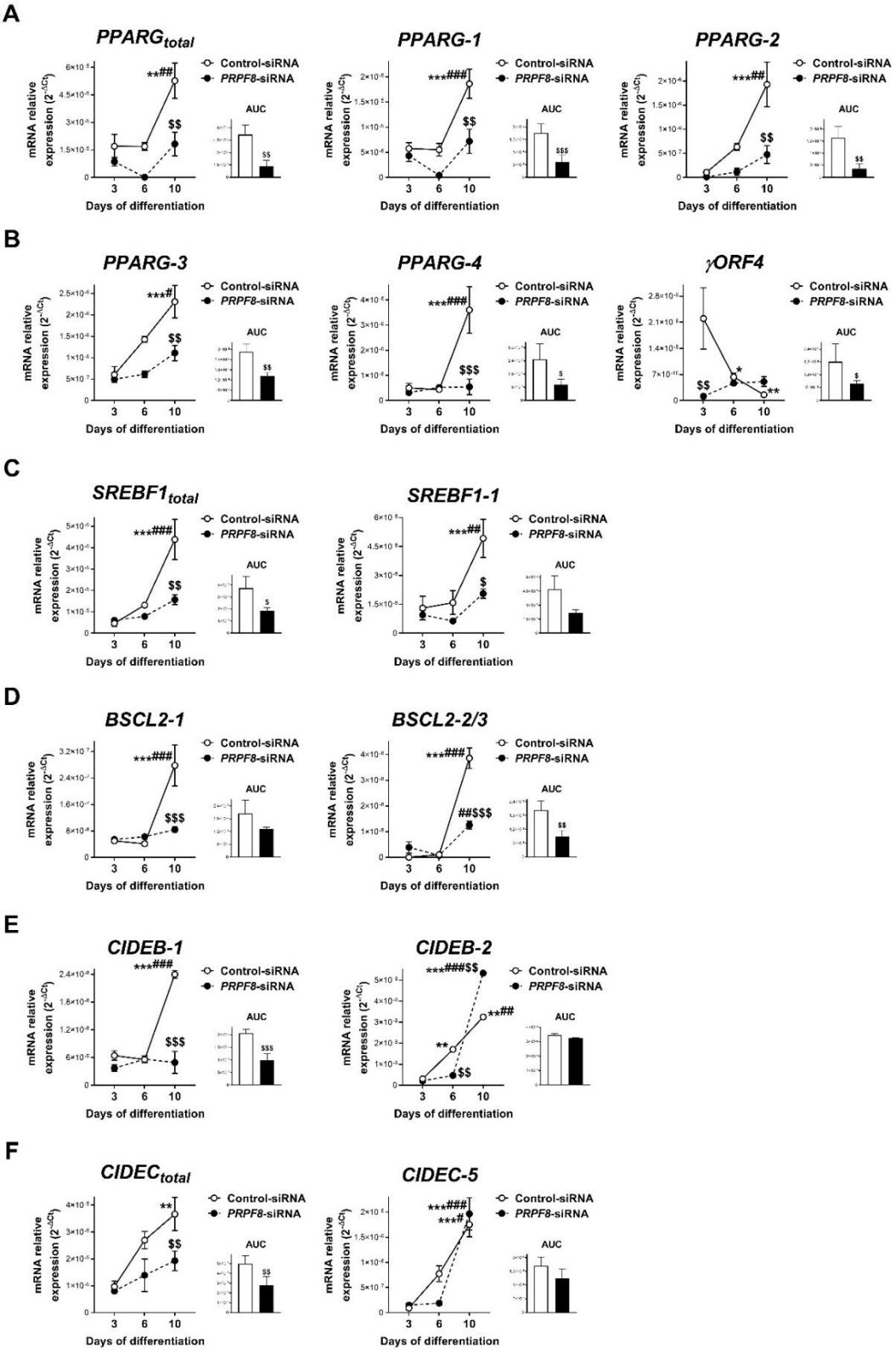

Figure 64. (A-F) mRNA levels of splicing variants of the genes indicated in hADSCs cells transfected with *PRPF8*-siRNA or Control-siRNA during *in vitro* differentiation (days 3-10). *****P<0.05, ******P<0.01, *******P<0.001 *vs.* day 3; $^{\#}$P<0.05, $^{\#\#}$P<0.01, $^{\#\#\#}$P<0.001 *vs.* day 6; $^{\$}$P<0.05, $^{\$\$}$P<0.01, $^{\$\$\$}$P<0.001 *vs.* control-siRNA.

Interestingly, these effects were observed together with an increase in the release of pro-inflammatory markers such as IL-10, IL-6, MCP-1, and MIF by *PRPF8*-silenced hADSCs as compared with control cells (**Figure 65**).

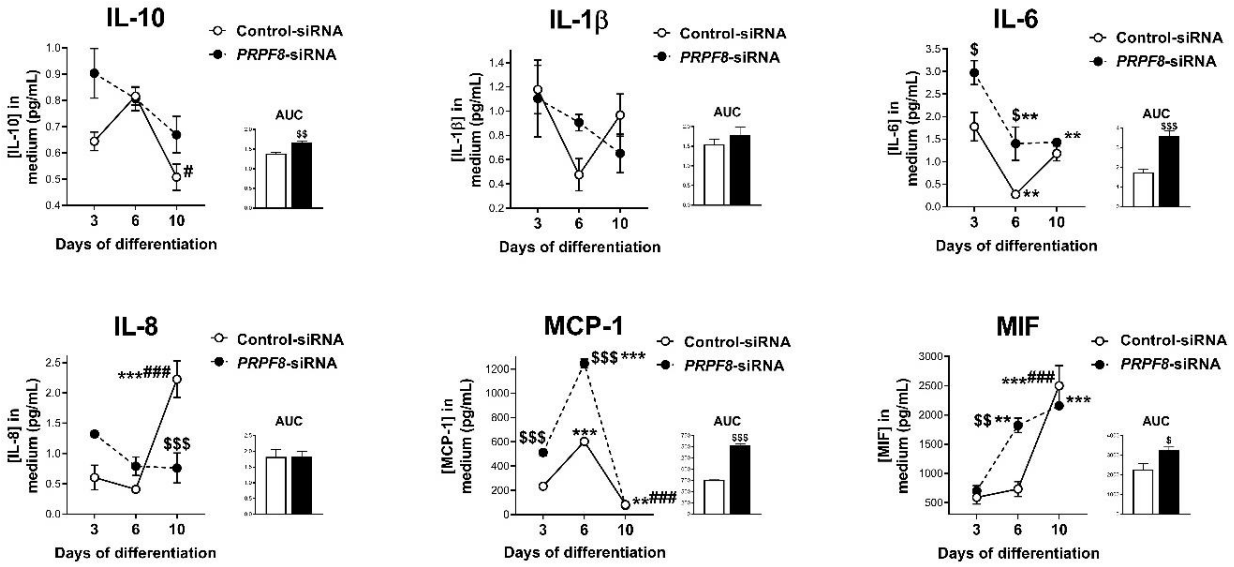

Figure 65. Protein levels of proteins indicated in the culture medium of hADSCs cells transfected with *PRPF8*-siRNA or Control-siRNA during *in vitro* differentiation (days 3-10). ******P<0.01, *******P<0.001 *vs.* day 3; $^{\#}$P<0.05, $^{\#\#\#}$P<0.001 *vs.* day 6; $^{\$}$P<0.05, $^{\$\$}$P<0.01, $^{\$\$\$}$P<0.001 *vs.* control-siRNA.

To clarify, the observed effects of *PRPF8*/PRP8 silencing in preadipocytes has been summarize in the following cartoon (**Figure 66**).

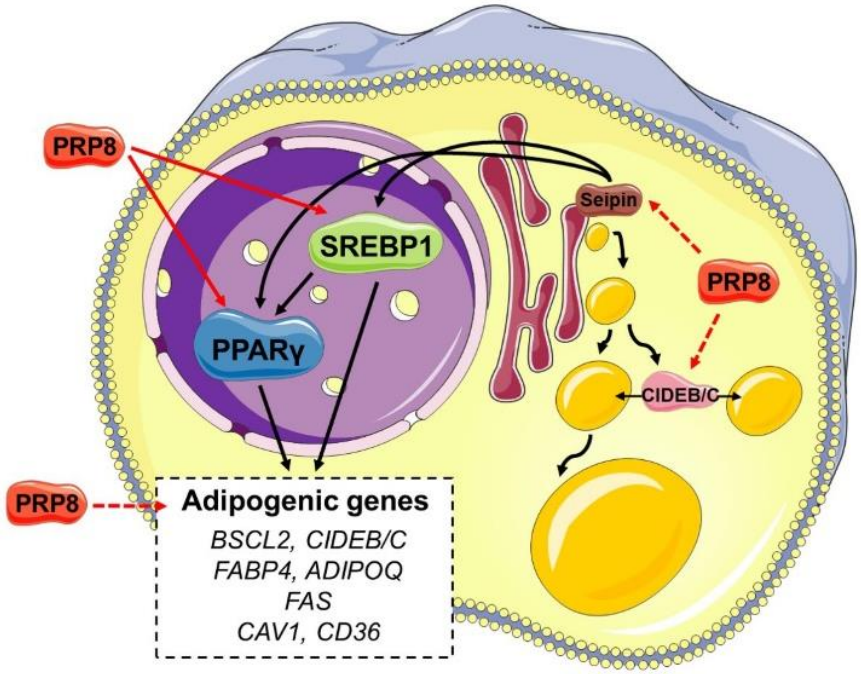

Figure 66. Schematic representation of the proposed mechanism of action of PRP8 on adipocyte differentiation. Solid arrows indicate direct effect and dashed arrows indicated indirect effect. Graphical elements have been from Servier Medical Art (SMART) repository.

1.7. Recovery of *PRPF8* and adipogenesis markers expression in response to bariatric surgery-induced weight loss

In order to unveil the regulation of *PRPF8* upon a substantial weight loss, we measured *PRPF8* mRNA expression in paired SC adipose tissue (SAT) samples from a third cohort including morbidly obese subjects undergoing bariatric surgery (BS) at the moment of the surgery (Pre-BS) and after an average of 16 months (Post-BS) when undergoing abdominoplasty (cohort 4) (**Table 4**; *Material and Methods* section).

These studies revealed significantly higher *PRPF8* expression levels in SAT after BS *vs.* Pre-BS (**Figure 67A**). Next, we analysed the contribution of obesity duration prior to the surgery in this regulation (**Figure 67B**). To test this, the subjects were sub-classified into two groups: short-standing obese (SSO), and long-standing obese (LSO), with an average of 15 ± 2 and 32 ± 2 years of obesity medical history, respectively (**Table 5*;*** *Material and Methods*). As shown in **Figure 67B**, the increase at mRNA level of *PRPF8* in SAT after BS reached statistical significance in the SSO group, but not in the LSO group.

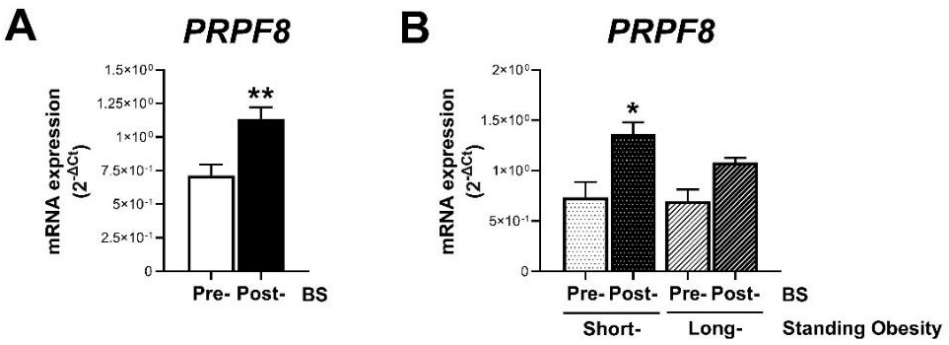

Figure 67. mRNA levels of *PRPF8* in SAT from obese subjects before and after BS (Pre- and Post-BS, respectively) independently **(A)**, and dependently **(B)** of obesity time. *****P<0.05, ******P<0.01 *vs.* Pre-BS.

BS-induced changes were accompanied by an increase in the mRNA/protein levels of the adipogenesis markers *PPARG*, and FABP4, but not ADIPOQ (**Figure 68A**). No differences between SSO and LSO groups were detected except for FABP4, whose protein levels were significantly increased after BS exclusively in the SSO group (**Figure 68B**).

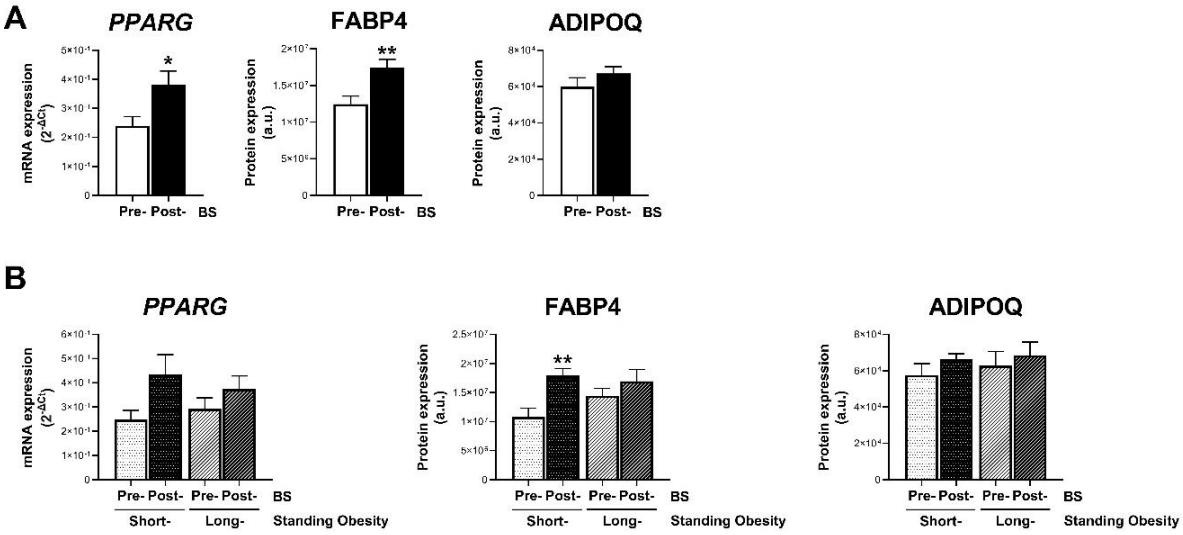

Figure 68. mRNA levels of the genes indicated in SAT from obese subjects before and after BS (Pre- and Post-BS, respectively) independently **(A)**, and dependently **(B)** of obesity time. *****P<0.05, ******P<0.01 *vs.* Pre-BS.

1.8. The UPR is altered in preadipocytes of IR/T2D obese subjects

As mentioned earlier, pathway analysis of iTRAQ proteomic data indicated that ER stress-related pathways were among the most significantly altered pathways in both SC and OM preadipocytes from T2D obese individuals when compared to NG obese subjects (**Figures 35B** and **35C**).

Immunoblotting studies of additional human preadipocyte samples to those employed for iTRAQ studies confirmed and extended the proteomic data by demonstrating the up- or down-regulation of mRNA/protein levels of several UPR components in SC and OM preadipocytes from IR/T2D obese groups as compared to NG obesity (**Figures 69-72**). Among those UPR-related components that were higher in T2D and/or IR vs. NG, we found the ER stress-inducible gene, BiP, pPERK and pPERK/PERK ratio in SC and OM preadipocytes, and the spliced form of *XBP1* in OM preadipocytes (**Figure 69**).

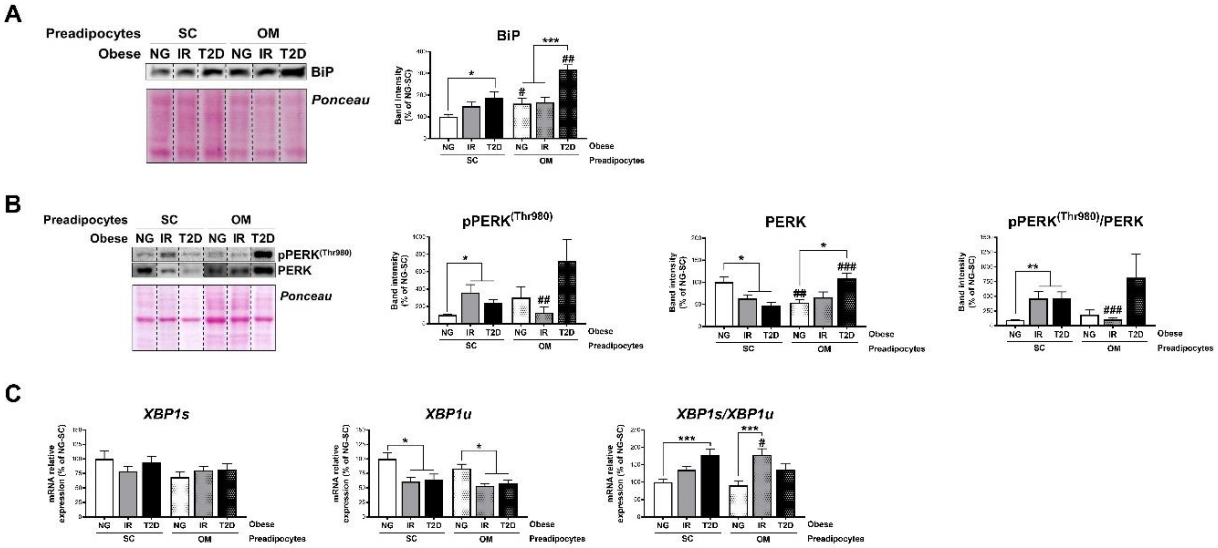

Figure 69. Representative blots and protein level quantifications of the proteins indicated **(A-B)** in SC and OM preadipocytes from NG, IR and T2D obese subjects (cohort 1, n=12). **(C)** mRNA levels of *XBP1s* and *XBP1u* in SC and OM preadipocytes from NG, IR and T2D obese subjects (n=12). *****P<0.05, ******P<0.01, *******P<0.001 *vs.* NG and/or IR subjects; $^{\#}$P<0.05, $^{\#\#}$P<0.01, $^{\#\#\#}$P<0.001 *vs.* SC preadipocytes from the same subjects.

In addition, the ER chaperones, GRP94 and PDI, were more abundant in T2D preadipocytes than in NG preadipocytes from both SC and OM fat (**Figure 70**). As indicated by our proteomic data, 11 additional ER chaperones were up-regulated in T2D *vs*. NG SC preadipocytes (**Appendix 2**).

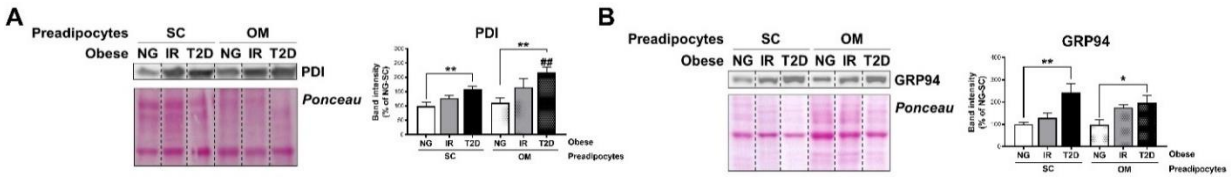

Figure 70. Representative blots and protein level quantifications of PDI **(A)**, and GRP94 **(B)** in SC and OM preadipocytes from NG, IR and T2D obese subjects (cohort 1, n=12). *****P<0.05, ******P<0.01 *vs.* NG and/or IR subjects; $^{\#\#}$P<0.01 *vs.* SC preadipocytes from the same subjects.

On the other hand, we observed decreased levels of cleaved/full-length ATF6 ratio in SC preadipocytes, and peIF2α and peIF2α/eIF2α ratio as well as the eIF2α-target, CHOP, in OM preadipocytes in T2D and/or IR *vs*. NG (**Figure 71**).

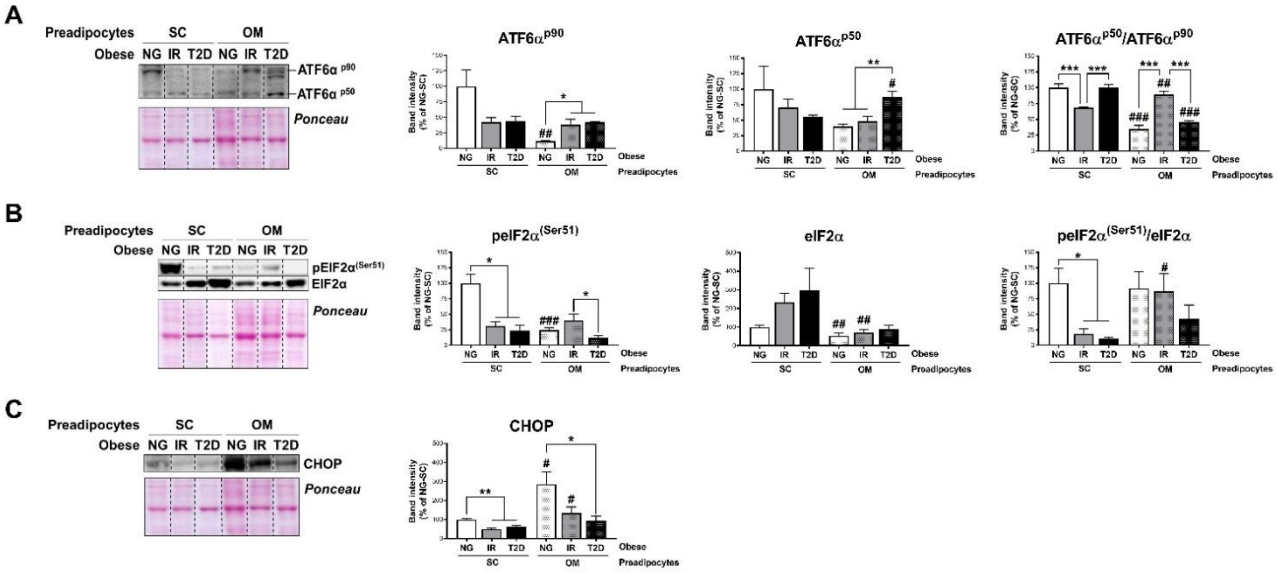

Figure 71. (A-C) Representative blots and protein level quantifications of the proetins indicated in SC and OM preadipocytes from NG, IR and T2D obese subjects (cohort 1, n=6-12). *****P<0.05, ******P<0.01, *******P<0.01 *vs.* NG and/or IR subjects; #P<0.05, ##P<0.01, ###P<0.001 *vs.* SC preadipocytes from the same subjects.

Finally, IR/T2D also modified the protein content of p90 and p50 as well as cleaved/full-length ATF6 ratio in OM preadipocytes (**Figure 71A**), and as compared to NG, IR enhanced IRE1α levels and decreased pIRE1α/IRE1α ratio in OM preadipocytes (**Figure 72**).

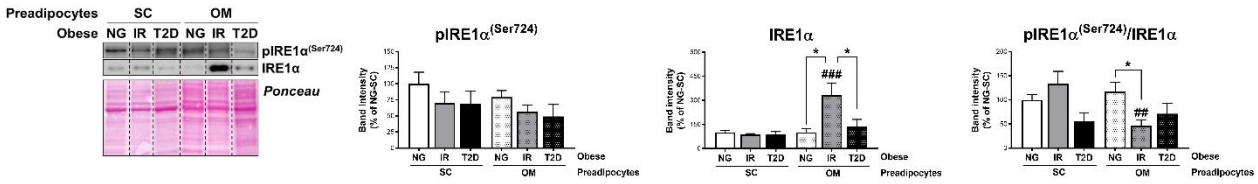

Figure 72. Representative blots and protein level quantifications of pIRE1α(Ser724) and IRE1α in SC and OM preadipocytes from NG, IR and T2D obese subjects (cohort 1, n=12). *****P<0.05 *vs.* NG and/or IR subjects; ##P<0.01, ###P<0.001 *vs.* SC preadipocytes from the same subjects.

1.9. Hyperactivation of ER-associated protein degradation (ERAD) in IR/T2D obese preadipocytes

In association with the UPR, the ERAD represents a key quality-control machinery that recruits unfolded/misfolded ER proteins via ER chaperones and targets these proteins for cytosolic degradation by the proteasome (Qi et al., 2017). In fact, the accumulation of misfolded proteins in the ER stimulates protein degradation via the ERAD (Christianson and Ye, 2014). Given our results on the UPR, we next explored the ERAD in human preadipocytes and observed a marked up-regulation of proteins involved in all the steps comprising this process, including protein recognition (*BIP*;

Figure 73A), retrotranslocation through the ER membrane (*DERL1*, *SEC61A1*, *STT3A*, and *STT3B*; **Figure 73B**), ubiquitination (*HRD1* and *RNF185*; **Figure 73C**), and targeting of misfolded proteins to the proteasome (*RAD23A* and *UBQLN1*; **Figure 73D**) in IR/T2D *vs.* NG obesity. These changes occurred in both SC and OM preadipocytes, which split into two clusters (NG and IR/T2D) when ERAD data was represented in a two-way hierarchical clustering heatmap (**Figure 73E**).

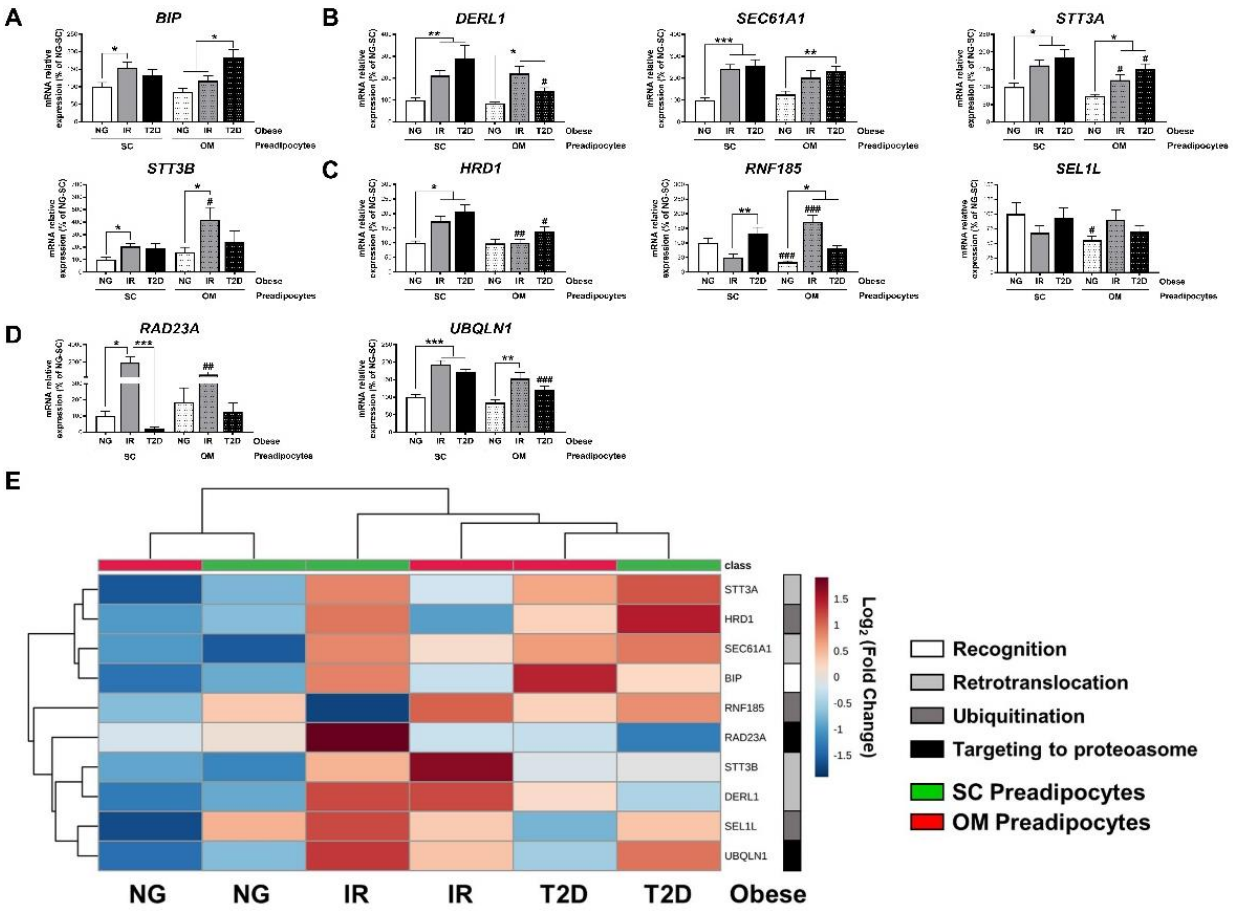

Figure 73. (A-D) mRNA levels of the genes indicated in SC and OM preadipocytes from NG, IR, and T2D obese subjects (cohort 1, n=12). *****P<0.05, ******P<0.01, *******P<0.001 *vs.* NG and/or IR subjects; #P<0.05, ##P<0.01, ###P<0.001 *vs.* SC preadipocytes from the same subjects. **(E)** Hierarchical clustering dendrogram heatmap of these genes. SC, green; OM, red. Rows stand for ERAD-related steps, while columns stand for subject groups. The scale in the colour bar represents -Log_2(Fold Change).

Interestingly, as we observed for IR/T2D preadipocytes *vs*. NG preadipocytes (either SC or OM), increasing BiP expression levels by overexpression of a vector coding for this ER chaperone, enhanced the mRNA content of ERAD genes in SGBS adipocytes (**Figure 74**).

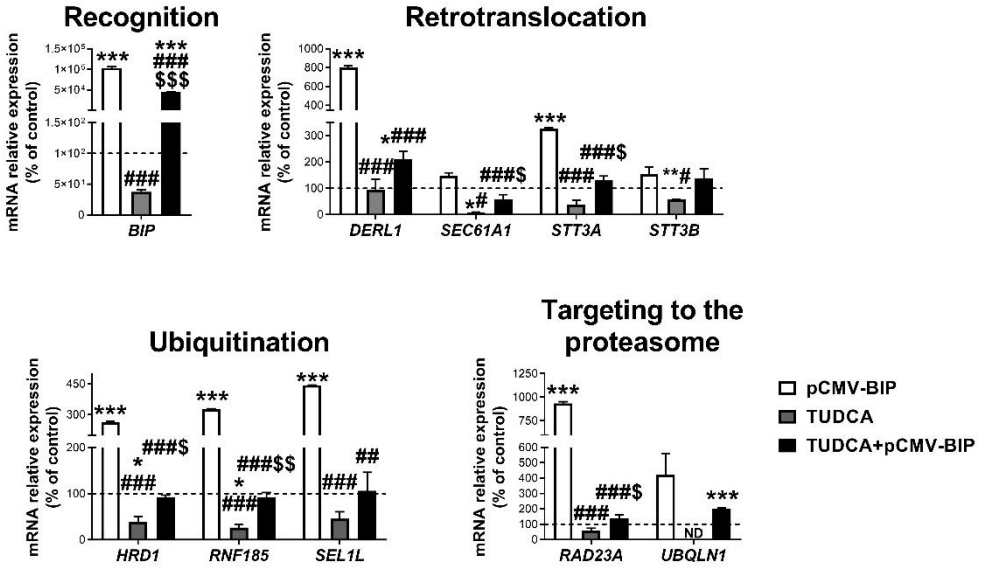

Figure 74. mRNA levels of ERAD-related genes in SGBS preadipocytes overexpressing BiP (pCMV-BIP, white), exposed 14 h to 0.5 mg/mL TUDCA (TUDCA, grey), or a combination of both (TUDCA+pCMV-BIP, black). ND, non-detected; *****P<0.05, ******P<0.01. *******P<0.001 *vs.* control; #P<0.05, ##P<0.01, ###P<0.001 *vs.* pCMV-BIP; $P<0.05, $$P<0.01, $$$P<0.001 *vs.* TUDCA.

BiP overexpression also caused a concomitant decrease in the expression levels of several adipogenic markers (**Figure 75**).

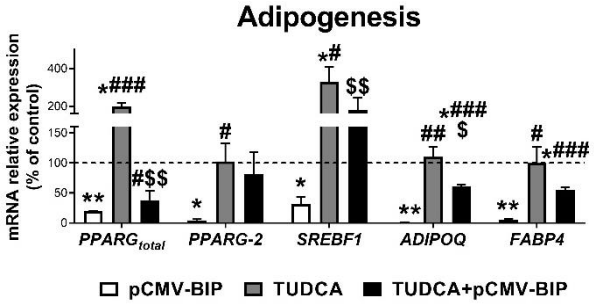

Figure 75. mRNA levels of adipogenesis-related genes in SGBS preadipocytes overexpressing BiP (pCMV-BIP, white), exposed 14 h to 0.5 mg/mL TUDCA (TUDCA, grey), or a combination of both (TUDCA+pCMV-BIP, black). *****P<0.05, ******P<0.01 *vs.* control; #P<0.05, ##P<0.01, ###P<0.001 *vs.* pCMV-BIP; $P<0.05, $$P<0.01 *vs.* TUDCA.

When the ERAD system was analysed in human preadipocyte samples, we also observed a trend to increase in representative genes of ERAD when data from T2D individuals with simple obesity were compared to their NG counterparts or to lean individuals (cohort 2) (**Figure 76**). Nevertheless, the expression of some of these ERAD genes, such as *RAD23A*, which was higher in SC preadipocytes from NG obese individuals as compared to lean individuals, decreased in the transition from NG to T2D in obesity (**Figure 76D**), an effect that was also observed in morbid obesity (**Figure 73D**).

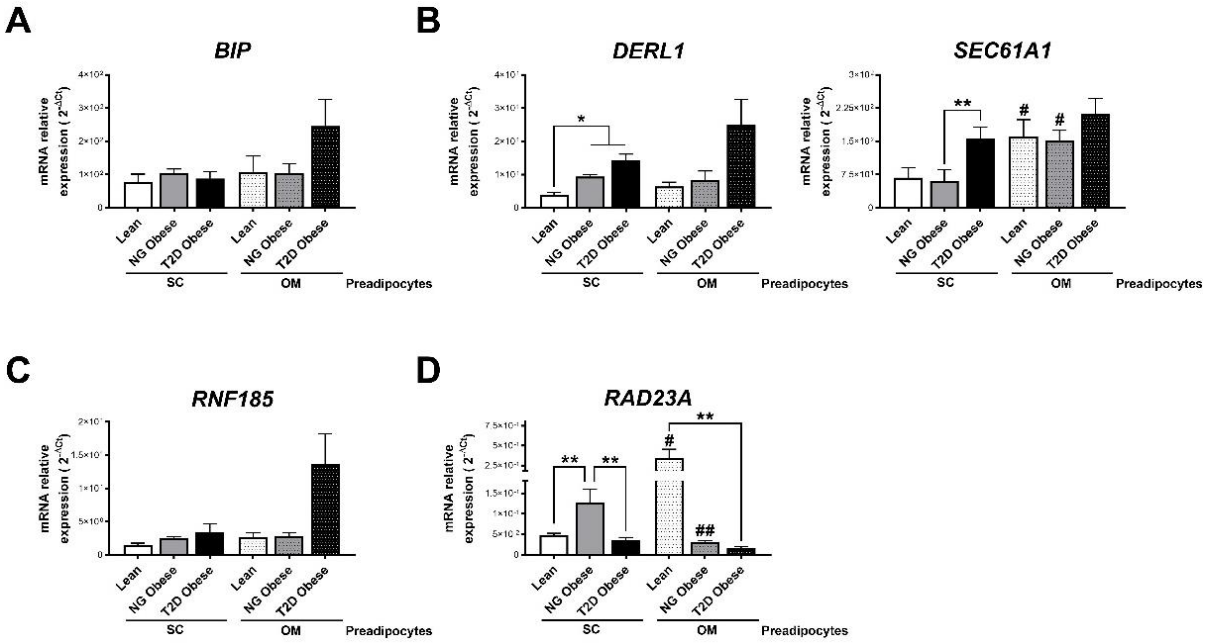

Figure 76. mRNA levels of the genes indicated in SC and OM preadipocytes from lean subjects and NG, and T2D obese subjects (cohort 2, n=5-11 per group). *****P<0.05, ******P<0.01 *vs.* lean and/or NG obese subjects; #P<0.05, ##P<0.01 *vs.* SC preadipocytes from the same subjects.

In view of these findings, we explored the regulation of ERAD genes during adipocyte differentiation. In the case of primary preadipocytes isolated from obese individuals (cohort 1), we observed that mRNA levels of ERAD genes increased during differentiation, especially in IR preadipocytes, which resulted in higher overall transcript contents of these genes in IR preadipocytes than in NG preadipocytes (measured as AUC) (**Figure 77**).

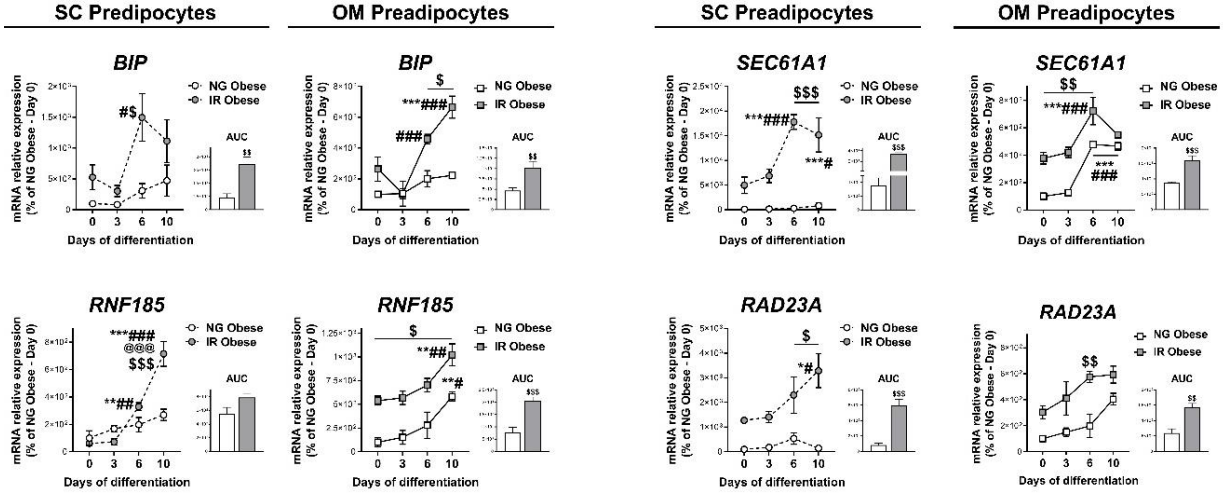

Figure 77. mRNA levels of the genes indicated during *in vitro* differentiation (days 0-10) of SC and OM preadipocytes from NG and IR obese subjects (cohort 1, n=6). *****P<0.05, ******P<0.01, *******P<0.001 *vs.* day 0; #P<0.05, ##P<0.01, ###P<0.001 *vs.* day 3; @@@P<0.001 *vs.* day 6; $P<0.05, $$P<0.01, $$$P<0.001 *vs.* NG obese.

Finally, *in-silico* analysis of transcriptomic data from differentiation studies of hADSCs obtained from SC fat from a lean individual (Ehrlund et al., 2017) revealed that genes related to ER proteostasis separate into two clusters with opposite expression trends during adipogenesis (**Figure 78B**), with the expression levels of ERAD genes increasing at late stages of differentiation (**Figure 78C**).

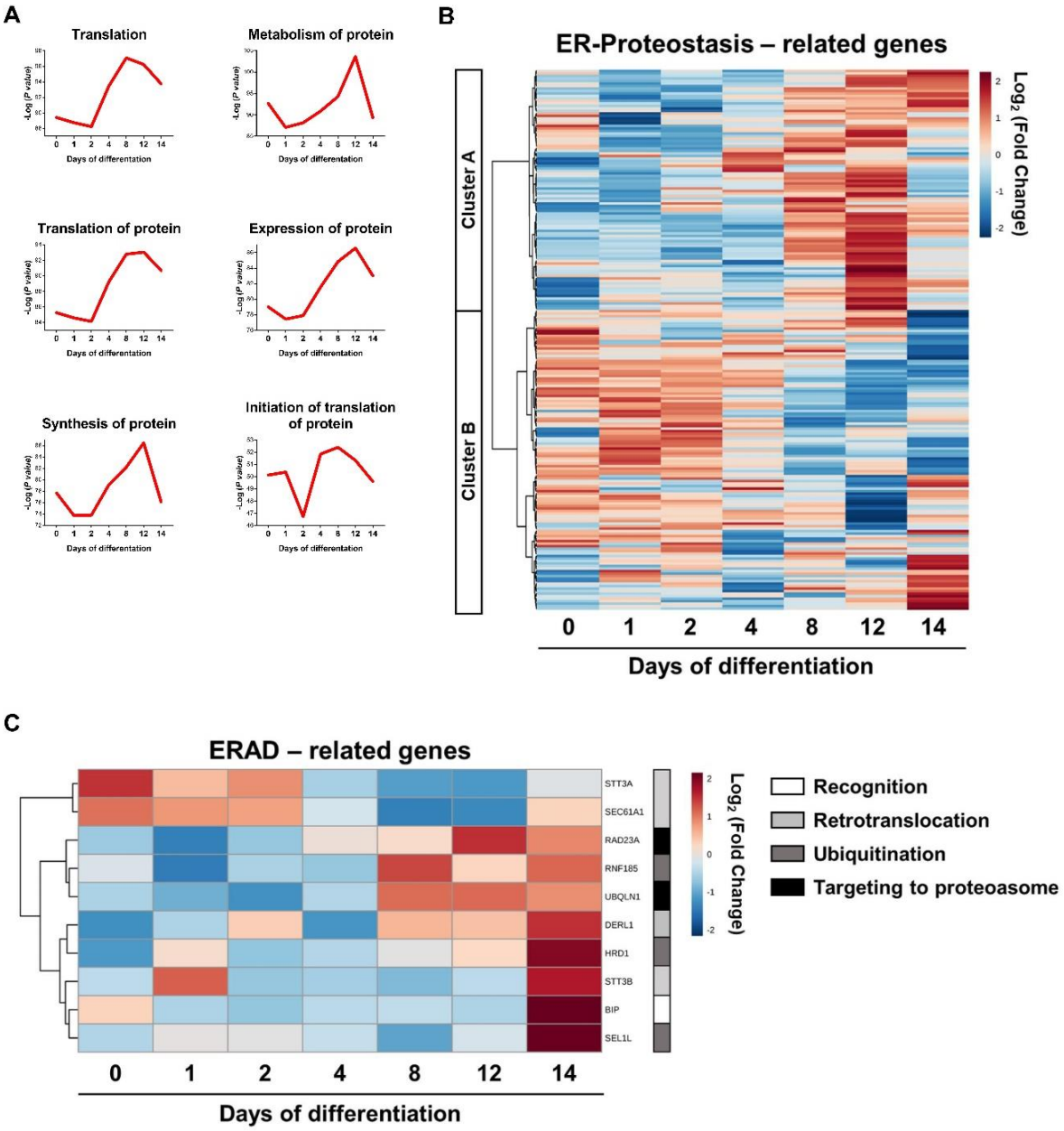

Figure 78. **(A)** Protein metabolism-related IPA pathways **(A)**, hierarchical clustering dendrogram heatmap of the mRNA expression of ER-Proteostasis GO pathway-related genes **(B)**, and ERAD-related genes in hADSCs during *in vitro* differentiation. Rows stand for genes, while columns stand for differentiation time (0-14 days). The scale in the colour bar is Log_2(Fold Change).

Likewise, the expression of most ERAD genes also increased during differentiation of SGBS cells, though low BIP and STT3A mRNA levels were observed at day 10 (**Figure 79**).

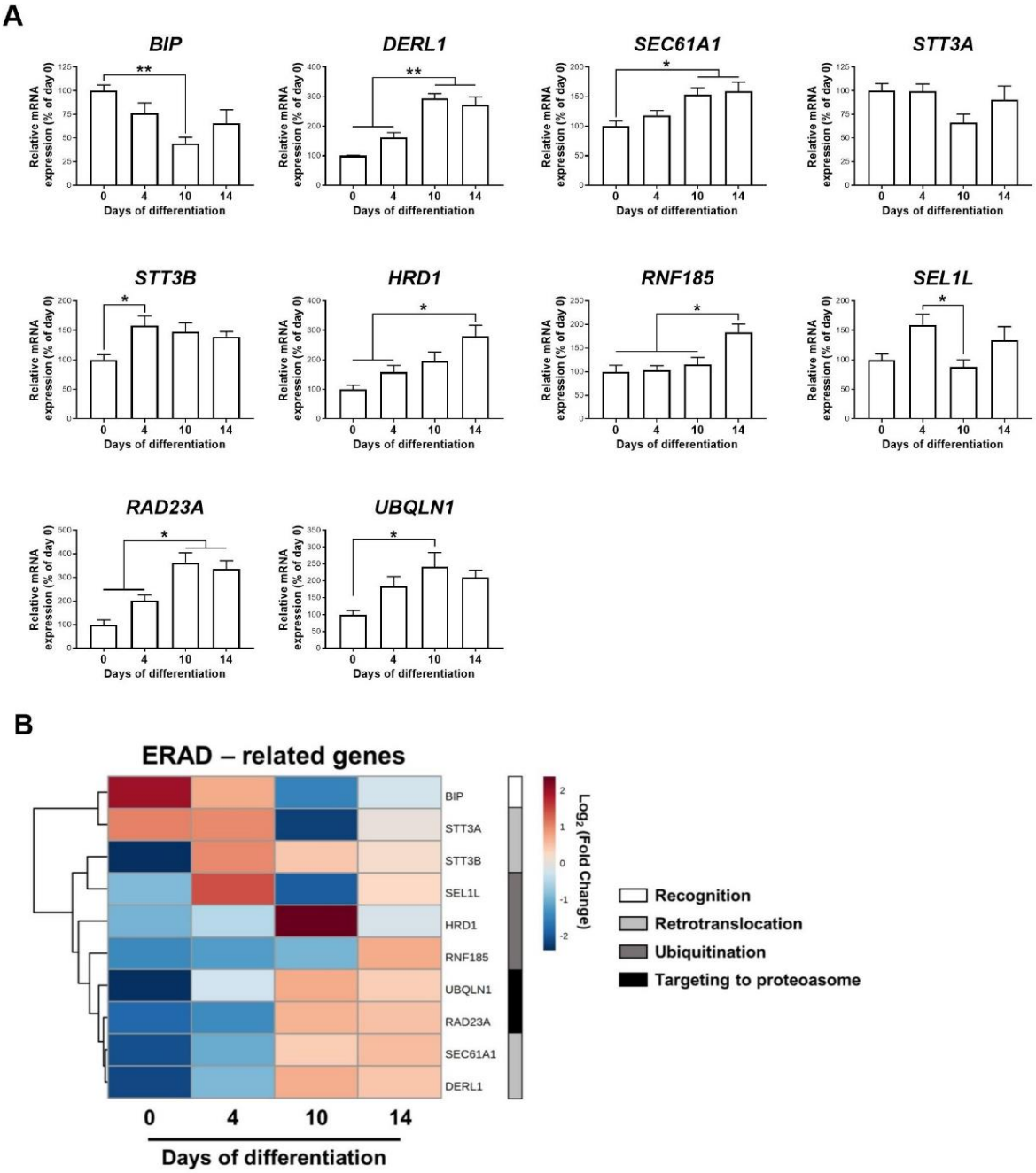

Figure 79. mRNA levels represented in bar chart **(A)**, or hierarchical clustering dendrogram heatmap **(B)** of ERAD-related genes in SGBS cells during adipogenesis. Rows stand for genes, while columns stand for differentiation time (0-14 days). The scale in the colour bar is Log_2(Fold Change). *****P<0.05, ******P<0.01 *vs.* precedent days.

1.10. Regulation of ERAD in response to bariatric surgery-induced weight loss

To unveil the regulation of ERAD upon weight loss and the contribution of obesity duration on this change, we measured the mRNA expression of both the inductor of ERAD, *XBP1*, and ERAD components in paired SAT samples from morbidly obese subjects undergoing BS at the moment of the surgery and after (Pre- and Post-BS,

respectively; cohort 4), separated or not according to their obesity time (**Table 4** and **5**; *Material and Methods* section).

These analyses showed that the *XBP1s*/*XBP1u* ratio was significantly reduced in SAT of individuals at the Post-BS state, irrespective of the duration of obesity (**Figure 80**).

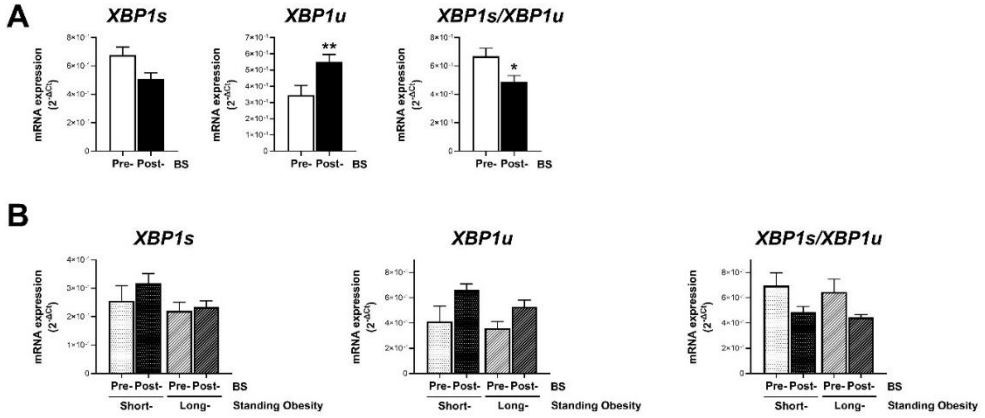

Figure 80. mRNA levels of *XBP1s*, *XBP1u* and their ratio in SAT from obese subjects before and after BS (Pre- and Post-BS, respectively) independently **(A)**, and dependently **(B)** of obesity time evolution. *****P<0.05, ******P<0.01 *vs.* Pre-BS.

No differences were observed in *BIP* mRNA levels, while we observed a down-regulation of *STT3B*, together with an up-regulation of *HRD1*, *SEL1L*, and UBQLN1 in SAT at post-BS (**Figure 81**).

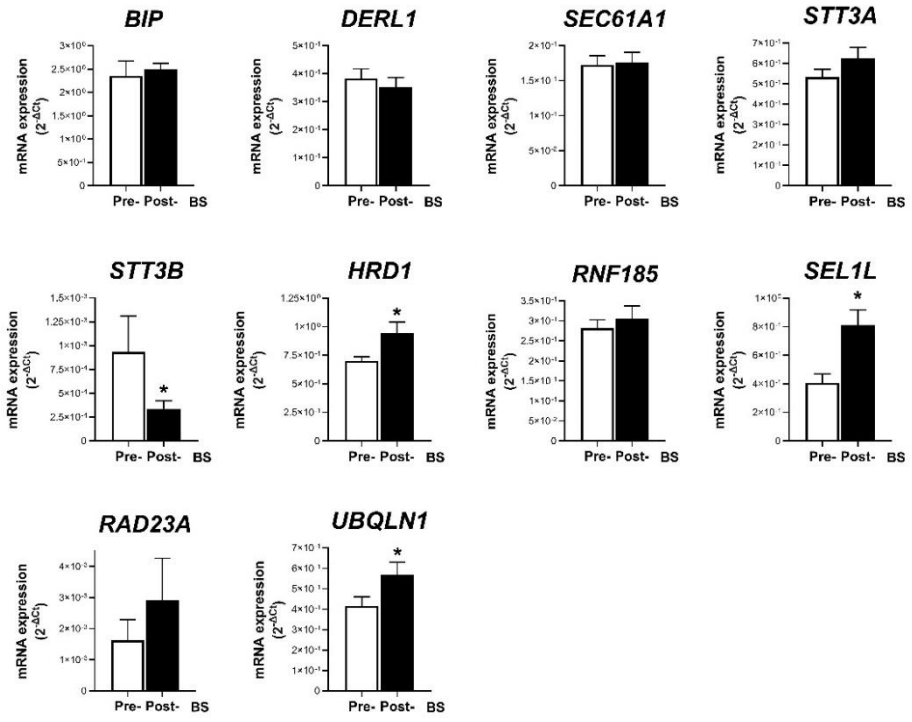

Figure 81. mRNA levels of the genes indicated in SAT from obese subjects before and after BS (Pre- and Post-BS, respectively). *****P<0.05 *vs.* Pre-BS.

Regarding the influence of obesity duration, differences in the behaviour of *STT3A*, *HRD1*, and *RNF185* at post-BS were observed between SSO and LSO groups (**Figure 82**).

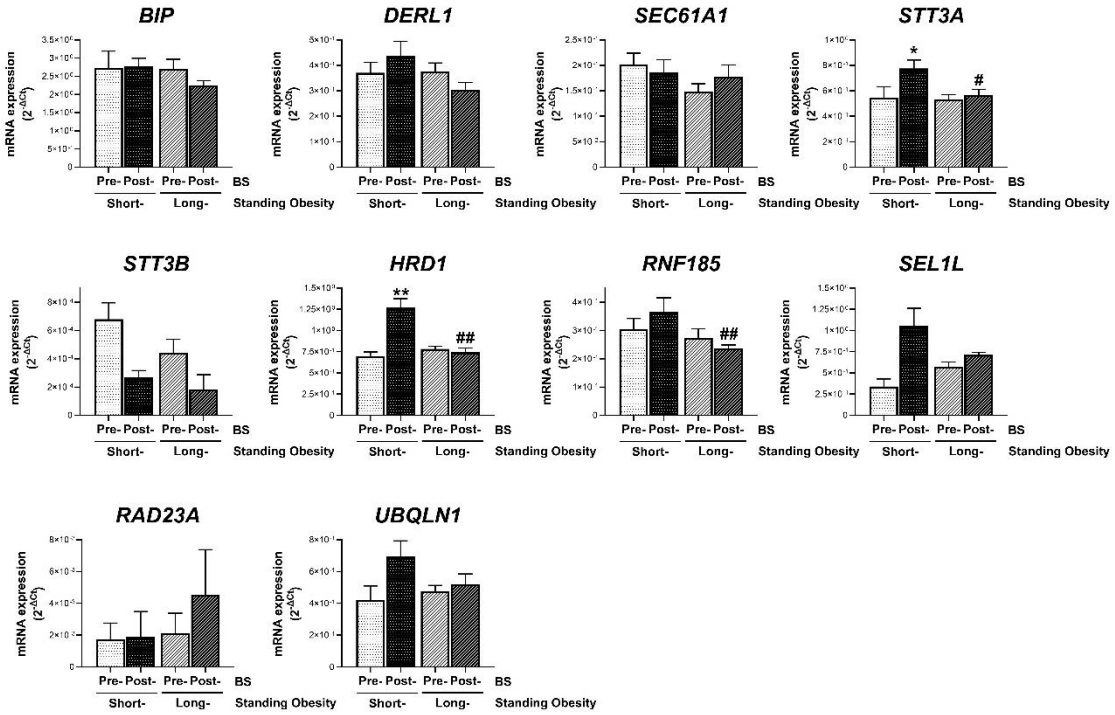

Figure 82. mRNA levels of the genes indicated in SAT from obese subjects before and after BS (Pre- and Post-BS, respectively) dependently of obesity time evolution. *****P<0.05, ******P<0.01 *vs.* Pre-BS; #P<0.05, ##P<0.01 *vs.* SSO.

In particular, when expression data from ERAD components were represented in a two-way hierarchical clustering heatmap (**Figure 83**), differences in the expression levels of these genes were clearly evident in the SSO group, which split into two clusters.

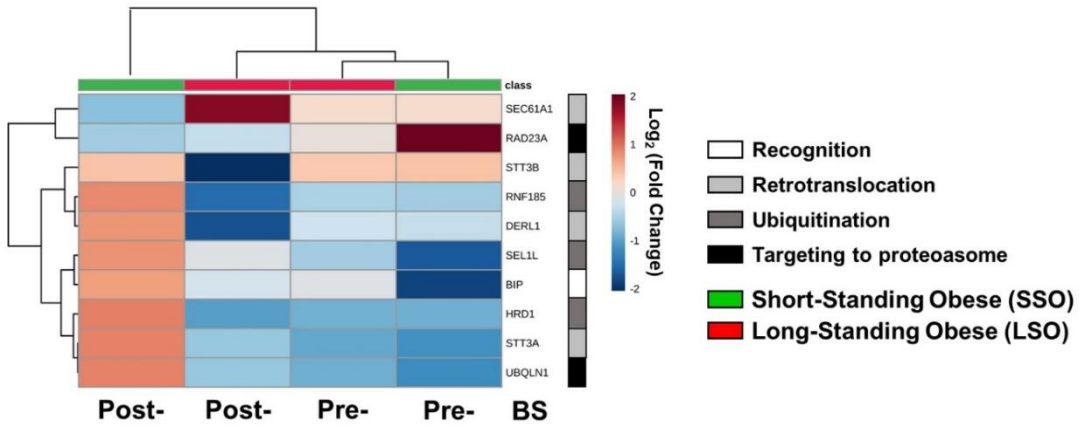

Figure 83. Hierarchical clustering dendrogram heatmap of mRNA levels of ERAD-related genes in SAT from obese subjects before and after BS (Pre- and Post-BS, respectively) dependently of obesity time evolution. SSO (green) and LSO (red) subjects. Rows stand for genes, while columns stand for subject groups. The scale in the colour bar represents -Log_2(Fold Change).

1.11. Hyperglycaemia/hyperinsulinemia alters preadipocyte ER proteostasis

We next explored whether obesogenic insults such as hyperglycaemia/hyperinsulinemia, inflammation, and hypertrophy due to lipid overload, could alter the expression of ERAD genes. To this end, SGBS preadipocytes were exposed to high concentrations of glucose and insulin (HGHI), TNFα, or fatty acids (palmitate or oleate) using *in vitro* models previously validated in our laboratory (Díaz-Ruiz et al., 2015). None of the treatments compromised cell viability but, except for oleate, they impaired insulin-induced Akt phosphorylation (**Figure 84**).

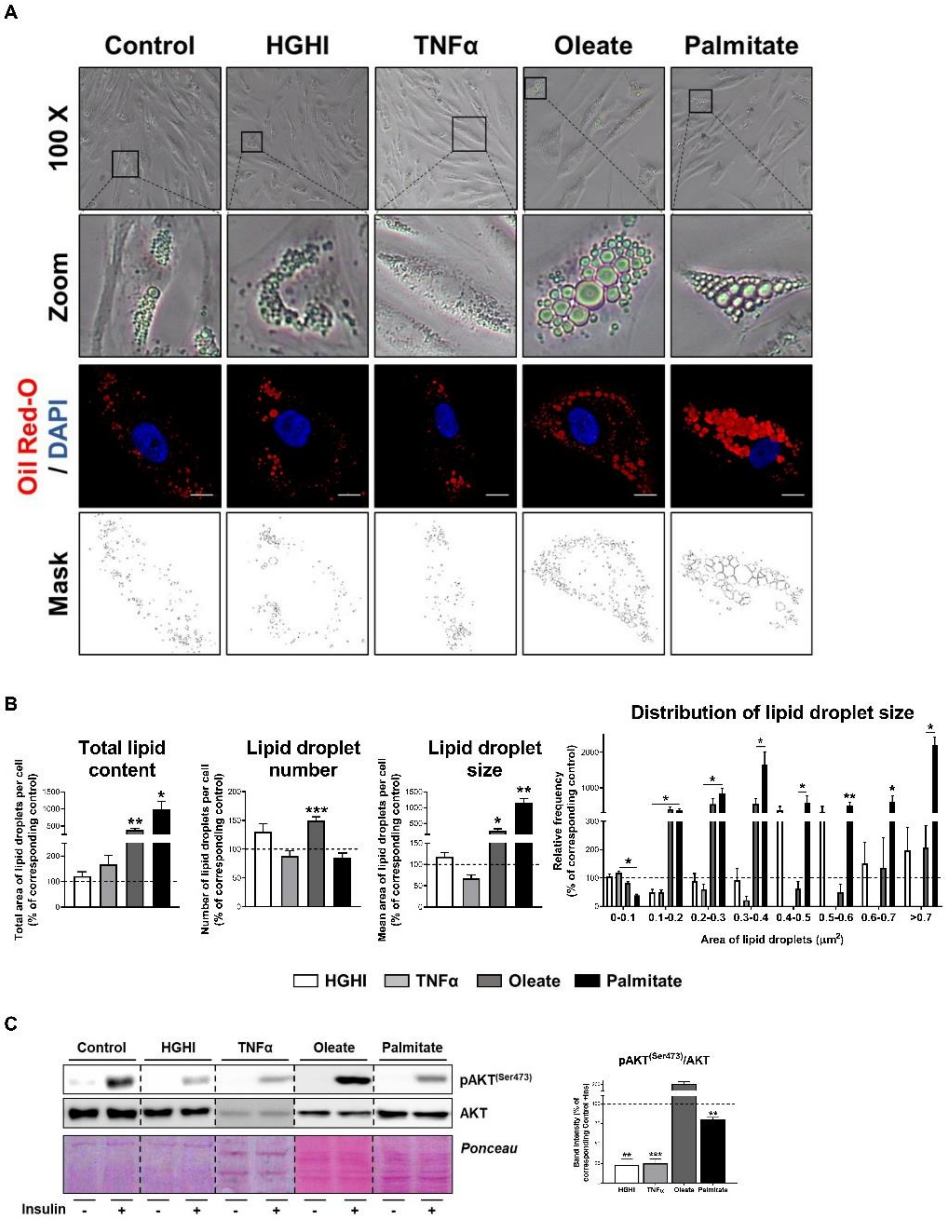

Figure 84. Representative light and confocal micrographs **(A)**, and LD morphometric analysis **(B)** of SGBS preadipocytes exposed during 30 h to HGHI (white), TNFα (grey), oleate (dark grey), or palmitate (black). Cells were stained with Oil Red-O (LDs, red) and DAPI (nuclei, blue). *****P<0.05, ******P<0.01, *******P<0.001 *vs.* control. **(C)** Representative blots and protein level quantification of pAKT$^{(Ser473)}$ and AKT in SGBS preadipocytes *in vitro* models after exposure to insulin (100 nM, 15 min) or medium alone. ******P<0.01, *******P<0.001 *vs.* corresponding control with insulin.

Among them, exposure to HGHI increased the expression of BiP and nearly all the other ERAD components tested (**Figure 85A**). As shown in **Figure 85B**, expression levels of ERAD genes enabled discrimination of HGHI-treated from control SGBS cells.

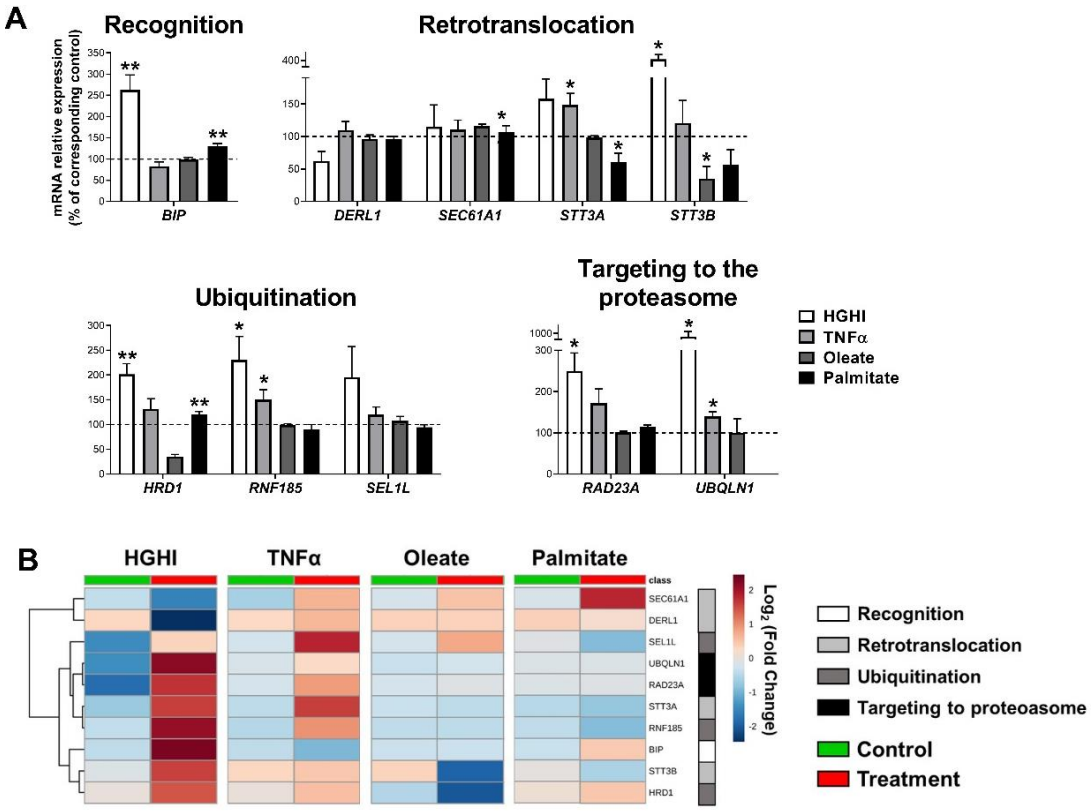

Figure 85. mRNA levels represented in bar chart **(A)**, or hierarchical clustering dendrogram heatmap **(B)** of ERAD-related genes in SGBS preadipocytes exposed during 30 h to high glucose (4.5 g/L)/high insulin (100 nMl/L) (HGHI; white), 5 nM TNFα (light grey), 500 µM oleate (dark grey) or 500 µM palmitate (black); and control (green), or treatments (red). *****P<0.05, ******P<0.01 *vs.* corresponding control. Rows stand for ERAD-related steps, while columns stand for subject groups. The scale in the colour bar represents -Log_2(Fold Change).

Given these observations, we next examined the activity of the protein degradation machinery in the cytosol, the proteasome (Bard et al., 2018), in cells exposed to HGHI. These studies showed that hyperglycaemic/hyperinsulinemic conditions decreased the activity of the 26S proteasome while increasing the amount of ubiquitinated proteins in SGBS preadipocytes (**Figures 86** and **87B**).

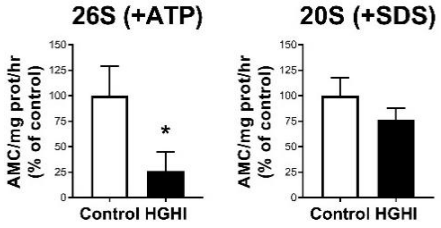

Figure 86. Proteasome activity of the 26S, and 20S proteasome in SGBS preadipocytes exposed during 30 h to high glucose (4.5 g/L)/high insulin (100 nM) (HGHI). *****P<0.05 *vs.* control.

Interestingly, ER homeostasis can be restored in ER-stressed cells by exposure to the naturally occurring bile acid, tauroursodeoxycholic acid (TUDCA) (Zhang et al., 2018). We thus tested whether exposure of SGBS preadipocytes at day 4 of differentiation to TUDCA prior to HGHI treatment could prevent HGHI-induced up-regulation of ERAD genes and accumulation of ubiquitinated proteins in these cells, which was proven to be the case (**Figures 87A** and **87B**). TUDCA also reverted the inhibitory effects of HGHI on *PPARγ* and *FABP4* expression levels (**Figure 84C**). Notably, TUDCA also blocked the effects induced by BiP overexpression on both ERAD genes and adipogenic markers in SGBS cells (**Figures 74** and **75**).

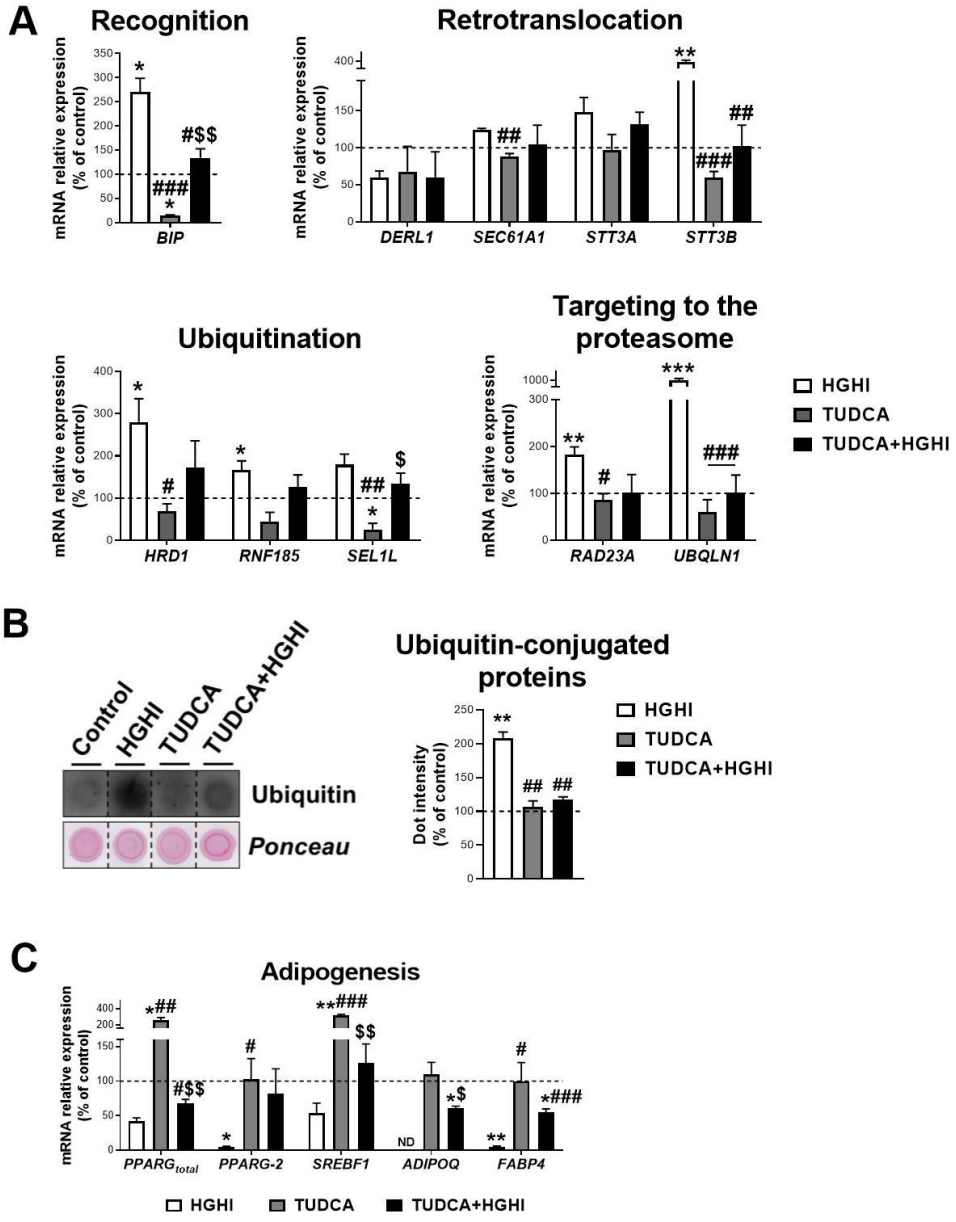

Figure 87. mRNA levels of ERAD **(A)**, and adipogenesis-related **(B)** genes, and representative dot-blot and protein quantification of ubiquitin-conjugated proteins **(C)** in SGBS preadipocytes exposed 14 h to 0.5 mg/mL TUDCA (TUDCA, grey), 30 h to HGHI conditions (white), or a combination of both (TUDCA+HGHI, black). ND, non-detected; *****P<0.05, ******P<0.01, *******P<0.001 *vs.* control; $^{\#}$P<0.05, $^{\#\#}$P<0.01, $^{\#\#\#}$P<0.001 *vs.* HGHI; $^{\$}$P<0.05, $^{\$\$}$P<0.01 *vs.* TUDCA.

This study has been deposited to the bioRxiv preprint server and can be accessible scanning this QR code.

2. Study 2: Characterization of miRNAs as markers of dysfunctional adipose tissue in type 2 diabetes (T2D)

2.1. Circulating miRNA levels and adipose tissue insulin resistance

We first explored the correlation between plasma levels of 9 miRNAs that had been previously associated with the incidence of T2D in the CORDIOPREV study (*miR-9*, *miR-28-3p*, *miR-29a*, *miR-30a-5p*, *miR-103*, *miR-126*, *miR-150*, *miR-223-3p*, and *miR-375*) (Jiménez-Lucena et al., 2018) and the indicator of insulin resistance at the adipose tissue, ATIRI (ter Horst et al., 2017). Baseline plasma *miR-223-3p* levels, which was 28.2% lower in incident-T2D subjects than in non-T2D subjects (p=0.016) (Jiménez-Lucena et al., 2018), exhibited a significant and negative correlation with ATIRI (**Figure 88**).

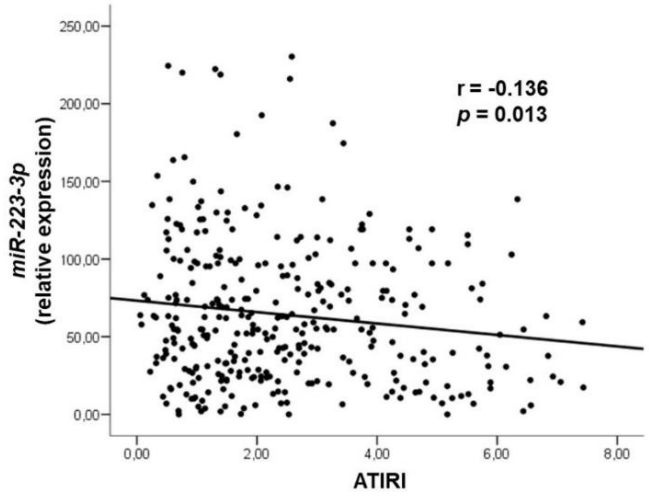

Figure 88. Correlation analysis between baseline circulating *miR-223-3p* expression levels and Adipose Tissue Insulin Resistance Index (ATIRI) determined in CORDIOPREV-DIAB study patients (n = 462). r, Pearson's correlation coefficient.

However, none of the other eight miRNAs exhibited significant correlation with ATIRI (**Table 9**).

Table 9. Correlation analysis between baseline circulating levels of the miRNAs indicated and ATIRI determined in the CORDIOPREV-DIAB study patients (n = 462).

	ATIRI	
	r	***p***
hsa-miR-150	0.002	0.974
hsa-miR-103	-0.040	0.417
hsa-miR-28-3p	-0.035	0.470
hsa-miR-126	-0.032	0.511
hsa-miR-9	0.013	0.789
hsa-miR-30a-5p	-0.046	0.345
hsa-miR-375	0.024	0.620
hsa-miR-29a	-0.059	0.229

Correlations were determined by Pearson's correlation coefficient test. r, correlation coefficient.

The relationship between ATIRI and miRNA plasma levels and clinical and anthropometric data was also examined by the Akaike Information Criterion (AIC) multivariate regression analysis with step AIC method (Akaike, 1974; Heinze et al., 2018). This analysis indicated that the best model (*i.e*., with the lowest AIC value) to explain ATIRI included *miR-223-3p* plasma levels together with gender, BMI, glucose, and triglycerides (**Table 10**).

Table 10. Stepwise Akaike information criterion (AIC) multivariate logistic regression analysis including ATIRI as dependent variable and the plasma levels of the nine studied miRNAs (*miR-9*, *miR-28-3p*, *miR-29a*, *miR-30a-5p*, *miR-103*, *miR-126*, *miR-150*, *miR-223-3p*, and *miR-375*), and anthropometrical and clinical parameters as independent variables.

Model	**1**	**2**	**3**
AIC	297.15	295.19	293.94
hsa-miR-223-3p	X	X	X
Gender	X	X	X
Glucose	X	X	X
Triglycerides	X	X	X
BMI	X	X	X
Age	X	X	
CRP	X		

CRP, C-Reactive Protein; **BMI**, Body Mass Index.

ATIRI was also significantly higher in incident-T2D subjects (**Figure 89**). These results, together with the significant contribution of the adipose tissue to the pool of circulating miRNAs (Thomou et al., 2017), suggested a potential relationship between *miR-223-3p* and adipose tissue dysfunction.

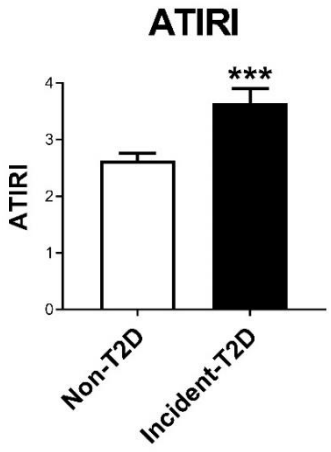

Figure 89. Baseline ATIRI in patients who did not develop T2D (non-T2D, n=355), and patients who developed T2D (incident-T2D, n=107) during the median follow-up of 60 months from the CORDIOPREV-DIAB study. ***P<0.001 *vs.* non-T2D.

2.2. *In silico* analysis of *miR-223-3p* target genes and pathways

We next examined *miR-223-3p* target genes in search of pathways related to adipose tissue function. *In silico* analysis of the top 50 genes in four different databases (miRDB, microRNA, TargetScan, and miRTarBase) enabled the identification of 157 target genes of *miR-223-3p*, 50 of which have been experimentally validated, including GLUT4, and FOXO, while 107 were predicted *in silico*, such as IRS-1 (**Appendix 5**). In this line, among the 166 significantly over-represented pathways revealed by IPA software analysis (**Appendix 5**), insulin receptor signalling and PI3K/AKT signalling pathways were ranked in the top 10 most significant overrepresented pathways (**Figure 90A**). IPA analysis also revealed TNFα as the second most significant upstream regulator of *miR-223-3p* target genes (**Figure 90B** and **Appendix 5**). Indeed, multiple over-represented pathways in the *miR-223-3p* regulatory network were related to inflammation (**Appendix 5**).

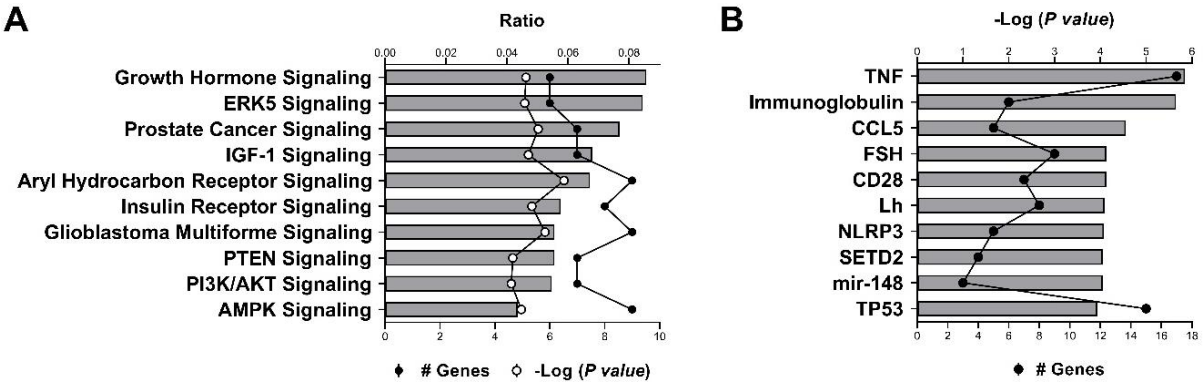

Figure 90. Top 10 most significantly enriched IPA pathways **(A)**, and upstream regulators **(B)** of the *miR-223-3p* target genes set. Bars indicate Ratio **(A)** and -Log (*P value* of overlap) **(B)**, respectively. Black lines indicate number of proteins and white line indicates -Log (*P value*).

In this line, *in silico* analysis of the potential target genes of the eight miRNAs that were identified together with *miR-223-3p* by Jiménez-Lucena et al. (2018) for their predictive value of T2D (**Figures 91** and **92**), suggest that none of them are likely involved in insulin resistance-related pathways, as it is the case for *miR-223-3p*.

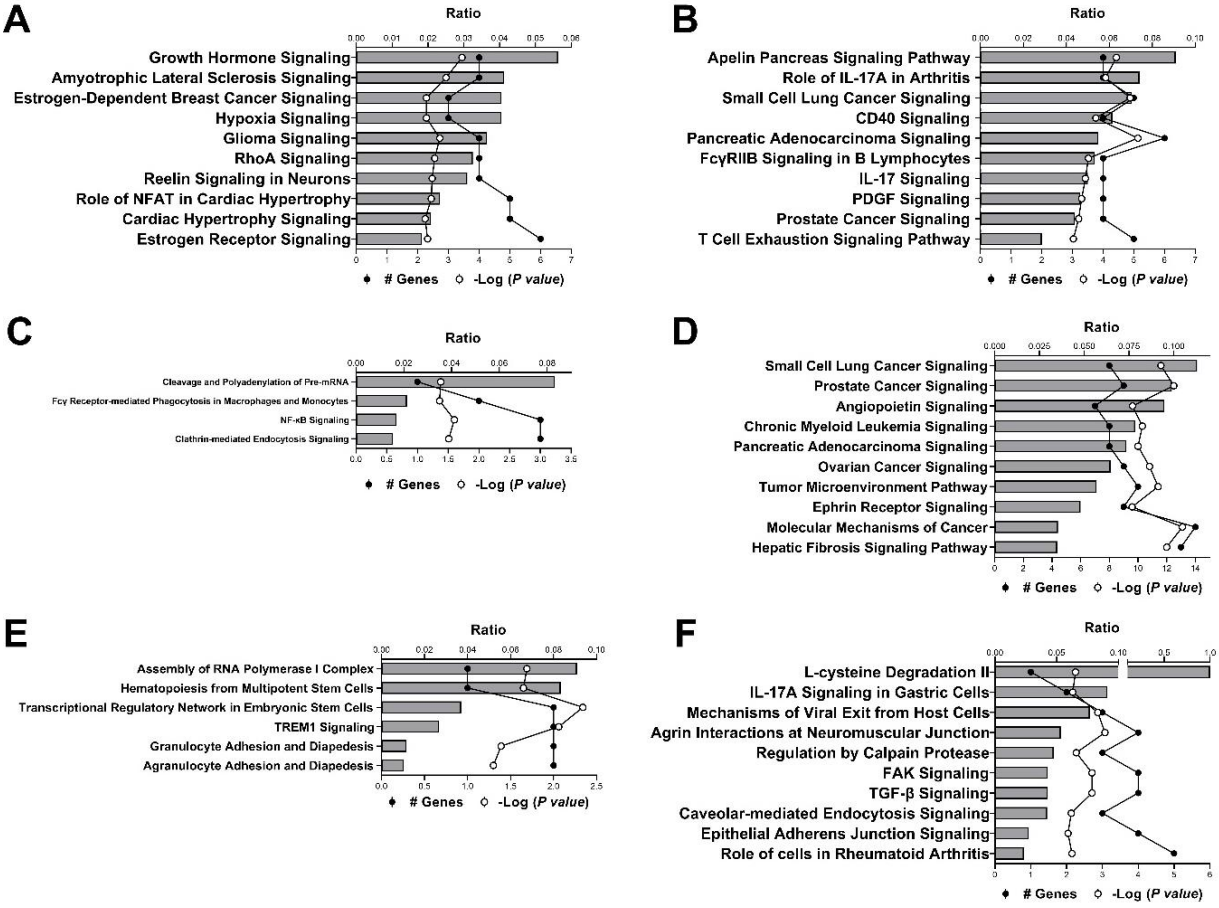

Figure 91. Top 10 most significantly enriched IPA pathways of *miR-150-3p* **(A)**, *miR-103-3p* **(B)**, *miR-28-3p* **(C)**, *miR-126-3p* **(D)**, *miR-9-3p* **(E)**, *miR-30a-5p* **(F)** target genes set. Bars indicate Ratio, black lines indicate number of proteins and white line indicates -Log (*P value*).

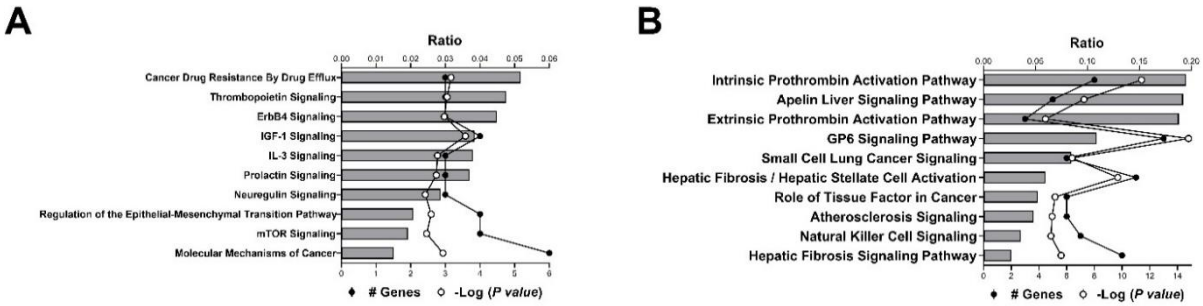

Figure 92. Top 10 most significantly enriched IPA pathways of *miR-375-3p* **(A)**, and *miR-29a-3p* **(B)** target genes set. Bars indicate Ratio, black lines indicate number of proteins and white line indicates -Log (*P value*).

2.3. Exposure of adipocytes to baseline serum from non-incident and incident-T2D patients.

In order to investigate the influence of circulating factors on adipose tissue function previous to T2D onset, we next assessed the response of adipocytes upon exposure to sera obtained from a subgroup of non-T2D and incident-T2D subjects from the CORDIOPREV-DIAB cohort (n = 32 for each group) at baseline, when differences in the biochemical and anthropometric profiles have not yet become apparent (**Table 3**; *Material and Methods* section).

These experiments showed significant reduced protein content of the insulin signalling mediator, IRS-1, in 3T3-L1 adipocytes treated with incident-T2D sera as compared to non-T2D sera (**Figure 93A**). Akt content was also altered in the former group (**Figure 93B**).

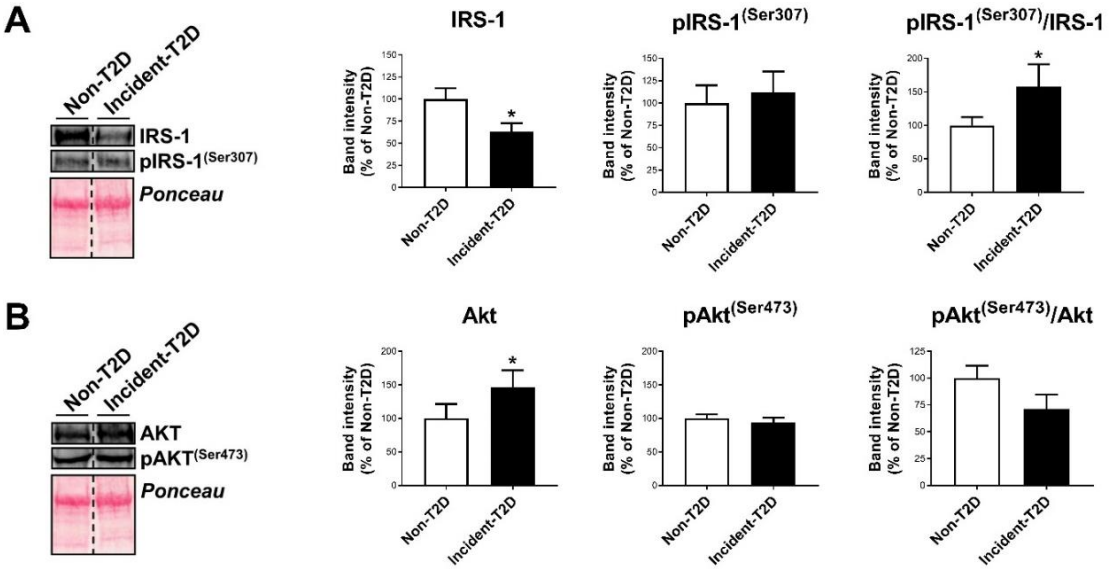

Figure 93. (A-B) Representative blots and quantification of the proteins indicated in 3T3-L1 cells at day 6 of differentiation upon 24h of exposure to 10% baseline serum from patients who did not develop T2D (Non-T2D, n=32) and patients who developed T2D (Incident-T2D, n=32) during the median follow-up of 60 months from the CORDIOPREV-DIAB study. *****P<0.05 *vs.* non-T2D.

Notably, cells exposed to incident-T2D sera exhibited significantly higher levels of the active (*i.e.*, phosphorylated) form of the inflammatory marker, JNK, which resulted in a higher pJNK/JNK ratio in these cells (**Figure 94**).

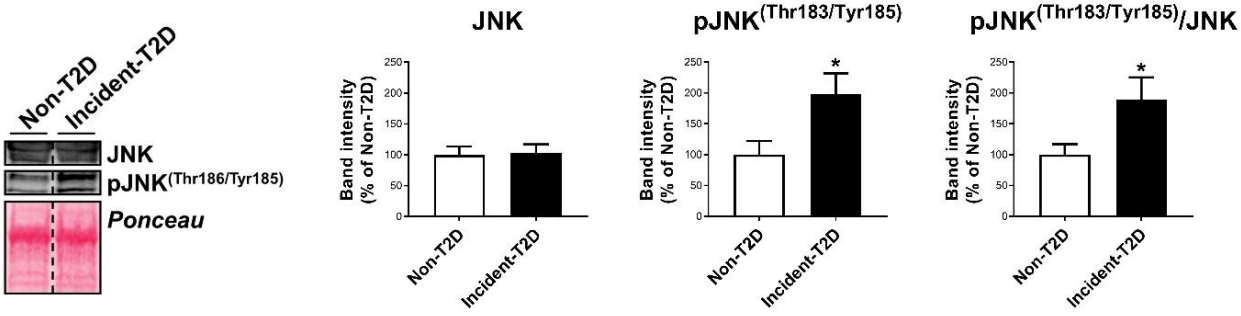

Figure 94. Representative blots and quantification of JNK and pJNK$^{(Thr183/Tyr185)}$ and its corresponding ratio in 3T3-L1 cells at day 6 of differentiation upon 24h of exposure to 10% baseline serum from patients who did not develop T2D (Non-T2D, n=32) and patients who developed T2D (Incident-T2D, n=32) during the median follow-up of 60 months from the CORDIOPREV-DIAB study. *****P<0.05 *vs.* non-T2D.

No effects were observed in relation to markers of ER stress (BIP, CHOP) (**Figure 95A**), or oxidative stress (SOD-1, GSS) (**Figure 95B**), yet a decrease in mitochondrial markers (UCP-1, PGC-1α), was observed after treatment with incident-T2D *vs.* non-T2D serum (**Figure 95C**).

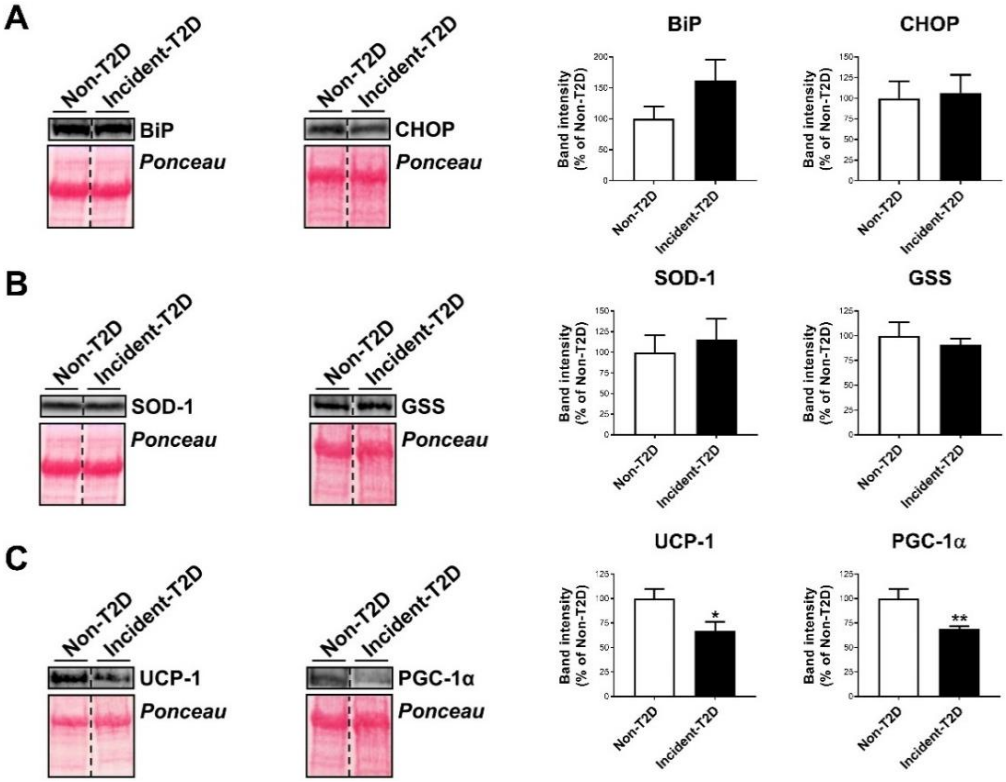

Figure 95. Representative blots and quantification of the proteins indicated in 3T3-L1 cells at day 6 of differentiation upon 24h of exposure to 10% baseline serum from patients who did not develop T2D (Non-T2D, n=32) and patients who developed T2D (Incident-T2D, n=32) during the median follow-up of 60 months from the CORDIOPREV-DIAB study. *****P<0.05, ******P<0.01 *vs.* non-T2D.

2.4. Regulation of *miR-223-3p* expression and secretion in adipocytes

Given the association between adipose tissue insulin resistance and low circulating *miR-223-3p* levels, and the previous observations from Thomou et al. (2017) demonstrating that adipose tissue is a major source of circulating miRNAs, we explored the ability of adipocytes to store and release *miR-223-3p* at different stages of differentiation. Likewise, based on the relationship observed *in silico* between *miR-223-3p* and inflammatory pathways, and the proven link between adipose tissue dysfunction and inflammation (Longo et al., 2019), we also examined *miR-223-3p* secretory dynamics in adipocytes challenged with TNFα.

2.4.1. miR-223-3p expression and secretory profiles during adipogenesis

miR-223-3p expression, as a measure of intracellular *miR-223-3p* content, was investigated in 3T3-L1 cells at different days of differentiation (D0, D3, D6, and D10). The amount of *miR-223-3p* released by these cells into the culture media in the previous 24 h-period at the indicated days was also evaluated. As shown in **Figure 96A**, *miR-223-3p* release into the culture media was significantly higher for preadipocytes (D0-D3) than for adipocytes at later stages of differentiation (D6-D10). Intracellular *miR-223-3p* levels were 2.9-, 3.4-, and 2.9-fold higher in fully differentiated adipocytes than in adipose cells at D0, D3 and D6, respectively (**Figure 96B**). These results indicated that preadipocytes primarily secrete *miR-223-3p* rather than keeping it intracellularly, while adipocytes preferentially retain this miRNA intracellularly, as illustrated by the *miR-223-3p* extracellular/intracellular ratios (**Figure 96C**).

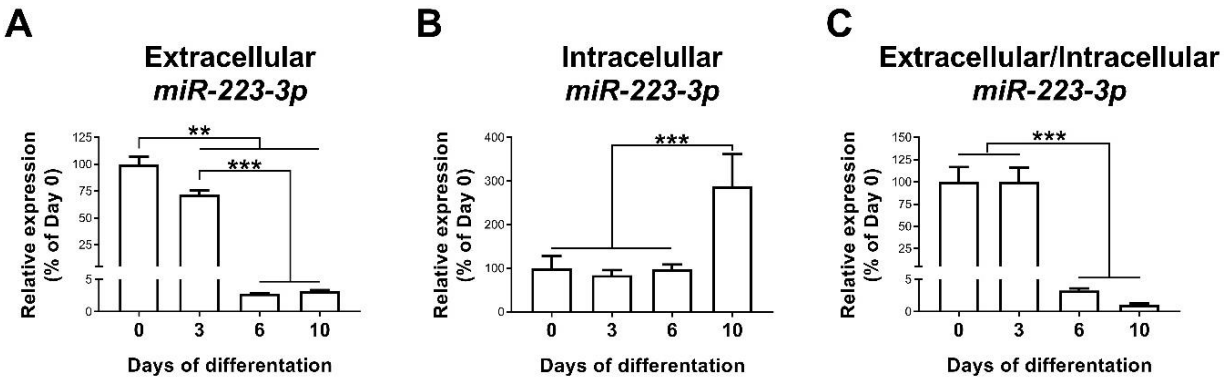

Figure 96. Extracellular **(A)**, and intracellular **(B)** levels of *miR-223-3p*, and its ratio **(C)** in 3T3-L1 cells during differentiation. ******P<0.01, *******P<0.001 *vs.* previous days.

In keeping with these results, we observed a decline in the mRNA and/or protein content of *Ago-2* (involved in miRNA processing), *Hnrnpa2b1* (involved in miRNA sorting

into exosomes), and the exosome marker, CD63, during 3T3-L1 cell differentiation (**Figures 97A-D**). Furthermore, the mRNA levels of *Ybx1*, which specifically participates in *miR-223-3p* sorting into exosomes (Gebert and MacRae, 2019), also decreased during adipogenesis (**Figure 97E**).

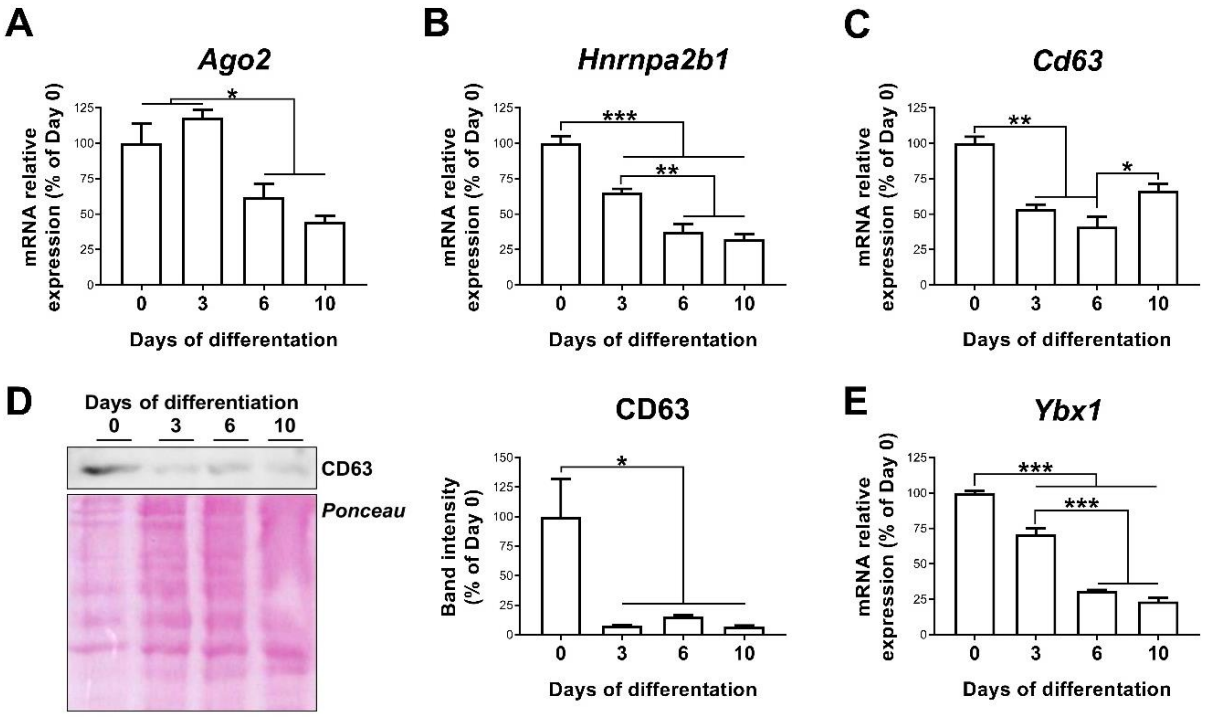

Figure 97. mRNA expression of the genes indicated **(A-C, E)**, and representative immunoblotting and quantification of CD63 **(D)** in 3T3-L1 cells during differentiation (days 0-10). *****P<0.05, ******P<0.01, *******P<0.001 *vs.* previous days.

In order to further explore the mechanisms mediating *miR-223-3p* release, extracellular vesicles (EVs) secreted by 3T3-L1 cells at D0 or D10 of differentiation were isolated from cell culture medium by serial ultracentrifugation. The purified particles were examined by electron microscopy (TEM), nanoparticle tracking analysis (NTA), and immunoblotting (**Figure 98**).

Consistent with other reports on exosomes (Tkach and Théry, 2016), these analyses revealed that EVs released by 3T3-L1 cells displayed a typical exosome morphology (i.e., cup-shaped and rounded vesicles) (**Figure 98A**), and size (~100 nm) (**Figure 98B**). A higher abundance of CD63 was found in the exosomal preparation in comparison with the total cell lysate (**Figure 98C**), thus validating the procedure employed for exosome isolation.

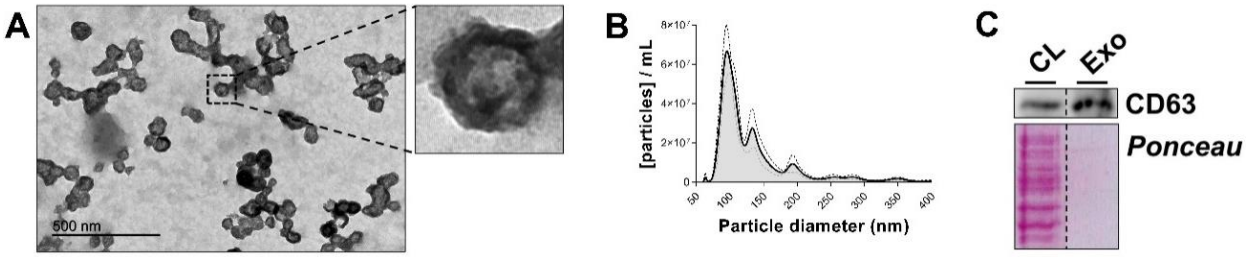

Figure 98. Representative TEM micrographs **(A)**, and representative size/concentration distribution by NTA **(B)** of exosome purification fraction from 3T3-L1 cells media. Scale bar = 500 nm. Mean is represented as a continue line and ±SEM is represented as dotted lines. **(C)** Representative blot of CD63 in 3T3-L1 cells total lysate (CL) and exosome purification fraction (Exo).

In accordance with our expression data, exosome production was significantly lower at D10 compared to D0 (**Figure 99**).

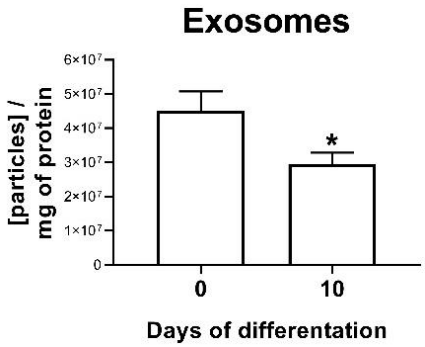

Figure 99. Exosome concentration in cell culture supernatant from 3T3-L1 cells at day 0 or 10 of differentiation. *P<0.05 *vs.* day 0.

To analyse whether the observed regulation of *miR-223-3p* is specific or not for this miRNA, we studied other miRNAs identified in the study by Jimenez-Lucena et al. (2018) and whose expression had been previously studied during adipogenesis (Ortega et al., 2010; Sun et al., 2009; Xie et al., 2009), but their secretion had not been explored yet, namely *miR-30a-5p* and *miR-103-3p*. We confirmed that the intracellular levels of both *miR-30a-5p* and *miR-103-3p* increased at late stages of adipogenesis (**Figures 100B** and **96E**), as observed in our studies for *miR-223-3p* (**Figure 96B**). However, while *miR-103-3p* and *miR-30a-5p* exhibited similar secretory profiles (**Figures 100A** and **100D**), they partially differed from that of *miR-223-3p*, specially at early stages of differentiation (D0) (**Figure 96A**).

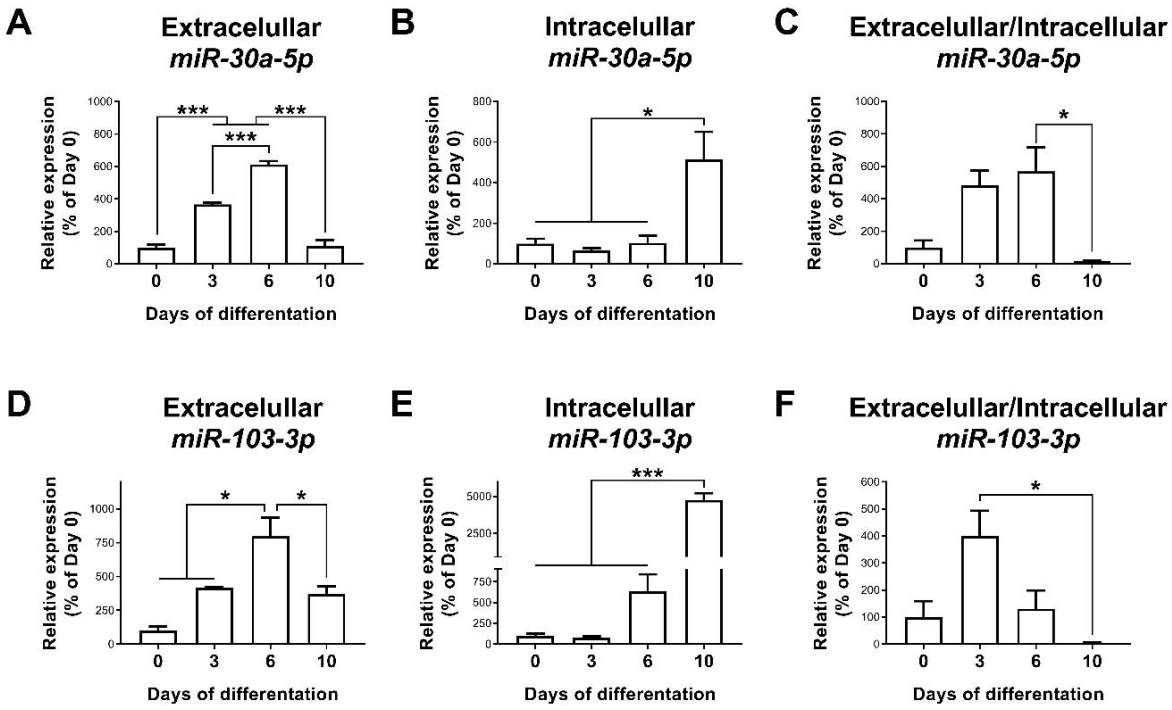

Figure 100. Extracellular **(A, D)**, and intracellular **(B, E)** levels of *miR-30a-5p* **(A, B)**, and *miR-103-3p* **(D, E)**, and its ratio **(C, F)** in 3T3-L1 cells during differentiation. *****P<0.05, *******P<0.001 *vs.* previous days.

2.4.2. *miR-223-3p* expression and secretory profiles in response to inflammation

We next explored the influence of inflammation on *miR-223-3p* secretion by exposing 3T3-L1 adipocytes to TNFα. The effects of TNFα on inflammation and insulin signalling were validated by the increase in the pJNK/JNK ratio (**Figure 101A**), and the decrease in insulin-induced stimulation of Akt activation (*i.e.*, pAkt/Akt ratio), respectively (**Figure 101B**).

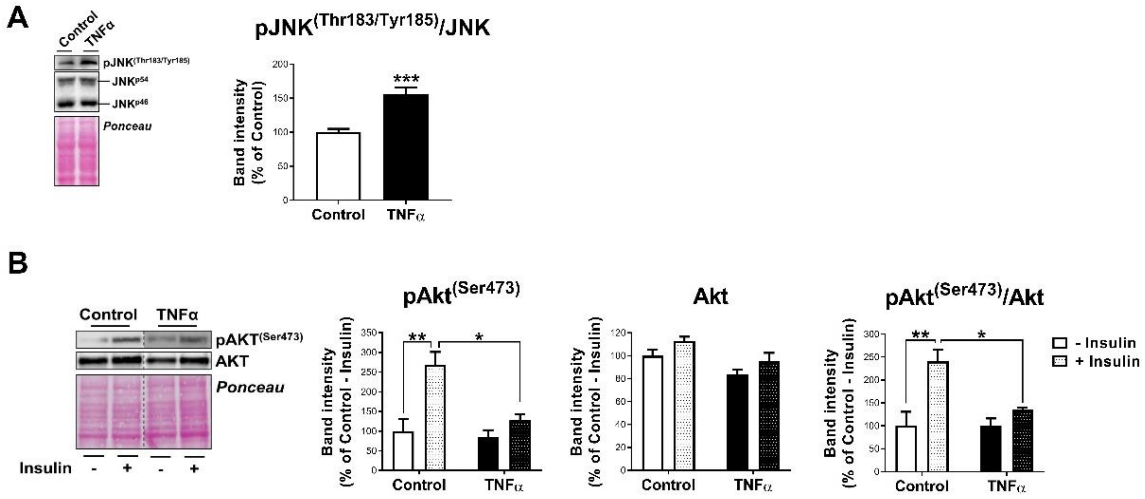

Figure 101. (A) Representative blot and quantification of pJNK(Thr183/Tyr185)/JNK in 3T3-L1 cells at day 6 of differentiation (D6) upon 24h of treatment with 5nM TNFα or vehicle (control). ***P<0.001 *vs.* control. **(B)** Representative blot and quantification of pAkt(Ser473), Akt, and its ratio in control or TNFα-treated 3T3-L1 cells (D6) stimulated or not with insulin (100nM, 5min). *P<0.05, **P<0.01 *vs.* indicated.

TNFα significantly reduced *miR-223-3p* secretion while increasing *miR-223-3p* intracellular content as compared to control conditions when exposed to either preadipocytes or adipocytes (**Figure 102A-C**, and **Figure 102D-F**, respectively).

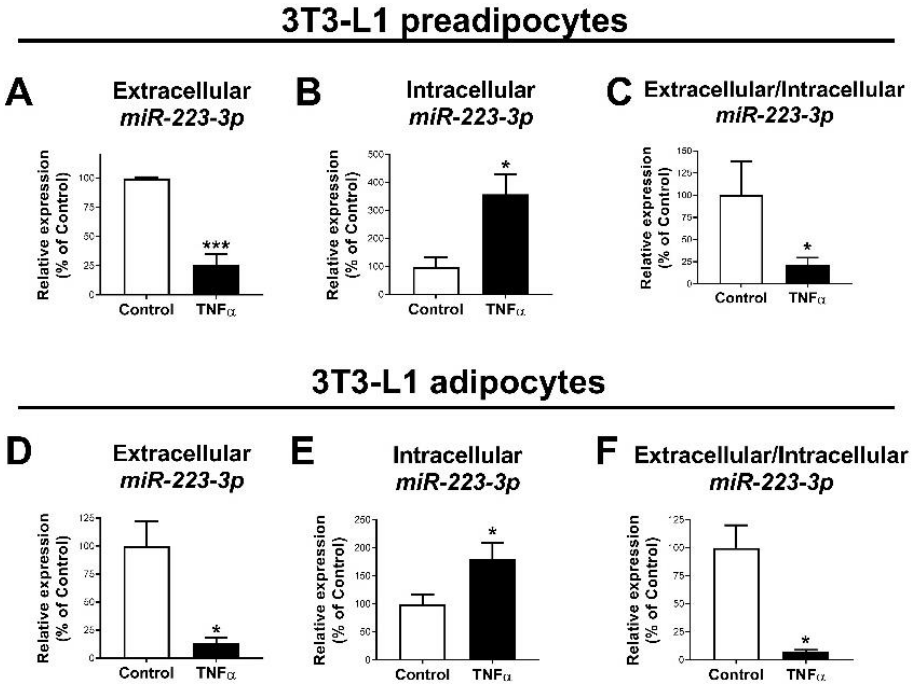

Figure 102. Extracellular **(A, D)**, and intracellular **(B, E)** levels of *miR-223-3p*, and its ratio in control or TNFα-treated 3T3-L1 preadipocytes (D3) and adipocytes (D6) **(C, F)**. *****P<0.05, *******P<0.001 *vs.* control.

Furthermore, *Ago2*, *Cd63*, and *Hnrnpa2b1* mRNA expression levels were reduced by TNFα (**Figure 103A-C** for preadipocytes; and **Figure 103E-G** for adipocytes), while *Ybx1* mRNA levels were not changed (preadipocytes) or significantly increased (adipocytes) compared to control conditions (**Figures 103D** and **103H**, respectively).

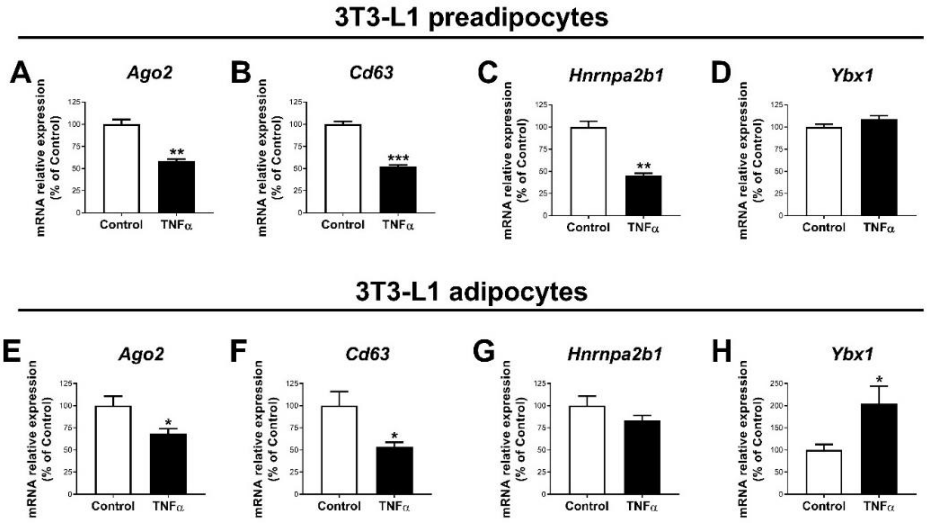

Figure 103. mRNA expression of the genes indicated in Control or TNFα-treated 3T3-L1 preadipocytes (D3) **(A-D)** or adipocytes (D6) **(E-H)**. *****P<0.05, ******P<0.01, *******P<0.001 *vs.* control.

Accordingly, exosome concentration was significantly lower in the culture supernatant from 3T3-L1 adipocytes exposed to TNFα than controls (**Figure 104**).

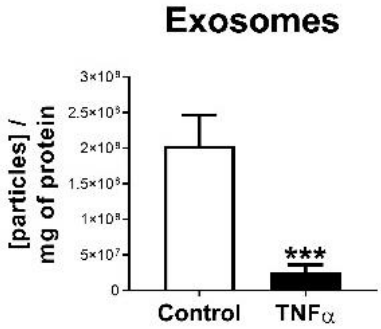

Figure 104. Concentration of exosomes in cell culture supernatant from 3T3-L1 cells upon 24 h of treatment with 5 nM TNFα or vehicle (control). *******P<0.001 *vs.* control.

Due to the relevant role of macrophages on AT inflammatory homeostasis and the proposed anti-inflammatory role of *miR-223-3p* (Deiuliis, 2016), we also analysed *miR-223-3p* response to TNFα in THP-1 monocytes. Notably, exposure of these cells to TNFα, which promotes the expression of classic pro-inflammatory markers (**Figure 105C**), did increase *miR-223-3p* intracellular content but not its secretion (**Figures 105D-F**).

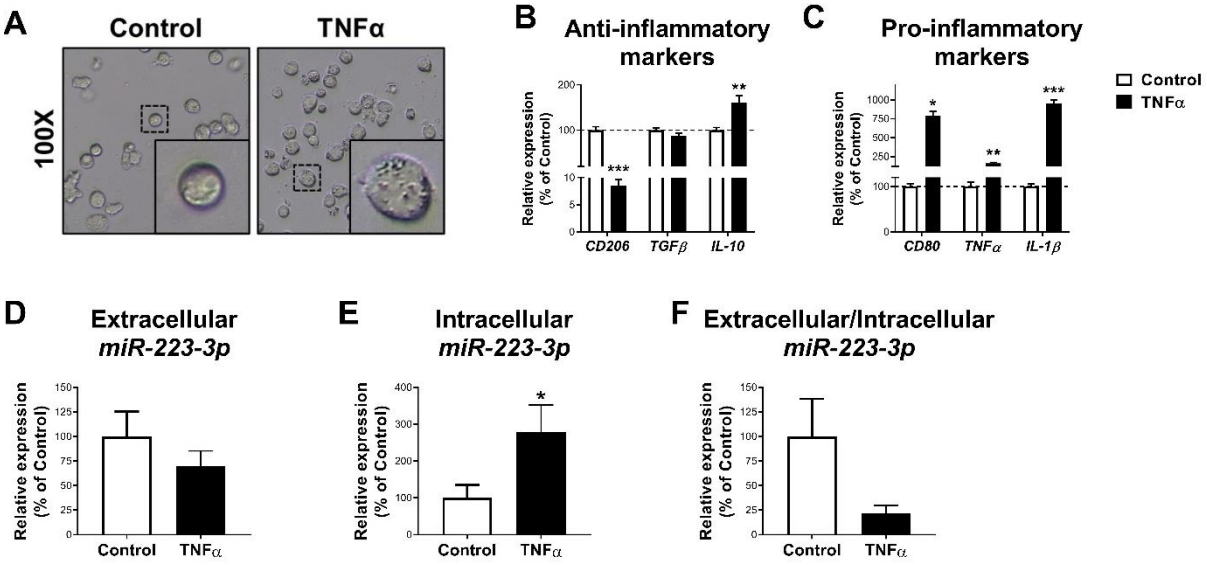

Figure 105. Representative images from light microscopy **(A)**, mRNA expression of the genes indicated **(B-C)**, and extracellular **(D)**, intracellular **(E)** levels of *miR-223-3p*, and its ratio **(F)** of THP-1 cells upon 24h of treatment with 5nM TNFα or vehicle (control). *P<0.05, **P<0.01, ***P<0.001 *vs.* control.

We also examined the regulation of *miR-30a-5p* and *miR-103-3p* secretion in response to TNFα and observed that the former decreased and the latter increased upon exposure to this inflammatory cytokine (**Figure 106A** and **106C**). When these results are

viewed together with the data on TNFα-induced decreased expression levels of *Ago2*, *Cd63*, and *Hnrpa2b1* (**Figure 103E-G**), it appears that at least for *miR-103-3p*, there must be additional mechanisms participating in the regulation of its secretion.

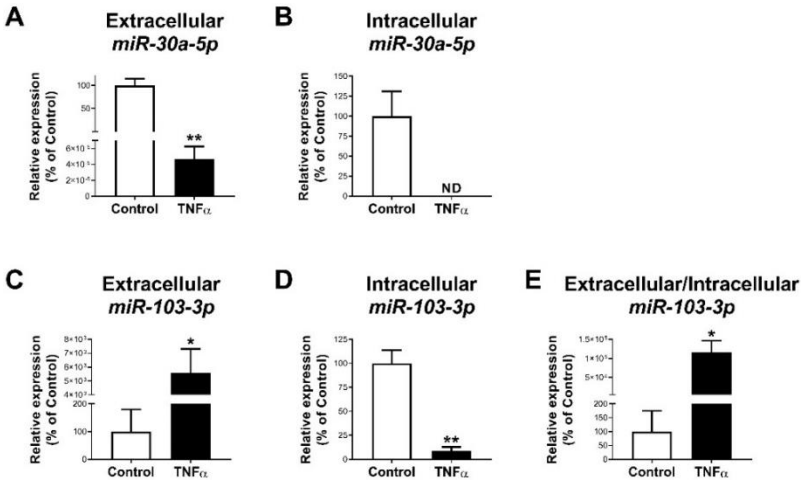

Figure 106. Extracellular **(A-C)**, intracellular **(B-D)** levels of *miR-30a-5p* **(A-B)**, and *miR-103-3p* **(C-E)**, and its ratio **(E)** in 3T3-L1 cells at day 6 of differentiation upon 24h of treatment with 5nM TNFα or vehicle (control) *****P<0.05, ******P<0.01 *vs.* control; ND, non-detected.

2.5. Effects of *miR-223-3p* overexpression on glucose metabolism in adipocytes

To address whether intracellular *miR-223-3p* accumulation might have consequences on adipose cell function, we overexpressed *miR-223-3p* in 3T3-L1 adipocytes at different stages of differentiation using a *miR-223-3p* mimic (**Figures 107-111 and 115-118**). Transfection efficiency was validated as shown in **Figure 107**, confirming that these cells accumulate *miR-223-3p* intracellularly.

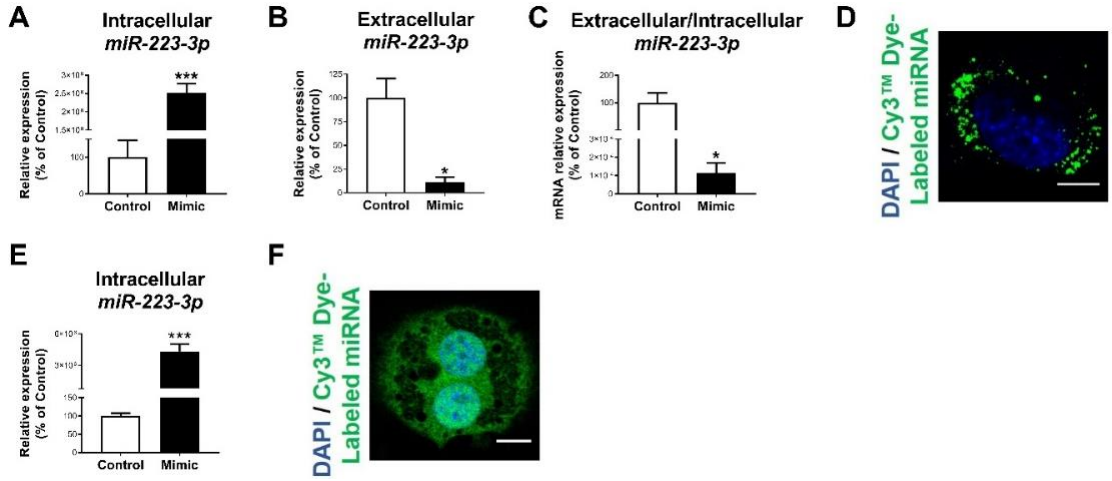

Figure 107. Intracellular **(A, E)**, extracellular **(B)** levels and its ratio **(C)** of *miR-223-3p*, and representative confocal micrographs **(D, F)** of 3T3-L1 cells transfected with negative miRNA-Control (control) or *miR-223-3p* (mimic) at day 3 **(A-D)** and day 6 **(E-F)** of differentiation. For confocal imaging cells were co-transfected with Cy3^{TM} labelled miRNA (green) and nuclei were stained with DAPI (blue). Scale bar = 10μm. *P<0.05, ***P<0.001 *vs.* control.

3T3-L1 cells transfected with *miR-223-3p* mimic at D3 of differentiation exhibited similar mRNA levels but lower protein content of the *miR-223-3p* target, GLUT4, than control cells (**Figures 108A** and **108B**). *miR-223-3p* mimic-overexpressing cells also exhibited significant decreases of several insulin signalling mediators, including IRS-1, Akt, and AS-160 protein content as compared to their control counterparts (**Figure 108C**). In contrast, a significant increase in the protein content of ARF6, which has been involved in GLUT4 incorporation into intracellular GLUT4 storage vesicles (Leto and Saltiel, 2012), was observed in cells overexpressing *miR-223-3p* (**Figure 108D**).

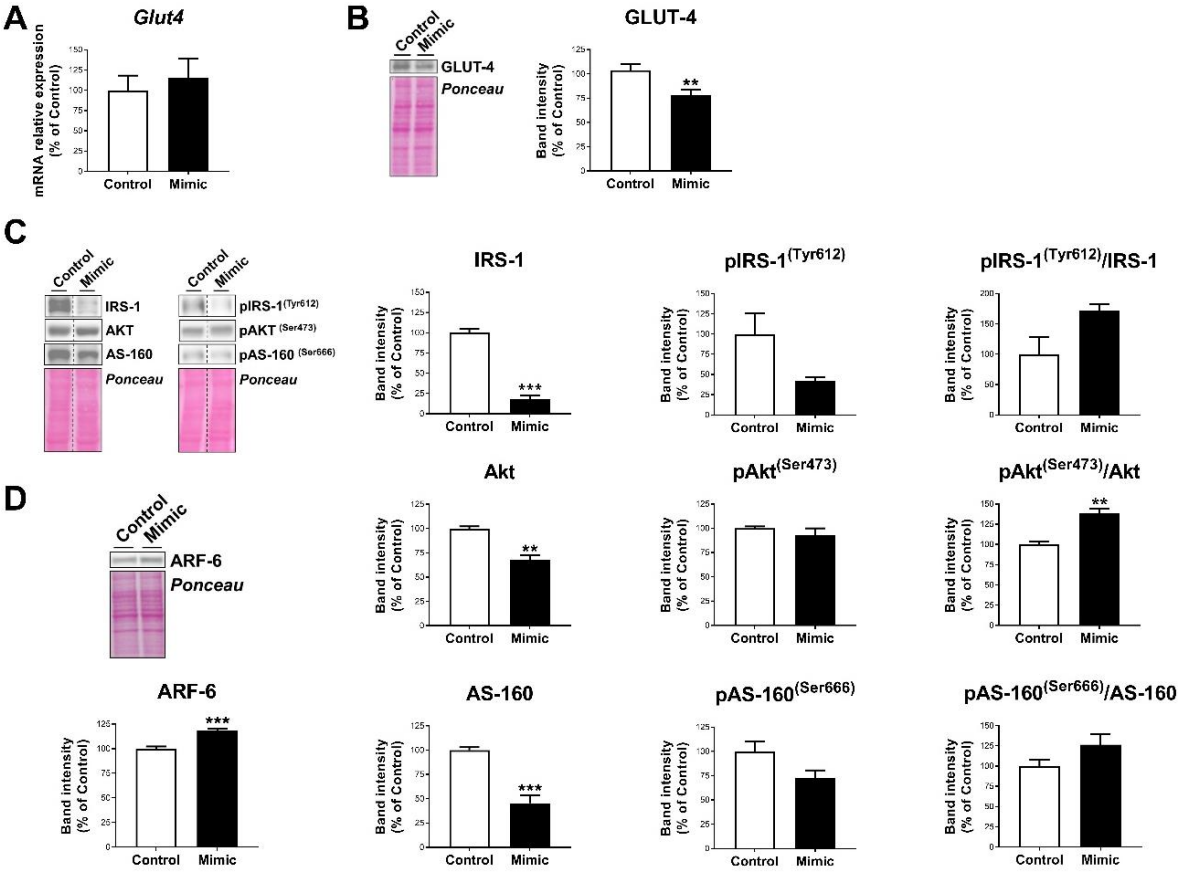

Figure 108. mRNA expression of *Glut4* **(A)**, representative blot and quantification of GLUT4 **(B)**, and representative blots and quantification of the proteins indicated **(C-D)** in 3T3-L1 cells transfected with negative miRNA-Control (control) or *miR-223-3p* mimic (mimic) at day 3 of differentiation. ******P<0.01, *******P<0.001 *vs.* control.

To evaluate whether *miR-223-3p* may also affect GLUT4 translocation to the plasma membrane, we employed a cMyc-GLUT4-EGFP expression vector (kindly donated by Dr. JA Pessin; Albert Einstein College of Medicine, NY), which was co-transfected with *miR-223-3p* mimic or negative miRNA control. Quantification of intracellular and plasma membrane-associated GLUT4 in confocal micrographs revealed that 3T3-L1 cells overexpressing *miR-223-3p* exhibited more GLUT4 located in the plasma membrane than control adipocytes under both basal and insulin-stimulated conditions (**Figure**

109A). In contrast to that observed in control cells, plasma membrane-associated GLUT4 levels in *miR-223-3p*-overexpressing cells were similar in the absence or presence of insulin (**Figure 109A**). In all groups, glucose uptake values changed in parallel to GLUT4 translocation to the plasma membrane (**Figure 109B**).

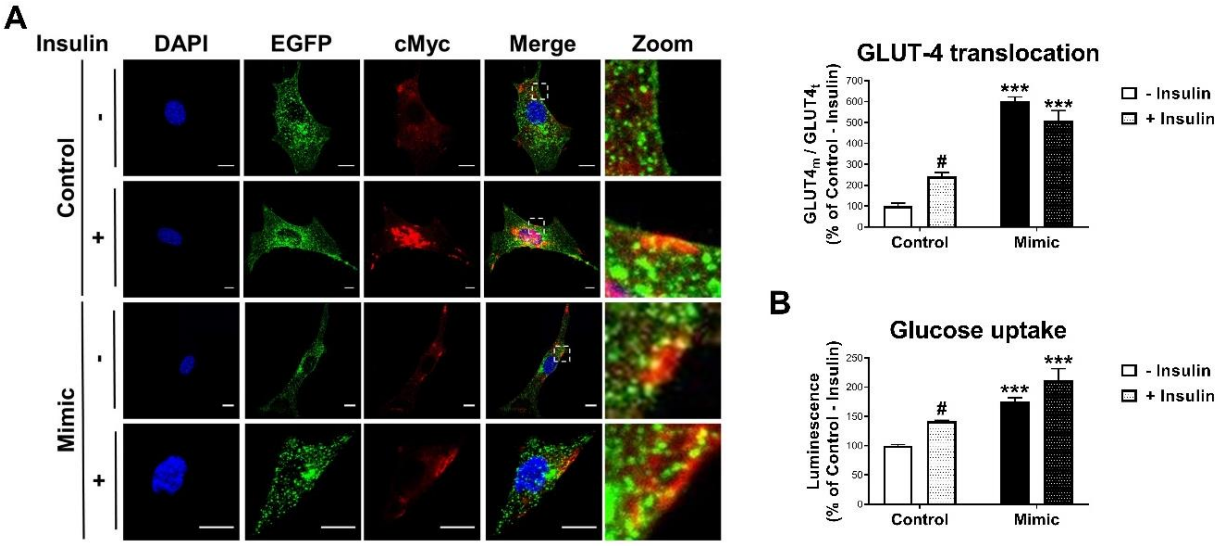

Figure 109. Representative confocal micrographs and quantification of GLUT4 translocation **(A)**, and glucose uptake **(B)** of cells transfected with negative miRNA-Control (control) or *miR-223-3p* mimic (mimic) at day 3 of differentiation stimulated or not with insulin (100nM, 20/60min). Cells were co-transfected with cMyc-GLUT4-EGFP expression plasmid and immunostained with anti-cMyc antibody, showing total GLUT4 (GLUT4t, green) and membrane-associated GLUT4 (GLUT4m, red). Nuclei were stained with DAPI (blue). Scale bar = 10 µm. *******P<0.001 *vs.* control; #P<0.05 *vs.* non-stimulated cells.

The effects of *miR-223-3p* overexpression were also examined in 3T3-L1 adipocytes at later stages of differentiation (D6) (**Figures 110**, **111**, and **115-118**). D6-transfected 3T3-L1 cells overexpressing *miR-223-3p* also exhibited decreased GLUT4 protein levels, but similar GLUT4 mRNA levels than control cells (**Figure 110A** and **110B**). There were also significant decreases in IRS-1 and AS-160 protein content as well as in Akt phosphorylation levels (**Figure 110C**), whereas ARF6 levels remained unchanged (**Figure 110D**).

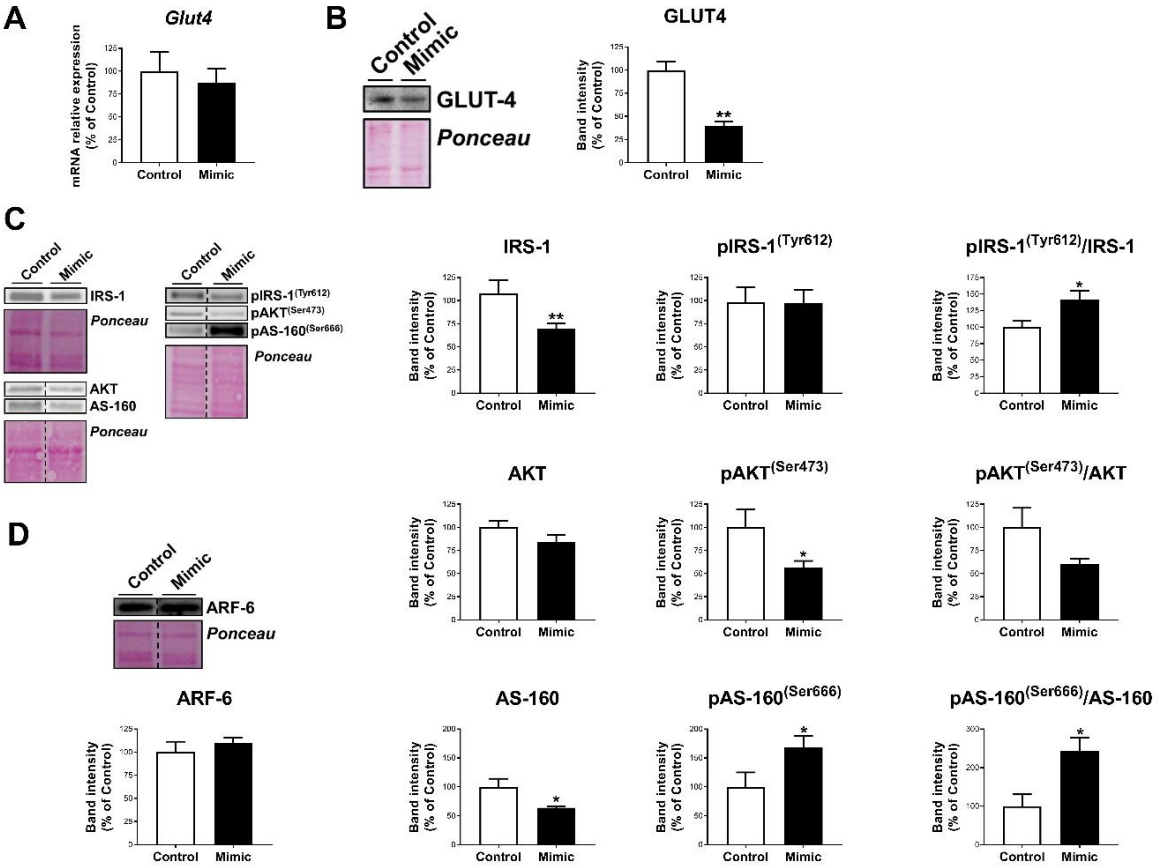

Figure 110. mRNA expression of *Glut4* **(A)**, representative blot and quantification of GLUT4 **(B)**, and representative blots and quantification of the proteins indicated **(C-D)** in 3T3-L1 cells transfected wit negative miRNA-Control (control) or *miR-223-3p* mimic (mimic) at day 6 of differentiation. *****P<0.05, ******P<0.01 *vs.* control.

Regarding GLUT4 translocation, no differences were observed in basal values between 3T3-L1 adipocytes overexpressing *miR-223-3p* mimic and control cells (**Figure 111A**). However, insulin-induced GLUT4 translocation was reduced by 6.4-fold in adipocytes overexpressing *miR-223-3p* (**Figure 111A**). Functional studies showed that both basal and insulin-stimulated glucose uptake was lower in adipocytes expressing *miR-223-3p* mimic than in control cells (**Figure 111B**).

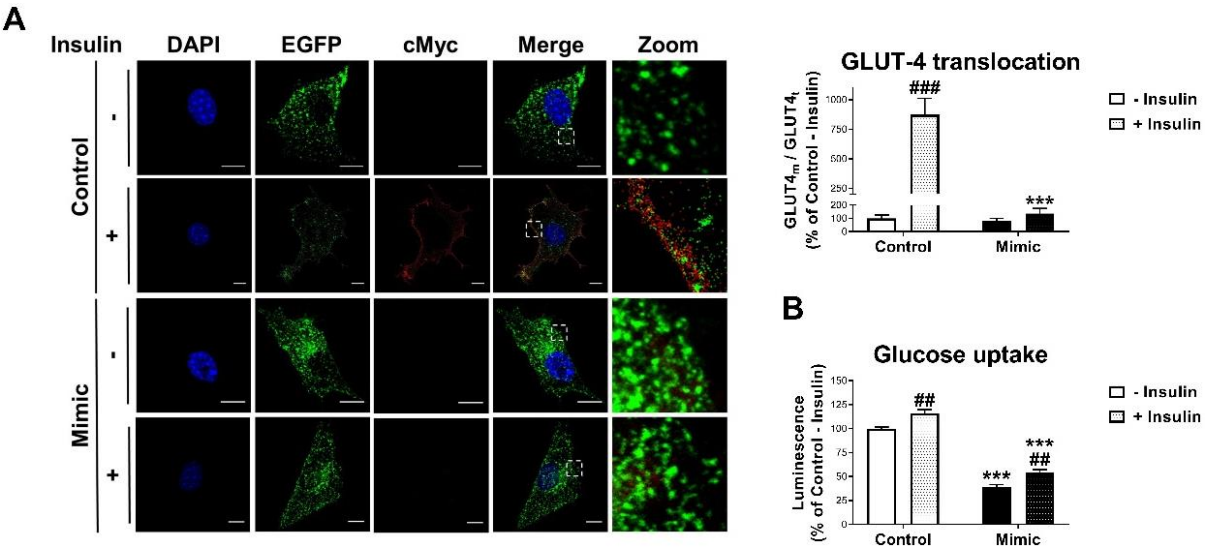

Figure 111. Representative confocal micrographs and quantification of GLUT4 translocation **(A)**, and glucose uptake **(B)** of cells transfected with negative miRNA-Control (control) or *miR-223-3p* mimic (mimic) at day 6 of differentiation stimulated or not with insulin (100 nM, 20/60 min). Cells were co-transfected with cMyc-GLUT4-EGFP expression plasmid and immunostained with anti-cMyc antibody, showing total GLUT4 (GLUT4t, green) and membrane-associated GLUT4 (GLUT4m, red). Nuclei were stained with DAPI (blue). Scale bar = 10 µm. *******P<0.001 *vs.* control; ##P<0.01 and ###P<0.001 *vs.* non-stimulated cells.

2.6. Regulation of *miR-223-3p* and glucose uptake in response to BS-induced weight loss

To further investigate the regulation of *miR-223-3p* in the context of BS-induced weight loss, we investigated the influence of circulating factors on *miR-223-3p* accumulation in adipocytes.

First, *miR-223-3p* expression was investigated in SGBS cells throughout differentiation. As shown in **Figure 112,** and similarly to the observed for 3T3-L1 cells (**Figure 96B**), SGBS cells also exhibited increased intracellular *miR-223-3p* levels at the end of differentiation.

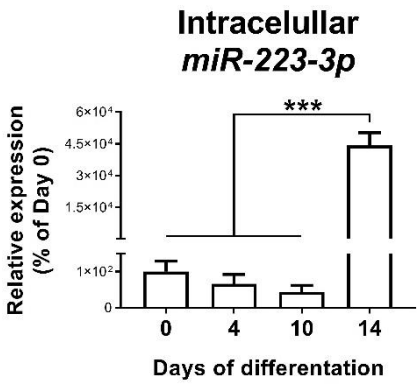

Figure 112. *miR-223-3p* intracellular levels of SGBS cells during differentiation (days 0-14) *******P<0.001 *vs.* previous days.

Next, we measured *miR-223-3p* intracellular levels in SGBS adipocytes upon exposure to sera obtained from subjects before and after BS (Pre- and Post-BS, respectively; cohort 4), separated or not according to obesity duration (**Tables 4** and **5**; *Material and Methods* section). This study showed a significant reduction in the amount of *miR-223-3p* accumulated within the cells treated with Post-BS sera as compared to Pre-BS sera (**Figure 113A**). This reduction only reached statistical significance in response to sera from SSO subjects (**Figure 113B**).

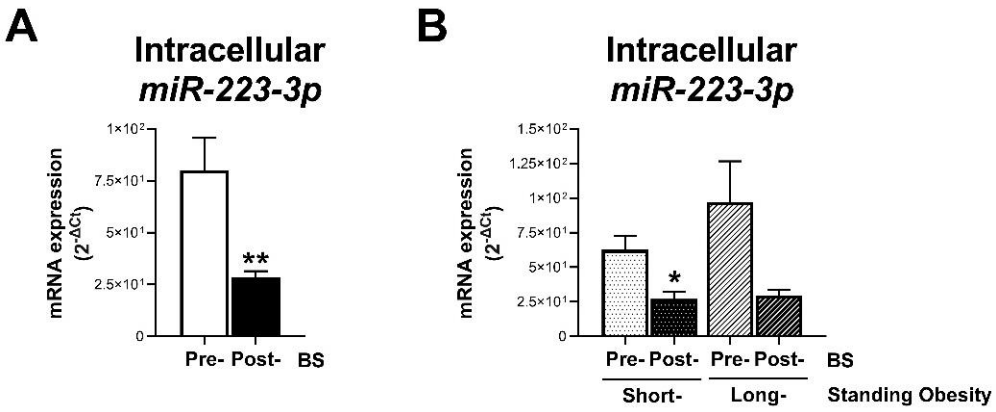

Figure 113. *miR-223-3p* intracellular levels of SGBS cells at day 14 of differentiation upon 24h of exposure to 10% baseline serum from obese subjects before and after BS (Pre- and Post-BS, respectively) independently **(A)** and dependently **(B)** of obesity time. *****P<0.05, ******P<0.01 *vs.* Pre-BS.

Moreover, exposure to Post-BS sera improved glucose uptake in response to insulin, irrespective of obesity duration (**Figure 114**).

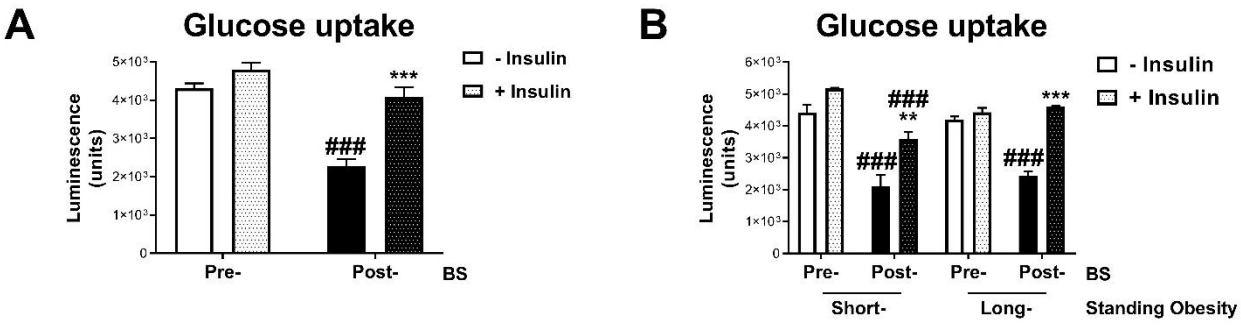

Figure 114. Glucose uptake of SGBS at day 14 of differentiation upon 24h of exposure to 10% baseline serum from obese subjects before and after BS (Pre- and Post-BS, respectively) independently **(A)** and dependently **(B)** of obesity time, stimulated with/without insulin (100nM, 60min). ******P<0.01, *******P<0.001 *vs.* without insulin; ###P<0.001 *vs.* Pre-BS.

2.7. Effects of *miR-223-3p* overexpression on lipid metabolism in adipocytes

Lipid accumulation assessed by quantification of Oil Red-O staining in confocal micrographs revealed lower lipid content in cells transfected at D3 with *miR-223-3p*

mimic than control cells, which was attributable to a reduction in LD number (**Figure 115**).

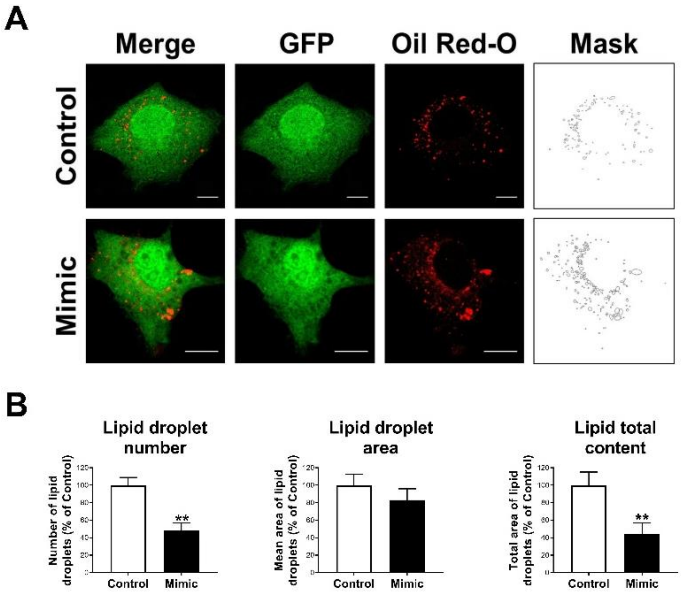

Figure 115. Representative confocal micrographs **(A)**, and LD morphological analysis **(B)** of 3T3-L1 cells transfected with negative miRNA-Control (control) or *miR-223-3p* mimic (mimic) at day 3 of differentiation. Cells were co-transfected with phrGFP-N1 encoding GFP alone (green) to validate transfection and LDs were stained with Oil Red-O (red). Scale bar = 10 µm. ******P<0.01 *vs.* control.

When transfected at D6, 3T3-L1 adipocytes expressing *miR-223-3p* mimic contained more but smaller LDs than control cells, so that no changes in total lipid content were observed as consequence of *miR-223-3p* overexpression (**Figure 116**).

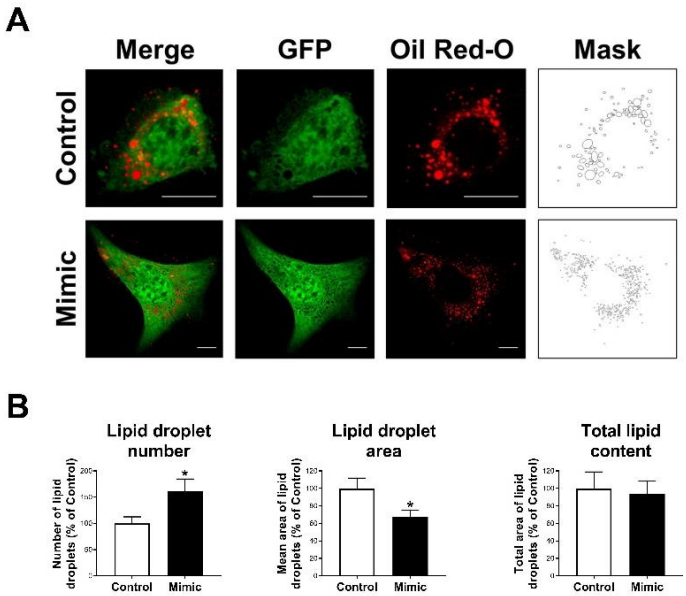

Figure 116. Representative confocal micrographs **(A)**, and LD morphological analysis **(B)** of 3T3-L1 cells transfected with negative miRNA-Control (control) or *miR-223-3p* mimic (mimic) at day 6 of differentiation. Cells were co-transfected with phrGFP-N1 encoding GFP alone (green) to validate transfection and LDs were stained with Oil Red-O (red). Scale bar = 10 µm. *****P<0.05 *vs.* control.

Finally, 3T3-L1 cells overexpressing *miR-223-3p* at either early or late differentiation stages exhibited enhanced lipolytic rates (measured as glycerol release into the medium) compared to their respective control cells (**Figures 117A** and **117B**, respectively).

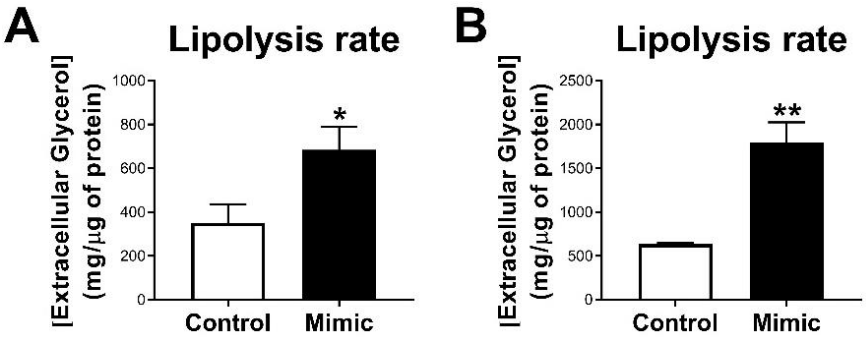

Figure 117. Lipolysis rate of 3T3-L1 cells transfected with negative miRNA-Control (control) or *miR-223-3p* mimic (mimic) at day 3 **(A)**, and 6 **(B)** of differentiation. *****P<0.05, ******P<0.01 *vs.* control.

These findings were in agreement with a significantly reduced mRNA content of several markers of adipogenesis, lipogenesis, and LD biogenesis and growth, and the increase of lipolysis-related genes observed in these cells (**Figure 118**).

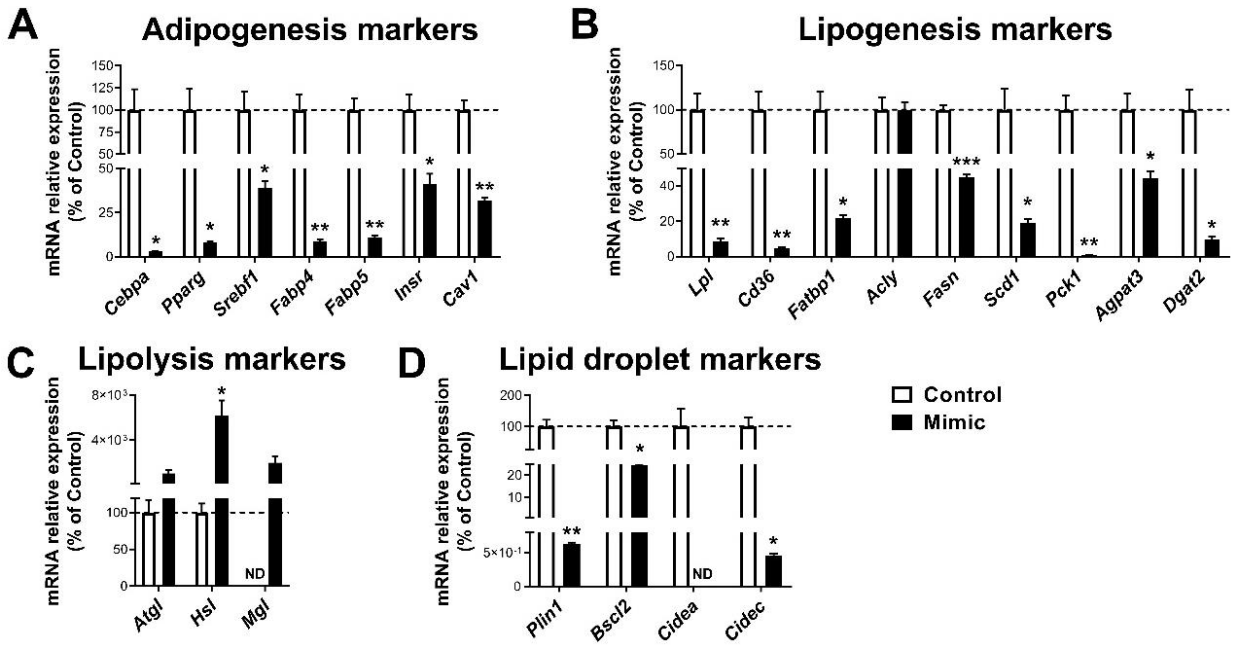

Figure 118. (A-C) mRNA levels of the genes indicated in 3T3-L1 cells transfected with negative miRNA-Control (control) or *miR-223-3p* mimic (mimic) at day 3 of differentiation. *****P<0.05, ******P<0.01, *******P<0.001 *vs.* control.

This study has been published in *Molecular Therapy – Nucleic Acids* in January 2021. https://doi.org/10.1016/j.omtn.2021.01.014

DISCUSSION

Health, including metabolic health, represents a compendium of organizational and dynamic features that maintain physiology. The biological causes or hallmarks of health include from the maintenance of homeostasis over time, to the triggering of adequate responses to stress. Disruption of any of these interrelated features is broadly pathogenic, causing an acute or progressive derailment of the system and health loss (López-Otín and Kroemer, 2020).

Thus, both cells and organisms have evolved mechanisms that display a high degree of flexibility (and/or buffering capacity) to perform adequate responses to adapt and/or cope with multiple external factors and alterations, and, eventually, stabilize the internal medium. This “phenotypic flexibility” is crucial for facing fluctuating and pathological conditions and it is determinant of health, and, therefore, its impairment represents a key component for the development of several diseases, including metabolic disorders (Westneat et al., 2019). In this context, the adipose tissue is considered one of the most plastics organs in the body and a major contributor to the maintenance of systemic metabolic homeostasis. In fact, adipose tissue dysfunction in obesity is relevant in the instauration of insulin resistance (IR) and type 2 diabetes (T2D) (Longo et al., 2019).

Despite the wealth of knowledge gathered to date on the regulation of the adipose tissue in humans under normal and pathological situations, there are several actions and players which remain not completely elucidated or, even, to be discovered. Indeed, finding novel molecular mechanisms and mediators should not be unexpected given the complexity of the system that ensure the precise control of the adipose tissue function and its constant crosstalk with other organs. In the aim to unveiling the molecular factors and signalling pathways related to adipose tissue dysfunction that may contribute to phenotypic flexibility impairment, we employed human samples in combination with both human and murine cell lines. The use of state-of-the-art methodologies applied to the study of these different models has enable to generate the results included in this Doctoral Thesis, which have been structured in two chapters, corresponding to two related scientific projects.

To be more specific, we have unveiled several pathological processes that likely contribute to the lack of phenotypic flexibility in the adipose tissue of obese individuals with metabolic disease, including their modulation in response to therapeutic interventions. The results obtained contribute to the identification of processes (i.e., alternative mRNA splicing and endoplasmic reticulum proteostasis), and signals (i.e., *miR-223-3p*) relevant to adipose tissue biology. These studies define their pathogenic role in the development of metabolic disease in obesity and highlight their potential value in the predisposition and susceptibility of an individual to develop IR/T2D.

Our data on preadipocytes not only define the impairment of alternative splicing to be specific of SC adipose tissue, while maladaptive ER stress-UPR-ERAD system seems to be a ubiquitous feature of both SC and OM fat, but also that these alterations disrupt adipocyte differentiation, and, therefore, hamper the necessary renewal capacity of this tissue. Moreover, our studies have established that adipocyte *miR-223-3p* release is prevented under pathological conditions (i.e., inflammation), which might contribute to the lower circulating *miR-223-3p* levels observed in patients who are going to develop T2D, and likely alter adipocyte function as well.

Herein, the multifactorial information recapitulated support the importance of identifying molecular regulators of phenotypic plasticity in the adipose tissue to comprehensively understand the development of metabolic disease in obesity. An improved knowledge about the molecular mechanisms underlying adipocyte dysfunction at intracellular level, may pave the way for the design of prevention strategies and better therapeutic approaches to tackle obesity.

1. Study 1: Identification of pathogenic markers of metabolic disease in preadipocytes of obese individuals

In the first study of this Doctoral Thesis, we found that alternative splicing in the SC adipose tissue, and the ER stress-UPR-ERAD system in both SC and OM fat represent essential components of the adipogenic process that are altered in obese individuals with IR/T2D. Specifically, IR/T2D obesity is characterized by reduced expression levels of multiple members of the major and minor spliceosome, and splicing factors in SC preadipocytes. We provide experimental evidence demonstrating that decreasing the expression of a key component of the major spliceosome, *PRPF8*/PRP8, by siRNA is sufficient to hamper the expression of both markers of adipogenesis and regulators of LD biogenesis and growth, thus supporting a relevant role for this protein and the splicing machinery in the regulation of adipocyte differentiation. Our results are also indicative of IR/T2D-dependent ERAD hyperactivation in preadipocytes of the two major fat depots, SC and OM, in obese individuals. Maladaptive UPR and ERAD signalling upon ER stress induction may contribute to impair adipocyte differentiation and to the progression of metabolic disease in obesity.

Alternative splicing of mRNA enables cells to acquire protein diversity, which is essential for cell differentiation and tissue growth and identity (Baralle and Giudice,

2017). It is accepted that both mRNA transcription and processing contribute to the changes in gene expression patterns leading to the transition of progenitor cells toward a mature phenotype (Fiszbein and Kornblihtt, 2017). In this regard, recent reports suggest a role for alternative splicing in adipocyte differentiation (Lin, 2015). It has been shown that inhibition of the splicing factor, SF3B1, blocks 3T3-L1 adipocyte differentiation (Kaida, 2019), and recent RNA-seq studies support the occurrence of alternative splicing events during adipogenesis of bone marrow-derived human mesenchymal stem cells (Yi et al., 2019). Furthermore, certain naturally PPARγ isoforms generated by alternative splicing act as dominant-negative isoforms that prevent adipocyte differentiation (Aprile et al., 2018). However, few studies have addressed the relevance of the splicing machinery in human preadipocytes and whether this system is altered in obesity. To the best of our knowledge, this is the first study demonstrating the down-regulation of multiple members of the splicing machinery in human SC preadipocytes in relation to obesity-associated IR/T2D.

To analyse the relevance of alternative splicing on adipogenesis, we reduced the expression of a major spliceosome component found to be markedly down-regulated in SC preadipocytes from IR/T2D obese individuals, *PRPF8*/PRP8, by siRNA treatment of SGBS preadipocytes. In this context, recent work combining RNA-seq and proteomics demonstrated that PRP8 depletion altered the expression of more than 1,500 proteins in Cal51 breast cancer cells, supporting the relevance of this protein in defining the human proteome (Liu et al., 2017). In fact, as part of the core of the major spliceosome, PRP8 is potentially involved in the removal of most introns from precursor mRNAs (99.5% of non-coding regions are removed by the major spliceosome) (Turunen et al., 2013). Our studies showed that decreasing PRP8 protein levels by 2-fold (as observed in IR/T2D vs. NG obese SC preadipocytes) in SGBS preadipocytes evoked gene/protein expression changes indicative of altered adipogenesis, which was confirmed by the decreased accumulation of lipids observed in SGBS cells at late stages of differentiation. These results were replicated in another SC adipocyte cell line, hADSCs, derived from a lean donor, reinforcing the key contribution of *PRPF8*/PRP8 to human adipocyte differentiation.

Two different yet functionally interrelated pathways were impaired in *PRPF8*-silenced SGBS and hADSCs cells in terms of both total gene expression levels and isoform balance of the proteins involved, i.e., adipogenic transcriptional program, and LD biogenesis and growth (**Figure 65**). Thus, PRP8 down-regulation altered the expression of *PPARG* and *SREBP1*, as well as of seipin and two members of the CIDE family (*CIDEB*, *CIDEC*). In particular, the overall decrease in *PPARG* and *SREBP1* isoforms

observed in SGBS cells upon PRP8 down-regulation may account for the reduction observed in mRNA and/or protein levels of known downstream target genes of these transcription factors (*ADIPOQ*, *FABP4*, *CIDEC*, and FAS) (Lowe et al., 2011; Slayton et al., 2019). Likewise, the dramatic changes in LD size and number observed in *PRPF8*-silenced adipocytes might be related to the low expression levels of the canonical *BSCL2*/seipin variant, seipin1 (Craveiro Sarmento et al., 2018), observed in these cells. Indeed, our observations in SGBS adipocytes are in line with previous data on seipin knockout A431 cells, which also exhibited more numerous but smaller LDs than controls (Salo et al., 2016). Interestingly, seipin knock-down has been shown to suppress *PPARG* and *SREBF1* expression (Fei et al., 2011), thus suggesting that the phenotype of SGBS cells silenced for *PRPF8*/PRP8 may be the result of the action of this spliceosome component on multiple key genes contributing to adipogenesis and lipogenesis. In line with this notion, analysis of CLIP-sep data in the ENCORI database revealed the presence of PRP8 binding sites in *PPARG*, *SREBP1*, *BSCL2*, *CIDEB*, and *CIDEC* mRNAs. Further research is needed to fully establish the splicing targets for PRP8 in preadipocytes and to characterize the relevance of the resulting protein isoforms (and/or their ratio) in adipogenesis. Notwithstanding this, the observation that PRP8 re-expression in *PRPF8*-silenced SGBS cells can restore the expression and/or isoform balance of genes such as *PPARG*, *BSCL2*, *CIDEB* or *CIDEC*, as well as normal LD content, supports a prominent role for this protein in lipid accumulation in adipocytes. In this scenario, it is reasonable to propose that the decreased expression of splicing-related genes in SC preadipocytes in IR/T2D obesity as compared to NG obesity could be responsible, at least in part, of the loss of adipogenic capacity displayed by SC preadipocytes from obese individuals with metabolic disease. In support of this proposal are our results on the up-regulation of *PRPF8* expression levels as well as of adipogenic markers (PPARγ, FABP4, and ADIPOQ), in the SC adipose tissue in response to bariatric surgery (BS)-induced weight loss, especially in obese individuals that exhibited a healthier metabolic profile (i.e., short-standing obesity, SSO) in terms of circulating parameters (glucose, HbA1) before surgery.

In this line, we and others have pointed to the mRNA splicing process as determinant of a correct cellular function and its dysregulation in adipose tissue to be associated with obesity and the development of metabolic disturbances (Vernia et al., 2016). Although the exact pathways regulated by mRNA splicing are only partially known, it is important to note that this process is regulated by both genetic variation and environmental cues (Kelemen et al., 2013), allowing an organism to adapt to the alterations in the environment and, therefore, the regulation of mRNA splicing in BS is of relevance.

Previous studies suggested that obesity-surgery induced by weight loss modulate splicing of genes such as *TCF7L2*, *INSR* and *MSH5* in SAT (Kaminska et al., 2016). This regulation is mediated, at least in part, by component of the splicing machinery such as HNRNPA1, SF3A1 and SFRS7 (Kaminska et al., 2014). However, a systematic analysis regarding the component of the splicing machinery in adipose tissue upon BS has never been addressed. Here, we show that the key component of the spliceosome, *PRPF8*, is upregulated in SAT after BS (more prominently in SSO subjects). Although further experiments are needed, we could hypothesize that weight loss in BS is improving the splicing capacity of these cells and it could contribute to the adipogenesis promotion observed.

When viewed together, our data strongly support the notion that splicing deregulation in SC preadipocytes may represent a pathogenic factor that contributes to the development of obesity-related complications. Changes in splicing components between groups were negligible in OM preadipocytes as compared to their SC counterparts. These inter-depot differences, which appear to be cell autonomous, might contribute, at least partly, to the distinct differentiation capacity of SC and OM preadipocytes observed in this and other studies (Martyniak and Masternak, 2017). Future studies using human primary preadipocytes with altered expression levels of selected splicing-related genes will be important to elucidate the precise splicing events that are critical for adipogenesis.

Interestingly, along with altered splicing, SC preadipocytes in IR/T2D obesity also exhibited molecular features indicative of ER stress response failure, a hallmark process associated with the development of metabolic diseases (Bhattarai et al., 2020). In fact, our data suggest that this pathogenic process also occurs in OM preadipocytes in IR/T2D obesity. In accordance with these findings, previous studies from our laboratory have established that IR obesity is associated with enhanced levels of ER stress markers in mature adipocytes isolated from either SC or OM fat (Díaz-Ruiz et al., 2015). Herein we report, for the first time, that the three UPR signal transducers, IRE1α, PERK, and ATF6 (Hetz and Papa, 2018), and two effector systems downstream the UPR branches, CHOP and XBP1 splicing, are dysregulated in primary SC and OM preadipocytes in IR/T2D obesity with respect to NG obesity, in terms of total protein content and/or phosphorylation rate (i.e., activation). It is noteworthy that changes in these proteins did not always follow the same trends between SC and OM preadipocytes in response to IR/T2D, indicating the existence of depot-specific (mal)adaptative responses to obesity-associated ER stress. Notwithstanding this notion, a feature common to SC and OM preadipocytes was the up-regulation of both the master initiator of the UPR signalling pathway, BiP, and *XBP1s*/*XBP1u* ratio, in IR/T2D obesity. Given the role of BiP in

mediating the targeting of misfolded/unfolded ER proteins for cytosolic degradation via ERAD, and the stimulatory effect of *XBP1s* on the expression of ERAD components (Karagöz et al., 2019), these observations supported that IR/T2D obesity could not only alter the UPR but also the activity of this branch of the quality-control system in the ER (Hwang and Qi, 2018). Interestingly, ERAD is activated when the protein folding capacity of the ER is exceeded (Hwang and Qi, 2018), which seems to be the case for SC and OM preadipocytes of IR/T2D obese individuals according to their enhanced expression levels of ER chaperones as compared to NG obesity. In fact, our studies show, for the first time, that SC and OM preadipocytes from IR/T2D obese individuals, as compared to NG obese individuals, display enhanced levels of proteins participating in all the steps comprising the ERAD, thus suggesting that this pathway is hyperactivated in preadipocytes during the progression to IR/T2D in obese individuals. An increase in the expression of ERAD genes was also observed in SGBS cells overexpressing BiP, further demonstrating the functional link between UPR and ERAD in preadipocytes.

In all, our data on the UPR and ERAD strongly support the notion that metabolic disease in obesity is characterized by the perturbation of ER proteostasis network components in preadipocytes. They also support the link between unresolved ER stress and adipogenesis dysregulation (Longo et al., 2016).

Our gene expression results show that ER stress and the UPR is reduced in SAT of obese subjects after weight loss induced by surgery, as indicated by the downregulation of *XBP1s*/*XBP1u* ratio mRNA levels. These results support the notion that the amelioration of ER stress and related stress signalling pathways in adipose tissue may be an important mechanisms underlying adipocyte re-function (such as adipogenesis), and metabolic improvements after BS (Sun et al., 2019). However, the effect of BS-induced weight loss on ERAD pathway in adipose tissue has not been studied before. It is interesting that despite marked suppression of ER stress and UPR markers in this tissue upon BS-induced weight loss, there was a marked upregulation in the expression levels of key ERAD components (i.e. *HRD1*, *SEL1L*, *UBQLN1*), which is generally considered to be downstream the UPR (Tepedelen and Kirmizibatrak, 2019). These findings, found to be more consistent in those subjects with less persistent obesity (SSO subjects), suggest that the hyperactivation observed in IR/T2D, at least in preadipocytes, is not only no corrected but even seems to be exacerbated after BS. It is plausible to argue that ERAD is regulated through other signals such as oxidative stress (Bagheri-Yarmand et al., 2019), and does not respond to changes in fat mass per se.

Our studies using *in vitro* models mimicking different obesogenic inputs indicate that inflammation, adipocyte hypertrophy and, specially, hyperglycaemia/hyperinsulinemia

(HGHI), as occurs in IR obese individuals, may contribute to alter ER proteostasis in preadipocytes. To be more specific, exposure to hyperglycaemic/hyperinsulinemic conditions represented the most active stimulus inducing ERAD hyperactivation, as well as BiP expression, in SGBS preadipocytes. Intriguingly, HGHI-induced ERAD expression was accompanied by a concomitant decrease in the activity of the cell machinery involved in misfolded/unfolded protein degradation, the proteasome, and the accumulation of ubiquitinated proteins in preadipocytes. These results suggest that the preadipocytes are unable to counteract the proteostatic stress evoked by HGHI-conditions, and proteotoxicity ensues. In agreement with these findings, we have reported the occurrence of proteotoxicity, i.e., decreased activity of the proteasome and accumulation of ubiquitinated proteins, in *in vitro* differentiated preadipocytes and in mature adipocytes isolated from SC and OM fat of diet-induced obese mice as compared to lean animals, as well as in mature adipocytes isolated from IR *vs.* NG obese individuals (Díaz-Ruiz et al., 2015). Unfortunately, the limited amount of human preadipocytes available from adipose tissue biopsy samples, prevented to extend our experiments to primary cell cultures. Notwithstanding these limitations, in all, our studies strongly support the notion that dysregulated ERAD in preadipocytes represents a relevant pathological mechanism linked to the development of metabolic disease in obese individuals. In this line, altered ERAD expression levels in SGBS cells by exposure to HGHI or BiP overexpression were accompanied by changes in adipogenic markers demonstrative of impaired adipocyte differentiation. These effects were reverted by pre-exposure of SGBS cells to the ER stress-reducing agent, TUDCA (Zhang et al., 2018). Together, these findings suggest that TUDCA may represent a potentially useful treatment for preadipocyte damage prevention in obesity, as it has been proposed for this bile acid in other ER stress-related pathologies (Kusaczuk, 2019).

In summary, the results obtained in this section unveil an important role for alternative splicing in SC preadipocyte differentiation thus paving the way for the development of novel therapeutic strategies to modulate adipose tissue expansion. Our studies on altered ER dynamics, that affect not only the UPR but also the ERAD pathway, in SC and OM preadipocytes are in line with our previous results in mature adipocytes (Díaz-Ruiz et al., 2015) and, in all, indicate that the maintenance of ER proteostasis in adipose tissue cells is key to ensure metabolic health in obesity.

2. Study 2: Characterization of miRNAs as markers of dysfunctional adipose tissue in type 2 diabetes (T2D)

Herein, we provide experimental evidence supporting that adipose tissue dysfunction precedes T2D onset and that decreased circulating *miR-223-3p* may represent a potential biomarker for this event. More specifically, low-circulating *miR-223-3p* levels have been associated with compromised adipose tissue insulin sensitivity previously to T2D onset. Furthermore, decreased *miR-223-3p* secretion concomitant with its intracellular accumulation as occurs under inflammatory conditions, has pathological effects on both preadipocyte and adipocyte physiology which may have further consequences on systemic metabolic homeostasis.

We and others have previously reported an association between plasma levels of various miRNA and T2D incidence (Jiménez-Lucena et al., 2018; Liu et al., 2014; Zampetaki et al., 2010; T. Zhang et al., 2013). However, despite the increasing number of studies reporting circulating miRNAs as metabolic biomarkers, the cause and physiological consequences of the alterations in these circulating miRNAs have been poorly explored. This knowledge might be of relevance to elucidate the underlying mechanisms of T2D development and to establish novel therapeutic strategies. In this scenario, adipose tissue is especially relevant due to its role as a major contributor of circulating miRNAs, as stated by foregoing reports (Heneghan et al., 2011; N. H. Kim et al., 2019; Thomou et al., 2017), and as a regulator of whole body metabolic homeostasis (Gentile et al., 2019; Landrier et al., 2019). In this line, we specifically found that low circulating *miR-223-3p* levels, previously associated with T2D incidence (Jiménez-Lucena et al., 2018), are related to impaired adipose tissue insulin sensitivity, placing circulating *miR-223-3p* as a potential biomarker for adipose tissue functionality.

Concordant with this hypothesis, our *in vitro* analyses revealed that adipocytes secrete *miR-223-3p*, especially at early stages of differentiation, while an inflammatory stimulus hampering insulin signalling, i.e., TNFα, prevented adipocyte *miR-223-3p* secretion, likely due to the dysregulation of general miRNA processing and exosome production. This is noteworthy since inflammation is a hallmark of dysfunctional adipose tissue that has been widely proposed as a central mechanism leading to metabolic disturbances (Clemente-Postigo et al., 2019; Ghaben and Scherer, 2019). Notably, inflammation was triggered and insulin signalling cascade altered in adipocytes upon exposure to baseline sera collected from the patients who were going to develop T2D in

the next 5-years. In view of these results, it is tempting to speculate that, unlike patients who did not developed T2D, a pro-inflammatory environment present before the establishment of T2D, would favour adipose tissue insulin resistance and would impair *miR-223-3p* secretion. This is in accordance to previous reports supporting that adipose tissue dysregulation may precede the development of metabolic complications (Korf and van der Merwe, 2017). Therefore, low circulating *miR-223-3p* levels, may not only represent a marker for T2D onset as previously reported (Jiménez-Lucena et al., 2018), but also for adipose tissue insulin resistance. In addition, our results raised the question as to whether an inflamed adipose tissue with diminished *miR-223-3p* secretion capacity might contribute to the decreased levels of circulating *miR-223-3p*. Taking into consideration the ubiquitous expression of this miRNA, the possible contribution of metabolic organs other than the adipose tissue to the circulating *miR-223-3p* pool should be also assessed in future studies. Likewise, other miRNAs, among other factors produced by the adipose tissue, might be involved in the metabolic dysregulation preceding T2D onset. Previous studies showed a correspondence between the adipose tissue expression of specific miRNAs and their circulating levels (N. H. Kim et al., 2019) but the relationship of these miRNAs and the functional state of adipose tissue was not explored. Apart from the pathogenic alteration of *miR-223-3p* secretion, the differences found in *miR-223-3p* dynamics in relation to adipocyte differentiation stage suggest that this miRNA may play distinct roles in preadipocytes and adipocytes. These differences might have physiological relevance and concur with the previously described distinct secretory profile, including extracellular vesicles, of preadipocytes and adipocytes (Sarantopoulos et al., 2018), as it has been confirmed in the present study.

Interestingly, intracellular *miR-223-3p* accumulation in adipocytes, rather than diminished *miR-223-3p* expression, accounted for the impaired *miR-223-3p* secretion by these cells during adipogenesis and in response to inflammation-induced insulin resistance. Although adipocyte *miR-223-3p* secretion has not been previously analysed, several studies have explored intracellular *miR-223-3p* expression in adipocytes and adipose tissue. In agreement with our results, an increase in *miR-223-3p* expression during adipogenesis (Qin et al., 2019) and after TNF-α treatment in adipocytes (Chuang et al., 2015) has been reported. Furthermore, higher adipose tissue *miR-223*-3p expression in insulin resistant obese patients compared to either lean or non-insulin resistant obese subjects (Deiuliis et al., 2016) and a decrease after bariatric surgery (Macartney-Coxson et al., 2020) were described, supporting the notion of *miR-223-3p* retention in adipose cells during metabolic dysregulation.

Previous studies found that stromal vascular fraction (SVF), rather than mature adipocytes, accounted for most *miR-223-3p* expression in obese visceral adipose tissue (Deiuliis et al., 2016). Taking this and the anti-inflammatory function attributed to this miRNA into consideration, a role for *miR-223-3p* in macrophages and adipose tissue inflammation has been proposed (Mori et al., 2019). In line with previous studies, herein we observed that, similar to that found in preadipocytes and adipocytes, THP-1 macrophages release *miR-223-3p*, suggesting that adipose macrophages might also contribute to the circulating *miR-223-3p* pool. Nevertheless, TNFα exposure did not affect *miR-223-3p* secretion but increased its accumulation inside these cells, further supporting the previously proposed role for this miRNA in inflammation-related processes (G. D. Kim et al., 2019). By contrast, the consequences of *miR-223-3p* dysregulation on adipocyte differentiation and function have been scarcely explored. However, previous findings (Qin et al., 2019) and our results suggest a relevant regulatory role of this miRNA on adipose tissue physiology beyond the already reported role in modulating adipose tissue immunity (Mori et al., 2019). Therefore, we also aimed at carrying out a comprehensive analysis of the effect of intracellular *miR-223-3p* accumulation on preadipocyte and adipocyte function, by overexpressing *miR-223-3p*.

We experimentally demonstrated that *miR-223-3p* overexpression impaired the expression and activation of insulin signalling mediators at both early and late stages of adipocyte differentiation. Nonetheless, the consequences of insulin signalling disruption, determined by glucose uptake and GLUT4 translocation, differed depending on the differentiation stage. Early adipocytes exhibited constitutive insulin-independent glucose uptake and GLUT4 translocation to the plasma membrane. This could be construed as a compensatory mechanism mediated by the upregulation of the GLUT4 recycling marker, ARF6, to fulfil the concomitant diminished GLUT4 protein content. In keeping with this, increased insulin-independent glucose uptake has been previously associated with decreased insulin responsiveness in adipose cells (Lee and Pratley, 2005). In accordance to previous reports (Chuang et al., 2015), this contrasts the reduced glucose uptake, either basal or insulin-stimulated, by late adipocytes upon *miR-223-3p* overexpression. Our results indicate that this phenomenon is likely due to impaired insulin signalling and reduced presence of GLUT4 at the plasma membrane, which is in line with the reduced glucose uptake seen in adipose tissue from diabetic humans (Ferrannini et al., 2018). The apparent contradictory findings relative to adipocyte differentiation stage could be accounted for by the demonstrated increase in insulin-independent glucose uptake at earlier stages of adipogenesis, that declines during

adipogenic differentiation (Hauner et al., 1998). This suggests that, despite the fact that GLUT4 is a validated *miR-223-3p* target gene, cell type-specific *miR-223-3p* regulatory networks can be triggered with disparate effects on GLUT4 expression and activity.

Importantly, proper adipocyte lipid storage into LDs is crucial for maintaining metabolic homeostasis, and defects on adipose tissue lipogenesis have been related to metabolic disorders (Ghaben and Scherer, 2019). Thus, we also examined the effect of *miR-223-3p* on lipid metabolism, finding a reduction in both the expression of markers of adipogenesis and lipogenesis and LD biogenesis and growth in early adipocytes, which was consistent with their reduced number of LDs. This suggests that early *miR-223-3p* overexpression during adipogenesis may prevent adipocyte differentiation due to an impaired capacity of these cells for accumulating lipids, which represents a hallmark of adipose tissue-associated metabolic disorders (Oliva-Olivera et al., 2017). LD size was reduced by *miR-223-3p* overexpression in late differentiated adipocytes. These changes were concomitant to an increased lipolytic rate regardless of the differentiation stage. Both adipose tissue inability to store lipids and increased lipolysis are associated with ectopic lipid storage and lipotoxic effects on other metabolic tissues and are considered risk factors for insulin resistance and T2D (Guilherme et al., 2008). Whether the effects of *miR-223-3p* on lipid turnover are directly mediated or secondary to the effects on GLUT4 translocation and glucose uptake, required for *de novo* lipogenesis, remains to be clarified.

Moreover, here, we have demonstrated that the changes in the circulating milieu after weight-loss induced by BS modulate *miR-223-3p* secretion and/or expression by adipocytes. We have observed that Post-BS serum, containing lower levels of inflammatory mediators (i.e., C-reactive protein), reduce *miR-223-3p* content in adipocytes, likely due to an increase in its secretion. These results are in line with the our and other's reported effect of inflammatory markers (i.e., TNFα) on *miR-223-3p* secretion and content in these cells (Chuang et al., 2015), and *miR-223-3p* down-regulation in SAT after BS (Macartney-Coxson et al., 2020). The relevance of these observations was further supported by our functional studies of glucose uptake induced by insulin in the adipocytes exposed to Pre- and Post-BS serum. Post-BS serum also improved the insulin-stimulated glucose uptake in adipocytes in comparison with those exposed to Pre-BS serum. This improvement has been also observed in SAT, where pre-surgery, insulin-stimulated SAT glucose uptake was impaired and increased significantly post-surgery (Dadson et al., 2016). This could be related to a better insulin signalling and a better recycling of GLUT4 in the basal state (Varela-Rodríguez et al.,

2020). Accordingly, GLUT4 (*miR-223-3p* target gene) is upregulated in SAT after BS (Albers et al., 2015). These findings further support the notion that inflammatory mediators present in either the serum or locally in the adipose tissue may be responsible for the alterations in *miR-223-3p* regulation.

To sum up, our *in vitro* analyses have shown for the first time that *miR-223-3p* has an effect not only on GLUT4 protein expression in differentiated adipocytes (Chuang et al., 2015), but also globally affects early and late adipocyte physiology by altering both glucose and lipid metabolism. Our results suggest that pathogenic intracellular *miR-223-3p* accumulation impairs adipogenesis and energy storage in differentiated adipocytes. This could have detrimental consequences for metabolic health, as it has been proposed that it is the adipose tissue expandability, rather than adipose tissue size, which led to adipose tissue dysfunction (Ghaben and Scherer, 2019). This hypothesis explains the existence of lean diabetic patients and the so-called metabolically healthy obese subjects. Within the context of our cohort study, this could explain why some individuals developed T2D whereas others remained healthy after a median follow-up of 60 months.

In conclusion, we have undertaken a comprehensive study of the relationship between circulating and adipose tissue *miR-223-3p* in the context of T2D predisposition. Our results indicate that adipose tissue insulin resistance may precede T2D development. Within this context, we identified that adipocyte *miR-223-3p* release was prevented under pathological conditions (i.e., inflammation), which might contribute to the lower circulating *miR-223-3p* levels observed in patients who are going to develop T2D. These results are in line with the previously proposed notion of adipose tissue as an important source of circulating miRNAs and pave the way to future studies on miRNAs release from this organ in the field of metabolic diseases. We also reported that the resulting pathological accumulation of *miR-223-3p* in preadipocytes and adipocytes under inflammatory conditions compromises cellular function. *miR-223-3p* overexpression not only inhibited GLUT4 and insulin-stimulated glucose uptake in these cells, but also led to impaired insulin signalling, GLUT4 trafficking, and lipid metabolism. Considering the major role of adipocyte dysfunction in the development of multiple metabolic diseases, these results unveil adipose *miR-223-3p* as a relevant player in tissue dysfunction and consequently, in the associated establishment of T2D. Altogether, our results provide novel molecular and cellular cues underlying the development of metabolic disturbances that may be helpful to design novel therapeutic strategies to prevent T2D.

Taken into account both studies developed in the present Doctoral Thesis, we can conclude that impaired splicing and disturbed ER proteostasis are components of the pathogenic molecular fingerprint of preadipocytes that could be targeted to prevent and/or improve adipose tissue dysfunction in obesity and its related metabolic disorders, and that *miR-223-3p* may have a role as a potential predictor of adipose dysfunction related to T2D development thus unveiling a novel molecular target that may be helpful to design novel therapeutic strategies to prevent T2D.

CONCLUSIONS

The results presented in this Doctoral Thesis constitute novel and valuable information supporting the existence of pathological mechanisms in the adipose tissue associated with the onset, development, and remission of metabolic diseases such insulin resistance (IR) and type 2 diabetes (T2D). The main conclusions associated to each objective included in the Thesis are described below:

1. Study 1: Identification of pathogenic markers of metabolic disease in preadipocytes of obese individuals

1. Down-regulation of several components of the splicing machinery is a hallmark of subcutaneous (SC) preadipocytes that likely contributes to the development of metabolic disturbances in obese individuals.
2. The spliceosome component, *PRFP8*/PRP8, modulates the splicing profile of important factors involved in adipogenesis and lipid droplet biogenesis, and it is required for proper adipogenesis.
3. The ER proteostasis system, including ER stress-related UPR and ERAD, is disturbed in SC and omental (OM) preadipocytes from IR/T2D obese individuals. This unbalance may be associated with SC/OM preadipocyte dysfunction and the development of metabolic diseases.
4. Adipogenesis is impaired upon ERAD hyperactivation, which may be triggered by the hyperglicemic/hyperinsulinemic environment in IR/T2D obesity.

2. Study 2: Characterization of miRNAs as markers of dysfunctional adipose tissue in type 2 diabetes (T2D)

1. Dysregulated circulating *miR-223-3p* levels in patients who develop T2D compared to those who do not develop T2D are related to adipose tissue dysfunction preceding T2D instauration.
2. *miR-223-3p* secretion by preadipocytes and adipocytes is prevented under inflammatory conditions, which may contribute to the alteration of its circulating levels observed in patients who are going to develop T2D.
3. *miR-223-3p* pathological accumulation in preadipocytes and adipocytes compromises their cellular function in terms of both glucose and lipid metabolism. This effect may have further consequences at systemic level.

REFERENCES

Acosta-Alvear D, Karagöz GE, Fröhlich F, Li H, Walther TC, Walter P. 2018. The unfolded protein response and endoplasmic reticulum protein targeting machineries converge on the stress sensor IRE1. *eLife* **7**:e43036. doi:10.7554/eLife.43036

ADA. 2020. 2. Classification and Diagnosis of Diabetes: Standards of Medical Care in Diabetes—2020. *Diabetes Care* **43**:S14 LP-S31. doi:10.2337/dc20-S002

Adams TD, Davidson LE, Litwin SE, Kim J, Kolotkin RL, Nanjee MN, Gutierrez JM, Frogley SJ, Ibele AR, Brinton EA, Hopkins PN, McKinlay R, Simper SC, Hunt SC. 2017. Weight and Metabolic Outcomes 12 Years after Gastric Bypass. *New England Journal of Medicine* **377**:1143–1155. doi:10.1056/NEJMoa1700459

Agarwal V, Bell GW, Nam JW, Bartel DP. 2015. Predicting effective microRNA target sites in mammalian mRNAs. *eLife* **4**:1–38. doi:10.7554/eLife.05005

Aghamohammadzadeh R, Greenstein AS, Yadav R, Jeziorska M, Hama S, Soltani F, Pemberton PW, Ammori B, Malik RA, Soran H, Heagerty AM. 2013. Effects of bariatric surgery on human small artery function: evidence for reduction in perivascular adipocyte inflammation, and the restoration of normal anticontractile activity despite persistent obesity. *Journal of the American College of Cardiology* **62**:128–135. doi:10.1016/j.jacc.2013.04.027

Akaike H. 1974. A new look at the statistical model identification. *IEEE Transactions on Automatic Control* **19**:716–723. doi:10.1109/TAC.1974.1100705

Åkra S, Aksnes TA, Flaa A, Eggesbø HB, Opstad TB, Njerve IU, Seljeflot I. 2020. Markers of remodeling in subcutaneous adipose tissue are strongly associated with overweight and insulin sensitivity in healthy non-obese men. *Scientific Reports* **10**:14055. doi:10.1038/s41598-020-71109-4

Alarcón CR, Lee H, Goodarzi H, Halberg N, Tavazoie SF. 2015. N6-methyladenosine marks primary microRNAs for processing. *Nature* **519**:482–485. doi:10.1038/nature14281

Albers PH, Bojsen-Møller KN, Dirksen C, Serup AK, Kristensen DE, Frystyk J, Clausen TR, Kiens B, Richter EA, Madsbad S, Wojtaszewski JFP. 2015. Enhanced insulin signaling in human skeletal muscle and adipose tissue following gastric bypass surgery. *American Journal of Physiology-Regulatory, Integrative and Comparative Physiology* **309**:R510–R524. doi:10.1152/ajpregu.00228.2014

Alcalá M, Calderon-Dominguez M, Bustos E, Ramos P, Casals N, Serra D, Viana M, Herrero L. 2017. Increased inflammation, oxidative stress and mitochondrial respiration in brown adipose tissue from obese mice. *Scientific Reports* **7**:16082. doi:10.1038/s41598-017-16463-6

Amen OM, Sarker SD, Ghildyal R, Arya A. 2019. Endoplasmic Reticulum Stress Activates Unfolded Protein Response Signaling and Mediates Inflammation,

Obesity, and Cardiac Dysfunction: Therapeutic and Molecular Approach . *Frontiers in Pharmacology* .

Ameres SL, Zamore PD. 2013. Diversifying microRNA sequence and function. *Nature Reviews Molecular Cell Biology* **14**:475–488. doi:10.1038/nrm3611

Andersen CL, Jensen JL, Ørntoft TF. 2004. Normalization of real-time quantitative reverse transcription-PCR data: A model-based variance estimation approach to identify genes suited for normalization, applied to bladder and colon cancer data sets. *Cancer Research* **64**:5245–5250. doi:10.1158/0008-5472.CAN-04-0496

Andersen DC, Jensen CH, Schneider M, Nossent AY, Eskildsen T, Hansen JL, Teisner B, Sheikh SP. 2010. MicroRNA-15a fine-tunes the level of Delta-like 1 homolog (DLK1) in proliferating 3T3-L1 preadipocytes. *Experimental Cell Research* **316**:1681–1691. doi:10.1016/j.yexcr.2010.04.002

Andersson DP, Eriksson Hogling D, Thorell A, Toft E, Qvisth V, Näslund E, Thörne A, Wirén M, Löfgren P, Hoffstedt J, Dahlman I, Mejhert N, Rydén M, Arner E, Arner P. 2014. Changes in Subcutaneous Fat Cell Volume and Insulin Sensitivity After Weight Loss. *Diabetes Care* **37**:1831 LP – 1836. doi:10.2337/dc13-2395

Aouida M, Eid A, Mahfouz MM. 2016. CRISPR/Cas9-mediated target validation of the splicing inhibitor Pladienolide B. *Biochimie open* **3**:72–75. doi:10.1016/j.biopen.2016.02.001

Aprile M, Ambrosio MR, D'Esposito V, Beguinot F, Formisano P, Costa V, Ciccodicola A. 2014. PPARG in human adipogenesis: Differential contribution of canonical transcripts and dominant negative isoforms. *PPAR Research* **2014**:18–20. doi:10.1155/2014/537865

Aprile M, Cataldi S, Ambrosio MR, D'Esposito V, Lim K, Dietrich A, Blüher M, Savage DB, Formisano P, Ciccodicola A, Costa V. 2018. PPARγΔ5, a Naturally Occurring Dominant-Negative Splice Isoform, Impairs PPARγ Function and Adipocyte Differentiation. *Cell Reports* **25**:1577-1592.e6. doi:10.1016/j.celrep.2018.10.035

Arias de la Rosa I, Escudero-Contreras A, Rodríguez-Cuenca S, Ruiz-Ponce M, Jiménez-Gómez Y, Ruiz-Limón P, Pérez-Sánchez C, Ábalos-Aguilera MC, Cecchi I, Ortega R, Calvo J, Guzmán-Ruiz R, Malagón MM, Collantes-Estevez E, Vidal-Puig A, López-Pedrera C, Barbarroja N. 2018. Defective glucose and lipid metabolism in rheumatoid arthritis is determined by chronic inflammation in metabolic tissues. *Journal of Internal Medicine* **284**:61–77. doi:10.1111/joim.12743

Arroyo JD, Chevillet JR, Kroh EM, Ruf IK, Pritchard CC, Gibson DF, Mitchell PS, Bennett CF, Pogosova-Agadjanyan EL, Stirewalt DL, Tait JF, Tewari M. 2011. Argonaute2 complexes carry a population of circulating microRNAs independent of vesicles in human plasma. *Proceedings of the National Academy of Sciences of the United*

States of America **108**:5003–5008. doi:10.1073/pnas.1019055108

Ayala-Sumuano J-T, Velez-delValle C, Beltrán-Langarica A, Marsch-Moreno M, Cerbón-Solorzano J, Kuri-Harcuch W. 2011. Srebf1a is a key regulator of transcriptional control for adipogenesis. *Scientific Reports* **1**:178. doi:10.1038/srep00178

Bagheri-Yarmand R, Sinha KM, Li L, Lu Y, Cote GJ, Sherman SI, Gagel RF. 2019. Combinations of Tyrosine Kinase Inhibitor and ERAD Inhibitor Promote Oxidative Stress-Induced Apoptosis through ATF4 and KLF9 in Medullary Thyroid Cancer. *Molecular cancer research : MCR* **17**:751–760. doi:10.1158/1541-7786.MCR-18-0354

Baglioni S, Cantini G, Poli G, Francalanci M, Squecco R, Di Franco A, Borgogni E, Frontera S, Nesi G, Liotta F, Lucchese M, Perigli G, Francini F, Forti G, Serio M, Luconi M. 2012. Functional Differences in Visceral and Subcutaneous Fat Pads Originate from Differences in the Adipose Stem Cell. *PLOS ONE* **7**:e36569.

Baldridge RD, Rapoport TA. 2016. Autoubiquitination of the Hrd1 Ligase Triggers Protein Retrotranslocation in ERAD. *Cell* **166**:394–407. doi:10.1016/j.cell.2016.05.048

Bard JAM, Goodall EA, Greene ER, Jonsson E, Dong KC, Martin A. 2018. Structure and Function of the 26S Proteasome. *Annual Review of Biochemistry* **87**:697–724. doi:10.1146/annurev-biochem-062917-011931

Bates DO, Morris JC, Oltean S, Donaldson LF. 2017. Pharmacology of Modulators of Alternative Splicing. *Pharmacological reviews* **69**:63–79. doi:10.1124/pr.115.011239

Bayraktar R, Van Roosbroeck K, Calin GA. 2017. Cell-to-cell communication: microRNAs as hormones. *Molecular oncology* **11**:1673–1686. doi:10.1002/1878-0261.12144

Belligoli A, Compagnin C, Sanna M, Favaretto F, Fabris R, Busetto L, Foletto M, Dal Prà C, Serra R, Prevedello L, Da Re C, Bardini R, Mescoli C, Rugge M, Fioretto P, Conci S, Bettini S, Milan G, Vettor R. 2019. Characterization of subcutaneous and omental adipose tissue in patients with obesity and with different degrees of glucose impairment. *Scientific reports* **9**:11333. doi:10.1038/s41598-019-47719-y

Benjamini, Yoav ; Hochberg Y. 1995. Controlling the False Discovery Rate - a Practical and Powerful Approach to Multiple Testing. Journal of the Royal Statistical Society Series B-Methodological 1995.pdf. *Journal of the Royal Statistical Society Series B (Methological)* **57**:289–300. doi:10.2307/2346101

Betel D, Koppal A, Agius P, Sander C, Leslie C. 2010. Comprehensive modeling of microRNA targets predicts functional non-conserved and non-canonical sites. *Genome Biology* **11**:R90. doi:10.1186/gb-2010-11-8-r90

Bhattacharyya S, Yu H, Mim C, Matouschek A. 2014. Regulated protein turnover:

snapshots of the proteasome in action. *Nature reviews Molecular cell biology* **15**:122–133. doi:10.1038/nrm3741

Bialesova L, Kulyté A, Petrus P, Sinha I, Laurencikiene J, Zhao C, Wright KD, Arner P, Dahlman I. 2017. Epigenetic Regulation of PLIN 1 in Obese Women and its Relation to Lipolysis. *Scientific Reports* **7**:1–11. doi:10.1038/s41598-017-09232-y

Bjørndal B, Burri L, Staalesen V, Skorve J, Berge RK. 2011. Different adipose depots: their role in the development of metabolic syndrome and mitochondrial response to hypolipidemic agents. *Journal of obesity* **2011**:490650. doi:10.1155/2011/490650

Blanco-Rojo R, Alcala-Diaz JF, Wopereis S, Perez-Martinez P, Quintana-Navarro GM, Marin C, Ordovas JM, van Ommen B, Perez-Jimenez F, Delgado-Lista J, Lopez-Miranda J. 2016. The insulin resistance phenotype (muscle or liver) interacts with the type of diet to determine changes in disposition index after 2 years of intervention: the CORDIOPREV-DIAB randomised clinical trial. *Diabetologia* **59**:67–76. doi:10.1007/s00125-015-3776-4

Bléher M, Meshko B, Gergondey R, Kovacs Y, Duprez D, L'Honoré A, Havis E. 2020. Egr1 loss-of-function promotes beige adipocyte differentiation and activation specifically in inguinal subcutaneous white adipose tissue. *Scientific Reports* **10**. doi:10.1101/2020.06.03.131342

Blüher M. 2016. Adipose tissue inflammation: A cause or consequence of obesity-related insulin resistance? *Clinical Science* **130**. doi:10.1042/CS20160005

Blüher M. 2013. Adipose tissue dysfunction contributes to obesity related metabolic diseases. *Best Practice and Research: Clinical Endocrinology and Metabolism* **27**:163–177. doi:10.1016/j.beem.2013.02.005

Bódis K, Roden M. 2018. Energy metabolism of white adipose tissue and insulin resistance in humans. *European Journal of Clinical Investigation* **48**:e13017. doi:https://doi.org/10.1111/eci.13017

Bogan JS. 2012. Regulation of Glucose Transporter Translocation in Health and Diabetes. *Annual Review of Biochemistry* **81**:507–532. doi:10.1146/annurev-biochem-060109-094246

Bogan JS, McKee AE, Lodish HF. 2001. Insulin-Responsive Compartments Containing GLUT4 in 3T3-L1 and CHO Cells: Regulation by Amino Acid Concentrations. *Molecular and Cellular Biology* **21**:4785–4806. doi:10.1128/mcb.21.14.4785-4806.2001

Botchlett R, Woo S-L, Liu M, Pei Y, Guo X, Li H, Wu C. 2017. Nutritional approaches for managing obesity-associated metabolic diseases. *The Journal of endocrinology* **233**:R145–R171. doi:10.1530/JOE-16-0580

Bradford MM. 1976. A Rapid and Sensitive Method for the Quantitation of Microgram

Quantities of Protein Utilizing the Principle of Protein-Dye Binding. *Analytical Biochemistry* **72**:248–254.

Brasaemle DL, Wolins NE. 2012. Packaging of fat: An evolving model of lipid droplet assembly and expansion. *Journal of Biological Chemistry* **287**:2273–2279. doi:10.1074/jbc.R111.309088

Bravo R, Parra V, Gatica D, Rodriguez AE, Torrealba N, Paredes F, Wang Z V, Zorzano A, Hill JA, Jaimovich E, Quest AFG, Lavandero S. 2013. Endoplasmic reticulum and the unfolded protein response: dynamics and metabolic integration. *International review of cell and molecular biology* **301**:215–290. doi:10.1016/B978-0-12-407704-1.00005-1

Brewer PD, Habtemichael EN, Romenskaia I, Mastick CC, Coster ACF. 2016. Glut4 is sorted from a Rab10 GTPase-independent constitutive recycling pathway into a highly insulinresponsive Rab10 GTPase-dependent sequestration pathway after adipocyte differentiation. *Journal of Biological Chemistry* **291**:773–789. doi:10.1074/jbc.M115.694919

Brovkina O, Nikitin A, Khodyrev D, Shestakova E, Sklyanik I, Panevina A, Stafeev I, Menshikov M, Kobelyatskaya A, Yurasov A, Fedenko V, Yashkov Y, Shestakova M. 2019. Role of MicroRNAs in the Regulation of Subcutaneous White Adipose Tissue in Individuals With Obesity and Without Type 2 Diabetes . *Frontiers in Endocrinology* .

Bryant NJ, Gould GW. 2011. SNARE Proteins Underpin Insulin-Regulated GLUT4 Traffic. *Traffic* **12**:657–664. doi:10.1111/j.1600-0854.2011.01163.x

Buchwald H, Oien DM. 2013. Metabolic/Bariatric Surgery Worldwide 2011. *Obesity Surgery* **23**:427–436. doi:10.1007/s11695-012-0864-0

Cao SS, Kaufman RJ. 2014. Endoplasmic reticulum stress and oxidative stress in cell fate decision and human disease. *Antioxidants & redox signaling* **21**:396–413. doi:10.1089/ars.2014.5851

Carvalho FG De, Sparks LM. 2019. Targeting White Adipose Tissue with Exercise or Bariatric Surgery as Therapeutic Strategies in Obesity. *Biology* **8**:16. doi:10.3390/biology8010016

Castro-Magdonel BE, Orjuela M, Alvarez-Suarez DE, Camacho J, Cabrera-Muñoz L, Sadowinski-Pine S, Medina-Sanson A, Lara-Molina C, García-Vega D, Vázquez Y, Durán-Figueroa N, Orozco-Romero M de J, Hernández-Ángeles A, Ponce-Castañeda MV. 2020. Circulating miRNome detection analysis reveals 537 miRNAS in plasma, 625 in extracellular vesicles and a discriminant plasma signature of 19 miRNAs in children with retinoblastoma from which 14 are also detected in corresponding primary tumors. *PLOS ONE* **15**:e0231394.

Castro JP, Tilma G, Bodo S. 2016. The two faces of reactive oxygen species (ROS) in adipocyte function and dysfunction. *Biological Chemistry*. doi:10.1515/hsz-2015-0305

Catalán V, Gómez-Ambrosi J, Rotellar F, Silva C, Rodríguez A, Salvador J, Gil MJ, Cienfuegos JA, Frühbeck G. 2007. Validation of endogenous control genes in human adipose tissue: Relevance to obesity and obesity-associated type 2 diabetes mellitus. *Hormone and Metabolic Research* **39**:495–500. doi:10.1055/s-2007-982502

Catanzaro G, Filardi T, Sabato C, Vacca A, Migliaccio S, Morano S, Ferretti E. 2020. Tissue and circulating microRNAs as biomarkers of response to obesity treatment strategies. *Journal of Endocrinological Investigation*. doi:10.1007/s40618-020-01453-9

Catrysse L, van Loo G. 2018. Adipose tissue macrophages and their polarization in health and obesity. *Cellular Immunology* **330**:114–119. doi:https://doi.org/10.1016/j.cellimm.2018.03.001

Chen F-J, Yin Y, Chua BT, Li P. 2020. CIDE family proteins control lipid homeostasis and the development of metabolic diseases. *Traffic* **21**:94–105. doi:https://doi.org/10.1111/tra.12717

Chen W, Chang B, Saha P, Hartig SM, Li L, Reddy VT, Yang Y, Yechoor V, Mancini MA, Chan L. 2012. Berardinelli-seip congenital lipodystrophy 2/seipin is a cell-autonomous regulator of lipolysis essential for adipocyte differentiation. *Molecular and cellular biology* **32**:1099–1111. doi:10.1128/MCB.06465-11

Chen X-W, Leto D, Xiao J, Goss J, Wang Q, Shavit JA, Xiong T, Yu G, Ginsburg D, Toomre D, Xu Z, Saltiel AR. 2011. Exocyst function is regulated by effector phosphorylation. *Nature cell biology* **13**:580–588. doi:10.1038/ncb2226

Chen X, Liang H, Zhang J, Zen K, Zhang C-Y. 2012. Secreted microRNAs: a new form of intercellular communication. *Trends in Cell Biology* **22**:125–132. doi:https://doi.org/10.1016/j.tcb.2011.12.001

Chong J, Yamamoto M, Xia J. 2019. MetaboAnalystR 2.0: From raw spectra to biological insights. *Metabolites* **9**. doi:10.3390/metabo9030057

Chooi YC, Ding C, Magkos F. 2019. The epidemiology of obesity. *Metabolism: Clinical and Experimental* **92**:6–10. doi:10.1016/j.metabol.2018.09.005

Chou CH, Shrestha S, Yang CD, Chang NW, Lin YL, Liao KW, Huang WC, Sun TH, Tu SJ, Lee WH, Chiew MY, Tai CS, Wei TY, Tsai TR, Huang HT, Wang CY, Wu HY, Ho SY, Chen PR, Chuang CH, Hsieh PJ, Wu YS, Chen WL, Li MJ, Wu YC, Huang XY, Ng FL, Buddhakosai W, Huang PC, Lan KC, Huang CY, Weng SL, Cheng YN, Liang C, Hsu WL, Huang H Da. 2018. MiRTarBase update 2018: A resource for

experimentally validated microRNA-target interactions. *Nucleic Acids Research* **46**:D296–D302. doi:10.1093/nar/gkx1067

Choudhary V, Ojha N, Golden A, Prinz WA. 2015. A conserved family of proteins facilitates nascent lipid droplet budding from the ER. *The Journal of cell biology* **211**:261–271. doi:10.1083/jcb.201505067

Christianson JC, Olzmann JA, Shaler TA, Sowa ME, Bennett EJ, Richter CM, Tyler RE, Greenblatt EJ, Harper JW, Kopito RR. 2011. Defining human ERAD networks through an integrative mapping strategy. *Nature cell biology* **14**:93–105. doi:10.1038/ncb2383

Christianson JC, Ye Y. 2014. Cleaning up in the endoplasmic reticulum: Ubiquitin in charge. *Nature Structural and Molecular Biology* **21**:325–335. doi:10.1038/nsmb.2793

Chuang T-Y, Wu H-L, Chen C-C, Gamboa GM, Layman LC, Diamond MP, Azziz R, Chen Y-H. 2015. MicroRNA-223 Expression is Upregulated in Insulin Resistant Human Adipose Tissue. *Journal of diabetes research* **2015**:943659. doi:10.1155/2015/943659

Church CD, Horowitz MC, Rodeheffer MS. 2012. WAT is a functional adipocyte ? © 2012 Landes Bioscience . Do not distribute . © 2012 Landes Bioscience . **1**:38–45.

Cignarelli A, Genchi VA, Perrini S, Natalicchio A, Laviola L, Giorgino F. 2019. Insulin and insulin receptors in adipose tissue development. *International Journal of Molecular Sciences* **20**:1–20. doi:10.3390/ijms20030759

Cisa-Wieczorek S, Hernández-Alvarez MI. 2020. Deregulation of Lipid Homeostasis: A Fa(c)t in the Development of Metabolic Diseases. *Cells* **9**:2605. doi:10.3390/cells9122605

Clemente-Postigo M, Oliva-Olivera W, Coin-Aragüez L, Ramos-Molina B, Giraldez-Perez RM, Lhamyani S, Alcaide-Torres J, Perez-Martinez P, El Bekay R, Cardona F, Tinahone FJ. 2019. Metabolic endotoxemia promotes adipose dysfunction and inflammation in human obesity. *American Journal of Physiology - Endocrinology and Metabolism* **316**:E319–E332. doi:10.1152/ajpendo.00277.2018

Cnop M, Foufelle F, Velloso LA. 2012. Endoplasmic reticulum stress, obesity and diabetes. *Trends in Molecular Medicine* **18**:59–68. doi:10.1016/j.molmed.2011.07.010

Coats BR, Schoenfelt KQ, Barbosa-Lorenzi VC, Peris E, Cui C, Hoffman A, Zhou G, Fernandez S, Zhai L, Hall BA, Haka AS, Shah AM, Reardon CA, Brady MJ, Rhodes CJ, Maxfield FR, Becker L. 2017. Metabolically Activated Adipose Tissue Macrophages Perform Detrimental and Beneficial Functions during Diet-Induced Obesity. *Cell Reports* **20**:3149–3161.

doi:https://doi.org/10.1016/j.celrep.2017.08.096

Coelho M, Oliveira T, Fernandes R. 2013. Biochemistry of adipose tissue: An endocrine organ. *Archives of Medical Science* **9**:191–200. doi:10.5114/aoms.2013.33181

Collins GA, Goldberg AL. 2017. The Logic of the 26S Proteasome. *Cell* **169**:792–806. doi:10.1016/j.cell.2017.04.023

Collins KH, Herzog W, MacDonald GZ, Reimer RA, Rios JL, Smith IC, Zernicke RF, Hart DA. 2018. Obesity, Metabolic Syndrome, and Musculoskeletal Disease: Common Inflammatory Pathways Suggest a Central Role for Loss of Muscle Integrity . *Frontiers in Physiology* .

Condrat CE, Thompson DC, Barbu MG, Bugnar OL, Boboc A, Cretoiu D, Suciu N, Cretoiu SM, Voinea SC. 2020. miRNAs as Biomarkers in Disease: Latest Findings Regarding Their Role in Diagnosis and Prognosis. *Cells* **9**:276. doi:10.3390/cells9020276

Corrêa LH, Heyn GS, Magalhaes KG. 2019. The Impact of the Adipose Organ Plasticity on Inflammation and Cancer Progression. *Cells* **8**:662. doi:10.3390/cells8070662

Cotillard A, Poitou C, Torcivia A, Bouillot J-L, Dietrich A, Klöting N, Grégoire C, Lolmede K, Blüher M, Clément K. 2014. Adipocyte Size Threshold Matters: Link with Risk of Type 2 Diabetes and Improved Insulin Resistance After Gastric Bypass. *The Journal of Clinical Endocrinology & Metabolism* **99**:E1466–E1470. doi:10.1210/jc.2014-1074

Cretu C, Agrawal AA, Cook A, Will CL, Fekkes P, Smith PG, Lührmann R, Larsen N, Buonamici S, Pena V. 2018. Structural Basis of Splicing Modulation by Antitumor Macrolide Compounds. *Molecular Cell* **70**:265-273.e8. doi:10.1016/j.molcel.2018.03.011

Creugny A, Fender A, Pfeffer S. 2018. Regulation of primary microRNA processing. *FEBS Letters* **592**:1980–1996. doi:10.1002/1873-3468.13067

Crewe C, An YA, Scherer PE. 2017. The ominous triad of adipose tissue dysfunction: Inflammation, fibrosis, and impaired angiogenesis. *Journal of Clinical Investigation*. doi:10.1172/JCI88883

Cristancho AG, Lazar MA. 2011. Forming functional fat: a growing understanding of adipocyte differentiation. *Nature reviews Molecular cell biology* **12**:722–734. doi:10.1038/nrm3198

Czech MP. 2020. Mechanisms of insulin resistance related to white, beige, and brown adipocytes. *Molecular Metabolism*. doi:10.1016/j.molmet.2019.12.014

Czech MP. 2017. Insulin action and resistance in obesity and type 2 diabetes. *Nature Medicine*. doi:10.1038/nm.4350

Dadson P, Landini L, Helmiö M, Hannukainen JC, Immonen H, Honka M-J, Bucci M,

Savisto N, Soinio M, Salminen P, Parkkola R, Pihlajamäki J, Iozzo P, Ferrannini E, Nuutila P. 2016. Effect of Bariatric Surgery on Adipose Tissue Glucose Metabolism in Different Depots in Patients With or Without Type 2 Diabetes. *Diabetes Care* **39**:292 LP – 299. doi:10.2337/dc15-1447

Danese E, Minicozzi AM, Benati M, Paviati E, Lima-Oliveira G, Gusella M, Pasini F, Salvagno GL, Montagnana M, Lippi G. 2017. Reference miRNAs for colorectal cancer: Analysis and verification of current data. *Scientific Reports* **7**:1–12. doi:10.1038/s41598-017-08784-3

Dasuri K, Zhang L, Ebenezer P, Fernandez-Kim SO, Bruce-Keller AJ, Szweda LI, Keller JN. 2011. Proteasome alterations during adipose differentiation and aging: Links to impaired adipocyte differentiation and development of oxidative stress. *Free Radical Biology and Medicine* **51**:1727–1735. doi:10.1016/j.freeradbiomed.2011.08.001

de sá PM, Richard AJ, Hang H, Stephens JM. 2017. Transcriptional regulation of adipogenesis. *Comprehensive Physiology* **7**:635–674. doi:10.1002/cphy.c160022

De Spiegelaere W, Dern-Wieloch J, Weigel R, Schumacher V, Schorle H, Nettersheim D, Bergmann M, Brehm R, Kliesch S, Vandekerckhove L, Fink C. 2015. Reference gene validation for RT-qPCR, a note on different available software packages. *PLoS ONE* **10**:1–13. doi:10.1371/journal.pone.0122515

Deiuliis JA. 2016. MicroRNAs as regulators of metabolic disease: Pathophysiologic significance and emerging role as biomarkers and therapeutics. *International Journal of Obesity*. doi:10.1038/ijo.2015.170

Deiuliis JA, Syed R, Duggineni D, Rutsky J, Rengasamy P, Zhang J, Huang K, Needleman B, Mikami D, Perry K, Hazey J, Rajagopalan S. 2016. Visceral Adipose MicroRNA 223 Is Upregulated in Human and Murine Obesity and Modulates the Inflammatory Phenotype of Macrophages. *PloS one* **11**:e0165962–e0165962. doi:10.1371/journal.pone.0165962

del Río-Moreno M, Alors-Pérez E, González-Rubio S, Ferrín G, Reyes O, Rodríguez-Perálvarez M, Sánchez-Frías ME, Sánchez-Sánchez R, Ventura S, López-Miranda J, Kineman RD, de la Mata M, Castaño JP, Gahete MD, Luque RM. 2019. Dysregulation of the Splicing Machinery Is Associated to the Development of Nonalcoholic Fatty Liver Disease. *The Journal of Clinical Endocrinology & Metabolism* **104**:3389–3402. doi:10.1210/jc.2019-00021

Delgado-Lista J, Perez-Martinez P, Garcia-Rios A, Alcala-Diaz JF, Perez-Caballero AI, Gomez-Delgado F, Fuentes F, Quintana-Navarro G, Lopez-Segura F, Ortiz-Morales AM, Delgado-Casado N, Yubero-Serrano EM, Camargo A, Marin C, Rodriguez-Cantalejo F, Gomez-Luna P, Ordovas JM, Lopez-Miranda J, Perez-

Jimenez F. 2016. CORonary Diet Intervention with Olive oil and cardiovascular PREVention study (the CORDIOPREV study): Rationale, methods, and baseline characteristics A clinical trial comparing the efficacy of a Mediterranean diet rich in olive oil versus a low-fat diet . *American Heart Journal* **177**:42–50. doi:10.1016/j.ahj.2016.04.011

Denton NF, Eghleilib M, Al-Sharifi S, Todorčević M, Neville MJ, Loh N, Drakesmith A, Karpe F, Pinnick KE. 2019. Bone morphogenetic protein 2 is a depot-specific regulator of human adipogenesis. *International Journal of Obesity*. doi:10.1038/s41366-019-0421-1

Dhiman R, Caesar S, Thiam AR, Schrul B. 2020. Mechanisms of protein targeting to lipid droplets: A unified cell biological and biophysical perspective. *Seminars in Cell & Developmental Biology* **108**:4–13. doi:https://doi.org/10.1016/j.semcdb.2020.03.004

Díaz-Ruiz A, Guzmán-Ruiz R, Moreno NR, García-Rios A, Delgado-Casado N, Membrives A, Túnez I, El Bekay R, Fernández-Real JM, Tovar S, Diéguez C, Tinahones FJ, Vázquez-Martínez R, López-Miranda J, Malagón MM. 2015. Proteasome Dysfunction Associated to Oxidative Stress and Proteotoxicity in Adipocytes Compromises Insulin Sensitivity in Human Obesity. *Antioxidants & Redox Signaling* **23**:597–612. doi:10.1089/ars.2014.5939

Dodson M V, Du M, Wang S, Bergen WG, Fernyhough-Culver M, Basu U, Poulos SP, Hausman GJ. 2014. Adipose depots differ in cellularity, adipokines produced, gene expression, and cell systems. *Adipocyte* **3**:236–241. doi:10.4161/adip.28321

Dufey E, Sepúlveda D, Rojas-Rivera D, Hetz C. 2014. Cellular Mechanisms of Endoplasmic Reticulum Stress Signaling in Health and Disease. 1. An overview. *American Journal of Physiology-Cell Physiology* **307**:C582–C594. doi:10.1152/ajpcell.00258.2014

Eckel J. 2018. Chapter 2 - Adipose Tissue: A Major Secretory Organ In: Eckel JBT-TCS and OC, editor. Academic Press. pp. 9–63. doi:https://doi.org/10.1016/B978-0-12-809518-8.00002-7

Ehrlund A, Mejhert N, Björk C, Andersson R, Kulyté A, Åström G, Itoh M, Kawaji H, Lassmann T, Daub CO, Carninci P, Forrest ARR, Hayashizaki Y, Sandelin A, Ingelsson E, Rydén M, Laurencikiene J, Arner P, Arner E. 2017. Transcriptional Dynamics During Human Adipogenesis and Its Link to Adipose Morphology and Distribution. *Diabetes* **66**:218–230. doi:10.2337/db16-0631

Ejarque M, Ceperuelo-Mallafré V, Serena C, Maymo-Masip E, Duran X, Díaz-Ramos A, Millan-Scheiding M, Núñez-Álvarez Y, Núñez-Roa C, Gama P, Garcia-Roves PM, Peinado MA, Gimble JM, Zorzano A, Vendrell J, Fernández-Veledo S. 2019.

Adipose tissue mitochondrial dysfunction in human obesity is linked to a specific DNA methylation signature in adipose-derived stem cells. *International Journal of Obesity* **43**:1256–1268. doi:10.1038/s41366-018-0219-6

Ejarque M, Ceperuelo-Mallafré V, Serena C, Pachón G, Núñez-Álvarez Y, Terrón-Puig M, Calvo E, Núñez-Roa C, Oliva-Olivera W, Tinahones FJ, Peinado MA, Vendrell J, Fernández-Veledo S. 2017. Survivin, a key player in cancer progression, increases in obesity and protects adipose tissue stem cells from apoptosis. *Cell death & disease* **8**:e2802. doi:10.1038/cddis.2017.209

Engin AB. 2017. Adipocyte-Macrophage Cross-Talk in Obesity BT - Obesity and Lipotoxicity In: Engin AB, Engin A, editors. Cham: Springer International Publishing. pp. 327–343. doi:10.1007/978-3-319-48382-5_14

Faria SL, Faria OP, Cardeal M de A, Ito MK. 2015. Effects of a very low calorie diet in the preoperative stage of bariatric surgery: a randomized trial. *Surgery for Obesity and Related Diseases* **11**:230–237. doi:10.1016/j.soard.2014.06.007

Feng S, Reuss L, Wang Y. 2016. Potential of Natural Products in the Inhibition of Adipogenesis through Regulation of PPARγ Expression and/or Its Transcriptional Activity. *Molecules (Basel, Switzerland)* **21**:1278. doi:10.3390/molecules21101278

Fernández-Vega A, Chicano-Gálvez E, Prentice BM, Anderson D, Priego-Capote F, López-Bascón MA, Calderón-Santiago M, Avendaño MS, Guzmán-Ruiz R, Tena-Sempere M, Fernández JA, Caprioli RM, Malagón MM. 2020. Optimization of a MALDI-Imaging protocol for studying adipose tissue-associated disorders. *Talanta* **219**:121184. doi:https://doi.org/10.1016/j.talanta.2020.121184

Fernando R, Wardelmann K, Deubel S, Kehm R, Jung T, Mariotti M, Vasilaki A, Gladyshev VN, Kleinridders A, Grune T, Castro JP. 2020. Low steady-state oxidative stress inhibits adipogenesis by altering mitochondrial dynamics and decreasing cellular respiration. *Redox Biology* **32**. doi:10.1016/j.redox.2020.101507

Ferrannini E, Iozzo P, Virtanen KA, Honka M-J, Bucci M, Nuutila P. 2018. Adipose tissue and skeletal muscle insulin-mediated glucose uptake in insulin resistance: role of blood flow and diabetes. *The American Journal of Clinical Nutrition* **108**:749–758. doi:10.1093/ajcn/nqy162

Ferrero R, Rainer P, Deplancke B. 2020. Toward a Consensus View of Mammalian Adipocyte Stem and Progenitor Cell Heterogeneity. *Trends in Cell Biology* **30**:937–950. doi:10.1016/j.tcb.2020.09.007

Ferro E, Enrico Bena C, Grigolon S, Bosia C. 2019. From Endogenous to Synthetic microRNA-Mediated Regulatory Circuits: An Overview. *Cells* **8**:1540. doi:10.3390/cells8121540

Festuccia WT, Blanchard PG, Deshaies Y. 2011. Control of brown adipose tissue

glucose and lipid metabolism by PPARγ. *Frontiers in Endocrinology* **2**:1–6. doi:10.3389/fendo.2011.00084

Fiszbein A, Kornblihtt AR. 2017. Alternative splicing switches: Important players in cell differentiation. *BioEssays* **39**:1–11. doi:10.1002/bies.201600157

Frikke-Schmidt H, O'Rourke RW, Lumeng CN, Sandoval DA, Seeley RJ. 2016. Does bariatric surgery improve adipose tissue function? *Obesity reviews : an official journal of the International Association for the Study of Obesity* **17**:795–809. doi:10.1111/obr.12429

Frühbeck G. 2015. Bariatric and metabolic surgery: a shift in eligibility and success criteria. *Nature Reviews Endocrinology* **11**:465–477. doi:10.1038/nrendo.2015.84

Fujimoto BA, Young M, Carter L, Pang APS, Corley MJ, Fogelgren B, Polgar N. 2019. The exocyst complex regulates insulin-stimulated glucose uptake of skeletal muscle cells. *American Journal of Physiology-Endocrinology and Metabolism* **317**:E957–E972. doi:10.1152/ajpendo.00109.2019

Gaggini M, Carli F, Gastaldelli A. 2017. The color of fat and its central role in the development and progression of metabolic diseases. *Hormone Molecular Biology and Clinical Investigation* **31**:1–14. doi:10.1515/hmbci-2017-0060

Gahete MD, del Rio-Moreno M, Camargo A, Alcala-Diaz JF, Alors-Perez E, Delgado-Lista J, Reyes O, Ventura S, Perez-Martínez P, Castaño JP, Lopez-Miranda J, Luque RM. 2018. Changes in Splicing Machinery Components Influence, Precede, and Early Predict the Development of Type 2 Diabetes: From the CORDIOPREV Study. *EBioMedicine* **37**:356–365. doi:10.1016/j.ebiom.2018.10.056

Gallagher CM, Walter P. 2016. Ceapins inhibit ATF6α signaling by selectively preventing transport of ATF6α to the Golgi apparatus during ER stress. *eLife* **5**:e11880. doi:10.7554/eLife.11880

Gao H, Volat F, Sandhow L, Galitzky J, Nguyen T, Esteve D, Åström G, Mejhert N, Ledoux S, Thalamas C, Arner P, Guillemot JC, Qian H, Rydén M, Bouloumié A. 2017. CD36 Is a Marker of Human Adipocyte Progenitors with Pronounced Adipogenic and Triglyceride Accumulation Potential. *Stem Cells* **35**:1799–1814. doi:10.1002/stem.2635

Gao M, Huang X, Song BL, Yang H. 2019. The biogenesis of lipid droplets: Lipids take center stage. *Progress in Lipid Research* **75**:100989. doi:10.1016/j.plipres.2019.100989

Gao Q, Binns DD, Kinch LN, Grishin N V, Ortiz N, Chen X, Goodman JM. 2017. Pet10p is a yeast perilipin that stabilizes lipid droplets and promotes their assembly. *The Journal of cell biology* **216**:3199–3217. doi:10.1083/jcb.201610013

Gardner BM, Pincus D, Gotthardt K, Gallagher CM, Walter P. 2013. Endoplasmic

reticulum stress sensing in the unfolded protein response. *Cold Spring Harbor perspectives in biology* **5**:a013169–a013169. doi:10.1101/cshperspect.a013169

Gebert LFR, MacRae IJ. 2019. Regulation of microRNA function in animals. *Nature reviews Molecular cell biology* **20**:21–37. doi:10.1038/s41580-018-0045-7

Gentile A, Lhamyani S, Coín-Aragüez L, Clemente-Postigo M, Oliva Olivera W, Romero-Zerbo S, García-Serrano S, García-Escobar E, Zayed H, Doblado E, Bermúdez-Silva F, Murri M, Tinahones FJ, El Bekay R. 2019. miR-20b, miR-296, and Let-7f Expression in Human Adipose Tissue is Related to Obesity and Type 2 Diabetes. *Obesity* **27**:245–254. doi:10.1002/oby.22363

Ghaben AL, Scherer PE. 2019. Adipogenesis and metabolic health. *Nature Reviews Molecular Cell Biology* **20**:242–258. doi:10.1038/s41580-018-0093-z

Gloy VL, Briel M, Bhatt DL, Kashyap SR, Schauer PR, Mingrone G, Bucher HC, Nordmann AJ. 2013. Bariatric surgery versus non-surgical treatment for obesity: a systematic review and meta-analysis of randomised controlled trials. *BMJ (Clinical research ed)* **347**:f5934–f5934. doi:10.1136/bmj.f5934

Gong J, Sun Z, Wu L, Xu W, Schieber N, Xu D, Shui G, Yang H, Parton RG, Li P. 2011. Fsp27 promotes lipid droplet growth by lipid exchange and transfer at lipid droplet contact sites. *The Journal of cell biology* **195**:953–963. doi:10.1083/jcb.201104142

Goossens GH, Blaak EE. 2015. Adipose tissue dysfunction and impaired metabolic health in human obesity: A matter of oxygen? *Frontiers in Endocrinology* **6**:1–5. doi:10.3389/fendo.2015.00055

Greene CS, Krishnan A, Wong AK, Ricciotti E, Zelaya RA, Himmelstein DS, Zhang R, Hartmann BM, Zaslavsky E, Sealfon SC, Chasman DI, Fitzgerald GA, Dolinski K, Grosser T, Troyanskaya OG. 2015. Understanding multicellular function and disease with human tissue-specific networks. *Nature Genetics* **47**:569–576. doi:10.1038/ng.3259

Groot M, Lee H. 2020. Sorting Mechanisms for MicroRNAs into Extracellular Vesicles and Their Associated Diseases. *Cells* **9**:1044. doi:10.3390/cells9041044

Guan B-J, Krokowski D, Majumder M, Schmotzer CL, Kimball SR, Merrick WC, Koromilas AE, Hatzoglou M. 2014. Translational control during endoplasmic reticulum stress beyond phosphorylation of the translation initiation factor eIF2α. *The Journal of biological chemistry* **289**:12593–12611. doi:10.1074/jbc.M113.543215

Guerriero CJ, Brodsky JL. 2012. The delicate balance between secreted protein folding and endoplasmic reticulum-associated degradation in human physiology. *Physiological reviews* **92**:537–576. doi:10.1152/physrev.00027.2011

Guilherme A, Virbasius J V, Puri V, Czech MP. 2008. Adipocyte dysfunctions linking

obesity to insulin resistance and type 2 diabetes. *Nature reviews Molecular cell biology* **9**:367–377. doi:10.1038/nrm2391

Gupta RK. 2014. Adipocytes. *Current Biology* **24**:R988–R993. doi:10.1016/j.cub.2014.09.003

Guzmán-Ruiz R, Tercero-Alcázar C, Rabanal-Ruiz Y, Díaz-Ruiz A, El Bekay R, Rangel-Zuñiga OA, Navarro-Ruiz MC, Molero L, Membrives A, Ruiz-Rabelo JF, Pandit A, López-Miranda J, Tinahones FJ, Malagón MM. 2020. Adipose tissue depot-specific intracellular and extracellular cues contributing to insulin resistance in obese individuals. *FASEB Journal* 1–20. doi:10.1096/fj.201902703R

Ha M, Kim VN. 2014. Regulation of microRNA biogenesis. *Nature Reviews Molecular Cell Biology* **15file:///**:509–524. doi:10.1038/nrm3838

Habtemichael EN, Brewer PD, Romenskaia I, Mastick CC. 2011. Kinetic evidence that Glut4 follows different endocytic pathways than the receptors for transferrin and α2-macroglobulin. *Journal of Biological Chemistry* **286**:10115–10125. doi:10.1074/jbc.M111.217935

Hammarstedt A, Gogg S, Hedjazifar S, Nerstedt A, Smith U. 2018. Impaired adipogenesis and dysfunctional adipose tissue in human hypertrophic obesity. *Physiological Reviews* **98**:1911–1941. doi:10.1152/physrev.00034.2017

Hanna J, Guerra-Moreno A, Ang J, Micoogullari Y. 2019. Protein Degradation and the Pathologic Basis of Disease. *The American journal of pathology* **189**:94–103. doi:10.1016/j.ajpath.2018.09.004

Hansen M, Lund MT, Gregers E, Kraunsøe R, Van Hall G, Helge JW, Dela F. 2015. Adipose tissue mitochondrial respiration and lipolysis before and after a weight loss by diet and RYGB. *Obesity* **23**:2022–2029. doi:10.1002/oby.21223

Hartig SM. 2013. Basic image analysis and manipulation in imageJ. *Current Protocols in Molecular Biology* 1–12. doi:10.1002/0471142727.mb1415s102

Harvey SE, Cheng C. 2016. Methods for Characterization of Alternative RNA Splicing. *Methods in molecular biology (Clifton, NJ)* **1402**:229–241. doi:10.1007/978-1-4939-3378-5_18

Hauner H, Röhrig K, Spelleken M, Liu LS, Eckel J. 1998. Development of insulin-responsive glucose uptake and GLUT4 expression in differentiating human adipocyte precursor cells. *International Journal of Obesity* **22**:448–453. doi:10.1038/sj.ijo.0800606

Heinonen S, Jokinen R, Rissanen A, Pietiläinen KH. 2020. White adipose tissue mitochondrial metabolism in health and in obesity. *Obesity Reviews* **21**:e12958. doi:https://doi.org/10.1111/obr.12958

Heinze G, Wallisch C, Dunkler D. 2018. Variable selection - A review and

recommendations for the practicing statistician. *Biometrical journal Biometrische Zeitschrift* **60**:431–449. doi:10.1002/bimj.201700067

Hendricks EJ. 2017. Off-label drugs for weight management. *Diabetes, metabolic syndrome and obesity : targets and therapy* **10**:223–234. doi:10.2147/DMSO.S95299

Heneghan HM, Miller N, McAnena OJ, O'Brien T, Kerin MJ. 2011. Differential miRNA expression in omental adipose tissue and in the circulation of obese patients identifies novel metabolic biomarkers. *Journal of Clinical Endocrinology and Metabolism* **96**:846–850. doi:10.1210/jc.2010-2701

Henne M, Goodman JM, Hariri H. 2020. Spatial compartmentalization of lipid droplet biogenesis. *Biochimica et Biophysica Acta (BBA) - Molecular and Cell Biology of Lipids* **1865**. doi:https://doi.org/10.1016/j.bbalip.2019.07.008

Hepler C, Gupta RK. 2017. The expanding problem of adipose depot remodeling and postnatal adipocyte progenitor recruitment. *Molecular and Cellular Endocrinology* **445**:95–108. doi:10.1016/j.mce.2016.10.011

Hetz C, Papa FR. 2018. The Unfolded Protein Response and Cell Fate Control. *Molecular Cell* **69**:169–181. doi:https://doi.org/10.1016/j.molcel.2017.06.017

Heyn GS, Corrêa LH, Magalhães KG. 2020. The Impact of Adipose Tissue-Derived miRNAs in Metabolic Syndrome, Obesity, and Cancer. *Frontiers in endocrinology* **11**:563816. doi:10.3389/fendo.2020.563816

Hillary RF, FitzGerald U. 2018. A lifetime of stress: ATF6 in development and homeostasis. *Journal of Biomedical Science* **25**:48. doi:10.1186/s12929-018-0453-1

Hipp MS, Park S-H, Hartl FU. 2014. Proteostasis impairment in protein-misfolding and -aggregation diseases. *Trends in Cell Biology* **24**:506–514. doi:https://doi.org/10.1016/j.tcb.2014.05.003

Hotamisligil GS, Shargill NS, Spiegelman BM. 1993. Adipose expression of tumor necrosis factor- (alpha): Direct. *Science* **259**:87–92.

Hou B, Zhao Y, He P, Xu C, Ma P, Lam SM, Li B, Gil V, Shui G, Qiang G, Liew CW, Du G. 2020. Targeted lipidomics and transcriptomics profiling reveal the heterogeneity of visceral and subcutaneous white adipose tissue. *Life Sciences* **245**:117352. doi:https://doi.org/10.1016/j.lfs.2020.117352

Hruby A, Hu FB. 2015. The Epidemiology of Obesity: A Big Picture. *PharmacoEconomics* **33**:673–689. doi:10.1007/s40273-014-0243-x

Huang W. 2017. MicroRNAs: Biomarkers, Diagnostics, and Therapeutics BT - Bioinformatics in MicroRNA Research In: Huang J, Borchert GM, Dou D, Huan J (Luke), Lan W, Tan M, Wu B, editors. New York, NY: Springer New York. pp. 57–

67. doi:10.1007/978-1-4939-7046-9_4

Hudak CS, Sul HS. 2013. Pref-1, a gatekeeper of adipogenesis. *Frontiers in Endocrinology* **4**:1–6. doi:10.3389/fendo.2013.00079

Hui HX, Feng T. 2018. Adipose Tissue as an Endocrine Organ In: Szablewski TFE-L, editor. Rijeka: IntechOpen. p. Ch. 10. doi:10.5772/intechopen.76220

Huot M-É, Vogel G, Zabarauskas A, Ngo CT-A, Coulombe-Huntington J, Majewski J, Richard S. 2012. The Sam68 STAR RNA-Binding Protein Regulates mTOR Alternative Splicing during Adipogenesis. *Molecular Cell* **46**:187–199. doi:https://doi.org/10.1016/j.molcel.2012.02.007

Jaldin-Fincati JR, Pavarotti M, Frendo-Cumbo S, Bilan PJ, Klip A. 2017. Update on GLUT4 Vesicle Traffic: A Cornerstone of Insulin Action. *Trends in Endocrinology and Metabolism* **28**:597–611. doi:10.1016/j.tem.2017.05.002

Janas Teresa, Janas MM, Sapoń K, Janas Tadeusz. 2015. Mechanisms of RNA loading into exosomes. *FEBS Letters* **589**:1391–1398. doi:https://doi.org/10.1016/j.febslet.2015.04.036

Ji C, Guo X. 2019. The clinical potential of circulating microRNAs in obesity. *Nature Reviews Endocrinology* **15**:731–743. doi:10.1038/s41574-019-0260-0

Jia Q, Morgan-Bathke ME, Jensen MD. 2020. Adipose tissue macrophage burden, systemic inflammation, and insulin resistance. *American Journal of Physiology-Endocrinology and Metabolism* **319**:E254–E264. doi:10.1152/ajpendo.00109.2020

Jiang J, Liu X, Liu C, Liu G, Li S, Wang L. 2017. Integrating Omics and Alternative Splicing Reveals Insights into Grape Response to High Temperature. *Plant physiology* **173**:1502–1518. doi:10.1104/pp.16.01305

Jiang S, Yan W. 2016. Current View of microRNA Processing. *Signal Transduction Insights* **5**:STI.S12317. doi:10.4137/STI.S12317

Jiménez-Lucena R, Rangel-Zúñiga OA, Alcalá-Díaz JF, López-Moreno J, Roncero-Ramos I, Molina-Abril H, Yubero-Serrano EM, Caballero-Villarraso J, Delgado-Lista J, Castaño JP, Ordovás JM, Pérez-Martinez P, Camargo A, López-Miranda J. 2018. Circulating miRNAs as Predictive Biomarkers of Type 2 Diabetes Mellitus Development in Coronary Heart Disease Patients from the CORDIOPREV Study. *Molecular Therapy - Nucleic Acids* **12**:146–157. doi:10.1016/j.omtn.2018.05.002

Jiménez-Vacas JM, Herrero-Aguayo V, Gómez-Gómez E, León-González AJ, Sáez-Martínez P, Alors-Pérez E, Fuentes-Fayos AC, Martínez-López A, Sánchez-Sánchez R, González-Serrano T, López-Ruiz DJ, Requena-Tapia MJ, Castaño JP, Gahete MD, Luque RM. 2019. Spliceosome Component SF3B1 as Novel Prognostic Biomarker and Therapeutic Target for Prostate Cancer. *Translational Research*. doi:10.1016/j.trsl.2019.07.001

Kadowaki T, Ueki K, Yamauchi T, Kubota N. 2012. SnapShot: Insulin signaling pathways. *Cell* **148**:624-624.e1. doi:10.1016/j.cell.2012.01.034

Kajimura S. 2017. Advances in the understanding of adipose tissue biology. *Nature Reviews Endocrinology* **13**:69–70. doi:10.1038/nrendo.2016.211

Kalkhof S, Krieg L, Büttner P, Wabitsch M, Küntzel C, Friebe D, Landgraf K, Hanschkow M, Schubert K, Kiess W, Krohn K, Blüher M, von Bergen M, Körner A. 2020. In Depth Quantitative Proteomic and Transcriptomic Characterization of Human Adipocyte Differentiation Using the SGBS Cell Line. *PROTEOMICS* **n/a**:1900405. doi:10.1002/pmic.201900405

Kaminska D, Hämäläinen M, Cederberg H, Käkelä P, Venesmaa S, Miettinen P, Ilves I, Herzig K-H, Kolehmainen M, Karhunen L, Kuusisto J, Gylling H, Laakso M, Pihlajamäki J. 2014. Adipose tissue INSR splicing in humans associates with fasting insulin level and is regulated by weight loss. *Diabetologia* **57**:347–351. doi:10.1007/s00125-013-3097-4

Kaminska D, Käkelä P, Nikkola E, Venesmaa S, Ilves I, Herzig K-H, Kolehmainen M, Karhunen L, Kuusisto J, Gylling H, Pajukanta P, Laakso M, Pihlajamäki J. 2016. Regulation of alternative splicing in human obesity loci. *Obesity (Silver Spring, Md)* **24**:2033–2037. doi:10.1002/oby.21587

Kaminska D, Pihlajamäki J. 2013. Regulation of alternative splicing in obesity and weight loss. *Adipocyte* **2**:143–147. doi:10.4161/adip.24751

Karastergiou K, Fried SK. 2013. Multiple Adipose Depots Increase Cardiovascular Risk via Local and Systemic Effects. *Current Atherosclerosis Reports* **15**:361. doi:10.1007/s11883-013-0361-5

Karpe F, Dickmann JR, Frayn KN. 2011. Fatty acids, obesity, and insulin resistance: Time for a reevaluation. *Diabetes* **60**:2441–2449. doi:10.2337/db11-0425

Keita M, Kaffy J, Troufflard C, Morvan E, Crousse B, Ongeri S. 2014. 19F NMR monitoring of the eukaryotic 20S proteasome chymotrypsin-like activity: An investigative tool for studying allosteric regulation. *Organic and Biomolecular Chemistry* **12**:4576–4581. doi:10.1039/c4ob00962b

Kelemen O, Convertini P, Zhang Z, Wen Y, Shen M, Falaleeva M, Stamm S. 2013. Function of alternative splicing. *Gene* **514**:1–30. doi:10.1016/j.gene.2012.07.083

Khorgami Z, Shoar S, Andalib A, Aminian A, Brethauer SA, Schauer PR. 2017. Trends in utilization of bariatric surgery, 2010-2014: sleeve gastrectomy dominates. *Surgery for Obesity and Related Diseases* **13**:774–778. doi:10.1016/j.soard.2017.01.031

Kim GD, Ng HP, Patel N, Mahabeleshwar GH. 2019. Kruppel-like factor 6 and miR-223 signaling axis regulates macrophage-mediated inflammation. *FASEB journal :*

official publication of the Federation of American Societies for Experimental Biology **33**:10902–10915. doi:10.1096/fj.201900867RR

Kim JI, Huh JY, Sohn JH, Choe SS, Lee YS, Lim CY, Jo A, Park SB, Han W, Kim JB. 2015. Lipid-Overloaded Enlarged Adipocytes Provoke Insulin Resistance Independent of Inflammation. *Molecular and Cellular Biology* **35**:1686–1699. doi:10.1128/mcb.01321-14

Kim NH, Ahn J, Choi YM, Son HJ, Choi WH, Cho HJ, Yu JH, Seo JA, Jang YJ, Jung CH, Ha TY. 2019. Differential circulating and visceral fat microRNA expression of non-obese and obese subjects. *Clinical Nutrition*. doi:10.1016/J.CLNU.2019.03.033

Kita S, Maeda N, Shimomura I. 2019. Interorgan communication by exosomes, adipose tissue, and adiponectin in metabolic syndrome. *Journal of Clinical Investigation*. doi:10.1172/JCI129193

Klip A, McGraw TE, James DE. 2019. Thirty sweet years of GLUT4. *Journal of Biological Chemistry* **294**:11369–11381. doi:10.1074/jbc.rev119.008351

Klip A, Sun Y, Chiu TT, Foley KP. 2014. Signal transduction meets vesicle traffic: The software and hardware of GLUT4 translocation. *American Journal of Physiology - Cell Physiology* **306**. doi:10.1152/ajpcell.00069.2014

Kojta I, Chacińska M, Błachnio-Zabielska A. 2020. Obesity, Bioactive Lipids, and Adipose Tissue Inflammation in Insulin Resistance. *Nutrients* **12**:1305. doi:10.3390/nu12051305

Konigorski S, Janke J, Drogan D, Bergmann MM, Hierholzer J, Kaaks R, Boeing H, Pischon T. 2019. Prediction of Circulating Adipokine Levels Based on Body Fat Compartments and Adipose Tissue Gene Expression. *Obesity Facts* **12**:590–605. doi:10.1159/000502117

Korf H, van der Merwe S. 2017. Adipose-derived exosomal MicroRNAs orchestrate gene regulation in the liver: Is this the missing link in nonalcoholic fatty liver disease? *Hepatology* **66**:1689–1691. doi:10.1002/hep.29343

Kors S, Geijtenbeek K, Reits E, Schipper-Krom S. 2019. Regulation of Proteasome Activity by (Post-)transcriptional Mechanisms. *Frontiers in molecular biosciences* **6**:48. doi:10.3389/fmolb.2019.00048

Kosaka N, Iguchi H, Hagiwara K, Yoshioka Y, Takeshita F, Ochiya T. 2013. Neutral sphingomyelinase 2 (nSMase2)-dependent exosomal transfer of angiogenic microRNAs regulate cancer cell metastasis. *The Journal of biological chemistry* **288**:10849–10859. doi:10.1074/jbc.M112.446831

Koscianska E, Starega-Roslan J, Krzyzosiak WJ. 2011. The role of Dicer protein partners in the processing of microRNA precursors. *PloS one* **6**:e28548–e28548. doi:10.1371/journal.pone.0028548

Koster A, Murphy RA, Eiriksdottir G, Aspelund T, Sigurdsson S, Lang TF, Gudnason V, Launer LJ, Harris TB. 2015. Fat distribution and mortality: the AGES-Reykjavik Study. *Obesity (Silver Spring, Md)* **23**:893–897. doi:10.1002/oby.21028

Kotake Y, Sagane K, Owa T, Mimori-Kiyosue Y, Shimizu H, Uesugi M, Ishihama Y, Iwata M, Mizui Y. 2007. Splicing factor SF3b as a target of the antitumor natural product pladienolide. *Nature Chemical Biology* **3**:570–575. doi:10.1038/nchembio.2007.16

Kreft SG, Hochstrasser M. 2011. An unusual transmembrane helix in the endoplasmic reticulum ubiquitin ligase Doa10 modulates degradation of its cognate E2 enzyme. *The Journal of biological chemistry* **286**:20163–20174. doi:10.1074/jbc.M110.196360

Krycer JR, Yugi K, Hirayama A, Fazakerley DJ, Quek LE, Scalzo R, Ohno S, Hodson MP, Ikeda S, Shoji F, Suzuki K, Domanova W, Parker BL, Nelson ME, Humphrey SJ, Turner N, Hoehn KL, Cooney GJ, Soga T, Kuroda S, James DE. 2017. Dynamic Metabolomics Reveals that Insulin Primes the Adipocyte for Glucose Metabolism. *Cell Reports* **21**:3536–3547. doi:10.1016/j.celrep.2017.11.085

Kwok KHM, Lam KSL, Xu A. 2016. Heterogeneity of white adipose tissue: Molecular basis and clinical implications. *Experimental and Molecular Medicine*. doi:10.1038/emm.2016.5

Lafontan M. 2014. Adipose tissue and adipocyte dysregulation. *Diabetes & Metabolism* **40**:16–28. doi:https://doi.org/10.1016/j.diabet.2013.08.002

Lago MEL, Cerqueira MT, Pirraco RP, Reis RL, Marques AP. 2018. 14 - Skin in vitro models to study dermal white adipose tissue role in skin healing In: Marques AP, Pirraco RP, Cerqueira MT, Reis RLBT-STM, editors. Boston: Academic Press. pp. 327–352. doi:https://doi.org/10.1016/B978-0-12-810545-0.00014-0

Lam F, Cladière D, Guillaume C, Wassmann K, Bolte S. 2017. Super-resolution for everybody: An image processing workflow to obtain high-resolution images with a standard confocal microscope. *Methods* **115**:17–27. doi:10.1016/j.ymeth.2016.11.003

Landrier J-F, Derghal A, Mounien L. 2019. MicroRNAs in Obesity and Related Metabolic Disorders. *Cells* **8**:859. doi:10.3390/cells8080859

Lass A, Zimmermann R, Oberer M, Zechner R. 2011. Lipolysis - A highly regulated multi-enzyme complex mediates the catabolism of cellular fat stores. *Progress in Lipid Research* **50**:14–27. doi:10.1016/j.plipres.2010.10.004

Lee H, Groot M, Pinilla-Vera M, Fredenburgh LE, Jin Y. 2019. Identification of miRNA-rich vesicles in bronchoalveolar lavage fluid: Insights into the function and heterogeneity of extracellular vesicles. *Journal of controlled release : official journal of the Controlled Release Society* **294**:43–52. doi:10.1016/j.jconrel.2018.12.008

Lee M-W, Lee M, Oh K-J. 2019. Adipose Tissue-Derived Signatures for Obesity and Type 2 Diabetes: Adipokines, Batokines and MicroRNAs. *Journal of clinical medicine* **8**:854. doi:10.3390/jcm8060854

Lee MJ, Wu Y, Fried SK. 2013. Adipose tissue heterogeneity: Implication of depot differences in adipose tissue for obesity complications. *Molecular Aspects of Medicine* **34**:1–11. doi:10.1016/j.mam.2012.10.001

Lee Y-H, Pratley RE. 2005. The evolving role of inflammation in obesity and the metabolic syndrome. *Current Diabetes Reports* **5**:70–75. doi:10.1007/s11892-005-0071-7

Lee Y, Rio DC. 2015. Mechanisms and Regulation of Alternative Pre-mRNA Splicing. *Annual review of biochemistry* **84**:291–323. doi:10.1146/annurev-biochem-060614-034316

Lemus L, Goder V. 2014. Regulation of Endoplasmic Reticulum-Associated Protein Degradation (ERAD) by Ubiquitin. *Cells* **3**:824–847. doi:10.3390/cells3030824

Lenz M, Arts ICW, Peeters RLM, de Kok TM, Ertaylan G. 2020. Adipose tissue in health and disease through the lens of its building blocks. *Scientific Reports* **10**:10433. doi:10.1038/s41598-020-67177-1

Lessard J, Laforest S, Pelletier M, Leboeuf M, Blackburn L, Tchernof A. 2014. Low abdominal subcutaneous preadipocyte adipogenesis is associated with visceral obesity, visceral adipocyte hypertrophy, and a dysmetabolic state. *Adipocyte* **3**:197–205. doi:10.4161/adip.29385

Lessard J, Tchernof A. 2012. Depot- and obesity-related differences in adipogenesis. *Clin Lipidol* **7**:587–596.

Leto D, Saltiel AR. 2012. Regulation of glucose transport by insulin: Traffic control of GLUT4. *Nature Reviews Molecular Cell Biology* **13**:383–396. doi:10.1038/nrm3351

Leung MYM, Carlsson NP, Colditz GA, Chang S-H. 2017. The Burden of Obesity on Diabetes in the United States: Medical Expenditure Panel Survey, 2008 to 2012. *Value in health : the journal of the International Society for Pharmacoeconomics and Outcomes Research* **20**:77–84. doi:10.1016/j.jval.2016.08.735

Li F, Zhang L, Craddock J, Bruce-Keller AJ, Dasuri K, Nguyen AT, Keller JN. 2008. Aging and dietary restriction effects on ubiquitination, sumoylation, and the proteasome in the heart. *Mechanisms of Ageing and Development* **129**:515–521. doi:10.1016/j.mad.2008.04.007

Li H, Cheng Y, Wu W, Liu Y, Wei N, Feng X, Xie Z, Feng Y. 2014. SRSF10 regulates alternative splicing and is required for adipocyte differentiation. *Molecular and cellular biology* **34**:2198–2207. doi:10.1128/MCB.01674-13

Li J-H, Liu S, Zhou H, Qu L-H, Yang J-H. 2013. starBase v2.0: decoding miRNA-ceRNA,

miRNA-ncRNA and protein–RNA interaction networks from large-scale CLIP-Seq data. *Nucleic Acids Research* **42**:D92–D97. doi:10.1093/nar/gkt1248

Li X, Zhang W, Xu T, Ramsey J, Zhang L, Hill R, Hansen KC, Hesselberth JR, Zhao R. 2013. Comprehensive in vivo RNA-binding site analyses reveal a role of Prp8 in spliceosomal assembly. *Nucleic acids research* **41**:3805–3818. doi:10.1093/nar/gkt062

Li Y, Yun K, Mu R. 2020. A review on the biology and properties of adipose tissue macrophages involved in adipose tissue physiological and pathophysiological processes. *Lipids in Health and Disease* **19**:164. doi:10.1186/s12944-020-01342-3

Lin C-L, Taggart AJ, Fairbrother WG. 2016. RNA structure in splicing: An evolutionary perspective. *RNA biology* **13**:766–771. doi:10.1080/15476286.2016.1208893

Lin J-C. 2015. Impacts of Alternative Splicing Events on the Differentiation of Adipocytes. *International journal of molecular sciences* **16**:22169–22189. doi:10.3390/ijms160922169

Lin JC. 2015. Impacts of alternative splicing events on the differentiation of adipocytes. *International Journal of Molecular Sciences* **16**:22169–22189. doi:10.3390/ijms160922169

Liu R, Nikolajczyk BS. 2019. Tissue immune cells fuel obesity-associated inflammation in adipose tissue and beyond. *Frontiers in Immunology*. doi:10.3389/fimmu.2019.01587

Liu W, Wang X. 2019. Prediction of functional microRNA targets by integrative modeling of microRNA binding and target expression data. *Genome Biology* **20**:1–10. doi:10.1186/s13059-019-1629-z

Liu Y, Gao G, Yang C, Zhou K, Shen B, Liang H, Jiang X. 2014. The Role of Circulating MicroRNA-126 (miR-126): A Novel Biomarker for Screening Prediabetes and Newly Diagnosed Type 2 Diabetes Mellitus. *International Journal of Molecular Sciences* **15**:10567–10577. doi:10.3390/ijms150610567

Liu Z, Lv Y, Zhao N, Guan G, Wang J. 2015. Protein kinase R-like ER kinase and its role in endoplasmic reticulum stress-decided cell fate. *Cell death & disease* **6**:e1822–e1822. doi:10.1038/cddis.2015.183

Livneh I, Cohen-Kaplan V, Cohen-Rosenzweig C, Avni N, Ciechanover A. 2016. The life cycle of the 26S proteasome: from birth, through regulation and function, and onto its death. *Cell research* **26**:869–885. doi:10.1038/cr.2016.86

Lizunov VA, Stenkula K, Troy A, Cushman SW, Zimmerberg J. 2013. Insulin Regulates Glut4 Confinement in Plasma Membrane Clusters in Adipose Cells. *PLoS ONE* **8**. doi:10.1371/journal.pone.0057559

Lo KA, Labadorf A, Kennedy NJ, Han MS, Yap YS, Matthews B, Xin X, Sun L, Davis RJ,

Lodish HF, Fraenkel E. 2013. Analysis of In Vitro Insulin-Resistance Models and Their Physiological Relevance to InVivo Diet-Induced Adipose Insulin Resistance. *Cell Reports* **5**:259–270. doi:10.1016/j.celrep.2013.08.039

Longo M, Zatterale F, Naderi J, Parrillo L, Formisano P, Raciti GA, Beguinot F, Miele C. 2019. Adipose Tissue Dysfunction as Determinant of Obesity-Associated Metabolic Complications. *International journal of molecular sciences* **20**. doi:10.3390/ijms20092358

Lopata A, Kniss A, Löhr F, Rogov V V, Dötsch V. 2020. Ubiquitination in the ERAD Process. *International journal of molecular sciences* **21**:5369. doi:10.3390/ijms21155369

López-Bascón MA, Calderón-Santiago M, Sánchez-Ceinos J, Fernández-Vega A, Guzmán-Ruiz R, López-Miranda J, Malagon MM, Priego-Capote F. 2018. Influence of sample preparation on lipidomics analysis of polar lipids in adipose tissue. *Talanta* **177**:86–93. doi:10.1016/j.talanta.2017.09.017

López-Otín C, Blasco MA, Partridge L, Serrano M, Kroemer G. 2013. The hallmarks of aging. *Cell* **153**:1194–1217. doi:10.1016/j.cell.2013.05.039

López-Otín C, Kroemer G. 2020. Hallmarks of Health. *Cell*. doi:https://doi.org/10.1016/j.cell.2020.11.034

Løvsletten NG, Vu H, Skagen C, Lund J, Kase ET, Thoresen GH, Zammit VA, Rustan AC. 2020. Treatment of human skeletal muscle cells with inhibitors of diacylglycerol acyltransferases 1 and 2 to explore isozyme-specific roles on lipid metabolism. *Scientific Reports* **10**:238. doi:10.1038/s41598-019-57157-5

Lowe CE, O'Rahilly S, Rochford JJ. 2011. Adipogenesis at a glance. *Journal of Cell Science* **124**:3726. doi:10.1242/jcs.101741

Luo L, Liu M. 2016. Adipose tissue in control of metabolism. *Journal of Endocrinology*. doi:10.1530/JOE-16-0211

Lynes MD, Tseng YH. 2018. Deciphering adipose tissue heterogeneity. *Annals of the New York Academy of Sciences* **1411**:5–20. doi:10.1111/nyas.13398

Macartney-Coxson D, Danielson K, Clapham J, Benton MC, Johnston A, Jones A, Shaw O, Hagan RD, Hoffman EP, Hayes M, Harper J, Langston MA, Stubbs RS. 2020. MicroRNA Profiling in Adipose Before and After Weight Loss Highlights the Role of miR-223-3p and the NLRP3 Inflammasome. *Obesity* **28**:570–580. doi:10.1002/oby.22722

Madsbad S, Dirksen C, Holst JJ. 2014. Mechanisms of changes in glucose metabolism and bodyweight after bariatric surgery. *The Lancet Diabetes & Endocrinology* **2**:152–164. doi:10.1016/S2213-8587(13)70218-3

Magré J, Delépine M, Khallouf E, Gedde-Dahl T, Van Maldergem L, Sobel E, Papp J,

Meier M, Mégarbané A, Bachy A, Verloes A, D'Abronzo FH, Seemanova E, Assan R, Baudic N, Bourut C, Czernichow P, Huet F, Grigorescu F, De Kerdanet M, Lacombe D, Labrune P, Lanza M, Loret H, Matsuda F, Navarro J, Nivelon-Chevalier A, Polak M, Robert JJ, Tric P, Tubiana-Rufi N, Vigouroux C, Weissenbach J, Savasta S, Maassen JA, Trygstad O, Bogalho P, Freitas P, Medina JL, Bonnicci F, Joffe BI, Loyson G, Panz VR, Raal FJ, O'Rahilly S, Stephenson T, Kahn CR, Lathrop M, Capeau J. 2001. Identification of the gene altered in Berardinelli-Seip congenital lipodystrophy on chromosome 11q13. *Nature Genetics* **28**:365–370. doi:10.1038/ng585

Makki K, Froguel P, Wolowczuk I. 2013. Adipose Tissue in Obesity-Related Inflammation and Insulin Resistance: Cells, Cytokines, and Chemokines. *ISRN Inflammation* **2013**:139239. doi:10.1155/2013/139239

Malhotra JD, Kaufman RJ. 2011. ER stress and its functional link to mitochondria: role in cell survival and death. *Cold Spring Harbor perspectives in biology* **3**:a004424–a004424. doi:10.1101/cshperspect.a004424

Małodobra-Mazur M, Cierzniak A, Pawełka D, Kaliszewski K, Rudnicki J, Dobosz T. 2020. Metabolic Differences between Subcutaneous and Visceral Adipocytes Differentiated with an Excess of Saturated and Monounsaturated Fatty Acids. *Genes* **11**:1092. doi:10.3390/genes11091092

Mardinoglu A, Heiker JT, Gärtner D, Björnson E, Schön MR, Flehmig G, Klöting N, Krohn K, Fasshauer M, Stumvoll M, Nielsen J, Blüher M. 2015. Extensive weight loss reveals distinct gene expression changes in human subcutaneous and visceral adipose tissue. *Scientific Reports* **5**:1–11. doi:10.1038/srep14841

Marshall RS, Vierstra RD. 2019. Dynamic Regulation of the 26S Proteasome: From Synthesis to Degradation . *Frontiers in Molecular Biosciences* .

Martín-Clemente B, Alvarez-Castelao B, Mayo I, Sierra AB, Díaz V, Milán M, Fariñas I, Gómez-Isla T, Ferrer I, Castaño JG. 2004. α-Synuclein expression levels do not significantly affect proteasome function and expression in mice and stably transfected PC12 cell lines. *Journal of Biological Chemistry* **279**:52984–52990. doi:10.1074/jbc.M409028200

Martín-Rodríguez JF, Cervera-Barajas A, Madrazo-Atutxa A, García-Luna PP, Pereira JL, Castro-Luque J, León-Justel A, Morales-Conde S, Castillo JR, Leal-Cerro A, Cano DA. 2014. Effect of bariatric surgery on microvascular dysfunction associated to metabolic syndrome: A 12-month prospective study. *International Journal of Obesity* **38**:1410–1415. doi:10.1038/ijo.2014.15

Masschelin PM, Cox AR, Chernis N, Hartig SM. 2020. The Impact of Oxidative Stress on Adipose Tissue Energy Balance. *Frontiers in Physiology*.

doi:10.3389/fphys.2019.01638

Matera AG, Wang Z. 2014. A day in the life of the spliceosome. *Nature Reviews Molecular Cell Biology* **15**:108–121. doi:10.1038/nrm3742

Matsumura Y, Sakai J, Skach WR. 2013. Endoplasmic Reticulum Protein Quality Control Is Determined by Cooperative Interactions between Hsp/c70 Protein and the CHIP E3 Ligase. *Journal of Biological Chemistry* **288**:31069–31079. doi:10.1074/jbc.M113.479345

Mattson MP, Arumugam T V. 2018. Hallmarks of Brain Aging: Adaptive and Pathological Modification by Metabolic States. *Cell Metabolism* **27**:1176–1199. doi:https://doi.org/10.1016/j.cmet.2018.05.011

McKenzie AJ, Hoshino D, Hong NH, Cha DJ, Franklin JL, Coffey RJ, Patton JG, Weaver AM. 2016. KRAS-MEK Signaling Controls Ago2 Sorting into Exosomes. *Cell Reports* **15**:978–987. doi:https://doi.org/10.1016/j.celrep.2016.03.085

McLaughlin T, Craig C, Liu L-F, Perelman D, Allister C, Spielman D, Cushman SW. 2016. Adipose Cell Size and Regional Fat Deposition as Predictors of Metabolic Response to Overfeeding in Insulin-Resistant and Insulin-Sensitive Humans. *Diabetes* **65**:1245–1254. doi:10.2337/db15-1213

Mehdiani A, Maier A, Pinto A, Barth M, Akhyari P, Lichtenberg A. 2015. An innovative method for exosome quantification and size measurement. *Journal of visualized experiments : JoVE* 50974. doi:10.3791/50974

Meijer HA, Smith EM, Bushell M. 2014. Regulation of miRNA strand selection: follow the leader? *Biochemical Society Transactions* **42**:1135–1140. doi:10.1042/BST20140142

Meister G. 2013. Argonaute proteins: functional insights and emerging roles. *Nature Reviews Genetics* **14**:447–459. doi:10.1038/nrg3462

Mendez AS, Alfaro J, Morales-Soto MA, Dar AC, McCullagh E, Gotthardt K, Li H, Acosta-Alvear D, Sidrauski C, Korennykh A V, Bernales S, Shokat KM, Walter P. 2015. Endoplasmic reticulum stress-independent activation of unfolded protein response kinases by a small molecule ATP-mimic. *eLife* **4**:e05434. doi:10.7554/eLife.05434

Meruvu S, Hugendubler L, Mueller E. 2011. Regulation of Adipocyte Differentiation by the Zinc Finger Protein ZNF638. *Journal of Biological Chemistry* **286**:26516–26523. doi:10.1074/jbc.M110.212506

Mi H, Muruganujan A, Ebert D, Huang X, Thomas PD. 2019. PANTHER version 14: More genomes, a new PANTHER GO-slim and improvements in enrichment analysis tools. *Nucleic Acids Research* **47**:D419–D426. doi:10.1093/nar/gky1038

Mintziori G, Nigdelis MP, Mathew H, Mousiolis A, Goulis DG, Mantzoros CS. 2020. The effect of excess body fat on female and male reproduction. *Metabolism* **107**:154193.

doi:https://doi.org/10.1016/j.metabol.2020.154193

Mizui Y, Sakai T, Iwata M, Uenaka T, Okamoto K, Shimizu H, Yamori T, Yoshimatsu K, Asada M. 2004. Pladienolides, New Substances from Culture of Streptomyces platensis Mer-11107. *the Journal of Antibiotics* **57**:188–196.

Mohan S, R PRM, Brown L, Ayyappan P, G RK. 2019. Endoplasmic reticulum stress: A master regulator of metabolic syndrome. *European Journal of Pharmacology* **860**:172553. doi:10.1016/j.ejphar.2019.172553

Montgomery MK, De Nardo W, Watt MJ. 2019. Impact of Lipotoxicity on Tissue “Cross Talk” and Metabolic Regulation. *Physiology* **34**:134–149. doi:10.1152/physiol.00037.2018

Moreno-Castellanos N, Guzmán-Ruiz R, Cano DA, Madrazo-Atutxa A, Peinado JR, Pereira-Cunill JL, García-Luna PP, Morales-Conde S, Socas-Macias M, Vázquez-Martínez R, Leal-Cerro A, Malagón MM. 2016. The Effects of Bariatric Surgery-Induced Weight Loss on Adipose Tissue in Morbidly Obese Women Depends on the Initial Metabolic Status. *Obesity Surgery* **26**:1757–1767. doi:10.1007/s11695-015-1995-x

Moreno-Castellanos N, Rodríguez A, Rabanal-Ruiz Y, Fernández-Vega A, López-Miranda J, Vázquez-Martínez R, Frühbeck G, Malagón MM. 2017. The cytoskeletal protein septin 11 is associated with human obesity and is involved in adipocyte lipid storage and metabolism. *Diabetologia* **60**:324–335. doi:10.1007/s00125-016-4155-5

Moreno-Navarrete J, Fernández-Real J. 2017. Adipocyte DifferentiationAdipose Tissue Biology: Second Edition. pp. 69–90. doi:10.1007/978-3-319-52031-5_3

Mori MA, Ludwig RG, Garcia-Martin R, Brandão BB, Kahn CR. 2019. Extracellular miRNAs: From Biomarkers to Mediators of Physiology and Disease. *Cell Metabolism* **8**:1–18. doi:10.1016/j.cmet.2019.07.011

Morito D, Nagata K. 2015. Pathogenic Hijacking of ER-Associated Degradation: Is ERAD Flexible? *Molecular Cell* **59**:335–344. doi:https://doi.org/10.1016/j.molcel.2015.06.010

Morten BC, Scott RJ, Avery-Kiejda KA. 2016. Comparison of Three Different Methods for Determining Cell Proliferation in Breast Cancer Cell Lines. *Journal of Visualized Experiments* **53**:1–11. doi:10.3791/54350

Moseti D, Regassa A, Kim W-K. 2016. Molecular Regulation of Adipogenesis and Potential Anti-Adipogenic Bioactive Molecules. *International journal of molecular sciences* **17**:124. doi:10.3390/ijms17010124

Moure R, Domingo P, Gallego-Escuredo JM, Villarroya J, Gutierrez MDM, Mateo MG, Domingo JC, Giralt M, Villarroya F. 2016. Impact of elvitegravir on human

adipocytes: Alterations in differentiation, gene expression and release of adipokines and cytokines. *Antiviral Research* **132**:59–65. doi:10.1016/j.antiviral.2016.05.013

Mueller E. 2014. Understanding the variegation of fat: Novel regulators of adipocyte differentiation and fat tissue biology. *Biochimica et Biophysica Acta - Molecular Basis of Disease* **1842**:352–357. doi:10.1016/j.bbadis.2013.05.031

Mullins GR, Wang L, Raje V, Sherwood SG, Grande RC, Boroda S, Eaton JM, Blancquaert S, Roger PP, Leitinger N, Harris TE. 2014. Catecholamine-induced lipolysis causes mTOR complex dissociation and inhibits glucose uptake in adipocytes. *Proceedings of the National Academy of Sciences of the United States of America* **111**:17450–17455. doi:10.1073/pnas.1410530111

Nettebrock NT, Bohnert M. 2020. Born this way – Biogenesis of lipid droplets from specialized ER. *BBA - Molecular and Cell Biology of Lipids* **1865**:158448. doi:10.1016/j.bbalip.2019.04.008

Ng M, Fleming T, Robinson M, Thomson B, Graetz N, Margono C, Mullany EC, Biryukov S, Abbafati C, Abera SF, Abraham JP, Abu-Rmeileh NME, Achoki T, Albuhairan FS, Alemu ZA, Alfonso R, Ali MK, Ali R, Guzman NA, Ammar W, Anwari P, Banerjee A, Barquera S, Basu S, Bennett DA, Bhutta Z, Blore J, Cabral N, Nonato IC, Chang JC, Chowdhury R, Courville KJ, Criqui MH, Cundiff DK, Dabhadkar KC, Dandona L, Davis A, Dayama A, Dharmaratne SD, Ding EL, Durrani AM, Esteghamati A, Farzadfar F, Fay DFJ, Feigin VL, Flaxman A, Forouzanfar MH, Goto A, Green MA, Gupta R, Hafezi-Nejad N, Hankey GJ, Harewood HC, Havmoeller R, Hay S, Hernandez L, Husseini A, Idrisov BT, Ikeda N, Islami F, Jahangir E, Jassal SK, Jee SH, Jeffreys M, Jonas JB, Kabagambe EK, Khalifa SEAH, Kengne AP, Khader YS, Khang YH, Kim D, Kimokoti RW, Kinge JM, Kokubo Y, Kosen S, Kwan G, Lai T, Leinsalu M, Li Y, Liang X, Liu S, Logroscino G, Lotufo PA, Lu Y, Ma J, Mainoo NK, Mensah GA, Merriman TR, Mokdad AH, Moschandreas J, Naghavi M, Naheed A, Nand D, Narayan KMV, Nelson EL, Neuhouser ML, Nisar MI, Ohkubo T, Oti SO, Pedroza A, Prabhakaran D, Roy N, Sampson U, Seo H, Sepanlou SG, Shibuya K, Shiri R, Shiue I, Singh GM, Singh JA, Skirbekk V, Stapelberg NJC, Sturua L, Sykes BL, Tobias M, Tran BX, Trasande L, Toyoshima H, Van De Vijver S, Vasankari TJ, Veerman JL, Velasquez-Melendez G, Vlassov VV, Vollset SE, Vos T, Wang C, Wang X, Weiderpass E, Werdecker A, Wright JL, Yang YC, Yatsuya H, Yoon J, Yoon SJ, Zhao Y, Zhou M, Zhu S, Lopez AD, Murray CJL, Gakidou E. 2014. Global, regional, and national prevalence of overweight and obesity in children and adults during 1980-2013: A systematic analysis for the Global Burden of Disease Study 2013. *The Lancet* **384**:766–781. doi:10.1016/S0140-6736(14)60460-8

Nguyen T-M, Schreiner D, Xiao L, Traunmüller L, Bornmann C, Scheiffele P. 2016. An

alternative splicing switch shapes neurexin repertoires in principal neurons versus interneurons in the mouse hippocampus. *eLife* **5**:e22757. doi:10.7554/eLife.22757

Nguyen TB, Olzmann JA. 2019. Getting a handle on lipid droplets: Insights into ER–lipid droplet tethering. *The Journal of Cell Biology* **218**:1089–1091. doi:10.1083/jcb.201902160

Nimptsch K, Konigorski S, Pischon T. 2019. Diagnosis of obesity and use of obesity biomarkers in science and clinical medicine. *Metabolism: Clinical and Experimental* **92**:61–70. doi:10.1016/j.metabol.2018.12.006

Nishimura T, Fabian MR. 2016. Scanning for a unified model for translational repression by microRNAs. *The EMBO journal* **35**:1158–1159. doi:10.15252/embj.201694324

O'Brien J, Hayder H, Zayed Y, Peng C. 2018. Overview of MicroRNA Biogenesis, Mechanisms of Actions, and Circulation. *Frontiers in endocrinology* **9**:402. doi:10.3389/fendo.2018.00402

O'Neill S, Bohl M, Gregersen S, Hermansen K, O'Driscoll L. 2016. Blood-Based Biomarkers for Metabolic Syndrome. *Trends in Endocrinology & Metabolism* **27**:363–374. doi:10.1016/j.tem.2016.03.012

Oliva-Olivera W, Coín-Aragüez L, Lhamyani S, Clemente-Postigo M, Torres JA, Bernal-López MR, El Bekay R, Tinahones FJ. 2017. Adipogenic Impairment of Adipose Tissue-Derived Mesenchymal Stem Cells in Subjects With Metabolic Syndrome: Possible Protective Role of FGF2. *The Journal of clinical endocrinology and metabolism* **102**:478–487. doi:10.1210/jc.2016-2256

Olson AL. 2012. Regulation of GLUT4 and Insulin-Dependent Glucose Flux. *ISRN Molecular Biology* **2012**:856987. doi:10.5402/2012/856987

Olzmann JA, Carvalho P. 2019. Dynamics and functions of lipid droplets. *Nature Reviews Molecular Cell Biology*. doi:10.1038/s41580-018-0085-z

Olzmann JA, Kopito RR, Christianson JC. 2013. The mammalian endoplasmic reticulum-associated degradation system. *Cold Spring Harbor perspectives in biology* **5**:a013185. doi:10.1101/cshperspect.a013185

Orliaguet L, Ejlalmanesh T, Alzaid F. 2020. Metabolic and Molecular Mechanisms of Macrophage Polarisation and Adipose Tissue Insulin Resistance. *International Journal of Molecular Sciences* . doi:10.3390/ijms21165731

Ortega FJ, Mercader JM, Catalán V, Moreno-Navarrete JM, Pueyo N, Sabater M, Gómez-Ambrosi J, Anglada R, Fernández-Formoso JA, Ricart W, Frühbeck G, Fernández-Real JM. 2020. Targeting the Circulating MicroRNA Signature of Obesity. *Clinical Chemistry* **59**:781–792. doi:10.1373/clinchem.2012.195776

Ortega FJ, Mercader JM, Moreno-Navarrete JM, Rovira O, Guerra E, Esteve E, Xifra G, Martínez C, Ricart W, Rieusset J, Rome S, Karczewska-Kupczewska M,

Straczkowski M, Fernández-Real JM. 2014. Profiling of Circulating MicroRNAs Reveals Common MicroRNAs Linked to Type 2 Diabetes That Change With Insulin Sensitization. *Diabetes Care* **37**:1375 LP – 1383. doi:10.2337/dc13-1847

Ortega FJ, Moreno-Navarrete JM, Pardo G, Sabater M, Hummel M, Ferrer A, Rodriguez-Hermosa JI, Ruiz B, Ricart W, Peral B, Fernández-Real JM. 2010. MiRNA expression profile of human subcutaneous adipose and during adipocyte differentiation. *PloS one* **5**:e9022–e9022. doi:10.1371/journal.pone.0009022

Ose J, Holowatyj AN, Nattenmüller J, Gigic B, Lin T, Himbert C, Habermann N, Achaintre D, Scalbert A, Keski-Rahkonen P, Böhm J, Schrotz-King P, Schneider M, Ulrich A, Kampman E, Weijenberg M, Gsur A, Ueland P-M, Kauczor H-U, Ulrich CM. 2020. Metabolomics profiling of visceral and abdominal subcutaneous adipose tissue in colorectal cancer patients: results from the ColoCare study. *Cancer causes & control : CCC* **31**:723–735. doi:10.1007/s10552-020-01312-1

Ozaki K, Awazu M, Tamiya M, Iwasaki Y, Harada A, Kugisaki S, Tanimura S, Kohno M. 2016. Targeting the ERK signaling pathway as a potential treatment for insulin resistance and type 2 diabetes. *American Journal of Physiology-Endocrinology and Metabolism* **310**:E643–E651. doi:10.1152/ajpendo.00445.2015

Pachón-Peña G, Serena C, Ejarque M, Petriz J, Duran X, Oliva-Olivera W, Simó R, Tinahones FJ, Fernández-Veledo S, Vendrell J. 2016. Obesity Determines the Immunophenotypic Profile and Functional Characteristics of Human Mesenchymal Stem Cells From Adipose Tissue. *STEM CELLS Translational Medicine* **5**:464–475. doi:10.5966/sctm.2015-0161

Pagliassotti MJ, Kim PY, Estrada AL, Stewart CM, Gentile CL. 2016. Endoplasmic reticulum stress in obesity and obesity-related disorders: An expanded view. *Metabolism: clinical and experimental* **65**:1238–1246. doi:10.1016/j.metabol.2016.05.002

Palazzo C, Nguyen C, Lefevre-Colau M-M, Rannou F, Poiraudeau S. 2016. Risk factors and burden of osteoarthritis. *Annals of Physical and Rehabilitation Medicine* **59**:134–138. doi:https://doi.org/10.1016/j.rehab.2016.01.006

Palumbo P, Lombardi F, Siragusa G, Cifone MG, Cinque B, Giuliani M. 2018. Methods of Isolation, Characterization and Expansion of Human Adipose-Derived Stem Cells (ASCs): An Overview. *International journal of molecular sciences* **19**:1897. doi:10.3390/ijms19071897

Pappachan JM, Viswanath AK. 2015. Metabolic surgery: A paradigm shift in type 2 diabetes management. *World journal of diabetes* **6**:990–998. doi:10.4239/wjd.v6.i8.990

Pareek M, Schauer PR, Kaplan LM, Leiter LA, Rubino F, Bhatt DL. 2018. Metabolic

Surgery. *Journal of the American College of Cardiology* **71**:670 LP – 687. doi:10.1016/j.jacc.2017.12.014

Parrettini S, Cavallo M, Gaggia F, Luca* RC and G. 2020. Adipokines: A Rainbow of Proteins with Metabolic and Endocrine Functions. *Protein & Peptide Letters*. doi:http://dx.doi.org/10.2174/0929866527666200505214555

Párrizas M, Novials A. 2016. Circulating microRNAs as biomarkers for metabolic disease. *Best Practice and Research: Clinical Endocrinology and Metabolism*. doi:10.1016/j.beem.2016.08.001

Patel R, Apostolatos A, Carter G, Ajmo J, Gali M, Cooper DR, You M, Bisht KS, Patel NA. 2013. Protein Kinase C delta (PKCδ) splice variants modulate apoptosis pathway in 3T3L1 cells during adipogenesis: Identification of PKCδII inhibitor. *Journal of Biological Chemistry* . doi:10.1074/jbc.M113.482638

Patki V, Buxton J, Chawla A, Lifshitz L, Fogarty K, Carrington W, Tuft R, Corvera S. 2001. Insulin action on GLUT4 traffic visualized in single 3T3-L1 adipocytes by using ultra-fast microscopy. *Molecular Biology of the Cell* **12**:129–141. doi:10.1091/mbc.12.1.129

Paul P, Chakraborty A, Sarkar D, Langthasa M, Rahman M, Bari M, Singha RKS, Malakar AK, Chakraborty S. 2018. Interplay between miRNAs and human diseases. *Journal of Cellular Physiology* **233**:2007–2018. doi:10.1002/jcp.25854

Payankaulam S, Raicu A-M, Arnosti DN. 2019. Transcriptional Regulation of INSR, the Insulin Receptor Gene. *Genes* **10**:984. doi:10.3390/genes10120984

Peinado JR, Jimenez-Gomez Y, Pulido MR, Ortega-Bellido M, Diaz-Lopez C, Padillo FJ, Lopez-Miranda J, Vazquez-Martínez R, Malagón MM. 2010. The stromal-vascular fraction of adipose tissue contributes to major differences between subcutaneous and visceral fat depots. *Proteomics* **10**:3356–3366. doi:10.1002/pmic.201000350

Pellegrinelli V, Carobbio S, Vidal-Puig A. 2016. Adipose tissue plasticity: how fat depots respond differently to pathophysiological cues. *Diabetologia*. doi:10.1007/s00125-016-3933-4

Perez-Riverol Y, Csordas A, Bai J, Bernal-Llinares M, Hewapathirana S, Kundu DJ, Inuganti A, Griss J, Mayer G, Eisenacher M, Pérez E, Uszkoreit J, Pfeuffer J, Sachsenberg T, Yilmaz Ş, Tiwary S, Cox J, Audain E, Walzer M, Jarnuczak AF, Ternent T, Brazma A, Vizcaíno JA. 2019. The PRIDE database and related tools and resources in 2019: Improving support for quantification data. *Nucleic Acids Research* **47**:D442–D450. doi:10.1093/nar/gky1106

Peschek J, Acosta-Alvear D, Mendez AS, Walter P. 2015. A conformational RNA zipper promotes intron ejection during non-conventional XBP1 mRNA splicing. *EMBO reports* **16**:1688–1698. doi:https://doi.org/10.15252/embr.201540955

Petersen MC, Shulman GI. 2018. Mechanisms of insulin action and insulin resistance. *Physiological Reviews*. doi:10.1152/physrev.00063.2017

Petushkova NA, Pyatnitskiy MA, Rudenko VA, Larina O V., Trifonova OP, Kisrieva JS, Samenkova NF, Kuznetsova GP, Karuzina II, Lisitsa A V. 2014. Applying of hierarchical clustering to analysis of protein patterns in the human cancer-associated liver. *PLoS ONE* **9**. doi:10.1371/journal.pone.0103950

Pfaffl MW, Tichopad A, Prgomet C, Neuvians TP. 2004. Determination of stable housekeeping genes, differentially regulated target genes and sample integrity: BestKeeper--Excel-based tool using pair-wise correlations. *Biotechnology letters* **26**:509–15.

Piperi C, Adamopoulos C, Dalagiorgou G, Diamanti-Kandarakis E, Papavassiliou AG. 2012. Crosstalk between advanced glycation and endoplasmic reticulum stress: Emerging therapeutic targeting for metabolic diseases. *Journal of Clinical Endocrinology and Metabolism* **97**:2231–2242. doi:10.1210/jc.2011-3408

Pong SK, Gullerova M. 2018. Noncanonical functions of microRNA pathway enzymes – Drosha, DGCR8, Dicer and Ago proteins. *FEBS Letters* **592**:2973–2986. doi:10.1002/1873-3468.13196

Preston GM, Brodsky JL. 2017. The evolving role of ubiquitin modification in endoplasmic reticulum-associated degradation. *The Biochemical journal* **474**:445–469. doi:10.1042/BCJ20160582

Pulido M, Diaz-Ruiz A, Jiménez-Gómez Y, Garcia-Navarro S, Gracia-Navarro F, Tinahones F, López-Miranda J, Frühbeck G, Vázquez-Martínez R, Malagón MM. 2011. Rab18 dynamics in adipocytes in relation to lipogenesis, lipolysis and obesity. *PLoS ONE* **6**. doi:10.1371/journal.pone.0022931

Qi L, Tsai B, Arvan P. 2017. New Insights into the Physiological Role of Endoplasmic Reticulum-Associated Degradation. *Trends in cell biology* **27**:430–440. doi:10.1016/j.tcb.2016.12.002

Qin L, Chen J, Tang L, Zuo T, Chen H, Gao R, Xu W. 2019. Significant Role of Dicer and miR-223 in Adipose Tissue of Polycystic Ovary Syndrome Patients. *BioMed Research International* **2019**. doi:10.1155/2019/9193236

Quail DF, Dannenberg AJ. 2019. The obese adipose tissue microenvironment in cancer development and progression. *Nature Reviews Endocrinology* **15**:139–154. doi:10.1038/s41574-018-0126-x

Ramakrishnan VM, Boyd NL. 2018. The Adipose Stromal Vascular Fraction as a Complex Cellular Source for Tissue Engineering Applications. *Tissue Engineering - Part B: Reviews* **24**:289–299. doi:10.1089/ten.teb.2017.0061

Rayner KJ, Hennessy EJ. 2013. Extracellular communication via microRNA: lipid

particles have a new message. *Journal of lipid research* **54**:1174–1181. doi:10.1194/jlr.R034991

Reddy P, Lent-Schochet D, Ramakrishnan N, McLaughlin M, Jialal I. 2019. Metabolic syndrome is an inflammatory disorder: A conspiracy between adipose tissue and phagocytes. *Clinica Chimica Acta* **496**:35–44. doi:https://doi.org/10.1016/j.cca.2019.06.019

Reilly SM, Saltiel AR. 2017. Adapting to obesity with adipose tissue inflammation. *Nature Reviews Endocrinology* **13**:633–643. doi:10.1038/nrendo.2017.90

Rodriguez A-M, Pisani D, Dechesne CA, Turc-Carel C, Kurzenne J-Y, Wdziekonski B, Villageois A, Bagnis C, Breittmayer J-P, Groux H, Ailhaud G, Dani C. 2005. Transplantation of a multipotent cell population from human adipose tissue induces dystrophin expression in the immunocompetent mdx mouse. *The Journal of experimental medicine* **201**:1397–1405. doi:10.1084/jem.20042224

Rodríguez A, Ezquerro S, Méndez-Giménez L, Becerril S, Frühbeck G. 2015. Revisiting the adipocyte: a model for integration of cytokine signaling in the regulation of energy metabolism. *American Journal of Physiology-Endocrinology and Metabolism* **309**:E691–E714. doi:10.1152/ajpendo.00297.2015

Rogers MA, Liu J, Song B-L, Li B-L, Chang CCY, Chang T-Y. 2015. Acyl-CoA:cholesterol acyltransferases (ACATs/SOATs): Enzymes with multiple sterols as substrates and as activators. *The Journal of steroid biochemistry and molecular biology* **151**:102–107. doi:10.1016/j.jsbmb.2014.09.008

Rosell M, Kaforou M, Frontini A, file:///C:/Users/Julia Sánchez Ceinos/Desktop/Nimptsch 309.pdfOkolo A, Chan Y-W, Nikolopoulou E, Millership S, Fenech ME, MacIntyre D, Turner JO, Moore JD, Blackburn E, Gullick WJ, Cinti S, Montana G, Parker MG, Christian M. 2014. Brown and white adipose tissues: intrinsic differences in gene expression and response to cold exposure in mice. *American Journal of Physiology-Endocrinology and Metabolism* **306**:E945–E964. doi:10.1152/ajpendo.00473.2013

Rottiers V, Näär AM. 2012. MicroRNAs in metabolism and metabolic disorders. *Nature reviews Molecular cell biology* **13**:239–250. doi:10.1038/nrm3313

Rubino F, Nathan DM, Eckel RH, Schauer PR, Alberti KGMM, Zimmet PZ, Del Prato S, Ji L, Sadikot SM, Herman WH, Amiel SA, Kaplan LM, Taroncher-Oldenburg G, Cummings DE. 2016. Metabolic Surgery in the Treatment Algorithm for Type 2 Diabetes: A Joint Statement by International Diabetes Organizations. *Diabetes Care* **39**:861 LP – 877. doi:10.2337/dc16-0236

Saito M, Yoneshiro T, Matsushita M. 2016. Activation and recruitment of brown adipose tissue by cold exposure and food ingredients in humans. *Best Practice and Research: Clinical Endocrinology and Metabolism* **30**:537–547.

doi:10.1016/j.beem.2016.08.003

Salo VT, Belevich I, Li S, Karhinen L, Vihinen H, Vigouroux C, Magré J, Thiele C, Hölttä-Vuori M, Jokitalo E, Ikonen E. 2016. Seipin regulates ER –lipid droplet contacts and cargo delivery . *The EMBO Journal* **35**:2699–2716. doi:10.15252/embj.201695170

Sams VG, Blackledge C, Wijayatunga N, Barlow P, Mancini M, Mancini G, Moustaid-Moussa N. 2016. Effect of bariatric surgery on systemic and adipose tissue inflammation. *Surgical Endoscopy* **30**:3499–3504. doi:10.1007/s00464-015-4638-3

Saponaro C, Gaggini M, Carli F, Gastaldelli A. 2015. The subtle balance between lipolysis and lipogenesis: A critical point in metabolic homeostasis. *Nutrients* **7**:9453–9474. doi:10.3390/nu7115475

Sarantopoulos CN, Banyard DA, Ziegler ME, Sun B, Shaterian A, Widgerow AD. 2018. Elucidating the Preadipocyte and Its Role in Adipocyte Formation: a Comprehensive Review. *Stem Cell Reviews and Reports*. doi:10.1007/s12015-017-9774-9

Sarjeant K, Stephens JM. 2012. Adipogenesis. *Cold Spring Harbor perspectives in biology* **4**:a008417–a008417. doi:10.1101/cshperspect.a008417

Schamberger A, Sarkadi B, Orbán TI. 2012. Human mirtrons can express functional microRNAs simultaneously from both arms in a flanking exon-independent manner. *RNA Biology* **9**:1177–1185. doi:10.4161/rna.21359

Schauer PR, Bhatt DL, Kirwan JP, Wolski K, Brethauer SA, Navaneethan SD, Aminian A, Pothier CE, Kim ESH, Nissen SE, Kashyap SR, Investigators S. 2014. Bariatric surgery versus intensive medical therapy for diabetes--3-year outcomes. *The New England journal of medicine* **370**:2002–2013. doi:10.1056/NEJMoa1401329

Scheja L, Heeren J. 2019. The endocrine function of adipose tissues in health and cardiometabolic disease. *Nature Reviews Endocrinology*. doi:10.1038/s41574-019-0230-6

Schleinitz D, Krause K, Wohland T, Gebhardt C, Linder N, Stumvoll M, Blüher M, Bechmann I, Kovacs P, Gericke M, Tönjes A. 2020. Identification of distinct transcriptome signatures of human adipose tissue from fifteen depots. *European Journal of Human Genetics* **28**:1714–1725. doi:10.1038/s41431-020-0681-1

Sebastiani G, Guarino E, Grieco GE, Formichi C, Delli Poggi C, Ceccarelli E, Dotta F. 2017. Circulating microRNA (miRNA) Expression Profiling in Plasma of Patients with Gestational Diabetes Mellitus Reveals Upregulation of miRNA miR-330-3p. *Frontiers in endocrinology* **8**:345. doi:10.3389/fendo.2017.00345

Sebo ZL, Rodeheffer MS. 2019. Assembling the adipose organ: adipocyte lineage segregation and adipogenesis in vivo *Development*

146:dev172098. doi:10.1242/dev.172098

Serena C, Keiran N, Ceperuelo-Mallafre V, Ejarque M, Fradera R, Roche K, Nuñez-Roa C, Vendrell J, Fernández-Veledo S. 2016. Obesity and Type 2 Diabetes Alters the Immune Properties of Human Adipose Derived Stem Cells. *Stem Cells* **34**:2559–2573. doi:10.1002/stem.2429

Sergi D, Naumovski N, Heilbronn LK, Abeywardena M, O'Callaghan N, Lionetti L, Luscombe-Marsh N. 2019. Mitochondrial (Dys)function and Insulin Resistance: From Pathophysiological Molecular Mechanisms to the Impact of Diet. *Frontiers in physiology* **10**:532. doi:10.3389/fphys.2019.00532

Sheng P, Flood KA, Xie M. 2020. Short Hairpin RNAs for Strand-Specific Small Interfering RNA Production . *Frontiers in Bioengineering and Biotechnology* .

Shi Y. 2017. Mechanistic insights into precursor messenger RNA splicing by the spliceosome. *Nature Reviews Molecular Cell Biology* **18**:655–670. doi:10.1038/nrm.2017.86

Shurtleff MJ, Temoche-Diaz MM, Karfilis K V, Ri S, Schekman R. 2016. Y-box protein 1 is required to sort microRNAs into exosomes in cells and in a cell-free reaction. *eLife* **5**:e19276. doi:10.7554/eLife.19276

Singh N, Parihar RK, Saini G, Mohan SK, Sharma N, Razaq M. 2013. Prevalence of metabolic syndrome in adolescents aged 10-18 years in Jammu, J and K. *Indian journal of endocrinology and metabolism* **17**:133–137. doi:10.4103/2230-8210.107849

Sjöström L, Peltonen M, Jacobson P, Sjöström CD, Karason K, Wedel H, Ahlin S, Anveden Å, Bengtsson C, Bergmark G, Bouchard C, Carlsson B, Dahlgren S, Karlsson J, Lindroos A-K, Lönroth H, Narbro K, Näslund I, Olbers T, Svensson P-A, Carlsson LMS. 2012. Bariatric Surgery and Long-term Cardiovascular Events. *JAMA* **307**:56–65. doi:10.1001/jama.2011.1914

Skorobogatko Y, Dragan M, Cordon C, Reilly SM, Hung CW, Xia W, Zhao P, Wallace M, Lackey DE, Chen XW, Osborn O, Bogner-Strauss JG, Theodorescu D, Metallo CM, Olefsky JM, Saltiel AR. 2018. RalA controls glucose homeostasis by regulating glucose uptake in brown fat. *Proceedings of the National Academy of Sciences of the United States of America* **115**:7819–7824. doi:10.1073/pnas.1801050115

Smorlesi A, Frontini A, Giordano A, Cinti S. 2012. The adipose organ: White-brown adipocyte plasticity and metabolic inflammation. *Obesity Reviews* **13**:83–96. doi:10.1111/j.1467-789X.2012.01039.x

Sohel MH. 2016. Extracellular/Circulating MicroRNAs: Release Mechanisms, Functions and Challenges. *Achievements in the Life Sciences* **10**:175–186. doi:https://doi.org/10.1016/j.als.2016.11.007

Solinas G, Borén J, Dulloo AG. 2015. De novo lipogenesis in metabolic homeostasis: More friend than foe? *Molecular Metabolism* **4**:367–377. doi:10.1016/j.molmet.2015.03.004

Song Z, Xiaoli AM, Yang F. 2018. Regulation and metabolic significance of De Novo lipogenesis in adipose tissues. *Nutrients* **10**:1–22. doi:10.3390/nu10101383

Spencer M, Unal R, Zhu B, Rasouli N, McGehee Jr. RE, Peterson CA, Kern PA. 2011. Adipose Tissue Extracellular Matrix and Vascular Abnormalities in Obesity and Insulin Resistance. *The Journal of Clinical Endocrinology & Metabolism* **96**:E1990–E1998. doi:10.1210/jc.2011-1567

Sriram S, Yuan C, Chakraborty S, Tay W, Park M, Shabbir A, Toh S-A, Han W, Sugii S. 2019. Oxidative stress mediates depot-specific functional differences of human adipose-derived stem cells. *Stem Cell Research & Therapy* **10**:141. doi:10.1186/s13287-019-1240-y

Stahl PD, Raposo G. 2019. Extracellular Vesicles: Exosomes and Microvesicles, Integrators of Homeostasis. *Physiology* **34**:169–177. doi:10.1152/physiol.00045.2018

Stavast CJ, Erkeland SJ. 2019. The Non-Canonical Aspects of MicroRNAs: Many Roads to Gene Regulation. *Cells* **8**:1465. doi:10.3390/cells8111465

Stenkula KG, Erlanson-Albertsson C. 2018. Adipose cell size: Importance in health and disease. *American Journal of Physiology - Regulatory Integrative and Comparative Physiology* **315**:R284–R295. doi:10.1152/ajpregu.00257.2017

Stöckli J, Fazakerley DJ, James DE. 2011. GLUT4 exocytosis. *Journal of Cell Science* **124**:4147–4159. doi:10.1242/jcs.097063

Stone TW, McPherson M, Gail Darlington L. 2018. Obesity and Cancer: Existing and New Hypotheses for a Causal Connection. *EBioMedicine* **30**:14–28. doi:10.1016/j.ebiom.2018.02.022

Stumvoll M, Goldstein BJ, Haeften TW Van. 2010. Seminar Type 2 diabetes: principles of pathogenesis and therapy. *Insulin* **365**.

Sun K, Lai EC. 2013. Adult-specific functions of animal microRNAs. *Nature reviews Genetics* **14**:535–548. doi:10.1038/nrg3471

Sun S, Kelekar S, Kliewer SA, Mangelsdorf DJ. 2019. The orphan nuclear receptor SHP regulates ER stress response by inhibiting XBP1s degradation. *Genes & development* **33**:1083–1094. doi:10.1101/gad.326868.119

Sun T, Fu M, Bookout AL, Kliewer SA, Mangelsdorf DJ. 2009. MicroRNA let-7 Regulates 3T3-L1 Adipogenesis. *Molecular Endocrinology* **23**:925–931. doi:10.1210/me.2008-0298

Świderska E. 2020. Role of PI3K/AKT Pathway in Insulin-Mediated Glucose Uptake In:

Strycharz J, editor. Rijeka: IntechOpen. p. Ch. 3. doi:10.5772/intechopen.80402

Syed SN, Frank A-C, Raue R, Brüne B. 2019. MicroRNA-A Tumor Trojan Horse for Tumor-Associated Macrophages. *Cells* **8**:1482. doi:10.3390/cells8121482

Tam CS, Xie W, Johnson WD, Cefalu WT, Redman LM, Ravussin E. 2012. Defining insulin resistance from hyperinsulinemic-euglycemic clamps. *Diabetes Care* **35**:1605–1610. doi:10.2337/dc11-2339

Tang J-Y, Lee J-C, Hou M-F, Wang C-L, Chen C-C, Huang H-W, Chang H-W. 2013. Alternative splicing for diseases, cancers, drugs, and databases. *TheScientificWorldJournal* **2013**:703568. doi:10.1155/2013/703568

Tapial J, Ha KCH, Sterne-Weiler T, Gohr A, Braunschweig U, Hermoso-Pulido A, Quesnel-Vallières M, Permanyer J, Sodaei R, Marquez Y, Cozzuto L, Wang X, Gómez-Velázquez M, Rayon T, Manzanares M, Ponomarenko J, Blencowe BJ, Irimia M. 2017. An atlas of alternative splicing profiles and functional associations reveals new regulatory programs and genes that simultaneously express multiple major isoforms. *Genome research* **27**:1759–1768. doi:10.1101/gr.220962.117

Tchkonia T, Karagiannides I, Armour Forse R, Kirkland JL. 2001. Different fat depots are distinct mini-organs. *Current Opinion in Endocrinology and Diabetes* **8**:227–234. doi:10.1097/00060793-200110000-00001

Tchkonia T, Thomou T, Zhu Y, Karagiannides I, Pothoulakis C, Jensen MD, Kirkland JL. 2013. Mechanisms and metabolic implications of regional differences among fat depots. *Cell Metabolism* **17**:644–656. doi:10.1016/j.cmet.2013.03.008

Tchoukalova YD, Harteneck DA, Karwoski RA, Tarara J, Jensen MD. 2003. A quick, reliable, and automated method for fat cell sizing. *Journal of Lipid Research* **44**:1795–1801. doi:10.1194/jlr.d300001-jlr200

Tepedelen BE, Kirmizibatrak PB. 2019. Endoplasmic Reticulum-Associated Degradation (ERAD) In: Català PBKE-A, editor. Rijeka: IntechOpen. p. Ch. 3. doi:10.5772/intechopen.82043

Ter Horst KW, Van Galen KA, Gilijamse PW, Hartstra A V., De Groot PF, Van Der Valk FM, Ackermans MT, Nieuwdorp M, Romijn JA, Serlie MJ. 2017. Methods for quantifying adipose tissue insulin resistance in overweight/obese humans. *International Journal of Obesity* **41**:1288–1294. doi:10.1038/ijo.2017.110

ter Horst KW, van Galen KA, Gilijamse PW, Hartstra A V, de Groot PF, van der Valk FM, Ackermans MT, Nieuwdorp M, Romijn JA, Serlie MJ. 2017. Methods for quantifying adipose tissue insulin resistance in overweight/obese humans. *International Journal of Obesity* **41**:1288–1294. doi:10.1038/ijo.2017.110

Théry C, Amigorena S, Raposo G, Clayton A. 2006. Isolation and Characterization of Exosomes from Cell Culture Supernatants and Biological Fluids. *Current Protocols*

in Cell Biology **30**:3.22.1-3.22.29. doi:10.1002/0471143030.cb0322s30

Thiam AR, Beller M. 2017. The why, when and how of lipid droplet diversity. *Journal of Cell Science* **130**:315 LP – 324. doi:10.1242/jcs.192021

Thomou T, Mori MA, Dreyfuss JM, Konishi M, Sakaguchi M, Wolfrum C, Rao TN, Winnay JN, Garcia-Martin R, Grinspoon SK, Gorden P, Kahn CR. 2017. Adipose-derived circulating miRNAs regulate gene expression in other tissues. *Nature* **542**. doi:10.1038/nature21365

Tkach M, Théry C. 2016. Communication by Extracellular Vesicles: Where We Are and Where We Need to Go. *Cell* **164**:1226–1232. doi:https://doi.org/10.1016/j.cell.2016.01.043

Toroney R, Nielsen KH, Staley JP. 2019. Termination of pre-mRNA splicing requires that the ATPase and RNA unwindase Prp43 acts on the catalytic snRNA U6. *bioRxiv* 659029. doi:10.1101/659029

Treiber T, Treiber N, Meister G. 2019. Regulation of microRNA biogenesis and its crosstalk with other cellular pathways. *Nature Reviews Molecular Cell Biology* **20**:5–20. doi:10.1038/s41580-018-0059-1

Tsai YC, Weissman AM. 2011. Ubiquitylation in ERAD: Reversing to Go Forward? *PLOS Biology* **9**:e1001038.

Tunduguru R, Thurmond DC. 2017. Promoting glucose transporter-4 vesicle trafficking along cytoskeletal tracks: PAK-ing them out. *Frontiers in Endocrinology* **8**:1–15. doi:10.3389/fendo.2017.00329

Turchinovich A, Tonevitsky AG, Cho WC, Burwinkel B. 2015. Check and mate to exosomal extracellular miRNA: new lesson from a new approach. *Frontiers in molecular biosciences* **2**:11. doi:10.3389/fmolb.2015.00011

Turchinovich A, Weiz L, Langheinz A, Burwinkel B. 2011. Characterization of extracellular circulating microRNA. *Nucleic acids research* **39**:7223–7233. doi:10.1093/nar/gkr254

Turunen JJ, Niemelä EH, Verma B, Frilander MJ. 2013. The significant other: Splicing by the minor spliceosome. *Wiley Interdisciplinary Reviews: RNA* **4**:61–76. doi:10.1002/wrna.1141

Ushioda R, Hoseki J, Nagata K. 2013. Glycosylation-independent ERAD pathway serves as a backup system under ER stress. *Molecular biology of the cell* **24**:3155–3163. doi:10.1091/mbc.E13-03-0138

Valley MP, Karassina N, Aoyama N, Carlson C, Cali JJ, Vidugiriene J. 2016. A bioluminescent assay for measuring glucose uptake. *Analytical Biochemistry* **505**:43–50. doi:10.1016/j.ab.2016.04.010

van de Weijer ML, Krshnan L, Liberatori S, Guerrero EN, Robson-Tull J, Hahn L, Lebbink

RJ, Wiertz EJHJ, Fischer R, Ebner D, Carvalho P. 2020. Quality Control of ER Membrane Proteins by the RNF185/Membralin Ubiquitin Ligase Complex. *Molecular Cell* **79**:768-781.e7. doi:https://doi.org/10.1016/j.molcel.2020.07.009

van Meerloo J, Kaspers GJL, Cloos J. 2011. Cell Sensitivity Assays: The MTT Assay In: Cree IA, editor. Cancer Cell Culture: Methods and Protocols. Totowa, NJ: Humana Press. pp. 237–245. doi:10.1007/978-1-61779-080-5_20

Vandesompele J, De Preter K, Pattyn F, Poppe B, Van Roy N, De Paepe A, Speleman F. 2002. Accurate normalization of real-time quantitative RT-PCR data by geometric averaging of multiple internal control genes. *Genome biology* **3**:RESEARCH0034.

Varela-Rodríguez BM, Juiz-Valiña P, Varela L, Outeiriño-Blanco E, Bravo SB, García-Brao MJ, Mena E, Noguera JF, Valero-Gasalla J, Cordido F, Sangiao-Alvarellos S. 2020. Beneficial Effects of Bariatric Surgery-Induced by Weight Loss on the Proteome of Abdominal Subcutaneous Adipose Tissue. *Journal of clinical medicine* **9**:213. doi:10.3390/jcm9010213

Vasic V, Denkert N, Schmidt CC, Riedel D, Stein A, Meinecke M. 2020. Hrd1 forms the retrotranslocation pore regulated by auto-ubiquitination and binding of misfolded proteins. *Nature Cell Biology* **22**:274–281. doi:10.1038/s41556-020-0473-4

Vembar SS, Brodsky JL. 2008. One step at a time : endoplasmic reticulum-associated degradation **9**. doi:10.1038/nrm2546

Verma B, Akinyi M V, Norppa AJ, Frilander MJ. 2018. Minor spliceosome and disease. *Seminars in Cell & Developmental Biology* **79**:103–112. doi:https://doi.org/10.1016/j.semcdb.2017.09.036

Vernia S, Edwards YJK, Han MS, Cavanagh-Kyros J, Barrett T, Kim JK, Davis RJ. 2016. An alternative splicing program promotes adipose tissue thermogenesis. *eLife* **5**:e17672. doi:10.7554/eLife.17672

Vickers KC, Palmisano BT, Shoucri BM, Shamburek RD, Remaley AT. 2011. MicroRNAs are transported in plasma and delivered to recipient cells by high-density lipoproteins. *Nature Cell Biology* **13**:423–433. doi:10.1038/ncb2210

Vijay J, Gauthier MF, Biswell RL, Louiselle DA, Johnston JJ, Cheung WA, Belden B, Pramatarova A, Biertho L, Gibson M, Simon MM, Djambazian H, Staffa A, Bourque G, Laitinen A, Nystedt J, Vohl MC, Fraser JD, Pastinen T, Tchernof A, Grundberg E. 2020. Single-cell analysis of human adipose tissue identifies depot- and disease-specific cell types. *Nature Metabolism* **2**:97–109. doi:10.1038/s42255-019-0152-6

Villarroya-Beltri C, Gutiérrez-Vázquez C, Sánchez-Cabo F, Pérez-Hernández D, Vázquez J, Martin-Cofreces N, Martinez-Herrera DJ, Pascual-Montano A, Mittelbrunn M, Sánchez-Madrid F. 2013. Sumoylated hnRNPA2B1 controls the sorting of miRNAs into exosomes through binding to specific motifs. *Nature*

Communications **4**. doi:10.1038/ncomms3980

Vincenz L, Jäger R, O'Dwyer M, Samali A. 2013. Endoplasmic Reticulum Stress and the Unfolded Protein Response: Targeting the Achilles Heel of Multiple Myeloma. *Molecular Cancer Therapeutics* **12**:831 LP – 843. doi:10.1158/1535-7163.MCT-12-0782

Vishvanath L, Gupta RK. 2019. Contribution of adipogenesis to healthy adipose tissue expansion in obesity Find the latest version : Contribution of adipogenesis to healthy adipose tissue expansion in obesity **129**:4022–4031.

Walter P, Ron D. 2011. The unfolded protein response: From stress pathway to homeostatic regulation. *Science* **334**:1081–1086. doi:10.1126/science.1209038

Wang H, Becuwe M, Housden BE, Chitraju C, Porras AJ, Graham MM, Liu XN, Thiam AR, Savage DB, Agarwal AK, Garg A, Olarte M-J, Lin Q, Fröhlich F, Hannibal-Bach HK, Upadhyayula S, Perrimon N, Kirchhausen T, Ejsing CS, Walther TC, Farese Jr R V. 2016. Seipin is required for converting nascent to mature lipid droplets. *eLife* **5**:e16582. doi:10.7554/eLife.16582

Wang QA, Tao C, Gupta RK, Scherer PE. 2013. Tracking adipogenesis during white adipose tissue development, expansion and regeneration. *Nature Medicine* **19**:1338–1344. doi:10.1038/nm.3324

Watson RT, Pessin JE. 2006. Bridging the GAP between insulin signaling and GLUT4 translocation. *Trends in Biochemical Sciences* **31**:215–222. doi:10.1016/j.tibs.2006.02.007

Westneat DF, Potts LJ, Sasser KL, Shaffer JD. 2019. Causes and Consequences of Phenotypic Plasticity in Complex Environments. *Trends in Ecology & Evolution* **34**:555–568. doi:https://doi.org/10.1016/j.tree.2019.02.010

White U, Ravussin E. 2019. Dynamics of adipose tissue turnover in human metabolic health and disease. *Diabetologia* **62**:17–23. doi:10.1007/s00125-018-4732-x

Wiese S, Reidegeld KA, Meyer HE, Warscheid B. 2007. Protein labeling by iTRAQ: A new tool for quantitative mass spectrometry in proteome research. *Proteomics* **7**:340–350. doi:10.1002/pmic.200600422

Will CL, Lührmann R. 2011. Spliceosome structure and function. *Cold Spring Harbor perspectives in biology* **3**:a003707. doi:10.1101/cshperspect.a003707

Williams JM, Inoue T, Banks L, Tsai B. 2013. The ERdj5-Sel1L complex facilitates cholera toxin retrotranslocation. *Molecular biology of the cell* **24**:785–795. doi:10.1091/mbc.E12-07-0522

Wu B, Guo W. 2015. The exocyst at a glance. *Journal of Cell Science* **128**:2957–2964. doi:10.1242/jcs.156398

Xie H, Lim B, Lodish HF. 2009. MicroRNAs induced during adipogenesis that accelerate

fat cell development are downregulated in obesity. *Diabetes* **58**:1050–1057. doi:10.2337/db08-1299

Xie M, Li M, Vilborg A, Lee N, Shu M-D, Yartseva V, Šestan N, Steitz JA. 2013. Mammalian 5'-capped microRNA precursors that generate a single microRNA. *Cell* **155**:1568–1580. doi:10.1016/j.cell.2013.11.027

Yan C, Wan R, Shi Y. 2019. Molecular Mechanisms of pre-mRNA Splicing through Structural Biology of the Spliceosome. *Cold Spring Harbor Perspectives in Biology* **11**. doi:10.1101/cshperspect.a032409

Yang Z, Wei Z, Wu X, Yang H. 2018. Screening of exosomal miRNAs derived from subcutaneous and visceral adipose tissues: Determination of targets for the treatment of obesity and associated metabolic disorders. *Molecular medicine reports* **18**:3314–3324. doi:10.3892/mmr.2018.9312

Yanovski JA. 2018. Obesity: Trends in underweight and obesity - scale of the problem. *Nature reviews Endocrinology* **14**:5–6. doi:10.1038/nrendo.2017.157

Yi X, Liu J, Wu P, Gong Y, Xu X, Li W. 2020a. The whole transcriptional profiling of cellular metabolism during adipogenesis from hMSCs. *Journal of Cellular Physiology* **235**:349–363. doi:https://doi.org/10.1002/jcp.28974

Yi X, Liu J, Wu P, Gong Y, Xu X, Li W. 2020b. The key microRNA on lipid droplet formation during adipogenesis from human mesenchymal stem cells. *Journal of Cellular Physiology* **235**:328–338. doi:https://doi.org/10.1002/jcp.28972

Yi X, Yang Y, Wu P, Xu X, Li W. 2020c. Alternative splicing events during adipogenesis from hMSCs. *Journal of Cellular Physiology* **235**:304–316. doi:https://doi.org/10.1002/jcp.28970

Ying W, Riopel M, Bandyopadhyay G, Dong Y, Birmingham A, Seo JB, Ofrecio JM, Wollam J, Hernandez-Carretero A, Fu W, Li P, Olefsky JM. 2017. Adipose Tissue Macrophage-Derived Exosomal miRNAs Can Modulate In Vivo and In Vitro Insulin Sensitivity. *Cell* **171**:372-384.e12. doi:https://doi.org/10.1016/j.cell.2017.08.035

Yoda M, Cifuentes D, Izumi N, Sakaguchi Y, Suzuki T, Giraldez AJ, Tomari Y. 2013. Poly(A)-specific ribonuclease mediates 3'-end trimming of Argonaute2-cleaved precursor microRNAs. *Cell reports* **5**:715–726. doi:10.1016/j.celrep.2013.09.029

Yue Y, Liu J, He C. 2015. RNA N6-methyladenosine methylation in post-transcriptional gene expression regulation. *Genes & development* **29**:1343–1355. doi:10.1101/gad.262766.115

Zampetaki A, Kiechl S, Drozdov I, Willeit P, Mayr U, Prokopi M, Mayr A, Weger S, Oberhollenzer F, Bonora E, Shah A, Willeit J, Mayr M. 2010. Plasma MicroRNA Profiling Reveals Loss of Endothelial MiR-126 and Other MicroRNAs in Type 2 Diabetes. *Circulation Research* **107**:810–817.

doi:10.1161/CIRCRESAHA.110.226357

Zatterale F, Longo M, Naderi J, Raciti GA, Desiderio A, Miele C, Beguinot F. 2020. Chronic Adipose Tissue Inflammation Linking Obesity to Insulin Resistance and Type 2 Diabetes . *Frontiers in Physiology* .

Zhang L, Li X, Zhao R. 2013. Structural analyses of the pre-mRNA splicing machinery. *Protein science : a publication of the Protein Society* **22**:677–692. doi:10.1002/pro.2266

Zhang L, Zhang C, Wang A. 2016. Divergence and Conservation of the Major UPR Branch IRE1-bZIP Signaling Pathway across Eukaryotes. *Scientific reports* **6**:27362. doi:10.1038/srep27362

Zhang P, Reue K. 2017. Lipin proteins and glycerolipid metabolism: Roles at the ER membrane and beyond. *Biochimica et Biophysica Acta (BBA) - Biomembranes* **1859**:1583–1595. doi:https://doi.org/10.1016/j.bbamem.2017.04.007

Zhang T, Lv C, Li L, Chen S, Liu S, Wang C, Su B. 2013. Plasma miR-126 is a potential biomarker for early prediction of type 2 diabetes mellitus in susceptible individuals. *BioMed research international* **2013**:761617. doi:10.1155/2013/761617

Zhang Y, Zheng Y, Fu Y, Wang C. 2019. Identification of biomarkers, pathways and potential therapeutic agents for white adipocyte insulin resistance using bioinformatics analysis. *Adipocyte* **8**:318–329. doi:10.1080/21623945.2019.1649578

Zhang Ying, Qu P, Ma X, Qiao F, Ma Y, Qing S, Zhang Yong, Wang Y, Cui W. 2018. Tauroursodeoxycholic acid (TUDCA) alleviates endoplasmic reticulum stress of nuclear donor cells under serum starvation. *PloS one* **13**:e0196785–e0196785. doi:10.1371/journal.pone.0196785

Zhao C, Sun X, Li L. 2019. Biogenesis and function of extracellular miRNAs. *ExRNA* **1**:38. doi:10.1186/s41544-019-0039-4

Zhao X, Yang Y, Sun BF, Shi Y, Yang X, Xiao W, Hao YJ, Ping XL, Chen YS, Wang WJ, Jin KX, Wang X, Huang CM, Fu Y, Ge XM, Song SH, Jeong HS, Yanagisawa H, Niu Y, Jia GF, Wu W, Tong WM, Okamoto A, He C, Danielsen JMR, Wang XJ, Yang YG. 2014. FTO-dependent demethylation of N6-methyladenosine regulates mRNA splicing and is required for adipogenesis. *Cell Research* **24**:1403–1419. doi:10.1038/cr.2014.151

Zhou L, Chen T, Li G, Wu C, Wang C, Li L, Sha S, Chen Lei, Liu G, Chen Ling. 2016. Activation of PPARγ ameliorates spatial cognitive deficits through restoring expression of AMPA receptors in seipin knock-out mice. *Journal of Neuroscience* **36**:1242–1253. doi:10.1523/JNEUROSCI.3280-15.2016

Zhu Q, Scherer PE. 2018. Immunologic and endocrine functions of adipose tissue:

implications for kidney disease. *Nature Reviews Nephrology* **14**:105–120. doi:10.1038/nrneph.2017.157

Zong L, Zhu Y, Liang R, Zhao H-B. 2016. Gap junction mediated miRNA intercellular transfer and gene regulation: A novel mechanism for intercellular genetic communication. *Scientific reports* **6**:19884. doi:10.1038/srep19884

Zuk P. 2013. Adipose-Derived Stem Cells in Tissue Regeneration: A Review. *ISRN Stem Cells* **2013**:1–35. doi:10.1155/2013/713959